

**Biosynthesis of novel glycolipids (Sophorolipids):  
Exploring the mechanism of assembling and biological  
properties**

**Thesis Submitted to AcSIR**

*For the Award of the Degree of*

**DOCTOR OF PHILOSOPHY**

*In*

**BIOLOGICAL SCIENCES**



By

**Parul Dubey**

(Registration Number: 10BB11A26057)

Under the guidance and co-guidance of  
**Dr. Narendra Kadoo and Dr. Asmita Prabhune**

Biochemical Sciences Division  
CSIR-National Chemical Laboratory  
Pune - 411008, India.

July 2016



# राष्ट्रीय रासायनिक प्रयोगशाला

(वैज्ञानिक तथा औद्योगिक अनुसंधान परिषद)

डॉ. होमी भाभा मार्ग पुणे - 411 008. भारत

## NATIONAL CHEMICAL LABORATORY

(Council of Scientific & Industrial Research)

Dr. Homi Bhabha Road, Pune - 411 008. India.



### Certificate of the Guide

This is to certify that work presented in the thesis entitled "Biosynthesis of novel glycolipids (Sophorolipids): Exploring the mechanism of assembling and biological properties" by **Parul Dubey**, submitted for the degree of **Doctor of Philosophy in Biological Sciences** was carried out under our supervision at the Biochemical Sciences Division, National Chemical Laboratory, Pune, 411008, India. All the materials from other sources have been duly acknowledged in the thesis.

**Dr. Narendra Kadoo**  
(Research Guide)

**Dr. Asmita Prabhune**  
(Research Co-Guide)

**July, 2016**

**Biochemical Sciences Division**

**CSIR-National Chemical Laboratory,**

**Pune-411008**

Communication  
Channels

NCL Level DID : 2590  
NCL Board No. : +91-20-25902000  
EPABX : +91-20-25893300  
+91-20-25893400

FAX

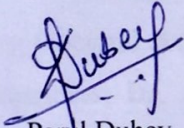
Director's Office : +91-20-25902601  
COA's Office : +91-20-25902660  
COS&P's Office : +91-20-25902664

WEBSITE

[www.ncl-india.org](http://www.ncl-india.org)

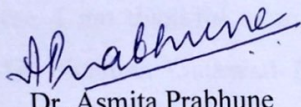
## Certificate

This is to certify that the work incorporated in this Ph.D. thesis entitled "**Biosynthesis of novel glycolipids (Sophorolipids): Exploring the mechanism of assembling and biological properties**" submitted by Ms. Parul Dubey to Academy of Scientific and Innovative Research (AcSIR) in fulfillment of the requirements for the award of the Degree of Doctor of Philosophy, embodies original research work under our supervision/guidance. We further certify that this work has not been submitted to any other University or Institution in part or full for the award of any degree or diploma. Research material obtained from other sources has been duly acknowledged in the thesis. Any text, illustration, table etc., used in the thesis from other sources, have been duly cited and acknowledged.



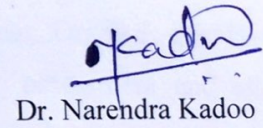
Parul Dubey

(Student)



Dr. Asmita Prabhune

(Co-Supervisor)



Dr. Narendra Kadoo

(Supervisor)

## **Acknowledgement**

My journey of pursuing Ph.D began in August 2011 and hereby I submit my thesis in July 2016. In this long period I came across many people who contributed in their own remarkable ways towards fulfillment of my thesis work and I would like to extend my heartfelt gratitude to them. First and foremost, I am thankful to my advisors, Dr. Asmita Prabhune and Dr. Narendra Kadoo for their constant support and encouragement. Asmita Ma'am is a very enthusiastic person, full of energy and innovative ideas. Her knowledge and contemporary ideas always helped me to give a different dimension to the work. Her positive attitude towards work has always boosted my moral. The faith and trust that she kept in me was a continual source of encouragement and I am deeply thankful to Asmita Ma'am for her support in professional and non-professional situations as well. This tenure in NCL was surely a pleasant journey because of her mentorship. I am obliged to Narendra Sir for his co-operation and timely help. His smiling face and serene attitude always allowed me to reach out to him without hesitation. I would like to extend a heartfelt thanks to Dr. Kaliaperumal Selvaraj for his perpetual support during my tenure in NCL. I admire him for his supervision and excellent teaching skills.

For the Ph.D degree, we students need to complete a course curriculum that is monitored by Doctoral Advisory Committee. I am thankful to my DAC chairman, Dr. D.S. Reddy and members, Dr. Absar Ahmed, Dr. Sushma Gaikwad for their timely assessment and expert comments that helped in successfully completing my courses and Ph.D work.

With a new work idea from Asmita Ma'am, we contacted Dr. Anuya Nisal from Polymer Science and Engineering Division and the collaboration proved to be very fruitful for my thesis work. The work conducted under her guidance helped me in learning several techniques and added to my knowledge. I am greatly thankful to Anuya Ma'am for her consistent support, encouragement and appreciation. She introduced me to various people who heartily helped me in smoothly conducting my experimental studies. For the same work we approached Dr. P. R. Rajamohanan and Dr. Sapna Ravindranathan from Central NMR facility. I feel indebted to both Rajamohanan Sir and Sapna Ma'am for putting their heart and soul in deciphering the intricate details of the study. Their knowledge and passion towards work helped us in decoding new unknown facets. I wish to thank Sapna Ma'am for tutoring me the intricate NMR experiments in comprehensible ways and for blithely sparing her time for my queries. I am also obliged to Dr.

Ashish Lele for extended scientific discussions and his intellectual suggestions that gave clarity to my work. Permission and co-operation from Dr. V. K. Aswal (Bhabha Atomic Research Centre, Mumbai) enabled me to conduct Small Angle Neutron Scattering studies at BARC. I am thankful to him and his student Dr. Sugam Kumar for their support and extensive discussions related to work. SANS data analysis done by Sugam aided in deducing the crucial information necessary to conclude the work.

The cell studies detailed in this thesis are performed at Dr. Dhiman Sarkar's Lab in Combi-Chem, Organic Chemistry Division. I am thankful to him for permitting me to avail the lab facilities and evaluating the work. I am also thankful to Dr. Sunil Bhagwat from Institute of Chemical Technology and Dr. Deopurkar from Savitribai Phule Pune University, for allowing me to conduct the surface tension measurements in their laboratory. Likewise, I am grateful to Dr. Sangeeta Kale from Defense Institute of Advanced Technology, Pune for permitting me to avail the facility of Field Emission Scanning Electron microscope at her institute. I would also like to thank Dr. S.K. Asha for allowing handling of FTIR-ATR instrument, Dr. Suresh Bhatt for allowing me to conduct lengthy light scattering experiments in his lab and Sujaya Ma'am for permitting me to use lyophilizer in Venture Center.

Be it professional or personal front, presence of friends makes life easy and I cannot end this note without thanking my dearest friends in and outside lab who made my journey in NCL memorable. Senior and friends like Dr. Kasturi Joshi-Navare, Dr. Vrushali Dengle-Pulate, Dr. Pradeep Kumar Singh and Dr. Debanjan Guin, always lended a helping hand whenever required. Assisting them in the beginning benefited me to learn the experimental techniques and they were very humble in advising me timely. I am also thankful to Snehal More Ma'am for her help and support. My labmates and friends, Philem Pushparani Devi, Pooja Singh, Priti Darne, Mihir Mehta, Pooja Ghushe, Avinash Sunder, Amrita Patil, Suman Jhajharia, Rajendra Prasad Meena, Zinoy Mandappan, Sandhya Aiyer, Krati Joshi, Meghana Okkutan, Ruchira Mukherji and Hrishikesh Mungi, were always present with me to encourage, support and help. I enjoyed fun and frolic days spend with them. Henceforth I carry memorable moments, conversations and time that I will cherish all my life. I thank them from the bottom of my heart for everything. I am also grateful to my friend Laxman Nawale who helped me in cell culture studies and endeavored hard to complete the experiments. It was merry working with him day and night. Project trainees like Jnanada Joshi, Devika Joshi and Sahana helped me discover new aspects in my personality.

While training them I myself learned many things that will definitely help me in future. They were very supportive; apart from their project work they often helped me with my experiments for which I am very thankful to them. Dr. Anuya's students Prachi Dhavale, Bhakti Khude, Chaitali Shete and Raeesa Sayyad often helped me in several aspects for which I am very thankful to them. Likewise, Rohini Kitture, Sameer, Ashwini, and Shobha Desai supported me for experimental work related to the thesis for which I am grateful to them.

As I was successfully able to complete my thesis work in Biochemical Sciences Division, National Chemical Laboratory Pune, I extend my heartfelt thanks to the Director of NCL and Head of Biochemical Division for giving me this great opportunity to work here and be a part of this renowned research institute. I acknowledge Council of Scientific and Industrial Research for providing the fellowship to conduct research at NCL.

Lastly I thank almighty God, for giving me strength and courage to carry out necessary chores and blessing me with loving family both before and after marriage. My endeavors paid off because of my family's trust, love and support. I dedicate this thesis to my loving Papa, who would have been the happiest person on earth to know that finally I have completed it. I am indebted to my parents Late Mr. Purushottam Dubey and Mrs. Rashmi Dubey for their struggle, undying support and trust in me. I wish to fulfill all your dreams and make you proud. I extend a heartfelt gratitude to my parents-in law for their support and encouragement. My brothers, Prashant and Rajat, have been a constant source of support and encouragement. Their presence fills me with strength and glee. Prashant's technical knowledge helped me in easy simplified processing of bulk experimental data for which I am thankful to him. I would also like to dedicate my accomplishments to the biggest strength in life, my best friend and loving husband Saurav Sharma. His backing and encouragement helped me to trek through this path gallantly. Advices from him always helped me in tough situations and his bearing attitude, patience kept me going through this journey, especially during the final stages.

Parul Dubey

*Dedicated to my Papa*

# Table of Contents

<b>List of Figures</b> .....	i
<b>List of Tables</b> .....	viii
<b>List of Abbreviations</b> .....	ix
<b>Chapter 1: Introduction</b> .....	1
1.1 Surfactants in general.....	2
1.2 Biosurfactants.....	2
1.3 Types of Biosurfactants.....	2
1.4 Sophorolipids.....	5
1.4.1 Sophorolipid structure .....	5
1.4.2 Producing organisms.....	6
1.4.3 Physiological role of sophorolipids .....	7
1.4.4 SL Biosynthetic pathway and substrates used for production.....	7
1.5 Self assembly in Sophorolipids.....	9
1.5.1 pH driven assembly in acidic sophorolipids.....	10
1.5.2 Changing morphology with concentration .....	10
1.5.3 Role of molecular structure in self assembly of acidic sophorolipid .....	11
1.5.4 Enhanced sophorolipid assembly by external forces.....	12
1.6 Sophorolipids in multiple areas.....	12
1.6.1 Sophorolipids in cosmetics .....	12
1.6.2 Sophorolipids as cleaning agents.....	13
1.6.3 Sophorolipids as germicide in vegetable and fruit wash .....	14
1.6.4 Sophorolipids in theranostic application.....	14
1.6.5 Environmental applications of Sophorolipids.....	14
1.6.6 Sophorolipids as adjuvants .....	15
1.6.7 Sophorolipids in nanomaterial synthesis.....	15
1.6.8 Sophorolipids as size reducing agents .....	16
1.6.9 Sophorolipids as therapeutic agents.....	16
1.7 Proteins and Surfactants .....	18

1.7.1 Protein-surfactant interactions.....	19
1.7.2 Introduction to silk fibroin .....	20
1.7.3 Silk as a biomaterial.....	21
<b>1.8 Scope of the work .....</b>	<b>22</b>
<b>1.9 Thesis outline.....</b>	<b>23</b>
<b>Chapter 2: Production and characterization of novel sophorolipids using primary</b>	
<b>fatty alcohol: their physico-chemical and antibacterial properties .....</b>	<b>25</b>
<b>2.1 Introduction .....</b>	<b>26</b>
<b>2.2 Materials and Method.....</b>	<b>28</b>
2.2.1 Chemicals .....	28
2.2.2 Microorganism and Maintenance .....	28
2.2.3 Production of Sophorolipids.....	28
2.2.4 Evaluation of surface active properties of SLCA .....	30
2.2.5 Characterization and structure determination.....	32
2.2.6 Assessment of antibacterial property of SLCA .....	33
<b>2.3 Results and Discussion .....</b>	<b>34</b>
2.3.1 Production of sophorolipid.....	34
2.3.2 Surface active properties of sophorolipid.....	34
2.3.3 Analytical characterization of SLCA .....	38
2.3.4 Antibacterial activity against Gram-positive and Gram-negative bacteria .....	46
<b>2.4 Conclusion.....</b>	<b>51</b>
<b>Chapter 3: Apoptosis mediated anti-proliferative effect of cetyl alcohol sophorolipid and</b>	
<b>their anti-angiogenic activity.....</b>	<b>52</b>
<b>3.1 Introduction.....</b>	<b>53</b>
<b>3.2 Materials and Method.....</b>	<b>54</b>
3.2.1 Sophorolipid production and extraction .....	54
3.2.2 Column purification of SLCA.....	54
3.2.3 LC-MS of purified cetyl alcohol sophorolipid .....	54
3.2.4 Cell lines and cell culture .....	55
3.2.5 High content screening analysis .....	55
3.2.6 Experimental assays.....	55

3.2.7	Anti-angiogenic activity of sophorolipids .....	59
<b>3.3</b>	<b>Results and Discussion</b> .....	60
3.3.1	Purified sophorolipid structure .....	60
3.3.2	Determination of cell viability .....	61
3.3.3	Monitoring cell cycle progression .....	63
3.3.4	SLCA induced apoptosis in HeLa cells .....	65
3.3.5	Evaluation of mitochondrial membrane potential.....	67
3.3.6	Ca <sup>2+</sup> release indicator of apoptosis .....	69
3.3.7	Functioning of caspase cascade .....	72
3.3.8	Cetyl alcohol sophorolipids as anti-angiogenic agents .....	73
<b>3.4</b>	<b>Conclusions</b> .....	77
<b>Chapter 4: Sophorolipid assisted tunable and rapid gelation of silk fibroin to form</b>		
	<b>porous biomedical scaffolds</b> .....	78
<b>4.1</b>	<b>Introduction</b> .....	79
<b>4.2</b>	<b>Materials and Method</b> .....	81
4.2.1	Preparation of regenerated silk fibroin solution .....	81
4.2.2	Sophorolipid synthesis and solutions.....	81
4.2.3	Formulation of hydrogels and characterization .....	82
4.2.4	Preparation of scaffolds and their characterization.....	83
4.2.5	Cell adhesion and proliferation studies on scaffolds.....	84
<b>4.3</b>	<b>Results and Discussion</b> .....	86
4.3.1	Studying time kinetics of gelation .....	86
4.3.2	Conformation changes in silk fibroin upon gelation .....	87
4.3.3	Compressive modulus of scaffolds .....	89
4.3.4	Morphology and pore size of scaffolds .....	89
4.3.5	Fibroblast adhesion and proliferation on scaffolds .....	90
<b>4.4</b>	<b>Conclusion</b> .....	94
<b>Chapter 5a: Silk Fibroin-Sophorolipid gelation: Deciphering the underlying</b>		
	<b>Mechanism</b> .....	96
<b>5a.1</b>	<b>Introduction</b> .....	97
<b>5a.2</b>	<b>Materials and Method</b> .....	99

5a.2.1	Preparation of regenerated silk fibroin .....	99
5a.2.2	Sophorolipid synthesis and solutions .....	100
5a.2.3	Nuclear Magnetic Resonance spectroscopy .....	100
5a.2.4	Bulk rheology measurements .....	102
5a.2.5	Small angle neutron scattering .....	102
<b>5a.3</b>	<b>Results and Discussion</b> .....	104
5a.3.1	Characterization of SF by NMR and SANS .....	105
5a.3.2	Characterization of Sophorolipids by NMR and SANS .....	107
5a.3.3	Bulk gelation in different SF-SL systems .....	116
5a.3.4	Molecular gelation in different SF-SL systems .....	118
5a.3.5	Mechanistic understanding of SF-SL systems.....	119
<b>5a.4</b>	<b>Conclusion</b> .....	124
<b>Chapter 5b: pH dependent sophorolipid assemblies and their influence on</b>		
	<b>gelation of silk fibroin protein</b> .....	125
5b.1	<b>Introduction</b> .....	126
5b.2	<b>Materials and method</b> .....	128
5b.2.1	Preparation of RSF and sophorolipid solutions.....	128
5b.2.2	NMR spectroscopy, rheology and SANS .....	128
5b.2.3	Fluorescence measurements .....	129
5b.3	<b>Results and Discussion</b> .....	129
5b.3.1	Influence of pH on sophorolipids .....	129
5b.3.2	Diffusion and size analysis of sophorolipid assemblies .....	131
5b.3.3	Gelation kinetics in SF+SL system at different pH .....	133
5b.3.4	SANS analysis of SF+ASL system at different pH .....	135
5b.3.5	Microenvironment change determination by fluorescent spectroscopy .....	138
5b.3.6	NMR diffusion analysis of SF+ASL system .....	140
<b>5b.4</b>	<b>Conclusion</b> .....	142
<b>Chapter 6: Conclusions and future work</b> .....		
<b>Chapter 6: Conclusions and future work</b> .....		143
<b>Bibliography</b> .....		152
<b>Synopsis</b> .....		169
<b>List of Publications</b> .....		172

## List of Figures

<b>Figure 1.1</b>	Two major forms of Sophorolipids produced by yeasts as a mixture-lactonic and acidic. <sup>[47]</sup>	6
<b>Figure 1.2</b>	Sophorolipid biosynthesis pathway adapted from Bogaert et al. (2007). Different enzymes carrying out the biochemical reactions are as follows: (1) cytochrome P450 monooxygenase, (2) alcohol dehydrogenase, (3) aldehyde dehydrogenase (4) lipase, (5) cytochrome P450 monooxygenase, (6) glucosyltransferase I, (7) glucosyltransferase II, (8) lactone esterase, (9) acetyl transferase. <sup>[21]</sup>	8
<b>Figure 1.3</b>	Acidic sophorolipid self assembles into various forms such as giant ribbons, spherical micelles and cylindrical micelles under different conditions. <sup>[58]</sup>	9
<b>Figure 1.4</b>	Schematic presentation of the two models used to describe protein-surfactant complexes at saturation. Left – Bead necklace model, the protein chain is wrapped around the surfactant micellar bead. Adapted from <sup>[118]</sup> Right – Decorated model, polypeptide chain passes through the micelles. Adapted from <sup>[116]</sup>	20
<b>Figure 1.5</b>	Secondary structure of silk fibroin protein. <sup>[123]</sup>	21
<b>Figure 2.1</b>	Main steps involved in sophorolipid synthesis	30
<b>Figure 2.2</b>	Diagram describing the Wilhelmy plate method (adapted from Kruss)	31
<b>Figure 2.3</b>	Oil displacement assay demonstrating surfactant property of SLCA in concentration dependent manner	35
<b>Figure 2.4</b>	Micelle formation in surfactants over critical micelle concentration	36
<b>Figure 2.5</b>	Graphical representation of surface tension reduction of SLCA	37
<b>Figure 2.6</b>	TLC of cetyl alcohol derived sophorolipid synthesized by <i>Candida bombicola</i> (ATCC 22214).	38
<b>Figure 2.7</b>	Fourier transform infrared (FT-IR) transmittance spectrum of CA-cetyl alcohol, SLCA-cetyl alcohol derived sophorolipid and glucose.	39

<b>Figure 2.8</b>	LC-MS chromatogram of SLCA	40
<b>Figure 2.9</b>	(a) Non-acetylated form of SLCA with methyl end group, (b) mono and (c) diacetylated form of SLCA with CH <sub>3</sub> end group	41
<b>Figure 2.10</b>	(a) mono-acetylated and (b) di-acetylated forms of SLCA with CH <sub>2</sub> OH end group	42
<b>Figure 2.11</b>	(a) Ion spectra of component A, (non-acetylated, -CH <sub>3</sub> end group). (b) Ion spectra of respective mono-acetylated (1-Ac- CH <sub>3</sub> end group) and (c) diacetylated (1-Diac CH <sub>3</sub> end group) form of component A, acquired using full-scan liquid chromatography– high-resolution accurate mass spectrometry. The encircled peaks highlight molecular ion and their sodium adducts.	43,44
<b>Figure 2.12</b>	(a) Ion spectra of component B, (mono-acetylated, -CH <sub>2</sub> OH end group) and (b) the corresponding ion spectra of the di-acetylated (2-Diac-CH <sub>2</sub> OH end group) form of component B, acquired using full-scan liquid chromatography–high-resolution accurate mass spectrometry.	45
<b>Figure 2.13</b>	Graph showing antibacterial activity of SLCA and cetyl alcohol against <i>E. coli</i> after different incubation time at 37°C	48
<b>Figure 2.14</b>	Antibacterial assay plates showing effective killing of <i>E. coli</i> with increasing time and concentration of SLCA.	48
<b>Figure 2.15</b>	Graph showing antibacterial activity of SLCA against <i>S. aureus</i> after different incubation time at 28°C	49
<b>Figure 2.16</b>	Antibacterial assay plates showing effective killing of <i>S. aureus</i> with increasing time and concentration of SLCA	50
<b>Figure 3.1a</b>	Ion Spectra and structure of sodium adduct of non-acetylated form of cetyl alcohol sophorolipid with methyl end group.	60
<b>Figure 3.1b</b>	Ion Spectra and structure of sodium adduct of monoacetylated form of cetyl alcohol sophorolipid with methyl end group.	61
<b>Figure 3.2</b>	MTT assay. HUVEC cells and varied cancer cell lines subjected to different concentrations of doxorubicin, SLCA B, SLCA C for 48 h and the % growth inhibition as calculated for different treatments; (a)	62

	doxorubicin <b>(b)</b> SLCA B <b>(c)</b> SLCA C by MTT assay, n=3, Mean value ± SD	
<b>Figure 3.3</b>	Effect of <b>SLCA B (16.32 µg/ml)</b> , <b>SLCA C (14.14 µg/ml)</b> , <b>Doxorubicin (1.45 µg/ml)</b> and <b>Paclitaxel (0.0048 µg/ml)</b> on cell cycle phases. The alterations in cell cycle were monitored with DAPI staining after time interval of 6, 12, 18 and 24 h of sophorolipid treatment. The highlighted values reflect the arrested cell percentage in different cell cycle phases.	65
<b>Figure 3.4</b>	(a) Apoptotic ratio in HeLa cells subjected to different drug treatments (b) Assay of Annexin V-FITC (green) binding and PI (red) incorporation in sophorolipid-treated HeLa cells after 72 h. The overlay images in the second last and last column represent the apoptotic cells and absence of necrosis respectively. The analysis was conducted using confocal microscopy, Magnification 20X (scale, 100 µm).	66,67
<b>Figure 3.5</b>	Alteration of mitochondrial transmembrane potential in sophorolipid stimulated HeLa cells. Sophorolipid treated cells were incubated for different time intervals and later stained with Mito Tracker Red. (a) Average dye intensity signifying depolarized cells. Data from triplicate experiments represented as mean±SD (b) Fluorescence intensity of bound dye as recorded by confocal microscope (20X magnification, scale-100 µm). Loss in red intensity exemplifies the disruption of MMP.	68,69
<b>Figure 3.6</b>	Elevation in intracellular $[Ca^{2+}]_i$ on sophorolipid treatment of <b>HeLa</b> cells. The treated cells were incubated for 4, 8 and 12 h, stained with DAPI (blue) and Fluo-4/AM (green). <b>(a)</b> Bar diagram represents cell percentage releasing calcium at different time intervals. <b>(b)</b> Overlay of confocal microscopy images exemplifying increased Fluo-4 AM intensity after 12 h that indicates increase in cytoplasmic calcium. Magnification 20X (scale, 100 µm).	70,71
<b>Figure 3.7</b>	Effect of <b>SLCA B</b> and <b>SLCA C</b> on activation of caspases. The sophorolipid treated cells were incubated for different time intervals and caspase activity was assessed by spectrometric method. <b>(a)</b> caspase-3, <b>(b)</b> caspase-8 and <b>(c)</b> caspase-9 activity was measured in comparison to	73

	the control. Data represented from three independent experiments as mean $\pm$ SD values.	
<b>Figure 3.8</b>	Inhibition of neovascularisation upon <b>SLCA B</b> and <b>SLCA C</b> treatment. HUVECs were plated on 96 well plate precoated with matrigel ( $\pm$ LVES+VEGF) as control. Sophorolipid treated cells were stained with rhodamine conjugated phalloidin (red) and DAPI (blue) to stain tubes and nuclei respectively. Cell imaging was done using HCS Reader Cellomics' ArrayScan®.	75
<b>Figure 4.1</b>	Time sweep rheology experiments on pure SF, S1, S3 and S5 samples.	86
<b>Figure 4.2</b>	(a) ATR-FTIR spectra of S3 solution as a function of time (b) % beta sheet change in S3 as a function of time after amide I peak deconvolution.	88
<b>Figure 4.3</b>	% Beta sheets of SF+SL hydrogel for S1, S3 and S5 samples.	88
<b>Figure 4.4</b>	Compressive modulus of SF+SL hydrogel as a function of SL concentration (i.e. 1%, 3% and 5% (w/v)) at 25°C.	89
<b>Figure 4.5</b>	Scanning electron micrographs of cut surface of lyophilized scaffolds for (a) S1, (b) S3 and (c) S5 samples. Scale bar for all images is 50 mm.	90
<b>Figure 4.6</b>	Adhesion of Mouse fibroblast (L929) cells as a function of time on lyophilized scaffolds prepared using S1, S3 and S5 solutions.	91
<b>Figure 4.7</b>	MTT assay showed that fibroblasts exhibited high metabolic activity cultured on three dimensional scaffold matrices for up to 7 days	92
<b>Figure 4.8</b>	a) Confocal images of DAPI and Nile red stained L929 fibroblast cells and scaffold matrices. (b) Adherent cell morphology on scaffolds 48 h post seeding and fixing with 2.5 % glutaraldehyde using Fluid® Cell Imaging System with fixed 20X Plan Fluorite objective having Image resolution – 1296 x 964 pixels. Scale bar for all images is 100 mm.	93
<b>Figure 5a.1</b>	(a) $^1\text{H}$ spectrum of SF in $\text{D}_2\text{O}$ obtained on a 700 MHz spectrometer at 298K. (b) $^1\text{H}$ - $^{15}\text{N}$ TROSY (transverse relaxation optimized spectroscopy) spectrum in $\text{H}_2\text{O}$ at 278K (left) and $^1\text{H}$ - $^{13}\text{C}$ HSQC spectrum in $\text{D}_2\text{O}$ at 298K (right) of SF. The tyrosine correlations are shown in the inset. In the multiplicity edited spectrum the positive $\text{CH}_3$	105,1 06

	and CH correlations are shown in blue while the negative CH <sub>2</sub> correlations are shown in green.	
<b>Figure 5a.2</b>	Small angle neutron scattering from 3% w/v pure silk fibroin in D <sub>2</sub> O. Inset depicts Guinier analysis of the initial data points.	106
<b>Figure 5a.3</b>	<sup>1</sup> H NMR spectra of LSL (green), ASL (red) and SLOA (blue) obtained on a 700 MHz spectrometer at 298 K. Signal assignments are indicated for LSL and ASL, with residual solvent signal marked by asterisks.	108
<b>Figure 5a.4</b>	Overlay of HSQC spectrum (red) showing single bond C-H correlations and HMBC spectrum (blue) showing long range C-H correlations in ASL and LSL at 298K.	109
<b>Figure 5a.5</b>	Parts of the multiplicity edited <sup>1</sup> H- <sup>13</sup> C HSQC spectra showing the sugar region (left) and aliphatic region (right). The positive "CH <sub>3</sub> " and "CH" group correlations are shown in blue while the negative "CH <sub>2</sub> " group correlations are shown in green. Spectra of Oleic acid derived SL from <i>Candida bombicola</i> (SLOA), column purified diacetylated lactonic SL (LSL) and non-acetylated acidic SL (ASL) are shown in separate panels.	110
<b>Figure 5a.6</b>	SANS on individual sophorolipids, namely mixed SL, acidic SL, lactonic SL at pH 8.0±0.2	111
<b>Figure 5a.7</b>	<sup>1</sup> H NMR spectra of a saturated solution of LSL (below), and solution of MSL with LSL:ASL ratio 1:3 (above) recorded on a 700 MHz spectrometer at 298 K with 128 scans. LSL spectrum is shown with 16 times magnification since signals were very weak due to poor solubility. The sharp signals in the LSL spectrum are from residual impurities.	113
<b>Figure 5a.8</b>	<sup>1</sup> H spectrum of ASL and LSL mixture in D <sub>2</sub> O obtained on a 700 MHz spectrometer at 298 K. The H <sub>2</sub> signals of ASL and LSL show a ratio of 3:1 for the two components in solution. The presence of signature corresponding to LSL molecule in the mixed solution of ASL and LSL confirms its enhanced solubility in the presence of acidic SL.	113
<b>Figure 5a.9</b>	Temperature dependence of the diffusion coefficients of ASL (red) and LSL (green) in a mixture of ASL and LSL forms in 3:1 molar ratio in D <sub>2</sub> O.	114

<b>Figure 5a.10</b>	NOESY spectrum of a mixture of ASL and LSL forms in 3:1 molar ratio in D <sub>2</sub> O obtained on a 700 MHz spectrometer at 298K. The mixing time employed was 800 ms. The cross peaks between ASL and LSL forms are indicated by asterisks.	115
<b>Figure 5a.11</b>	Diagrammatic representation of different SL systems in solution.	116
<b>Figure 5a.12</b>	Rheological time sweep experiment (a) (Filled symbols – G' ; Unfilled symbols - G'') and molecular gelation studies using <sup>1</sup> H NMR (b) on pure SF, SF+ASL, SF+LSL and SF+MSL systems	117
<b>Figure 5a.13</b>	SANS data and model fits for SF+LSL/ASL/MSL systems at pH 8.0 ± 0.2.	119
<b>Figure 5a.14</b>	SANS data of ASL, SF, SF+ASL. Experimental data of SF+ASL solution depict features of both SF and ASL.	120
<b>Figure 5a.15</b>	Schematic representation of SF-SL gelation mechanism, with individual SF chains shown in different colors.	121
<b>Figure 5a.16</b>	(a) HSQC spectra showing the aliphatic region upon successive addition of SF to MSL solution (b) Overlay of the HSQC spectra of a 3:1 mixture of ASL and LSL in the absence (blue) and presence (red) of SF. The well separated signals of LSL which are indicated in boxes are absent on addition of SF.	123
<b>Figure 5b.1</b>	Overlay of the HSQC spectra of MSL at pH 6 (blue) and pH 8 (red). The signal from the methylene group indicated in the structure is marked by a square in the spectrum.	130
<b>Figure 5b.2</b>	Proton spectra of (a) ASL and (b) MSL in D <sub>2</sub> O at pH 6 and 8. The signals marked by asterisks are from solvent, acetone (~1.8 ppm) and acetic acid (~ 2.2 ppm).	131
<b>Figure 5b.3</b>	Diffusion decay curve of ASL (in D <sub>2</sub> O) at pH 6.0 (blue) and 8.0 (red).	131
<b>Figure 5b.4</b>	SANS scattering data of ASL in D <sub>2</sub> O at pH 6.0 and 8.0.	132
<b>Figure 5b.5</b>	Rheological time sweep experiment on (a) MSL+SF and (b) ASL+SF in H <sub>2</sub> O at pH 6.0 and 8.0 (Filled symbols – G'; Unfilled symbols – G'').	133
<b>Figure 5b.6</b>	Gelation kinetics of MSL+SF (circles) and ASL+SF (squares) in D <sub>2</sub> O at	134

	pH 6 (blue) and 8 (red) monitored by NMR.	
<b>Figure 5b.7</b>	Comparison of difference in gelation time of SF+ASL samples prepared in D <sub>2</sub> O (filled circle) and H <sub>2</sub> O (empty circle) at pH 8.	135
<b>Figure 5b.8</b>	SANS scattering data of SF+ASL (in D <sub>2</sub> O) depicting as measured and summed up scattering from SF and ASL individually (a) at pH 6 (b) at pH 8. SF+ASL scattering data (c) in sol state (initial ~6h), (d) in gelled state.	136
<b>Figure 5b.9</b>	Schematic representation of SF-ASL interaction according to the bead necklace model.	137
<b>Figure 5b.10</b>	Fluorescence spectroscopy graph depicting I <sub>1</sub> /I <sub>3</sub> intensity ratio of pyrene (a) in different environments (comprising of components under study), (b) SF+SL system at different pH. Fluorescence emission data depicting the I <sub>1</sub> /I <sub>3</sub> intensity ratio of pyrene in (a) solutions of individual components and (b) solution of SF+MSL.	139,1 40
<b>Figure 5b.11</b>	(a) Variation of the diffusion coefficient (D) of ASL with time during gel formation in ASL+SF. (b) Gel formation kinetics in ASL+SF at pH 6. The time axis shift of the inflection in the two plots is highlighted.	141
<b>Figure 1a</b>	SEM images of SLCA solutions at different concentration before and after.	147
<b>Figure 2a</b>	SEM images of electrospun silk fibroin after different treatments.	149
<b>Figure 2b</b>	FTIR spectrum of electrospun SF fibers with acidic sophorolipids	150
<b>Figure 2c</b>	FTIR spectrum of electrospun SF fibers with mixed sophorolipids.	150
<b>Figure 2d</b>	MTT assay showing proliferation of L929 fibroblast cells in silk fibroin electrospun fibers subjected to different treatments	151
<b>Figure 2e</b>	MTT assay showing cytotoxicity studies on human lung cancer A549 cells in silk fibroin electrospun fibers subjected to different treatments.	151
<b>Scheme 5a.1</b>	Representation of acidic and lactonic SL molecules with labeling of atoms.	107

## List of Tables

<b>Table 1.1</b>	Classification of glycolipid biosurfactants.	3
<b>Table 2.1</b>	Media composition for sophorolipid production	29
<b>Table 2.2</b>	Emulsification activity of SLCA and other chemical surfactants.	36
<b>Table 2.3</b>	Comparison of minimum surface tension and CMC of different surfactants.	37
<b>Table 2.4</b>	Different forms of SLCA synthesized by <i>Candida bombicola</i> when supplemented with cetyl alcohol and glucose	46
<b>Table 2.5</b>	Comparative MIC <sub>100</sub> values of three different sophorolipids, SLCA <sup>a</sup> sophorolipid of cetyl alcohol, SLLA <sup>b</sup> -sophorolipid of lauryl alcohol, OASL <sup>c</sup> -oleic acid derived sophorolipid for Gram-positive and Gram-negative bacteria respectively.	51
<b>Table 3.1</b>	Growth Inhibition (GI): GI <sub>50</sub> /GI <sub>90</sub> in µg/ml values of Sophorolipids on different cell lines derived from MTT assay	63
<b>Table 5a.1</b>	The fitted parameters of the sophorolipid systems	111
<b>Table 5a.2</b>	The fitted parameters of SF+SL systems.	119
<b>Table 5b.1</b>	Fitted parameters for SANS data of ASL at different pH.	132
<b>Table 5b.2</b>	Fitted parameters of SF+ASL system at different pH.	137

## Abbreviations

A431	Human squamous carcinoma cell line
A549	Human lung carcinoma cell line
ASL	Acidic sphorolipid
ATR	Attenuated total reflectance
<i>C. bombicola</i>	<i>Candida bombicola</i>
CD <sub>3</sub> OD	Deuterated methanol
CdTe	Cadmium telluride
CHO KI cell line	Chinese Hamster ovary cell line
CMC	Critical micelle concentration
COSY	Correlation spectroscopy
DAPI	4',6-diamidino-2-phenylindole
DMEM	Dulbecco's Modified Eagle Medium
DMSO	Dimethyl Sulfoxide
DNA	Deoxyribonucleic acid
EMEM	Eagle's Minimum Essential Medium
E <sub>24</sub>	Emulsification index at 24 hours
<i>E. coli</i>	<i>Escherichia coli</i>
FBS	Fetal bovine serum
FITC	Fluorescein Isothiocyanate
FTIR	Fourier Transform Infrared Spectroscopy
GI	Growth inhibitory value
HCT 116	Human Colon carcinoma cell line
HCS	High Content Screening
HepG2	Human hepatocellular carcinoma cell line
HeLa	Human cervical carcinoma cell line
HUVEC	Primary Human umbilical vein endothelial cells
H7402	Human liver carcinoma cell line

HFIP	Hexafluoroisopropanol
HMBC	Heteronuclear multiple bond correlation
HSQC	Heteronuclear single quantum coherence spectroscopy
HR-MS	High Resolution Mass Spectroscopy
HPLC	High Performance Liquid Chromatography
KBr	Potassium Bromide
KYSE109, KYSE450	Human esophageal carcinoma cell lines
L929	Mouse fibroblast cell line
LC-MS	Liquid chromatography Mass Spectroscopy
LiBr	Lithium Bromide
LB	Luria Bertani
LSL	Lactonic sophorolipid
LSCM	Laser Scanning Confocal Microscope
LVES	Large vessel endothelial supplement
MALDI-TOF MS	Matrix assisted laser desorption/ionization-time of flight mass spectrometry
MCF-7	Human breast carcinoma cell line
MGYP	Malt Glucose Yeast Peptone
MMP	Mitochondrial Membrane Potential
MSL	Mixed sophorolipid
MIC	Minimum Inhibitory Concentration
MTT	3-(4,5-dimethylthiazol-2-yl)-2,5-diphenyltetrazolium bromide
NADPH	Nicotinamide Adenine Dinucleotide Phosphate
NCIM	National Collection of Industrial Microorganism
NaHCO <sub>3</sub>	Sodium bicarbonate
NMR	Nuclear Magnetic Resonance
NOESY	Nuclear Overhauser effect spectroscopy
PFGSE	Pulsed field gradient spin echo
PS	Phosphatidyl serine

PI	Propidium iodide
PANC-1	Human pancreatic carcinoma cell line
ROESY	Rotating frame Overhauser effect spectroscopy
RSF	Regenerated silk fibroin
<i>S. aureus</i>	<i>Staphylococcus aureus</i>
SEM	Scanning Electron Microscope
SF	Silk fibroin
SL	Sophorolipid
SDS	Sodium dodecyl sulfate
SLOA	Sophorolipid derived from oleic acid
SLCA	Cetyl alcohol derived sophorolipid
SLLA	Lauryl alcohol derived sophorolipid
SANS	Small Angle Neutron Scattering
THP-1	Acute monocytic leukemia cell line
TOCSY	Total correlation spectroscopy
VEGF	Vascular Endothelial Growth Factor
ZnSe	Zinc Selenide

# Chapter 1

---

## Introduction

### **Biosynthesis of novel glycolipids (Sophorolipids): Exploring the mechanism of assembling and biological properties**

*“Under normal conditions the research scientist is not an innovator but a solver of puzzles, and the puzzles upon which he concentrates are just those which he believes can be both stated and solved within the existing scientific tradition”.*

*Thomas Kuhn*

The scientific work enumerated in this thesis encircles around a magical glycolipid biosurfactant molecule known as Sophorolipid (SL). The novel and conventional SLs synthesized have been studied for their biological properties and assembling behaviour. Further the work has been justified by exemplifying SLs varied applicability as a potential anti-proliferative drug and gelling agent for structural protein. Owing to reported antimicrobial and anticancer potential of SLs, in this thesis we have explored the potential of novel SLs against different cancer cell lines with a view to find effective alternative, to conventional chemotherapy, that kills cancer cells and remains ineffective against normal human cells. Gelation of structural protein using biosurfactant has been reported for first time, thus it was more intriguing to decipher the mechanism of this uncommon combination.

### **1.1 *Surfactants in general***

Surfactants by definition are surface active agents that lower surface and interfacial tension. Although surfactants vary structurally, they commonly are amphiphilic in nature that makes them soluble in both aqueous and organic solvents. This behaviour marks their participation in several sectors ranging from cosmetics, detergents, foods, concrete additives to pharmaceuticals.<sup>[1]</sup> For centuries, typically synthetic surfactants have been employed for above mentioned applications. To fulfil the enormously growing need of surfactant over past decades continuous growth in surfactant market is witnessed. Global surfactant production in 2005 was ~13 million tonnes with 3.6 % increase p.a. since 1995.<sup>[2]</sup> Synthetic or chemical based surfactants though still dominate the market but stringent regulations and sustainability issues have driven a shift in the market towards biosurfactants. Increased importance of biosurfactants is based on the fact that they are eco-friendly, less toxic and biodegradable. These properties are essentially desirable to overcome sustainability issues linked to chemical surfactants that is negatively impacting our environment.

### **1.2 *Biosurfactants***

Biosurfactants constitute a structurally diverse group of molecules that are produced by variety of microorganisms. These natural molecules being synthesized by microbial conversion rather than chemical synthesis are considered superior over their chemical counterparts.<sup>[3]</sup> In addition to usual surfactant behaviour the non-conventional properties possessed by biosurfactants such as antimicrobial, biocompatibility, low toxicity etc. widen up their applicability in varied fields. Therefore, interest in biosurfactants has progressively escalated in various fields as multifunctional materials for the new century.

### **1.3 *Types of biosurfactants***

Unlike chemical surfactants that are mainly classified based on the nature of their hydrophilic head, biosurfactants are classified based on either chemical composition or microbial origin. In general the structural backbone of biosurfactants is made of hydrophilic head that may range from amino acid or peptide to saccharides (mono, di or poly) and hydrophobic tail that is mainly saturated or unsaturated fatty acids. Major classes of biosurfactants and their microbial origin have been discussed briefly in the following section

and different glycolipids, their producing organisms and properties have been additionally tabulated in Table 1.1. Elaborate classification has been reviewed by other groups.<sup>[4,5]</sup>

**Table 1.1** Classification of glycolipid biosurfactants.

Biosurfactants		Microorganism	Surface tension	Highest Yield	Economic Applications	Reference
Group	Class					
Glycolipids	Rhamnolipids	<i>Pseudomonas aeruginosa</i> , <i>Pseudomonas sp.</i> <i>Burkholderia sp.</i>	25-30 mN/m	>100 g/L	Remove metals from soil, disperse and degrade hydrocarbons, emulsify oils, antimicrobial	[6-8]
	Trehalose lipids	<i>Nocardia sp.</i> <i>Rhodococcus sp.</i> <i>Mycobacterium sp.</i> <i>Arthrobacter sp.</i>	30-36 mN/m	Up to 40 g/L	Hydrocarbon bioremediation, microbial enhanced oil recovery, additives in different industry	[9-12]
	Cellobiose lipids	<i>Ustilago sp.</i> <i>Pseudozyma sp</i>	37 mN/m	~23 g/L	Fungicidal	[13-16]
	Mannosyl erythritol lipids	<i>Candida antarctica</i> , <i>Ustilago sp.</i> <i>Pseudozyma sp.</i> <i>Kurtzmanomyces sp.</i>	30-33 mN/m	Up to 100 g/L	Used in detergents, Oil-in-water emulsions. Possess antimicrobial and immunological properties	[15,17-20]
	Sophorolipids	<i>Starmerella bombicola</i> , <i>Wickerhamiella domercqiae</i> , <i>Candida batistae</i> , <i>Rhodotorula Bogoriensis</i> , <i>Candida apicola</i> .	25-33 mN/m	<b>400 g/L</b>	Cosmetics, cleaning agents, germicidal formulations, nanomaterial synthesis, bioremediation, oil recovery, adjuvants, therapeutic agents – antimicrobial, anticancerous, antiviral etc.	[21-28]

- **Glycolipids:** As the name suggests these biosurfactants comprise of a carbohydrate group linked to a fatty acid by an ester group. Glycolipids form the major class of biosurfactants. The best known glycolipids are rhamnolipids, trehalose lipids, cellobiose lipids, mannosylerythritol lipids and sophorolipids.<sup>[29]</sup> The structure, properties and major producing organisms of these glycolipids are mention below:

- **Rhamnolipids:** Rhamnolipids structurally comprise of rhamnose sugar linked to hydroxydecanoic acid. It is bacterial surfactant synthesized by *Pseudomonas aeruginosa* species.<sup>[6]</sup> Rhamnolipids have shown to possess potential in removing oil from marine/sand and also in fighting phytopathogens. Rhamnolipids are also utilized for industrial L-rhamnose production for the purpose of high-quality flavour components.
- **Trehalose lipids:** Trehalose lipids comprise of non-reducing disaccharide trehalose as the hydrophilic moiety and diverse hydrophobic groups. These are mainly isolated from *Nocardia* and *Mycobacteri*.<sup>[29]</sup> The low productivity limits the practical use of this biosurfactant.
- **Cellobiose lipids:** Cellobiose lipids are mainly produced by *Ustilago species* and possess fungicide properties applicable in agriculture and medicine.<sup>[29]</sup> Structurally these biosurfactants are made up of disaccharide sugar, cellobiose, which is glycosidically linked to unusual long-chain fatty acid.
- **Mannosylerythritol lipids (MEL):** MELs are isolated from yeast *Pseudomonas* and *Ustilago* species. Structurally they comprise of 4-O-β-D mannopyranosyl-meso-erythritol as hydrophilic head and fatty acid tail. MELs tend to self assemble and thus display antimicrobial and gene delivery properties.<sup>[20]</sup>
- **Sophorolipids:** Sophorolipids in comparison to other glycolipids have gained wide recognition in past few decades owing to their biodegradability and low eco-toxicity. They are regarded as most promising biosurfactants as they are synthesized in large quantities by non -pathogenic yeasts (refer Table 1.1). Sophorolipids comprise of a disaccharide head group known as sophorose that is glycosidically linked to fatty acid tail.<sup>[30,31]</sup> As this work is primarily based on sophorolipids they are further described in detail later in this chapter.

Apart from glycolipids, other groups of biosurfactants are mentioned below.

- **Lipopeptides and oligopeptides:** This class of biosurfactants are mostly produced by bacteria, often into cyclic structures. Lipopeptide such as Surfactin from *Bacillus subtilis* is commonly used as antibiotic and possesses exceptional surfactant properties.<sup>[32]</sup> Other lipopeptides with antimicrobial and haemolytic properties include, daptomycin, mycosubtilin.<sup>[33,34]</sup>

- **Fatty acids, Neutral lipids and Phospholipid:** These biosurfactants are produced by *Corynebacterium lepus*, *Nocardia erythropolis* and *Thiobacillus thiooxidans* respectively when grown on n-alkanes.<sup>[11,35,36]</sup> They are considered essential for biomedical applications.
- **Polymeric Biosurfactants:** This class of surfactants are generally high-molecular weight biopolymers that possess properties such as high tensile strength, shear resistance, and high viscosity. Thus, they find application in cosmetic, pharmaceutical and food industry. Examples include, emulsan, biodispersan synthesized by *Acinetobacter calcoaceticus*<sup>[37,38]</sup> and liposan an extracellular emulsifier is synthesized by *Candida lipolytica*.<sup>[39]</sup>
- **Particulate Biosurfactants:** Whole microbial cell and extracellular vesicles form this group of surfactants. Certain *Cyanobacteria* species and hydrocarbon degrading microorganisms display affinity for air-water and hydrocarbon-water interfaces and thus themselves act as surfactants.<sup>[40]</sup> Certain *Pseudomonas* sp. and *Acinetobacter* sp. when grown on alkane form vesicles that act as surfactants.<sup>[40]</sup>

#### 1.4 Sophorolipids

Sophorolipids, as first described in 1961 by Gorin et al.,<sup>[41]</sup> are produced by various yeast species, among which *Candida bombicola* is studied most extensively. Among other class of glycolipid biosurfactants sophorolipids are regarded as most propitious as they are produced in high amounts by non-pathogenic yeasts, percentage of substrate conversion is high and the product can be recovered easily.<sup>[42-44]</sup> Sophorolipids, further abbreviated as “SL,” display remarkable surface activity and skin compatibility, thus suit well for personal care and cosmetic applications. In addition to surfactant properties such as dispersibility, emulsification, SLs additionally display several beneficial biological properties such as anti-microbial, anti-viral etc. and have been approved by Food and Drug Administration (FDA). The allowable intake limit is 5mg/mL.<sup>[45]</sup> This makes sophorolipids attractive for various commercial applications.

**1.4.1 Sophorolipid structure:** Sophorolipids are synthesized *de novo* by certain yeast species in low amount but when these yeast species are externally supplemented with glucose as a hydrophilic carbon source and fatty acid as lipophilic feed, the synthesized

amount of sophorolipids are fairly high. Thus, structurally SLs are composed of a polar disaccharide head group with an unusual  $\beta$  1-2 glycosidic linkage known as sophorose that is linked to the  $\omega$  or  $\omega$ -1 carbon of the hydrophobic fatty acid tail.<sup>[46]</sup> SLs are extracellularly produced by the yeast as a mixture that comprises of two forms: acidic and lactonic form (depicted in Figure 1.1). When the carboxylic end of the fatty acid tail remains free it is known as the acidic SL (ASL) whereas internal esterification of this carboxylic group to 4' OH of the sugar results in a closed ring structure i.e. lactonic SL (LSL).<sup>[46]</sup> The percentage of each form in the mixture entirely depends upon the duration for which SL production is carried out. Prolonged incubation results in higher conversion of ASL to LSL, thus leading to a predominance of lactonic SL in the mixture. Further variation in the SL structure occurs by acetylation of the sugars at 6' and/or 6'' positions, resulting into mixture of several forms. The physical appearance of end product depends upon the ratio of acidic and lactonic SL. Higher percentage of acidic SL results in brown viscous product, while larger production of LSL especially diacetylated form yields crystalline product.

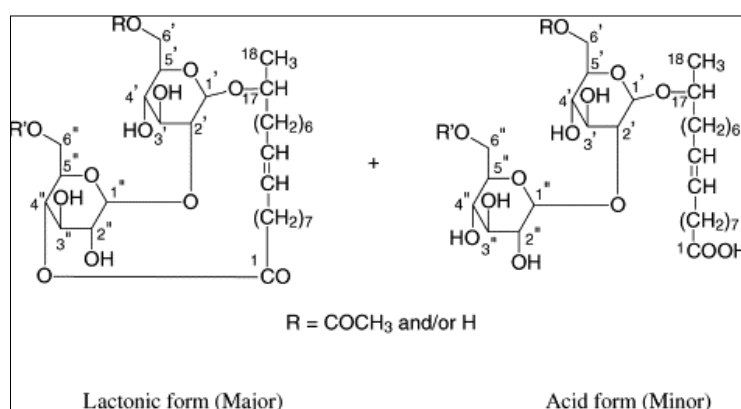


**Figure 1.1** Two major forms of Sophorolipids produced by yeasts as a mixture-lactonic and acidic.<sup>[47]</sup>

**1.4.2 Producing organisms:** As mentioned in section 1.4, first report in 1961 described synthesis of an extracellular glycolipid by *Torulopsis magnolia*.<sup>[41]</sup> Later in 1968 the yeast was correctly identified as *Torulopsis apicola*, now known as *Candida apicola*. With growing interest in alkane utilizing ability of the yeast, new strains were identified down the year that included *Candida bogoriensis* (*Rhodotorula bogoriensis*),<sup>[48]</sup> *Candida bombicola* (initially known as *Torulopsis bombicola*).<sup>[49]</sup> With increasing popularity of sophorolipid as potential biosurfactants after more than a decade, novel SL producing yeast species, teleomorph of

*Candida bombicola*, *Starmerella bombicola* was introduced. Recently, a new strain of *Wickerhamiella domericqiae* was reported to synthesize sophorolipid.<sup>[50]</sup>

**1.4.3 Physiological role of Sophorolipids:** Sophorolipids are synthesized by the yeast for following speculated physiological reasons: (1) in order to utilize and store the excess lipophilic substrate available in the environment,<sup>[51]</sup> (2) as SL producers are isolated from high osmotic strength environment, it may be their way of tackling the high sugar concentration by sequestering it in SL molecule and hence making it less available for other microorganisms.<sup>[52]</sup> Thus, SL production (specifically lactonic form that is more biologically active) may be considered as a defence strategy against competitive microorganisms. Ito et al. in 1980 demonstrated that hydroxyl fatty acid glycoside (identified as lactonic acid, 17-hydroxy octadecanoic acid) produced by *Torulopsis bombicola* significantly inhibited the growth yeasts such as *Pichia*, *Candida*, *Lodderomyces*, *Saccharomycopsis* and *Debaryomyces* that primarily utilize n-alkanes.<sup>[53]</sup>

**1.4.4 SL Biosynthetic pathway and substrates used for production:** Sophorolipids were first recognized by alkane utilizing ability of the yeasts. Certain yeasts, as described in section 1.4.2, are known to synthesize SLs *de novo*. Thus, these microorganisms possess necessary enzymes to process alkane and metabolize it for sequestering into SL molecules. The biosynthetic pathway adapted from Van Bogaert et al., 2007 is represented in Figure 1.2.<sup>[21]</sup> As can be seen after the processing of alkane to fatty acid, enzymatic process initiates by the action of NADPH dependent cytochrome P450 monooxygenase enzyme that converts fatty acid into  $\omega$  or  $\omega-1$  hydroxy fatty acid. In subsequent step to the hydroxylated fatty acid first glucose moiety is added at C1' position by glucosyltransferase I. In third step, second glucose moiety is coupled to the first glucose molecule at C2' position by the glucosyltransferase II and thus acidic sophorolipid is formed. Subsequently, by the action of lactone esterase, lactonic SL is formed by additional internal esterification step between carboxyl group of fatty acid and 4''OH group of the sophorose. Further, the action of acetyl-coenzyme A (CoA) dependent acetyl transferase acetylates the sugar at 6' and/or 6'' position.

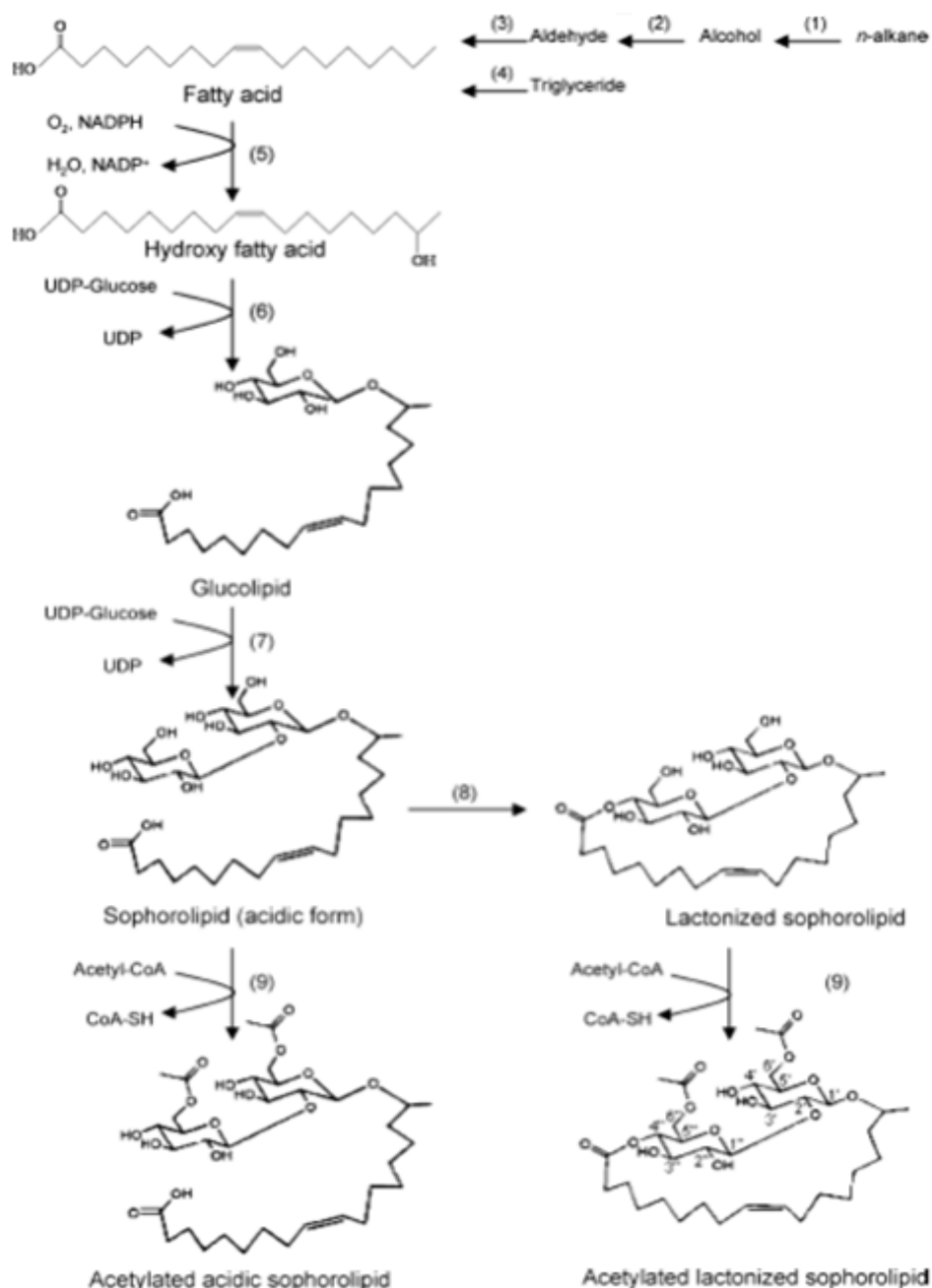


**Figure 1.2** Sophorolipid biosynthesis pathway adapted from Bogaert et al. (2007). Different enzymes carrying out the biochemical reactions are as follows: (1) cytochrome P450 monooxygenase, (2) alcohol dehydrogenase, (3) aldehyde dehydrogenase (4) lipase, (5) cytochrome P450 monooxygenase, (6) glucosyltransferase I, (7) glucosyltransferase II, (8) lactone esterase, (9) acetyl transferase.<sup>[21]</sup>

Sophorolipids have an additional advantage of being tailor made i.e., by varying the lipophilic carbon source, different SLs varying in physiochemical properties can be synthesized according to the need and applications. Apart from fatty acids, as we can see in Figure 1.2 other substrates such as alkane, alcohol, aldehyde and triglycerides can be used

for SL production as yeasts also contains necessary enzymatic machinery for their conversion into fatty acid. With this view, many researchers have synthesized sophorolipids by using different substrates such as alkanes,<sup>[54]</sup> saturated fatty acids,<sup>[55,56]</sup> unsaturated fatty acids,<sup>[57]</sup> oils<sup>[21]</sup> and fatty alcohol<sup>[27]</sup> etc. Whichever substrate is used, the basic SL structure remains the same. The hydrophilic head group and lipophilic fatty tail makes SLs amphiphilic in nature. Thus, sophorolipids display certain typical properties which are mentioned in following section.

**1.5 Self assembly in Sophorolipids:** The unique property of the molecules to form an organised arrangement driven by interaction among themselves is termed as self assembly that occurs above a certain concentration termed as critical aggregation concentration.<sup>[58]</sup> Acidic sophorolipid being an asymmetrical bolaamphiphile is structurally unique, hence is expected to self assembly in different molecular forms under various conditions.<sup>[59]</sup> Figure 1.3 depicts the different molecular assemblies adopted by ASL.

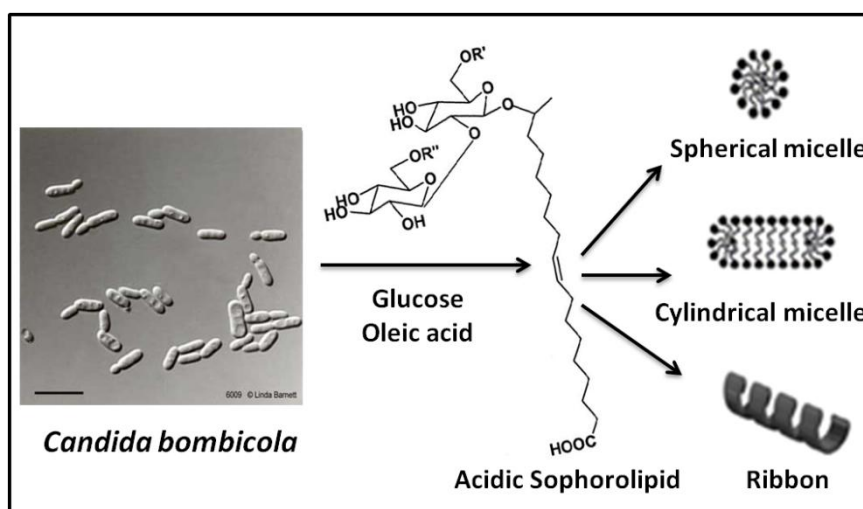


**Figure 1.3** Acidic sophorolipid self assembles into various forms such as giant ribbons, spherical micelles and cylindrical micelles under different conditions.<sup>[58]</sup>

Among the two major forms of sophorolipid, acidic SL has been extensively studied for its solution self assembling properties, as it is completely soluble in water and possess unique structural features that include asymmetrical polar groups (disaccharide head vs carboxylic end group), a kinked hydrophobic core (cis- 9-octadecanoic chain) and a non-amide polar-nonpolar linkage.<sup>[59]</sup> In contrast the closed ring structure of lactonic SL makes it

comparatively more hydrophobic than ASL and results into its poor water solubility. Thus, not many reports on self assembly of LSL are available in literature.

Several factors are known to influence the self assembling property of different molecules including acidic SL, such as pH, concentration, molecular structure etc. that have been discussed below.<sup>[58]</sup>

### **1.5.1 pH driven assembly in acidic sophorolipids**

First study conducted on ASL's assembling behavior reported formation of giant twisted and helical ribbons of 5-11 $\mu$ m width and several hundreds of micrometers length, in acidic conditions (pH 2.0 to 4.1)<sup>[59]</sup> Though the significance of pH was not emphasized in the study but the authors proposed that packing of acidic SL molecules was stabilized by strong hydrophobic association between the cis-9-octadecanoic chain and strong disaccharide-disaccharide hydrogen bonding. Later the effect of pH on the free carboxylic group of acidic SL and thus its assembling property was investigated. Interestingly the pH dependent behaviour of acidic SL emphasized on its potential use as stimuli-responsive molecule.<sup>[60]</sup> Based on the small-angle neutron scattering (SANS) study's authors reported that in three different pH regimes i.e. pH<5 to 5<pH<8 and pH>8 the micellar nature of acidic SL varied from neutral micelles to charged micelles and to large netlike aggregates respectively. This molecular evolution in shape, aggregation state and surface properties resulted from the increase in degree of ionization of the carboxylic end group that introduced negative charge at the micellar surface. Such a behaviour indicated that sophorolipids constitute a versatile micellar system driven by pH, thus they could be tuned for a number of applications in nanoscience and related fields. Similar reports presented pH dependent behaviour of rhamnolipids with their morphology in the pH range between 4.5 to 7.0 changing from vesicles to micelles.<sup>[61]</sup>

### **1.5.2 Changing morphology with concentration**

As mentioned previously the self assembly of molecules is strongly governed by number hence concentration of molecules in solution. The effect of acidic sophorolipid concentration on evolution in its assembled structures was clearly evident from SANS study. SANS being an extremely powerful technique to study shape, size, volumes and specific area of surfactant derived micelle revealed that spherical SL micelles of 3.0 nm average size exist

in solution for sophorolipid concentration  $<1$  wt%.<sup>[62]</sup> While with increasing concentration from  $> 0.5$  wt% to 5 wt% the spherical assemblies elongate into cylindrical micelles. These findings were in good correlation with other reports on alkyl polyglucoside (APG) surfactants which also tend to orient in spherical and cylindrical assemblies based on their concentration, head-to tail geometry and presence of a co-solvent.<sup>[63,64]</sup>

The packing constraints due to closed ring structure of lactonic SLs results in formation of small unilamellar vesicles at low surfactant concentrations (0.2 to 3mM) that evolve via a large unilamellar vesicle structure at 7 mM to a disordered dilute phase of tubules at higher concentrations (10 to 30 mM).

### ***1.5.3 Role of molecular structure in self assembly of acidic sophorolipids***

Apart from factors like pH and concentration, the changes in structure at the molecular level can also influence the self assembling behaviour of sophorolipids. This was evidently exemplified by using three different sophorolipids of oleic acid (OASL), stearic acid (SASL) and eladic acid (EASL).<sup>[65]</sup> The OASL formed ribbon like structure similar to those reported by Zhou et al.,<sup>[59]</sup> whereas in the case of SASL (saturated analogue of oleic acid) the self assembled structures appeared like several open sheets lying on top of each other. For EASL (with a trans double bond) authors reported formation of twisted ribbon structures, which was attributed to a favourable  $\pi$  overlap, leading to squeeze in the middle of the molecule. This resulted into higher stearic repulsion of the sophorose moieties, ensuing a twist and leading to the helicity.

The effect of unsaturation was clearly evident from study conducted by Dhasaiyan et al. (2014). With the help of experimental and simulation studies the author reported that the presence of double bond in the hydrophobic core of the SL molecule greatly impacts the morphology of the self assembled structures. They showed that oleic acid SL with one unsaturated bond forms ribbon like structures (also reported previously), whereas linolenic acid SL with three double bonds assembles into vesicles.<sup>[66]</sup> Supporting this recently Pandey et al. (2016) also performed simulation studies and reported that linolenic acid sophorolipid with three double bonds, assembled into vesicle and aggregates depending upon SL to water ratio. Lately, Cuvier et al. reported that the saturated version of non-acetylated acidic sophorolipid (18:0) at neutral pH in water yield monodisperse ( $13.5 \pm 1.5$  nm) twisted ribbons. Additionally the quality of fibre dispersion could be improved by a simple additional

step of dialysis that removes residual salt responsible for aggregation of ribbons into bundles.<sup>[67]</sup> The impact of molecular structure on self assembling behavior of sophorolipids nullifies when subject to pH above 10. Cuvier et al. (2015) demonstrated that both oleic acid SL (unsaturated) and stearic acid SL (saturated) self assemble into platelets of nanoscale length at basic pH. The force responsible for the assembling nature at this pH was reported to be electrostatic repulsion between  $\text{COO}^-$  groups in contrast to hydrogen bonding and weak van der Waals forces that essentially drive self assembly at pH near neutrality.<sup>[68]</sup>

#### **1.5.4 Enhanced sophorolipid assembly by external forces**

With time and ongoing research the potential applications of sophorolipids and other biosurfactants has been realized, thus giving a new dimension to their applicability in varied developing fields. In agreement to it lately, Singh et al. (2013) reported highly spherical mesoscale molecular self assembly of sophorolipid created by pulsed UV laser (248 nm), which were remarkably biocompatible and had strong green fluorescence.<sup>[69]</sup> They reported that fluorescence character appeared to be driven by oleic component whereas assembly process was assisted by glucose component. Further they successfully loaded the mesostructures with magnetic nanoparticles, for inducing hyperthermic effect.

### **1.6 Sophorolipids in multiple areas**

Even though SLs belong to surfactant class of molecules yet they possess several additional properties due to which they find application in numerous fields. Such different areas that utilize SL have been discussed below.

#### **1.6.1 Sophorolipids in cosmetics**

Sophorolipids properties such as moisturizing, antioxidant, antimicrobial and skin compatibility makes it highly preferred biosurfactants for cosmetic applications.<sup>[70]</sup> SLs synthesized from *Candida bombicola* have been reported to possess excellent wetting, foaming, emulsifying properties, additionally SLs ability to stimulate dermal fibroblasts and collagen neosynthesis<sup>[71]</sup> has been exploited in acne treatment, skin smoothing and anti-wrinkle products.<sup>[72,73]</sup> Soliance French based company (<http://www.groupe-soliance.com>) excels in innovative cosmetic products with ingredients derived from green sources for sustainable development. Sopholiance S, is a sophorolipid based product with hydrophilic

head from wheat and non-polar tail from rapeseed oil. It has been designed by Soliance with an objective to fight the root cause of body odours and acne i.e. microorganisms. Sophorolipids being antimicrobial biosurfactants serve the purpose and product can thus be used as deodorants and to cure acne.<sup>[74]</sup>

### **1.6.2 Sophorolipids as cleaning agents**

Low eco-toxicity, biodegradability and production from renewable feedstock make sophorolipid a potential surfactant that overcomes the drawbacks imposed by its chemical counterparts to the environment. With this view there has been a growing demand of sophorolipid in detergent industry to replace and reduce the chemical load flushed in the environment upon usage of chemical surfactants. Major share of the surfactant production worldwide gets consumed for cleaning applications.

Sophorolipids among other glycolipid is preferred biosurfactants for cleaning purpose as it is antimicrobial wash active, emulsifier and low-high foaming surfactant. Japan-based company Saraya has commercialised “Sophoron”, a sophorolipid based low-foam dishwasher detergent. “Sophogreen” first bio-solubilizer has been recently designed by Soliance using sophorolipids that serves as a better alternative to petroleum based solubilizers. Other companies such as, Belgian-based Ecover (<http://www.ecover.com>) and South Korea-based MG Intobio also commercialize products made using Sophorolipids. The skin irritability test (Episkin test) conducted by Ecover on SL based product confirmed that SL does not causes skin irritation. Toxicity and biodegradability test conducted on Ecover product SL18 revealed that SL based product was in orders of magnitude less toxic than non-ionic surfactants, alkyl polyglucosides (APG) and 100% biodegradable after 28 days. Sophorolipids mild nature, low aquatic toxicity and considerable surface activity has resulted in launching of SL based products by Ecover such as all-purpose cleaner, window cleaner, floor soap and wax cleaner.<sup>[75]</sup> Germany based Henkel has also been employing sophorolipid for its glass cleaning products such as Sidolin, Tenn, Instanet and Sonasol. A study conducted by Navare et al. (2013) also demonstrated that SL synthesized using jatropha oil, to curtail the production cost by using cheap sources, had potential to be used as a fabric cleaner.<sup>[76]</sup>

### **1.6.3 Sophorolipids as germicide in vegetable and fruit wash**

Owing to their antimicrobial properties SLs also find application in germicidal solutions designed for cleaning fruits and vegetables.<sup>[77]</sup> Pulate et al. (2014) formulated a germicidal composition using fatty alcohol sophorolipid. The SL formulated wash was effective for cleaning fruits and vegetables such as sapodilla, tomato, lemon and cucumber and it additionally increased their shelf life. The formulation was found to be effective in reducing the growth of Gram-negative bacteria affecting agricultural yield such as *Erwinia chrysanthemi*, *Escherichia coli*, *Salmonella typhimurium* and *Xanthomonas campestris*.<sup>[78]</sup>

### **1.6.4 Sophorolipids in theranostic application**

Quantum dots (QDs) known for their optical and electronic properties applicable in biomedical field as labelling and imaging tools, face restrictions due to their toxicity and biocompatibility issues. To introduce biocompatibility, without the loss of photoluminescence property Singh et al. (2013) synthesized non-toxic cadmium telluride (CdTe) QDs by using acidic SL as surface-functionalising agent. SL-CdTe QDs potential as a diagnostic tool was demonstrated by cellular internalization studies in ThP-1 (human acute monocytic leukemia) cells. The cytotoxicity studies confirmed their biocompatibility and hence applicability.<sup>[79]</sup>

### **1.6.5 Environmental applications of Sophorolipids**

Certain natural oil-degrading bacteria consume hydrophobic substrates and help in oil biodegradation in soil/seawater. The effectiveness of these bacteria can be enhanced by biosurfactants support as it could help in emulsification, adhesion/de-adhesion of bacteria to and from hydrocarbons, micellisation and contaminant desorption.<sup>[80]</sup> A study revealed that presence of sophorolipid increased micellar dispersion of hydrocarbons and had positive effects on biodegradative role of natural oil-degrading bacteria.<sup>[81]</sup> Similarly, bioremediation of lubricating oil contaminated soils using sophorolipids has been successfully demonstrated. SLs high emulsification index in oil such as toluene and n-heptane confirmed their potential applicability.<sup>[82]</sup>

Apart from this, SLs can be individually employed to remove heavy metal contaminants from soil. A study postulated that removal of heavy metal contaminants such as copper and zinc from sediments using sophorolipid/rhamnolipid/surfactin was due to surfactant sorption on

the soil surface followed by metal complexation resulting into detachment of metal from soil. The detached metal associates with the surfactant micelle and is removed from the sediments.<sup>[83]</sup> Not only this but successful utilization of metal (nickel) contaminated oil waste for sophorolipid production is encouraging to remediate these wastes for their safe removal and recovery. The obtained SL product with significantly low nickel level could be used for industrial cleaning applications.<sup>[55]</sup> Apart from oil spills and heavy metal contaminants, another threat to environment is harmful algal blooms (HAB). To combat HAB SLs have proved to possess remarkable algicidal activity against four common HAB species, *Heterosigma akashiwo*, *Prorocentrum minimum*, *Cochlodinium polykrikoides* and *Scirpsiella trochoidea*.<sup>[84]</sup>

#### **1.6.6 Sophorolipids as adjuvants**

To increase the efficacy and biological activity of pesticides used for crop protection adjuvants are generally added to the formulations. Use of lactonic sophorolipid as an adjuvant for pesticide preparation in form of tank mix additive showed that pesticides activity was increased by 10%.<sup>[85]</sup>

#### **1.6.7 Sophorolipids in nanomaterial synthesis**

The amphiphilic nature of SLs has made a special space for them in nanotechnology. Initially SLs were used as capping agent (as an alternative of oleic acid) for synthesis of polydisperse water-soluble nanoparticles such as cobalt.<sup>[86]</sup> Later the utilization of sophorolipid eliminated the necessity for exogenous reducing agent and imparted better stability to silver nanoparticles as compared to oleic acid capped analogues.<sup>[87]</sup> The applicability of SL was further extended to synthesis of sophorolipid grafted polymer scaffolds that reduced  $\text{Ag}^+$  ions to  $\text{Ag}^0$  without compromising with its antibacterial properties. Authors showed that bacteria did not survive on these silver studded scaffolds whereas CHO-K1 (Chinese hamster ovary) cells thrived, thus making them good candidates for tissue engineering and bio-implant applications. Dhar et al. (2011) reported a completely green process developed for the preparation of sophorolipid-conjugated-gellan gum capped/reduced- gold nanoparticles which showed greater efficacy in killing the glioma cell lines and more prominently glioma stem cell lines.<sup>[88]</sup> Recently in 2013, Baccile et al. reported the use of acidic form of sophorolipids to functionalize magnetic iron oxide nanoparticles.<sup>[89]</sup> The two-step approach

yielded classical gamma-Fe<sub>2</sub>O<sub>3</sub> nanoparticles. Authors showed that carboxylic group of the sophorolipids interacted with the iron oxide surface due to which the synthesized material was very stable in solution. Dhar et al. (2016) reported synthesis of gold nanoparticles of 8-10nm size using curcumin-sophorolipids nanocomposites as effective reducing and capping agents. The systematic bio-distribution of gold nanoparticles in vital organs of rat model suggested their potential use as drug delivery carriers.<sup>[90]</sup>

### **1.6.8 Sophorolipids as size reducing agents**

The amphiphilic nature of surfactants helps them to solubilise relative hydrophobic molecules into aqueous media. Curcumin widely known for its anti-inflammatory and chemo-preventive property has limited oral bioavailability due to its hydrophobic nature. Thus a study conducted to overcome the drawbacks associated with curcumins bio-applicability, synthesized a formulation using acidic sophorolipid and curcumin under sonication. Sonication resulted in size reduction of curcumin from 818 nm to 15.5 nm (SL+curcumin) and thus improved curcumin's delivery and therapeutic efficacy in breast cancer cells, whereas complexing of curcumin with SL increased its stability, solubility, bioavailability and fluorescence.<sup>[91]</sup> Additionally the pharmacokinetic studies performed on Wistar rats by Darne et al., revealed that curcumin-SL (Cur-SL) nanocomposites could be retained in the blood plasma for 2 h, thus reflecting enhanced bioavailability of curcumin.<sup>[90]</sup>

### **1.6.9 Sophorolipids as therapeutic agents**

Toxicological studies conducted on sophorolipid and its derivatives showed very low acute oral toxicity. Median lethal dose tested in rats and mice was found to be 10-16g/kg and 5.8-6.6g/kg on oral and subcutaneous administration. Additionally SL derivatives were found to be non-reactive in skin and eye irritation studies.<sup>[92]</sup> Thus these toxicological findings are encouraging to use SLs for different therapeutic applications mentioned below.

➤ **Cell differentiation inducer** - Uncontrolled division in cancer cell is generally attributed to certain abnormalities in their differentiation capacity. Induction of normal differentiation in cancer cells could be an alternative in regenerative medicines. Isoda et al. in 1997 first reported the cell differentiation inducing ability of sophorolipids in human promyelocytic leukemia cell line HL60.<sup>[93]</sup> After a decade, Navare et. al. (2011) successfully

presented the morphological evidence of SL's (derived from oleic acid and linoleic acid) potential to induce differentiation in glioma cell line LN-229.<sup>[94]</sup>

➤ **Anticancerous SLs** - Anticancer property of sophorolipids from different source has been reported against various cancer cells. SL synthesized from *Wickerhamiella domercqiae* (yeast isolated from oil containing waste water) displayed dose-dependent cytotoxic effect on human liver cancer cell-H7402, human lung cancer cell-A549, Human promyelocytic leukemia cells-HL60 and human erythroleukemic cancer cells-K562 at drug concentration  $\leq 62.5 \mu\text{g/mL}$ . The sophorolipid was identified as diacetylated lactonic SL.<sup>[50]</sup> Later the authors showed that cytotoxic effect of SL on H7402 cell line was mediated by apoptosis.<sup>[23]</sup> *Candida bombicola* synthesized sophorolipid were shown to display anticancer activity against pancreatic cancer. Among the different derivatives, methyl ester SL was reported as most cytotoxic.<sup>[95]</sup> Another study conducted to evaluate the cytotoxic effect of HPLC purified sophorolipids, synthesized by *Wickerhamiella domercqiae var.*, on human esophageal cancer cell lines KYSE 109 and KYSE 450 emphasized on importance of sophorolipid structure on its anticancer activity. Among the two sophorolipid forms, lactonic SL displayed cytotoxic effects whereas acidic SL hardly showed any activity. Acetylation and extent of unsaturation had marked effect on SLs cytotoxic effect. Diacetylated SL with mono-unsaturation in fatty acid tail was found to be most potent.<sup>[96]</sup> Sophorolipids produced by *Candida bombicola* NRRL Y-17069 supplemented with soyabean oil and sunflower oil cake demonstrated promising anticancer activity in HepG2 and A549. Inactivation of enzymes, urokinase and histone deacetylase was held responsible for SLs cytotoxicity.<sup>[97]</sup>

➤ **Antibacterial Sophorolipids** - Sophorolipids antimicrobial property makes it an excellent candidate for cosmetic and biomedical applications. Sophorolipids synthesized by *Candida bombicola* were found to be bactericidal against *Cupriavidus necator* and *Bacillus subtilis*. SLs ability to markedly disrupt the bacterial biofilm formation indicated their potential use for health care application where these biofilms are responsible for several infectious disease leading to chronic conditions.<sup>[98]</sup> Studies conducted to evaluate the antibacterial property of SLs and their derivatives has shown that these glycolipid biosurfactants show considerable activity against Gram-positive bacteria (*Bacillus subtilis*, *Staphylococcus aureus*, *Rhodococcus erythropolis*, *Propionobacterium acne* and

*Streptococcus agalactiae*) but are primarily ineffective or require high enough concentration to kill Gram-negative (*Escherichia coli*) bacteria that are hard to achieve for clinical applications.<sup>[99–102]</sup>

➤ ***Anti-viral, spermicidal and Immunomodulator sophorolipids*** - Apart from antimicrobial properties, sophorolipids also possess anti-viral properties. SL synthesized by *Candida bombicola* has been employed to treat herpes-related viral infection.<sup>[103]</sup> Shah et al. reported the spermicidal and anti-HIV activity of diacetylated ethyl ester form of SL.<sup>[104]</sup> Sophorolipids have also been demonstrated to possess ability to decrease mortality in rats caused due to septic shock by modulating inflammatory response. The immunomodulatory role was attributed to cytokine down regulation and decreased nitric oxide production instead of antibacterial activity.<sup>[105,106]</sup> In order to treat diseases caused by altered immunoglobulin E regulation such as asthma, SLs possess great potential, as they decrease IgE production by down-regulating the IgE pathobiology genes.<sup>[107]</sup>

➤ ***Synergistic sophorolipids*** - Sophorolipids being antimicrobial in nature when complexed with tetracycline and cefaclor not only increased the efficacy of antibiotics but also reduced the effective dose required for killing *Staphylococcus aureus* and *Escherichia coli* respectively. The synergistic effect of SL is speculated to be the result of its amphiphilic nature that results in its spanning through the cell membrane and thus facilitating entry of the drug molecules inside the microbial cells.<sup>[108]</sup>

Several properties of sophorolipids detailed above confirm their increased popularity over past few years. With growing interest in this class of biosurfactants, extensive research is being conducted on, up scaling its production for industrial application and commercialization, new strains, novel SL molecules, derivatization and applications.

### **1.7 Proteins and surfactants**

Proteins are multifunctional biomolecules that serve role as catalyst, signalling molecules and building blocks to confer rigidity and stiffness. Surfactants are amphiphilic molecules that are known to lower interfacial tension and act as emulsifiers, dispersants, detergents, and wetting agents. By combining the strength and function of proteins with physico-chemical properties of surfactants, material with the advantages of both the components

can be formed for protein based therapeutics. Protein surfactant interactions date back to practical applications from protein molecular weight estimation to efficient washing powder enzymes and personal hygiene products.<sup>[109]</sup> Though several studies have focused on protein-surfactant interactions yet their remains ambiguity in mechanism adopted by surfactants to denature proteins. Most studies have been dedicated to interaction of a model anionic surfactant sodium dodecyl sulphate (SDS) with model proteins such as bovine serum albumin (BSA) <sup>[110–112]</sup>, lysozyme<sup>[113,114]</sup> and others <sup>[115,116]</sup>. Interaction of another structural protein, silk fibroin from *Bombyx mori* with SDS <sup>[117]</sup> and other cationic and non-ionic surfactants <sup>[118]</sup> has also been recently studied.

### 1.7.1 Protein-surfactant interactions

Both protein and surfactants are amphiphilic in nature, thus interaction between the two depends upon the type (ionic, non-ionic) and concentration of surfactant. Ionic surfactants show strong interactions with proteins whereas non-ionic surfactant generally prefer to self associate.<sup>[119]</sup> Mostly, interactions between protein and surfactant is electrostatic and/or hydrophobic. Electrostatic interactions lead to specific binding of surfactant to protein and are observed at low surfactant concentration.<sup>[120]</sup> At intermediate surfactant concentration, non-cooperative binding, characterized by gradual binding of surfactant is observed. Further, as number of surfactant molecules increase the binding affinity enhances and cooperative binding takes place. Beyond this, at higher surfactant concentration the protein-surfactant complex gets saturated, and their remains no more surfactant binding sites on the protein polypeptide chain. In such conditions protein lose their tertiary structure but retain secondary structure. These stages of protein surfactant interactions have primarily been established based on studies conducted on SDS complexed with BSA <sup>[121]</sup> and lysozyme<sup>[119]</sup>. Protein-surfactant complexes formed at high surfactant concentrations have been described by different proposed models such as “rod-like particle model”, <sup>[122,123]</sup> “bead necklace model” <sup>[124]</sup> and “decorated micelle model” (shown in Figure 1.4). Among these bead-necklace model is widely supported. In this model, the protein chain is wrapped around the surfactant micelles. Decorated micelle model is a slight variation of bead-necklace model and it proposes that polypeptide chain passes through the surfactant micelle.

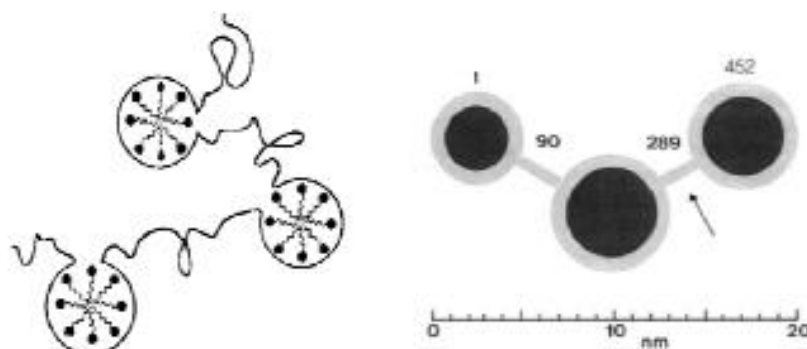


**Figure 1.4** Schematic presentation of the two models used to describe protein-surfactant complexes at saturation. Left – Bead necklace model, the protein chain is wrapped around the surfactant micellar bead. Adapted from<sup>[121]</sup> Right – Decorated model, polypeptide chain passes through the micelles. Adapted from<sup>[119]</sup>

In this thesis, instead of conventional model proteins such as BSA and lysozyme, another structural protein from *Bombyx mori* silk worm has been studied, towards fabrication of material for biomedical application. Similarly instead of conventionally studied anionic surfactant, sophorolipid biosurfactant has been employed in the process that will be described in later chapters. To study the interaction of silk fibroin with sophorolipid it is necessary to understand its structure, importance and properties that are described below.

### 1.7.2 Introduction to silk fibroin

Silk, a natural polymer generally woven into textiles, is produced by larvae of certain insects and mulberry silk worm *Bombyx mori*. The larvae spin the protein in the form of cocoon that can be degummed to separate the two constituent proteins in silk fibre i.e. fibroin and sericin. Sericin is a glue-like protein that holds the two filaments of fibroin intact.<sup>[125]</sup> The cocoon is simply boiled with salts in water to remove sericin, fibroin thus obtained after a repeated wash is dissolved in ionic liquid solvents to form Regenerated Silk Fibroin (RSF). This RSF solution can then be used for medical and tissue engineering applications. Fibroin protein is primarily made of a heavy (350 kDa) and light (25 kDa) chain, that remain linked by disulphide bond, as shown in Figure 1.5.<sup>[126]</sup> The primary structure of heavy chain comprise of repetitive amino acid sequence (Gly-Ala-Gly-Ala-Gly-Ser)<sub>n</sub> and tyrosine rich domains. The amino acid repeats present in the heavy chain participate in the beta sheet formation and impart crystalline nature, hence exceptional tensile strength to the protein.<sup>[127]</sup> While the light chain mainly constitutes the amorphous or non-crystalline region of the fibroin protein and connects the crystalline regions. Isoelectric pH of silk fibroin is

~3.8 and it carries overall negative charge at a neutral pH.<sup>[128]</sup> Several advantages of employing silk fibroin for material fabrication are; it is domestically reared in large quantities and displays excellent mechanical properties, thermal stability and biocompatibility. Silk fibroin has also gained wide recognition due to its biodegradability and aqueous processability.

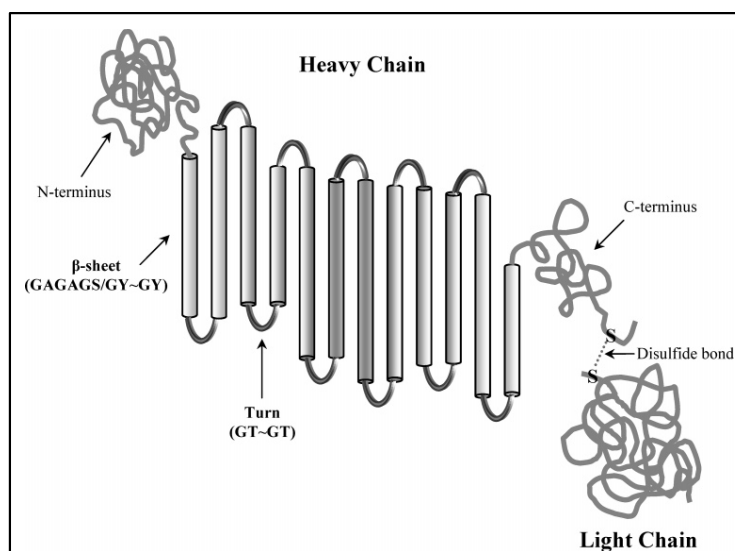


**Figure 1.5** Secondary structure of silk fibroin protein.<sup>[126]</sup>

### 1.7.3 Silk fibroin as a biomaterial

Unprocessed silk fibroin (virgin or degummed) has been used for surgical purposes since centuries. Processing of the native silk fibres in aqueous or organic solvents allowed researchers to exploit it for designing various biomaterials. Reprocessing of silk fibers or electrospinning is employed to fabricate non-woven fibroin mats that offer the advantage of increased surface area and rough surface for enhanced cell adhesion.<sup>[129]</sup> Silk films formed by casting fibroin in aqueous or organic solvent are advantageous due to the water vapour and oxygen permeability which supports wound healing.<sup>[130,131]</sup> For tissue engineering applications a three dimensional material that can support adhesion, proliferation, migration of cells along with transport of nutrients and waste material is desirable. With this view silk fibroin has been employed to form porous sponges by using methods such as gas foaming, lyophilisation and by employing salt or sugars as porogens.<sup>[132]</sup> Another form of biomaterial in which silk fibroin can be fabricated is hydrogels. Hydrogels are three

dimensional network made from polymers and are highly employed in biomedical field for wound healing, drug delivery and tissue engineering applications.<sup>[133]</sup>

### **1.8 Scope of the work**

The new potentials of sophorolipids are being realized ever since its introduction and unique facets are being added by carrying out extensive research on it. Multiple properties possessed by single class of molecules i.e. Sophorolipids, renders the opportunity of employing them in varied fields ranging from detergent industry to materials and biomedical. Such high variation in properties is due to additional advantage of SL being tailor made i.e. different SL molecules can be synthesized by supplementing the yeast with different lipophilic feed. Thus, the flexibility of modifying the sophorolipid's structure has prompted researchers to synthesize numerous forms of sophorolipids with a view to enhance their biological properties.

With the aim to synthesize novel SL, we have used cetyl alcohol as the lipophilic substrate along with glucose as a hydrophilic carbon source. In comparison to fatty acids, fatty alcohols lack carboxylic end, thus there remains no directionality for their incorporation into sophorolipid molecule. Due to the prior presence of hydroxyl group at one end of the cetyl alcohol, the hydroxylation step in the biosynthetic pathway carried out by cytochrome P450 monooxygenase may or may not be ruled out.<sup>[134]</sup> This would result into formation of different product that can be expected to have varied properties than the conventional sophorolipids. As mentioned above, SLs possess anti-bacterial properties, thus we have tried to explore the potential of newly synthesized cetyl alcohol sophorolipid as anti-bacterial agent. As discussed above, anti-cancer property of SLs has been extensively studied in past owing to their promising potential and biocompatibility. Here we have explored the anti-proliferative activity of cetyl alcohol derived sophorolipid and its mechanism of action. These properties in the synthesized novel SLs prove their potential for application as therapeutic agents.

Surfactant-protein interactions are widely studied for applications ranging from estimation of protein molecular weight to efficient detergent enzymes and personal hygiene products. Surfactants are known to denature proteins. Anionic surfactant like sodium dodecyl sulfate (SDS) has been reported to induce gelation in silk fibroin, a structural protein that takes few weeks to gel on its own. Chemical structure of sophorolipids resembles SDS

and thus it is likely for SLs to initiate gelation in silk fibroin and accelerate the process through hydrophobic interactions. Also, SLs display several properties that can prove to be advantageous over previously reported gelling agents. SLs are synthesized microbially by certain non-pathogenic yeasts. Being natural compounds derived biologically, SL's are biocompatible and have reduced environmental impact in comparison to their synthetic counterparts.<sup>[135]</sup> Thus, we for the first time evaluated the role of SLs as gelling agent. The biomedical application of three dimensional SF-SL scaffolds has also been reported. Further the silk fibroin and sophorolipid interactions were studied in depth to understand the mechanism and to know how the sophorolipid accelerates gelation process. The effect of certain parameters in driving the process was also ascertained.

### **1.9 Thesis outline**

The thesis has been divided into following five chapters:

#### ***Chapter 1. Introduction***

The first chapter is an introduction to the thesis. It includes brief account on surfactants and specifically biosurfactants. Sophorolipid, the centre of this thesis, has been reviewed with respect to its properties and application in different fields. Protein and surfactant interactions have been discussed and bio-medically significant protein, silk fibroin as a biomaterial has been introduced. With this background, the scope and objectives of the thesis have been defined.

#### ***Chapter 2. Production of Novel Sophorolipids using fatty alcohol, their physico-chemical, analytical and antimicrobial analysis***

The second chapter is about the synthesis of novel sophorolipid (SLCA) by using fatty alcohol i.e. cetyl alcohol as the lipophilic carbon source. The work involves physicochemical characterization to ascertain the effectiveness of SLCA as a biosurfactant and analytical characterization for structure identification. Antibacterial studies were conducted to check the applicability of these novel sophorolipids as a safe and effective therapeutic alternative.

#### ***Chapter 3. Apoptosis mediated anti-proliferative effect of cetyl alcohol sophorolipids and their anti-angiogenic activity***

In the third chapter the anti-proliferative effect of SLCA against different human cancer cell lines was evaluated. Various assays were conducted to ascertain the probable mechanism of cytotoxicity in HeLa cells. Further the anti-angiogenic ability of SLCA in HUVEC cells was investigated and reported for the first time.

#### ***Chapter 4. Sophorolipid assisted tunable and rapid gelation of silk fibroin to form porous biomedical scaffolds***

The fourth chapter for the first time reports the accelerated gelation of silk fibroin protein, under physiological conditions, using sophorolipid (SL) as a gelling agent. The hydrogels were further converted to three dimensional scaffolds with tunable porosity and pore size and their biocompatibility was demonstrated by different cell studies.

#### ***Chapter 5a. Silk Fibroin Sophorolipid gelation: Deciphering the underlying mechanism***

The fifth chapter (part a) is dedicated to deciphering the mechanism by which sophorolipid gels silk fibroin using multiple characterization techniques. The in-depth mechanism studied, also involves the assembling behaviour of different forms of SL and their interaction with the protein. This work significantly adds value to the growing literature of protein-surfactant systems that are of prime interest to the healthcare, food and cosmetic industry.

#### ***Chapter 5b. pH dependent sophorolipid assemblies and their influence on gelation of silk fibroin protein.***

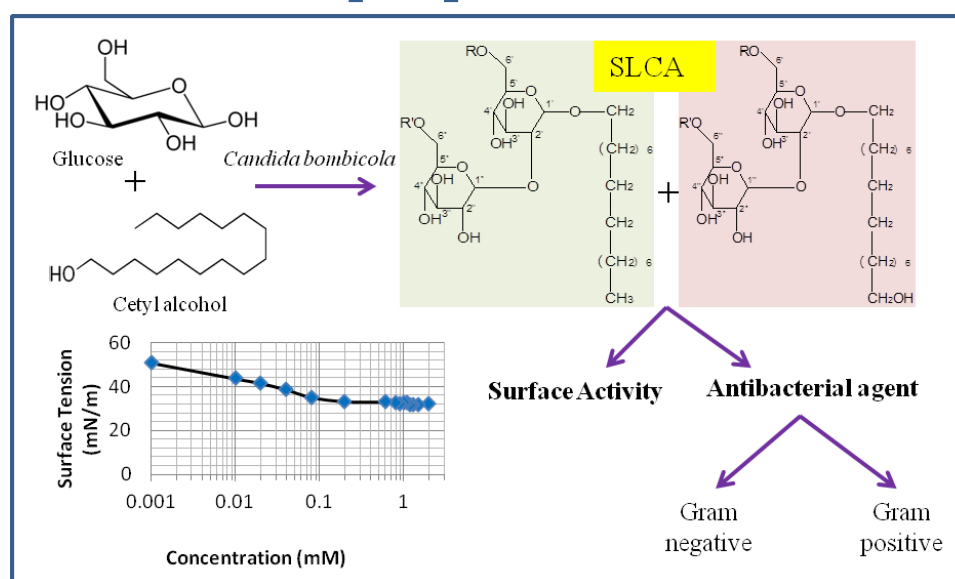
The fifth chapter (part b) is an extension of chapter 5a. It describes about the influence of pH on sophorolipids self assembling property and the way it dictates the gelation of sophorolipid-silk fibroin.

#### ***Chapter 6. Conclusions***

The sixth chapter summarizes the work presented in the thesis and emphasizes on possible further research in this area. Self assembling behaviour of cetyl alcohol derived sophorolipid has been shown. Also the applicability of sophorolipids in enhancing the bio applicability of electrospun silk fibres has been demonstrated.

## Chapter 2

# Production and characterization of novel sophorolipids using primary fatty alcohol: their physico-chemical and antibacterial properties



Sophorolipids are biologically derived amphiphilic glycolipids that have attracted much attention in recent past owing to their additional biological properties, such as antimicrobial and anticancerous apart from lowering interfacial tension. A novel sophorolipid was synthesized (sophorolipid derived from cetyl alcohol, SLCA), by supplementing non-pathogenic yeast *Candida bombicola* ATCC 22214, with glucose and cetyl alcohol as hydrophilic and lipophilic carbon source, respectively. Physicochemical characterization performed to ascertain the effectiveness of SLCA as a biosurfactant, revealed that it significantly lowered the surface tension of water to 31.349mN/m with critical micelle concentration of 104 mg/L. Structural characterization confirmed the incorporation of already hydroxylated lipidic carbon source, cetyl alcohol in sophorolipid molecule. Applicability of these novel sophorolipids as an effective therapeutic alternative to existing antibacterial agent was found remarkable. These interesting findings add a new facet to the known range of sophorolipids that can be explored for potential applications in diverse industries.

## 2.1 Introduction

As described in the previous chapter, sophorolipids constitute an interesting class of extracellular glycolipid biosurfactants, synthesized naturally by certain non-pathogenic yeasts; *Candida bombicola* ATCC 22214 being the most studied one. Sophorolipids (SL) are known to lower interfacial tension and similar to synthetic surfactants they exhibit physiochemical properties such as detergency, emulsification, foaming and wetting. SLs are widely gaining recognition due to additional possession of antimicrobial,<sup>[101]</sup> anticancerous,<sup>[136]</sup> cell-differentiation<sup>[94]</sup> and apoptosis inducing properties.<sup>[137]</sup> Recently, Singh et al. (2009) reported the role of sophorolipids in nanomaterial synthesis as reducing and capping agent.<sup>[87]</sup> Further a new dimension to application of sophorolipids was lately introduced by Singh et al. (2013) by synthesizing highly spherical mesoscale molecular self assembly that exhibited strong green fluorescence thus exemplifying its potential to be used in bio-imaging and drug delivery.<sup>[69]</sup>

Sophorolipids, consist of dimeric sugar, sophorose, linked glycosidically to a hydroxy fatty acid residue. This form of sophorolipid is known as acidic SL. Upon esterification of the carboxylic group of acidic SL with the 4'' OH of the sugar, a closed ring structural form of sophorolipid is formed, known as, lactonic SL.<sup>[46]</sup> The sophorose moiety may additionally contain acetyl groups at the 6' and/or 6'' positions that add to the variability of the SL mixture synthesized by the yeast. Sophorolipids have an additional advantage of being tailor made i.e., by varying the lipophilic carbon source, different SLs varying in physiochemical properties can be synthesized according to the need and applications. With this view, many researchers have synthesized sophorolipids by using different lipidic substrates such as alkanes,<sup>[138]</sup> saturated fatty acids,<sup>[56]</sup> unsaturated fatty acids,<sup>[57]</sup> and fatty alcohol<sup>[102]</sup> etc. Apart from these pure substrates, several edible and non-edible oils/oil cakes such as canola oil,<sup>[139]</sup> jatropha oil,<sup>[76]</sup> karanj oil,<sup>[140]</sup> bauhinia seed oil<sup>[141]</sup> mahua oil, waste cooking oil,<sup>[142]</sup> and sunflower oil cake<sup>[143]</sup> etc. have been employed with a view to reduce sophorolipid production cost for industrial applicability. Use of rapeseed oil in combination with deproteinized whey concentrate helped in attaining sophorolipid yield as high as 400g/L.<sup>[30]</sup>

Glucose is the most common hydrophilic substrate provided to the yeast. Although researchers have tried to use sucrose, galactose and lactose to lower the substrate cost but it also resulted in lower sophorolipid yield.<sup>[144-146]</sup> Similarly use of low cost soy molasses as

glucose substitute also gave lower sophorolipid yield.<sup>[147]</sup> In addition to lipidic feed when glycidic carbon source is supplemented to the yeast, sophorolipid production is considerably higher.

Thus, generally both carbon sources are supplemented to the yeast for SL production. Like glucose, fatty acids (pure or in oils) are preferably provided to the yeast but on supplementing the yeast with already hydroxylated products acid-free sophorolipids/alkyl sophorosides can be formed. Brakemeier et al. (1995) for the first time reported the use of secondary alcohols (2-dodecanol, 2-tetradodecanol) as the lipophilic carbon source along with glucose as hydrophilic source. They reported the direct incorporation of 2-alkanols in the novel sophorose lipids without further metabolization.<sup>[148]</sup> The shorter chain length of the sophorolipid molecule in comparison to the classical sophorolipids, resulted in increased solubility of these compounds and better ability to reduce surface tension of water. Although these novel sophorose lipids possessed remarkable properties advantageous for industrial application but they suffered from the disadvantage of high costs of secondary alcohols.<sup>[149]</sup>

The use of primary alcohols could offer a less expensive alternative to secondary alcohols which are quite expensive for commercial fermentation. Thus, later Brakemeier et al. (1998) demonstrated use of 1-dodecanol for sophorolipid production. In order to avoid metabolization of the lipidic substrate and its utilization in *de novo* synthesis of hydroxylated fatty acids (C16/C18) by the yeast, they experimented with the media nutrient content. Upon increasing the glucose and yeast extract concentration to 1.5 and 4-fold respectively, direct transformation of 1-dodecanol was achieved.<sup>[149]</sup> The synthesized product resembled with synthetic alkyl-polyglycosides. Recently, Dingle-Pulate et al. (2012) also demonstrated incorporation of lauryl alcohol C<sub>12-14</sub> into the sophorolipid molecule.<sup>[27]</sup>

In comparison to fatty acids, fatty alcohols lack carboxylic end, thus there remains no directionality for their incorporation into sophorolipid molecule. Due to the prior presence of hydroxyl group at one end of the fatty alcohol, the hydroxylation step in the biosynthetic pathway carried out by cytochrome P450 monooxygenase may or may not be ruled out.<sup>[134]</sup> This would result into formation of different product that can be expected to have varied properties than the conventional sophorolipids.

So far there are no reports on the successful use of primary cetyl alcohol (C<sub>16</sub>) for sophorolipid production. Thus, in order to synthesize novel SL, cetyl alcohol was used as the lipophilic substrate along with glucose as a hydrophilic carbon source in the present work. Till date techniques such as LC-MS<sup>[150]</sup> and MALDI-TOF MS<sup>[22]</sup> have been used for identification of sophorolipids. A highly evolved technique, liquid chromatography high resolution mass spectrometry (LC-HRMS) which provides sensitive, high-quality data has yet not been explored for the identification of sophorolipids. Hence for the first time, structural characterization of cetyl alcohol derived sophorolipids (SLCA) was carried out with the help of LC-HRMS. Towards the application, surface activity and antibacterial property of the as synthesized SLCA were also studied and compared with already reported SLs.

## **2.2 Materials and methods**

### **2.2.1 Chemicals**

All chemicals used in the study were of analytical grade. Glucose was purchased from Qualigens, India. Peptone, malt and yeast extract were purchased from Hi-media, India. Cetyl alcohol (C<sub>16</sub>) was received from Galaxy Surfactants, India. Cetyl alcohol also known as 1-hexadecanol or palmityl alcohol, is water insoluble white solid or flakes, derived from vegetable oils. It finds application in cosmetic industry as opacifier and thickening agent.

### **2.2.2 Microorganism and Maintenance**

The yeast used in this study was *Candida bombicola* ATCC 22214. It was grown in MGYP medium containing 0.3% Malt extract, 2% Glucose, 0.3% Yeast extract and 0.5% Peptone, at 28°C. The culture was maintained by periodic transfer on MGYP agar slants at 4°C. *Staphylococcus aureus* (ATCC 2079) and *Escherichia coli* (ATCC 8739) were acquired from National Collection of Industrial Microorganism (NCIM) Pune, India. The bacterial cultures, *S. aureus* and *E. coli* were grown at 28°C and 37°C, respectively and maintained on Luria-Bertani slants.

### **2.2.3 Production of Sophorolipids**

#### **a) Fermentation conditions for cetyl alcohol derived sophorolipid**

A loopful of *Candida bombicola* ATCC 22214 cells were taken from slant and seed culture was developed by transferring it to 10 mL medium, mentioned in Table 2.1, for 24 hours at 28°C with 180 rpm orbital shaking.<sup>[151]</sup>

**Table 2.1** Media composition for sophorolipid production

Media Components	Glucose	Yeast extract	MgSO <sub>4</sub> .7H <sub>2</sub> O	Na <sub>2</sub> HPO <sub>4</sub>	NaH <sub>2</sub> PO <sub>4</sub>	(NH <sub>4</sub> ) <sub>2</sub> SO <sub>4</sub>
Concentration (g/L)	100	1.0	0.3	2	7	1

The seed culture was transferred to 40 mL medium for developing the starter culture, and incubated for 24 hours at 28°C under constant orbital shaking at 180rpm. The grown starter culture was transferred into 200 mL of above mentioned medium in 1 litre Erlenmeyer flask and incubated for 120 h at 28°C with 180 rpm orbital shaking. The medium was supplemented with cetyl alcohol as lipophilic substrate at concentration of 1g/100mL dissolved in 0.5 mL ethanol.

### **b) Extraction of Sophorolipids**

*Candida bombicola* cells were harvested from the culture broth by centrifugation at 5,000 rpm, 10°C for 20 minutes. This cell mass was reutilized for sophorolipid production by resting cell method. Equal volume of ethyl acetate was added to supernatant for extracting the sophorolipid as described by Gupta & Prabhune (2012).<sup>[57]</sup> The aqueous layer was re-extracted until no emulsion was formed at the interface. Next, the water traces were removed by subjecting ethyl acetate to sodium sulphate treatment. The solvent was filtered to remove sodium sulphate and reduced by rotary evaporation under vacuum to yield a brown coloured viscous product, referred as SLCA and was stored at 4°C. The steps involved in sophorolipid production and extraction are depicted in Figure 2.1.

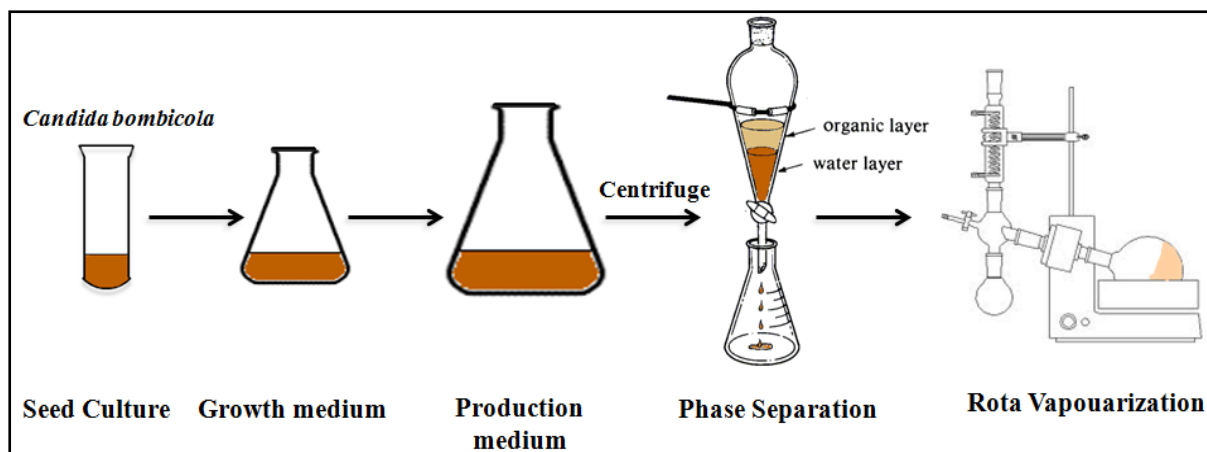


Figure 2.1 Main steps involved in sophorolipid synthesis

#### 2.2.4 Evaluation of surface active properties of SLCA

The surfactant properties of cetyl alcohol derived sophorolipid (SLCA) were evaluated by two screening methods that rely on interfacial activity i.e. oil displacement assay and emulsification capacity assay. The surface activity of SLCA was also determined by direct surface tension measurements.

##### a) Oil Spreading Assay

The surfactant property of as synthesized SLCA was qualitatively confirmed by conducting oil spreading assay developed by Morikawa et al.<sup>[152]</sup> For the assay, in a 55 mm petridish, 20mL distilled water was taken and a thin film of oil was formed by adding 500  $\mu$ l of jatropha oil. To the equilibrated oil film, 20  $\mu$ l of test sample solution varying in concentration (2-10 mg/mL) was added to the centre of oil film. Depending upon the concentration, a clear halo developed that related to the surfactant property of SLCA.

##### b) Emulsification capacity assay

The emulsification assay was conducted as described by Cooper and Goldenberg (1987).<sup>[153]</sup> Stock solution of SLCA and other chemical surfactants such as sodium dodecyl sulphate (SDS) and tween-80 were prepared in MilliQ water. 4mL oil (groundnut, sunflower and jatropha) was added to 2mL SLCA solutions in a test tube and vortexed for 2 mins. The test was allowed to stand for 24 h and then emulsification index was calculated by following formula:

$$E_{24} = \frac{H_e}{H_t} \times 100$$

where  $H_e$  represents height of the emulsion layer and  $H_t$  means total height of the mixture.  $E_{24}$  was calculated for SLCA and chemical surfactants. Distilled water was used as control. Emulsions formed were monitored for 15 days to check their stability.

**c) Surface tension and CMC:**

Wilhelmy plate method is widely used for measuring the surface tension of a liquid or interfacial tension between the two liquids. The instrument used is known as Tensiometer. In this method a thin platinum plate is perpendicularly suspended on the liquid surface, which when contacts with the liquid, a force  $F$  acts on it. This force correlates to the surface tension/interfacial tension ( $\sigma$ ) and contact angle according to following equation:

$$\sigma = \frac{F}{L * \cos\theta}$$

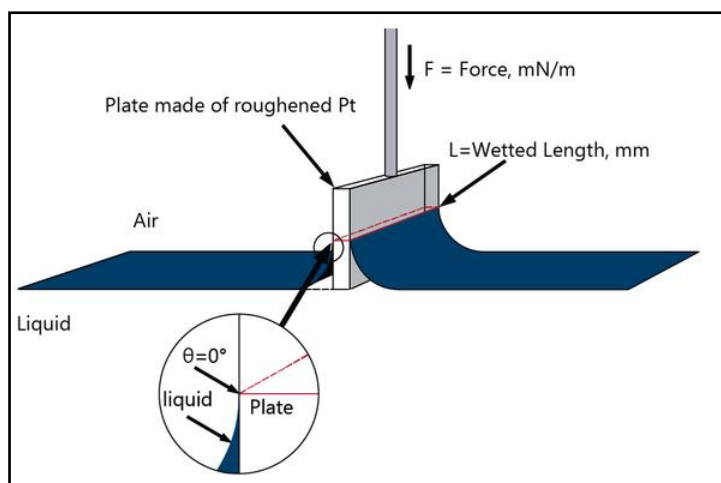


**Figure 2.2** Diagram describing the Wilhelmy plate method (adapted from Kruss)

As can be seen in Figure 2.2 the length  $L$  of the plate is equivalent to its perimeter. In the tensiometer the plate is attached to a force sensor that measures force  $F$ . This method was used to measure the equilibrium surface tension of SLCA aqueous solutions, using Kruss K-11 tensiometer with an accuracy of  $\pm 0.2$  mN/m at  $25 \pm 1^\circ\text{C}$ . Stock solution of SLCA was prepared in MilliQ water and diluted to concentration range of 0.001-2% w/v. First the calibration of instrument was carried out using distilled water and then surface tension measurements were carried out for different SLCA concentrations in triplicate and average

value was taken. The critical micelle concentration (CMC) of SLCA was calculated, as the concentration at which minimum surface tension was observed from the surface tension vs concentration graph.

### **2.2.5 Characterization and structure determination**

#### **a) Thin Layer chromatography (TLC)**

The presence of different components in the product was evaluated by TLC. Silica gel plates (Merck DC Kieselgel 60 F<sub>254</sub>) were used as the stationary phase and chloroform, methanol and water were used as the mobile phase in 65:15:2 (v/v) ratio.<sup>[154]</sup> To visualize the spots dried plate was sprayed with charring solution of acidified p-anisaldehyde prepared using absolute ethanol-135mL, conc. H<sub>2</sub>SO<sub>4</sub>-5mL, glacial acetic acid-1.5mL and p-anisaldehyde-3.7mL. The plate was air dried and heated at 140°C.<sup>[155]</sup> R<sub>f</sub> values of spots were calculated as ratio of distance travelled by sample to solvent.

#### **b) Fourier transformer infrared spectroscopy (FT-IR)**

In order to confirm the various functional groups present, SLCA was analysed by Infrared Spectroscopy. The SLCA mixture was crushed with finely grinded KBr powder, and the mix was dried under IR lamp for few minutes. The powder was then pelleted and used for recording FTIR spectra on a Perkin-Elmer Spectrum One instrument at 4 cm<sup>-1</sup> resolution. All measurements consisted of 64 scans.

#### **c) Liquid Chromatography Mass spectroscopy (LC-MS)**

SLCA mixture was separated by HPLC with Waters Acquity UPLC using a C18 column (5µm, 150 x 4.6mm). Water and acetonitrile were used as solvent system. The water/acetonitrile ratio was initially maintained as 90:10 v/v for initial 5 mins and then fraction of acetonitrile was gradually increased from 10 to 90 for remaining 10 mins. The flow rate was set as 0.5 mL/min. Effluent was connected to Micromass 2Q quadrapole mass analyzer with an electron spray ionization (ESI) probe in positive mode that scanned in m/z 100 to 900 mass range.

#### **d) High resolution mass spectroscopy (HR-MS)**

High resolution mass spectroscopy experiment was performed on Thermo Scientific, Hybrid Quadrupole Q-Exactive HR mass spectrometer for SLCA structure identification. Chromatographic separation was carried out using LC (Accela 1250 pump), Thermo Scientific™ Hypersil ODS C18 column, 150 mm X 4.6 mm, having 8 $\mu$ m particle size. The sample was prepared by dissolving SLCA in methanol to a final concentration of 100  $\mu$ g/mL. The gradient solvent system was used for eluting sophorolipid components. Similar to LC-MS, water and acetonitrile were used as the solvent system but profile varied. Elution was started with water/acetonitrile in 100:0, v/v ratio, which was held for 15 mins. The ratio of acetonitrile was gradually increased to a final composition of 0:100, v/v (water/acetonitrile). Flow rate was adjusted as 500  $\mu$ L/min. The mass spectrometer was operated in positive electrospray ionization mode in 25,000 full-width at half-height maximum resolution with mass range  $m/z$  300 to 800.<sup>[156]</sup>

The operation conditions were as follows: spray voltage at 3.6 kV, capillary temperature at 320 °C, S-lens RF level at 50, automatic gain control (AGC) at  $1 \times 10^6$ , and maximum injection time at 120ms. Nitrogen was used as the sheath gas, auxiliary gas, and sweep gas, set at 45, 10, and 2, respectively (arbitrary units).<sup>[156]</sup> A volume of 5  $\mu$ L of sample was injected and full HR-MS scan was performed using positive polarity. Data were analyzed with Thermo Scientific Xcalibur software.

The exact mass-to-charge ratios of molecular ions of the predicted SLCA mixture components were calculated and used to extract the ions from the full-scan total ion current (TIC).<sup>[156]</sup> The mass spectra corresponding to the chromatographic peaks were analyzed. Highest relative abundant peaks were correlated with the molecular mass of the different SLCA components and their protonated and sodium adducts. Thus, mass to charge ratio enabled to identify the structures of SLCA putatively.

### **2.2.6 Assessment of antibacterial property of SLCA**

Antibacterial activity of SLCA was determined using standard microdilution and spread plate method against a Gram-negative bacterium *Escherichia coli* (ATCC 8739) and an opportunistic Gram-positive bacterium *Staphylococcus aureus* (ATCC 2079). Both the microorganisms were grown in Luria-Bertani medium at their corresponding growth temperatures for 24 hours. The cell count was quantified by optical density (OD) at 600nm

and by counting CFU/mL. SLCA was diluted to 10, 50, 90, 300 µg/mL using sterile Millipore water, for *E. coli*. For *S. aureus* SLCA was diluted to 100, 500, 700, 1000 µg/mL.

Bacterial suspension maintained at a cell count of  $10^3$  per mL, was added to each of these dilutions of SLCA and incubated for 6 hours at their respective temperatures. Two controls were used in the study: 1) Without SLCA and 2) With lipophilic substrate i.e. cetyl alcohol only, at the corresponding maximum concentration of SLCA used. Then 50 µL aliquots were withdrawn at an interval of 2 hours and plated on Luria-Bertani plates. The plates were then incubated at 37°C for *E. coli* and 28°C for *S. aureus*. After 24 hours, colonies were counted manually. Experiments were performed in triplicates with standard deviation <5 %. The following formula was used to calculate the percentage of cell survival.<sup>[151]</sup>

$$\% \text{ Cell survival} = 100 \times \frac{N_e}{N_c}$$

$N_e$  and  $N_c$  refer to number of live bacterial colonies on test plate and control plate respectively.

### **Minimum Inhibitory concentration**

Minimum Inhibitory concentration (MIC) of the test compound is considered to be that concentration which inhibits more than 90% growth of the bacterial colony. The concentration of SLCA at which no bacterial colonies were observed on Luria-Bertani agar plate was considered as its MIC value.

## **2.3 Results and Discussion**

### **2.3.1 Production of Sophorolipid**

~11g/L of SLCA was produced by resting cell method with 1% v/v hydrophobic substrate feeding to *Candida bombicola*. Resting cell method allowed economic reuse of same yeast biomass for up to 3 times SL production. The synthesized SLCA was subjected to different assays and test in order to evaluate its surface and interfacial activity.

### **2.3.2 Surface active properties of sophorolipid**

#### **a) Oil displacement**

The surfactant property of SLCA synthesized by *Candida bombicola* was qualitatively confirmed by oil spreading assay. As can be seen in Figure 2.3 with increasing concentration

of SLCA from 2-10 mg/mL the size of the halo increased, thus signifying the phenomenon to be dose dependent. In comparison to SLCA, cetyl alcohol i.e. substrate used for SL production failed to displace the oil even at highest concentration studied. This clearly indicated the modification in cetyl alcohol resulted upon incorporation in SL molecule and the synthesized product possessed surfactant property.

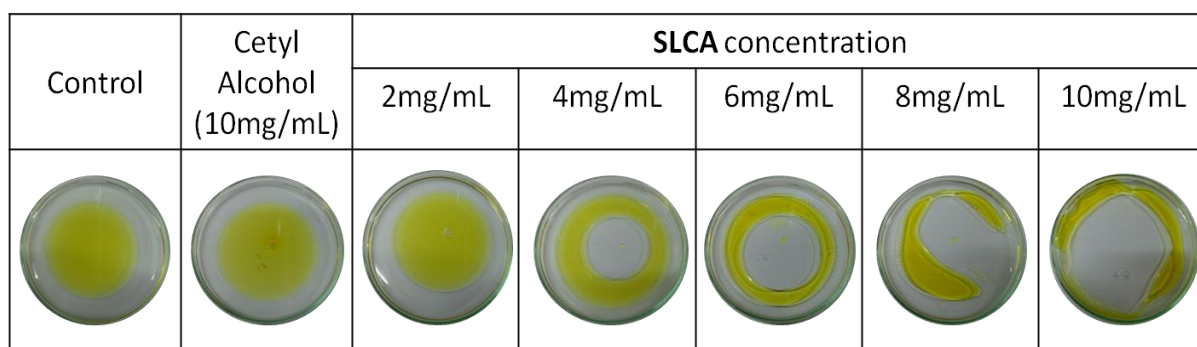


**Figure 2.3** Oil displacement assay demonstrating surfactant property of SLCA in concentration dependent manner.

### ***b) Emulsification Activity***

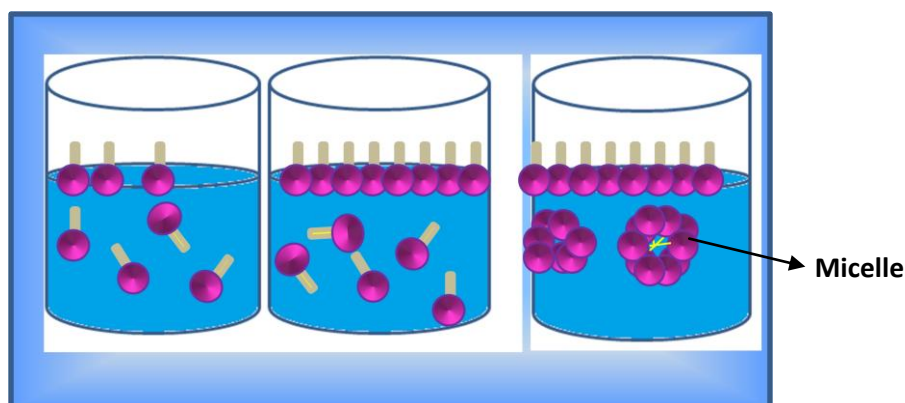
Emulsion is a two-phase system of liquids, which are generally immiscible. An emulsion is usually formed by the dispersion of one liquid phase as microscopic droplets in another liquid continuous phase. To increase the kinetic stability of these emulsions, surfactants are generally used due to their surface active properties. The amphiphilic nature of the biosurfactants allows them to align at the immiscible interfaces such as oil-water and then helps in dispersal of one into another. The emulsification index of different surfactants in different oil has been noted in Table 2.2. Stock concentration of each sample was taken as 2mg/mL. Emulsification activity of SLCA in groundnut and jatropha oil was found to be superior in comparison to standard chemical surfactants sodium dodecyl sulfate (SDS) and Tween-80. In sunflower oil  $E_{24}$  value of SLCA was higher than tween-80 but slightly lower than SDS.

**Table 2.2** Emulsification activity of SLCA and other chemical surfactants

Types of Surfactant	Emulsification Index (%) ( $E_{24}$ ) of surfactants in different oils		
	Groundnut oil	Jatropha oil	Sunflower oil
SLCA	71.7	88.88	54.54
SDS	46	65	62.50
Tween-80	30	65	45.71

### c) *Surface tension and CMC*

Surfactant solutions are known to often display unusual properties. In dilute solutions they act as a normal solute, whereas beyond certain concentrations abrupt changes in turbidity, electrical conductance, osmotic pressure and surface tension are observed. This eccentric behaviour is attributed to the formation of organized aggregates or micelles following adsorption of surfactant to reduce surface tension (as shown in Figure 2.4). The surfactant concentration at which micelle formation becomes discernible is termed as its critical micelle concentration (CMC) which can be measured with the help of any micelle-influenced physical property as a function of concentration.<sup>[157]</sup>

**Figure 2.4** Micelle formation in surfactants over critical micelle concentration

In the present study CMC was determined by measuring the surface tension of SLCA solutions ranging between 0.001 to 2% w/v. Reduction in surface tension was observed with increasing concentration of SLCA, attributed to their assembling as a monolayer at the surface. After certain concentration no significant decrease in surface tension was recorded, owing to formation of micelle in the bulk aqueous phase. The minimum surface tension of

cetyl alcohol ranges between 38-43 mN/m. As illustrated in Figure 2.5, SLCA lowered the surface tension of water from 72 to 31.349 mN/m. The critical micelle concentration was calculated as 104 mg/L. Our result is quiet comparable with the literature data, reporting CMC of 130 mg/L<sup>[158]</sup> and 140 mg/L,<sup>[51]</sup> for sophorolipid derived from oleic acid. In comparison to other surfactants, fatty alcohol sophorolipids ((lauryl alcohol SL (SLLA), cetyl alcohol SL (SLCA)) displayed best surface tension lowering ability (Table 2.3). The effect of fatty acid chain length on surface tension lowering capacity of fatty alcohol SL was clearly evident. Lauryl alcohol SL with shorter chain length (C<sub>12-14</sub>) as compared to cetyl alcohol SL (C<sub>16</sub>) lowered the surface tension to 24mN/m<sup>[159]</sup> and thus proved to have higher surface activity.

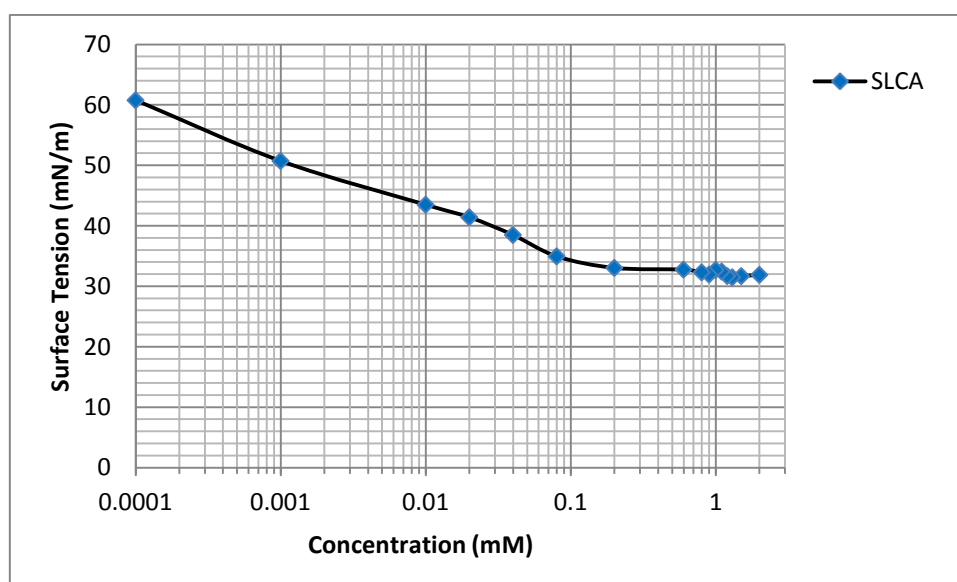


**Figure 2.5** Graphical representation of surface tension reduction of SLCA.

**Table 2.3** Comparison of minimum surface tension and CMC of different surfactants.

Surfactants	CMC	Surface tension (mN/m)	Reference
Cetyl alcohol SL	104 mg/L	31.34	[160]
Lauryl alcohol SL	0.68 mg/L	24	[27]
Oleic acid SL	130 mg/L	39	[158]
Xylolipid	1.0 mg/L	35.9	[161]

### 2.3.3 Analytical characterization of SLCA

#### a) Thin layer chromatography

The TLC (Figure 2.6) analysis of crude SLCA showed that it is a mixture comprising of components that resolved on TLC plate corresponding to their respective polarity. Non-polar components migrated more than the polar components. TLC showed distinct spots at  $R_f$  values 0.58, 0.51, 0.46, 0.34 and 0.25 and two faint spots at 0.90 and 0.74.



**Figure 2.6** TLC of cetyl alcohol derived sophorolipid synthesized by *Candida bombicola* (ATCC 22214).

#### b) FT-IR analysis

The FT-IR spectrum (Figure 2.7) of SLCA depicted in blue shows the presence of sugar in the sophorolipid molecule by C–O stretch of C–O–H groups at  $1,024\text{ cm}^{-1}$ . The attachment of the fatty alcohol is indicated by the peak at  $1068\text{ cm}^{-1}$  that corresponds to C–O stretch of fatty alcohol. The presence of alkyl chain corresponding to the fatty alcohol is also confirmed by symmetrical and asymmetrical stretching of methylene at  $2842\text{ cm}^{-1}$  and  $2914\text{ cm}^{-1}$  respectively. The peak at  $1,242\text{ cm}^{-1}$  signifies an ether linkage corresponding to the glycosidic bond between sugar-sugar and fatty alcohol-sugar moiety. Additional carbonyl group peak (absent in sugar and cetyl alcohol) at  $1733\text{ cm}^{-1}$  corresponds to the ester linked acetyl group at 6'/6'' position of the sugar molecule. The bond at  $3325\text{ cm}^{-1}$  corresponded to O–H stretching. The absence of  $1,624\text{ cm}^{-1}$  band corresponding to C=C stretching reveals that cetyl alcohol incorporated into the product is completely saturated. The C–O stretch ( $1,157\text{ cm}^{-1}$ ) of C (–O)–O–C corresponding to lactones was also found missing in crude SLCA. From FT-IR data it could be concluded that cetyl alcohol derived sophorolipids are being synthesized by *Candida bombicola* when supplemented with cetyl alcohol.

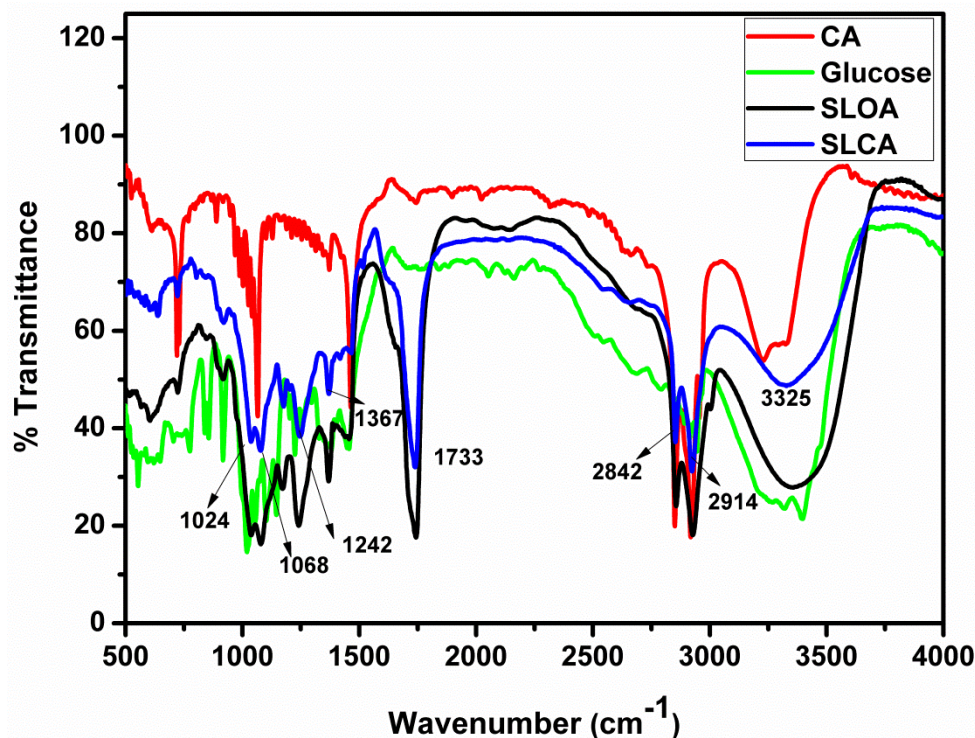


**Figure 2.7** Fourier transform infrared (FT-IR) transmittance spectrum of CA-cetyl alcohol, glucose SLOA-oleic acid derived sophorolipid and SLCA-cetyl alcohol derived sophorolipid.

### c) LC-MS analysis

Sophorolipid biosynthesis takes place by multi-step process, when *Candida bombicola* is supplemented with glucose and a lipophilic carbon source, cetyl alcohol (CA) in our case. Incorporation of CA into the sophorolipid molecule was ascertained by liquid chromatography-mass spectrometry (LC-MS). Components in SLCA mixture varied mainly in the type of terminal group present at the lipophilic end. Two major components are designated as A and B. Component A had a terminal methyl group, thus revealing that sophorose moiety is glycosidically incorporated to the hydroxyl group already present in the cetyl alcohol and therefore bypassing the hydroxylation step carried out by cytochrome P450 monooxygenase enzyme. On the other hand, component B had a more polar terminal ( $-\text{CH}_2\text{OH}$ ) group, which indicated that some percent of the cetyl alcohol provided to the yeast is being hydroxylated by cytochrome P450 monooxygenase enzyme. Two major different forms of SLCA present in the mixture product are given in Table 2.4, which further varied in degree of acetylation at 6' and 6'' position of the sophorose moiety. SLCA subjected to high performance liquid chromatography (HPLC), as mentioned in section 2.2.5c, separated inline based on its polarity. The separated components were ionized by

electrospray in positive mode. The chromatogram of the SLCA mixture is shown in Figure 2.8. Five distinct molecular masses were identified at different retention times that corresponded to different structural forms of SLCA. These molecular forms mainly varied in the end group of the hydrophobic tail. As shown in Figure 2.9a the molecular mass  $m/z$  567.26 of the peak at retention time 5.5 min corresponded to non-acetylated protonated form of component A i.e. SLCA with methyl end group. Similarly the molecular mass  $m/z$  608.30 and 651.26 at retention time of 6.0 min and 7.6 min corresponded to mono-acetylated and di-acetylated protonated forms of SLCA with  $\text{CH}_3$  end group (Figure 2.9 b, c). Molecular mass at two other peaks i.e. 4.6 and 4.9 min had  $m/z$  625.65 and 667.48 that corresponded to mono-acetylated and di-acetylated protonated forms of SLCA with  $\text{CH}_2\text{OH}$  end group (component B) (Figure 2.10 a,b).

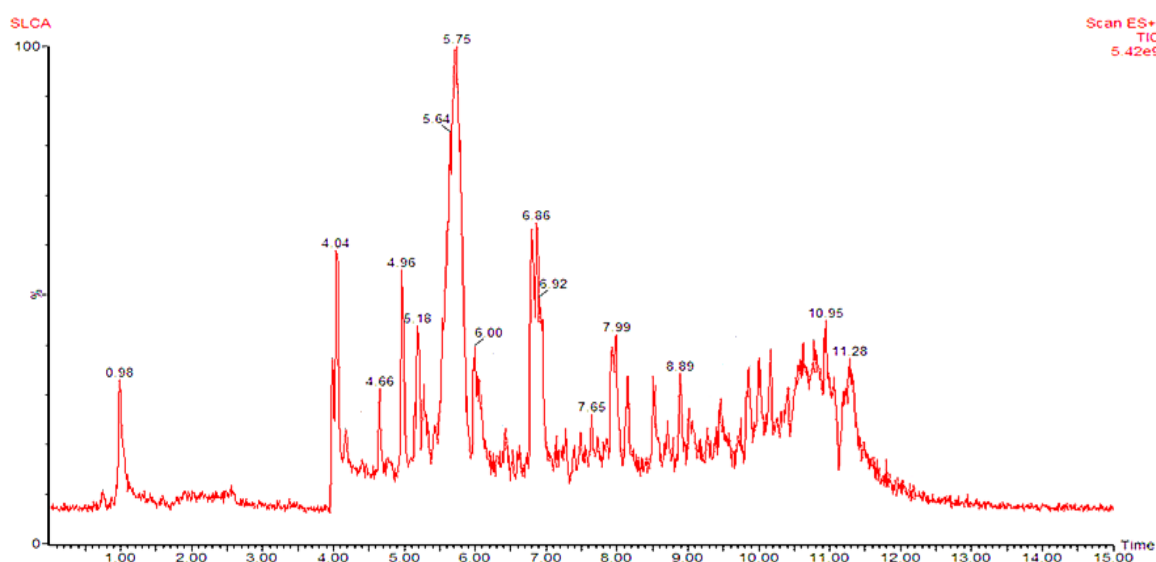


**Figure 2.8** LC-MS chromatogram of SLCA

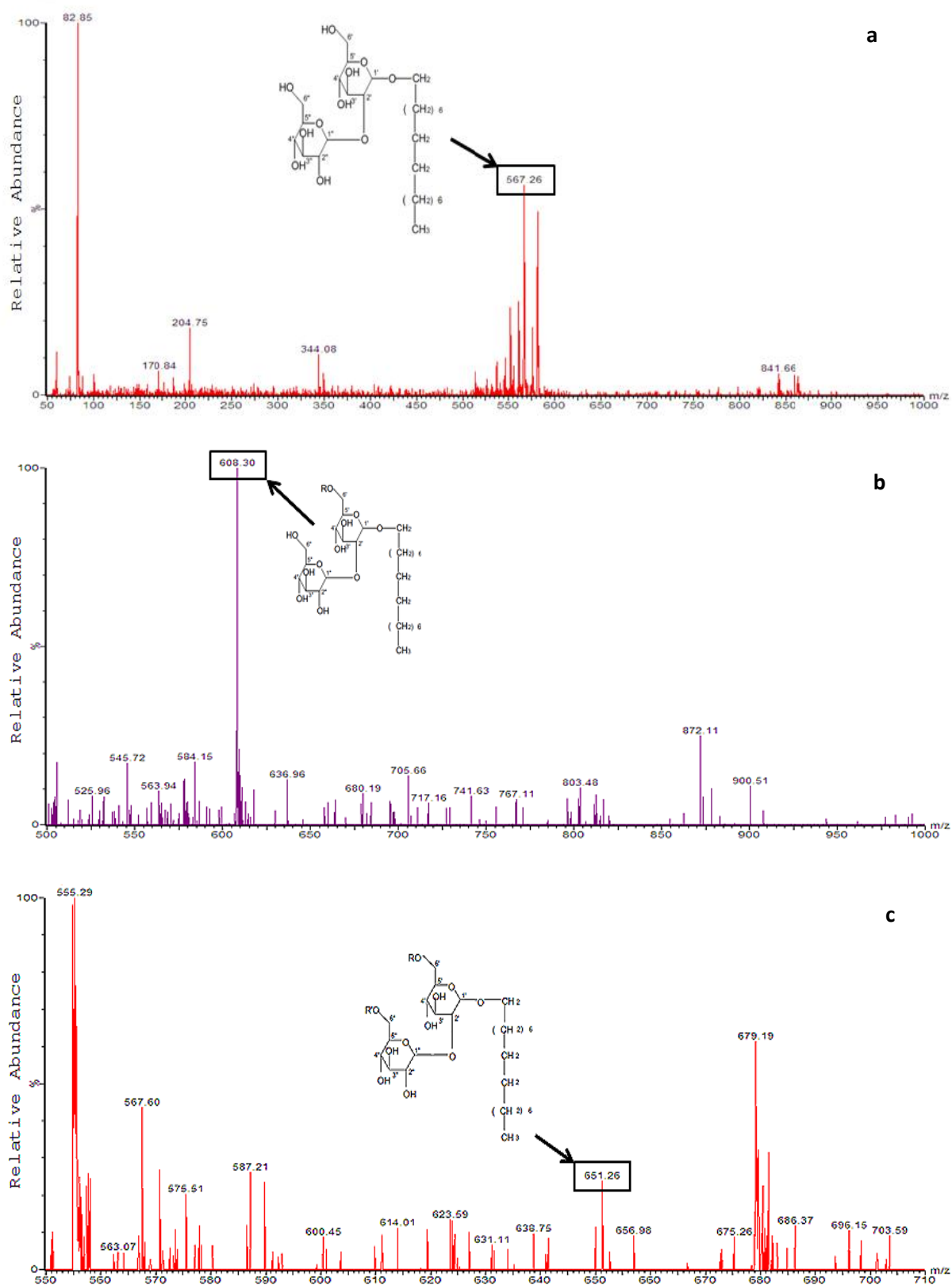


**Figure 2.9** (a) Non-acetylated form of SLCA with methyl end group, (b) mono and (c) diacetylated form of SLCA with CH<sub>3</sub> end group

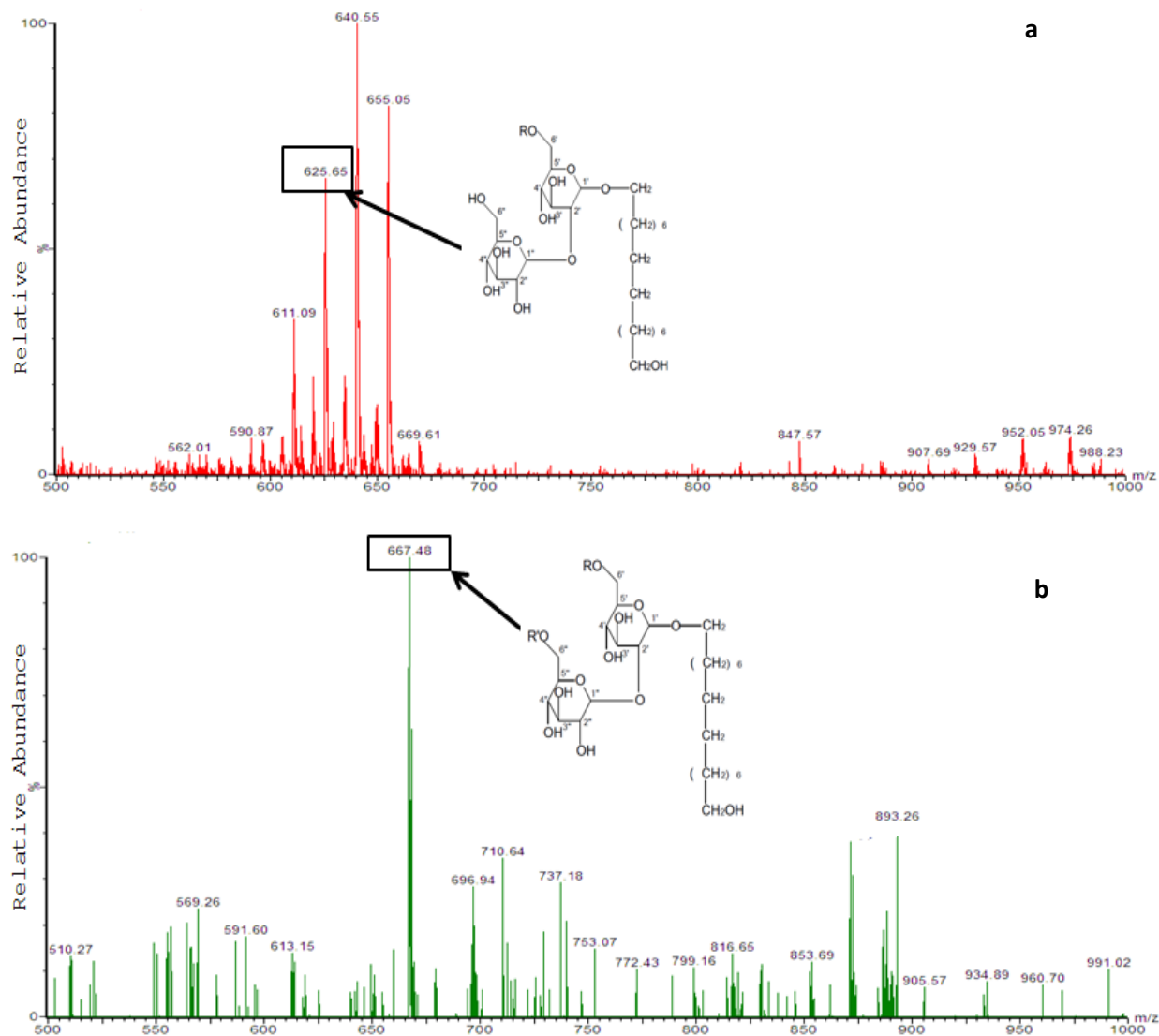
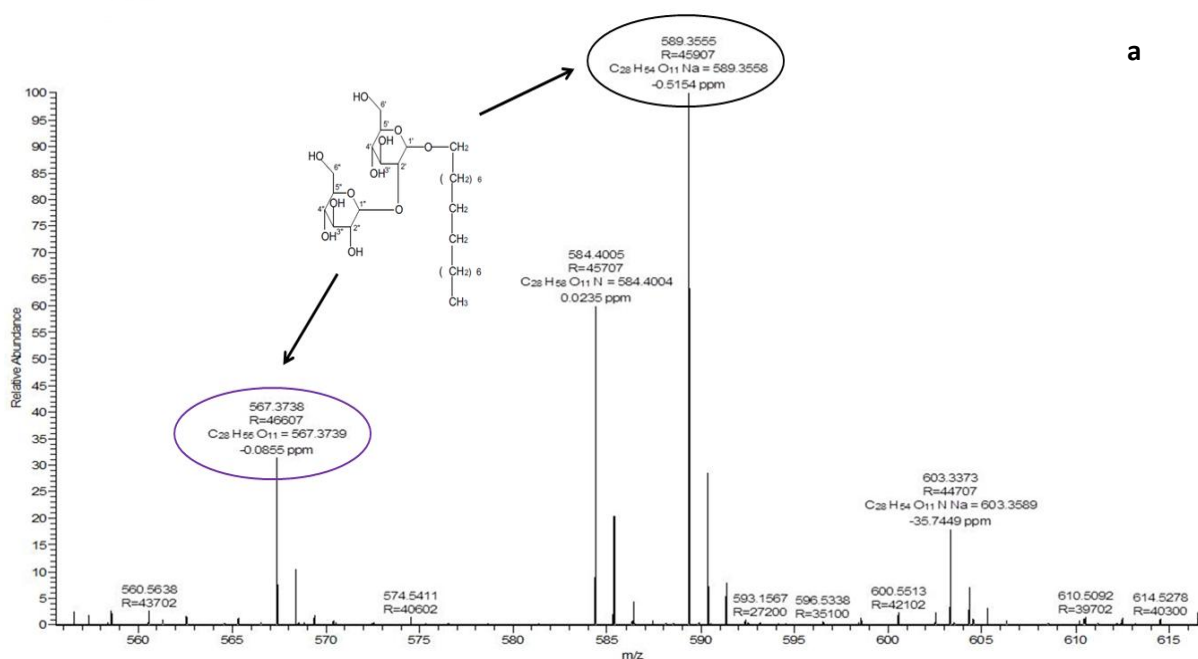


**Figure 2.10** (a) mono-acetylated and (b) di-acetylated forms of SLCA with CH<sub>2</sub>OH end group

#### d) HR-MS analysis

To confirm the different forms of SLCA identified by LC-MS, a highly evolved technique, liquid chromatography high resolution mass spectrometry (LC-HRMS) that provides sensitive, high-quality data was employed. Full-scan HR-MS analysis, followed by post-acquisition ion extraction, was used to identify and confirm different structural forms of SLCA. The ion spectra of component A (non-acetylated, -CH<sub>3</sub> end group), is illustrated in Figure 2.11a. The measured accurate mass (m/z 567.3738 (elemental composition C<sub>28</sub>H<sub>54</sub>O<sub>11</sub>)) of the peak at retention time (RT) 32.11 mins matched the calculated exact mass (m/z 567.3739) of its protonated form. The presence of component A in SLCA mixture was also confirmed by formation of its sodium adducts at m/z 589.3555. The corresponding ion

spectra of the mono-acetylated (1-Ac-CH<sub>3</sub> end group) and diacetylated (1-Diac-CH<sub>3</sub> end group) forms of component A (non-acetylated, -CH<sub>3</sub> end group) are shown in Figure 2.11b and 2.11c. The measured accurate mass ( $m/z$  609.3605) of the peak at RT 35.31 mins matched the calculated exact mass ( $m/z$  609.3695) of protonated mono-acetylated form of component A. Its presence in SLCA mixture was confirmed by formation of its sodium adducts at  $m/z$  631.3658. Similarly the measured accurate mass ( $m/z$  651.3951) of the peak at RT 38.71 mins matched the calculated exact mass ( $m/z$  651.3950) of protonated diacetylated form of component A. Its presence in SLCA mixture was also confirmed by formation of its sodium adducts at  $m/z$  673.3742. The mass accuracy for each compound was within 2 ppm of the corresponding theoretical  $m/z$  value.



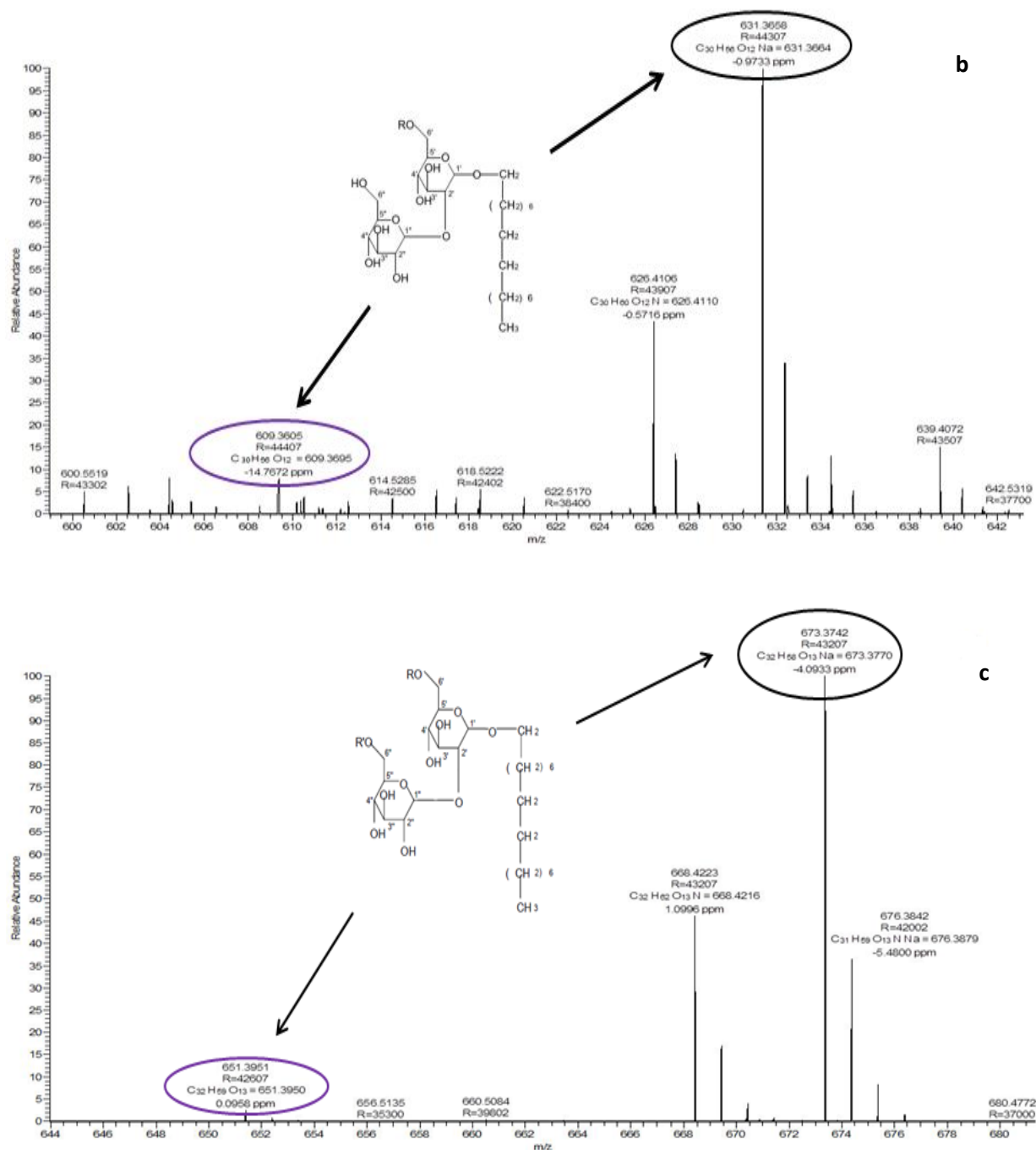


**Figure 2.11** (a) Ion spectra of component A, (non-acetylated, -CH<sub>3</sub> end group). (b) Ion spectra of respective mono-acetylated (1-Ac-CH<sub>3</sub> end group) and (c) diacetylated (1-Diac-CH<sub>3</sub> end group) form of component A, acquired using full-scan liquid chromatography–high-resolution accurate mass spectrometry. The encircled peaks highlight molecular ion and their sodium adducts.

Similarly the ion spectra of component B, (mono-acetylated, -CH<sub>2</sub>OH end group) is illustrated in Figure 2.12a. The measured accurate mass ( $m/z$  625.3796, (elemental composition C<sub>30</sub>H<sub>56</sub>O<sub>13</sub>)) of the peak at RT 24.88 min matched the calculated exact mass ( $m/z$

625.3794) of its protonated form. The corresponding ion spectra of the di-acetylated (2-Diac-CH<sub>2</sub>OH end group) form of component B (mono-acetylated, -CH<sub>2</sub>OH end group) is shown in Figure 2.12b. The measured accurate mass ( $m/z$  667.3885) of the peak at RT 27.04 mins matched the calculated exact mass ( $m/z$  667.3889) of protonated di-acetylated form of component B. Its presence in SLCA mixture was confirmed by formation of its sodium adduct at  $m/z$  689.3713.

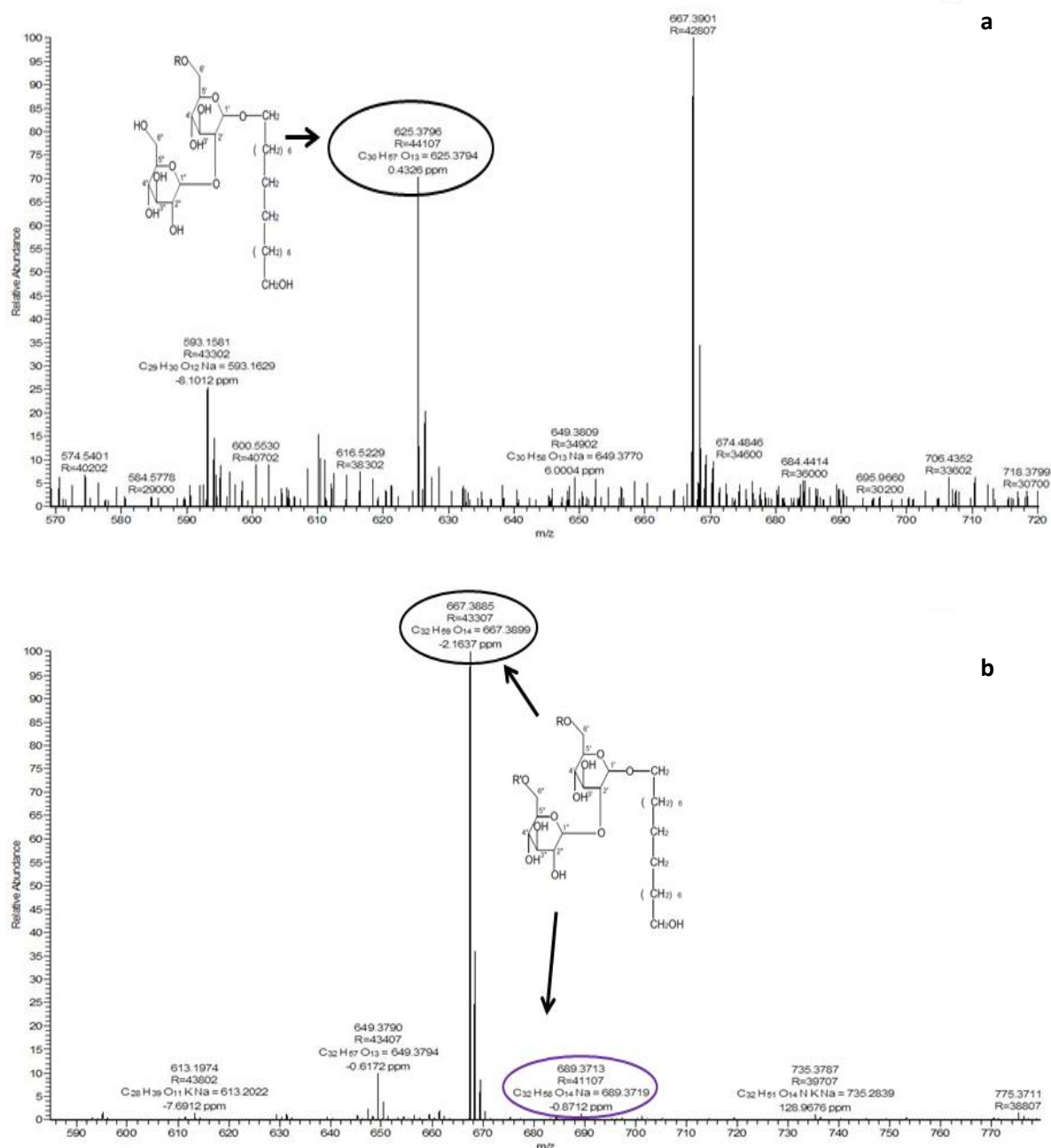


**Figure 2.12** (a) Ion spectra of component B, (mono-acetylated, -CH<sub>2</sub>OH end group) and (b) the corresponding ion spectra of the di-acetylated (2-Diac-CH<sub>2</sub>OH end group) form of component B, acquired using full-scan liquid chromatography–high-resolution accurate mass spectrometry.

**Table 2.4** Different forms of SLCA synthesized by *Candida bombicola* when supplemented with cetyl alcohol and glucose

SLCA components	Structure	Elemental Composition	Theoretical Mass	Practical Mass	PPM error
A) -end CH <sub>3</sub>		C <sub>28</sub> H <sub>54</sub> O <sub>11</sub>	567.3739	567.3738	-0.0855
Ac-end CH <sub>3</sub>		C <sub>30</sub> H <sub>56</sub> O <sub>12</sub>	609.3695	609.3605	-14.7672
Diac-end CH <sub>3</sub>		C <sub>32</sub> H <sub>58</sub> O <sub>13</sub>	651.3950	651.3951	0.0958
B) Ac-end CH <sub>2</sub> OH		C <sub>30</sub> H <sub>56</sub> O <sub>13</sub>	625.3794	625.3796	0.4326
Diac-end CH <sub>2</sub> OH		C <sub>32</sub> H <sub>58</sub> O <sub>14</sub>	667.3899	667.3885	-2.1637

### 2.3.4 Antibacterial activity against Gram-positive and Gram-negative bacteria

Current antimicrobial drugs are encountering increased problem of resistance by pathogenic microorganisms. Thus, there is an imperative need to discover new antimicrobials that are effective against treatment of drug-resistant microorganisms. Sophorolipids, reported to have antimicrobial activity are drawing attention as a safe and effective therapeutic alternative to already existing agents. The proposed underlying action mechanism of sophorolipids on microorganism is the membrane lipid order perturbation that results into their compromised viability.<sup>[162]</sup> With the view to ascertain the possession of antibacterial property by novel sophorolipids synthesized in this study (SLCA), Gram-positive coccus, *Staphylococcus aureus* and Gram-negative bacterium, *Escherichia coli* were chosen as index

bacterium. *S. aureus* is found colonizing anterior nares, skin and gastrointestinal tract of healthy individuals, but it can be markedly pathogenic causing cellulitis, abscesses, endocarditis and sepsis. It has rapidly developed resistance to most of the antibiotics. On the other hand *E. coli* colonizes the lower intestine of warm blooded animals, but its different strains can be highly versatile pathogen causing intestinal and extra-intestinal diseases. The effectiveness of SLCA as antibacterial agent was ascertained by plotting percentage of cell survival against incubation time. A decrease in colony count was observed with increasing amount of SLCA, as well as incubation time in case of both the bacteria.

Figure 2.13, shows that percentage cell survival for *E. coli* dropped to 2.1% (97.9% growth inhibition) after 4 h of exposure to SLCA (90 µg/mL). While in the case of cetyl alcohol (CA, lipophilic substrate), at concentration of 300 µg/mL the percentage cell survival dropped to 7.45% (92.55% growth inhibition) after 4 h of exposure, i.e., substrate concentration required for significantly inhibiting the growth of bacteria was three times more than the product (SLCA). It indicated that by attaching hydrophilic sophorose moiety to water insoluble cetyl alcohol, the organism (*Candida bombicola*) converted the lipophilic substrate into an amphiphilic molecule (SLCA), thus making it water soluble. This resulted into enhanced contact with the bacteria hence decreasing the percentage of cell survival. SLCA almost completely inhibited the growth of *E. coli* at concentration of 300 µg/mL, within 10 mins incubation whereas CA was not effective in completely inhibiting the growth even after 6 h of incubation at the same concentration. MIC value for SLCA was found to be 300 µg/mL, at 10 mins incubation time. The petriplate images depicting the antibacterial action of SLCA against *E. coli* are shown in Figure 2.14.

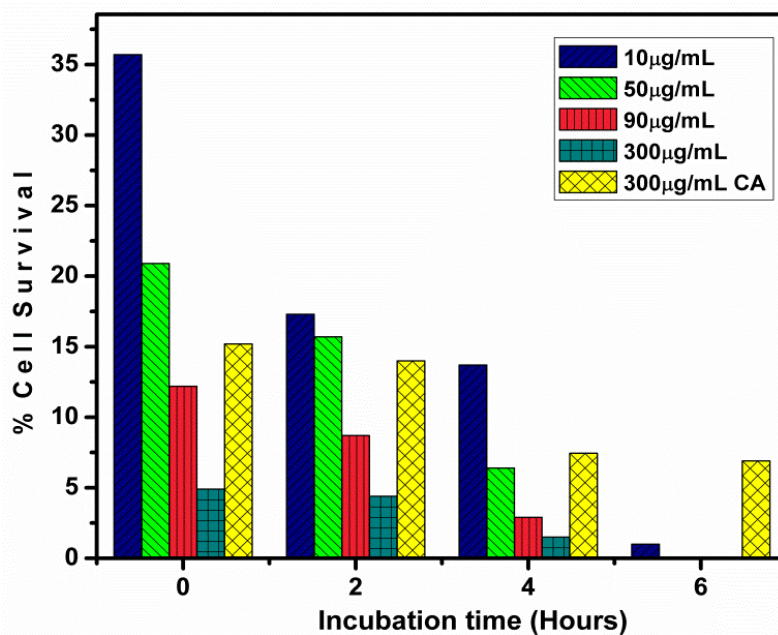


**Figure 2.13** Graph showing antibacterial activity of SLCA and cetyl alcohol against *E. coli* after different incubation time at 37°C

TIME	0 Hour	2 Hour	4 Hour	6 Hour
Conc. Of SLCA	0 Hour	2 Hour	4 Hour	6 Hour
Control				
10 µg/mL				
50 µg/mL				
90 µg/mL				
300 µg/mL				
300 µg/mL CA				

**Figure 2.14** Antibacterial assay plates showing effective killing of *E. coli* with increasing time and concentration of SLCA.

For *S. aureus* (Figure 2.15) the cell survival dropped to 0.26% (99.74% growth inhibition) within 4 h of exposure to SLCA at 300  $\mu\text{g}/\text{mL}$  concentration, whereas in case of cetyl alcohol the percentage survival dropped only to 39.63% (60.37% growth inhibition) after 4 h of exposure to its highest concentration (900  $\mu\text{g}/\text{mL}$ ). Similar to *E. coli*, in case of *S. aureus* also three times more substrate concentration was required to achieve comparable growth inhibition and cetyl alcohol being insoluble in water was not as effective as SLCA in inhibiting the growth of cells. SLCA completely inhibited the growth of *S. aureus* at 300  $\mu\text{g}/\text{mL}$  concentration, after 6 h of incubation whereas CA was not effective in completely inhibiting the growth even after 6 h of incubation at the same concentration. MIC value for SLCA against *S. aureus* was found to be 300  $\mu\text{g}/\text{mL}$ , at 6h incubation time. The petriplate images depicting the antibacterial action of SLCA against *S. aureus* are shown in Figure 2.16

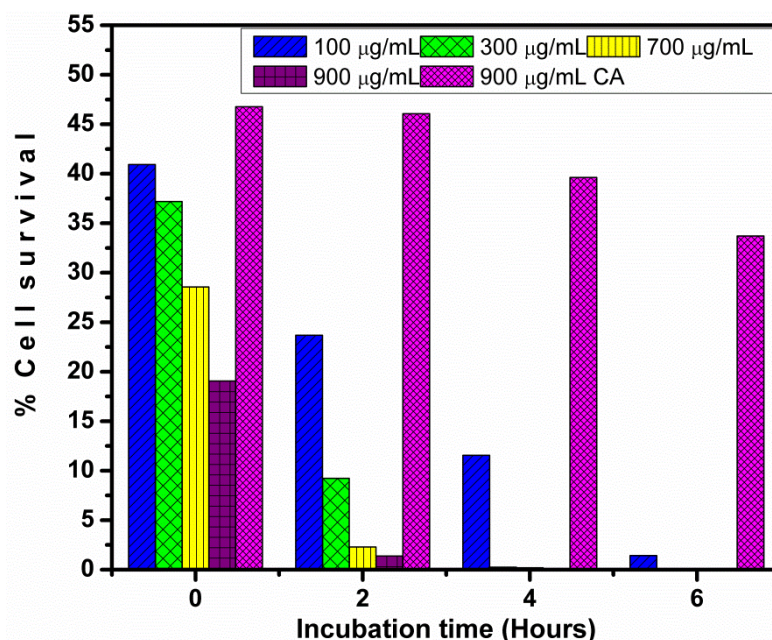


**Figure 2.15** Graph showing antibacterial activity of SLCA against *S. aureus* after different incubation time at 28°C

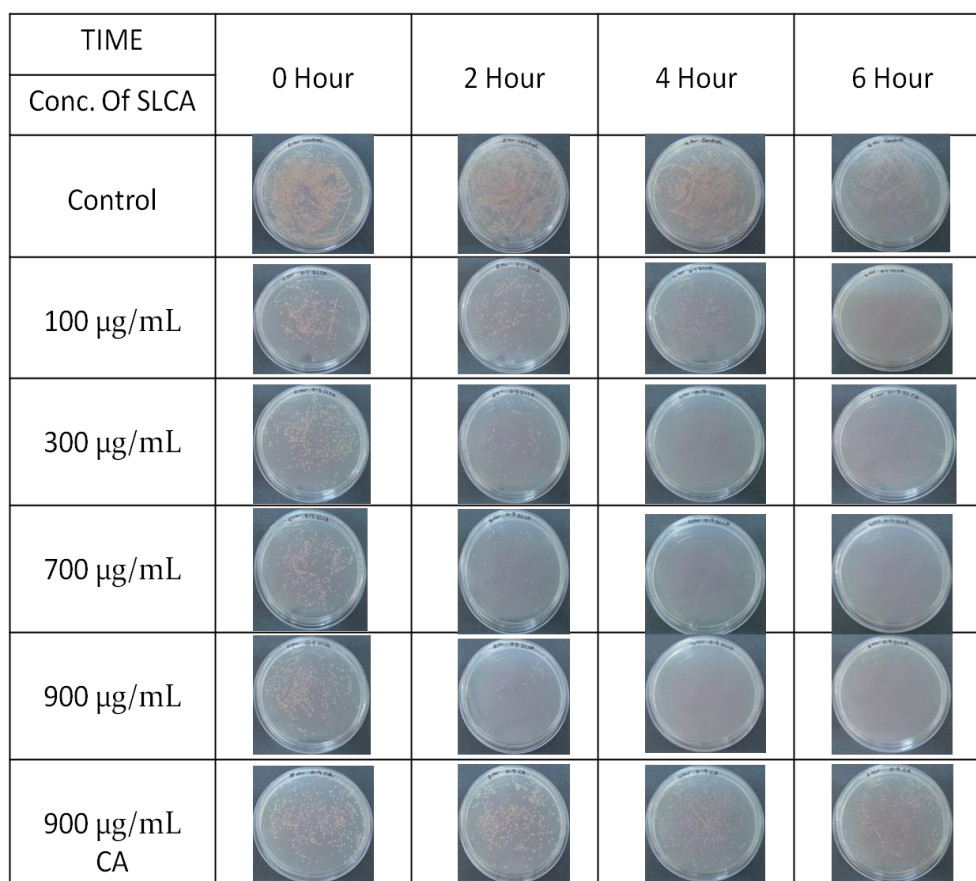


**Figure 2.16** Antibacterial assay plates showing effective killing of *S. aureus* with increasing time and concentration of SLCA.

The antibacterial study carried out by Shah et al. (2007) revealed that SLs are more effective against Gram-positive bacteria than Gram-negative bacteria.<sup>[100]</sup> In agreement to this Joshi-Navare and Prabhune (2011) reported that in case of *E. coli*, oleic acid derived sophorolipids (OASL), at concentration as high as 1000 µg/mL was not sufficient enough to completely inhibit the growth.<sup>[94]</sup> Whereas in our case, it is interesting to observe that inspite of established robustness of Gram-negative bacteria, SLCA proved to be effective against *E. coli* at remarkably low concentration (300 µg/mL). However, complete inhibition of *S. aureus* with same concentration of SLCA (300 µg/mL) required 6 h incubation time. This probably may be due to constitutional variation in the cell membrane of the two bacteria.<sup>[5]</sup> In both the cases it was observed that SLCA is more effective antibacterial agent than its lipophilic substrate, CA. When we compared the inhibitory action of SLCA, it clearly showed to be more potent than other sophorolipids derived from lauryl alcohol<sup>[102]</sup> and oleic acid,<sup>[99]</sup> against both Gram-positive and Gram-negative bacteria (Table 2.5). The substrate used in

the study is commercially used in cosmetics and reported to be non-irritating and non-mutagenic based on clinical studies.<sup>[163]</sup> Thus, as synthesized product retains potential to be used commercially and covers well under green technology approach.

**Table 2.5** Comparative MIC<sub>100</sub> values of three different sophorolipids, SLCA<sup>a</sup> sophorolipid of cetyl alcohol, SLLA<sup>b</sup>-sophorolipid of lauryl alcohol, OASL<sup>c</sup>-oleic acid derived sophorolipid for Gram-positive and Gram-negative bacteria respectively.

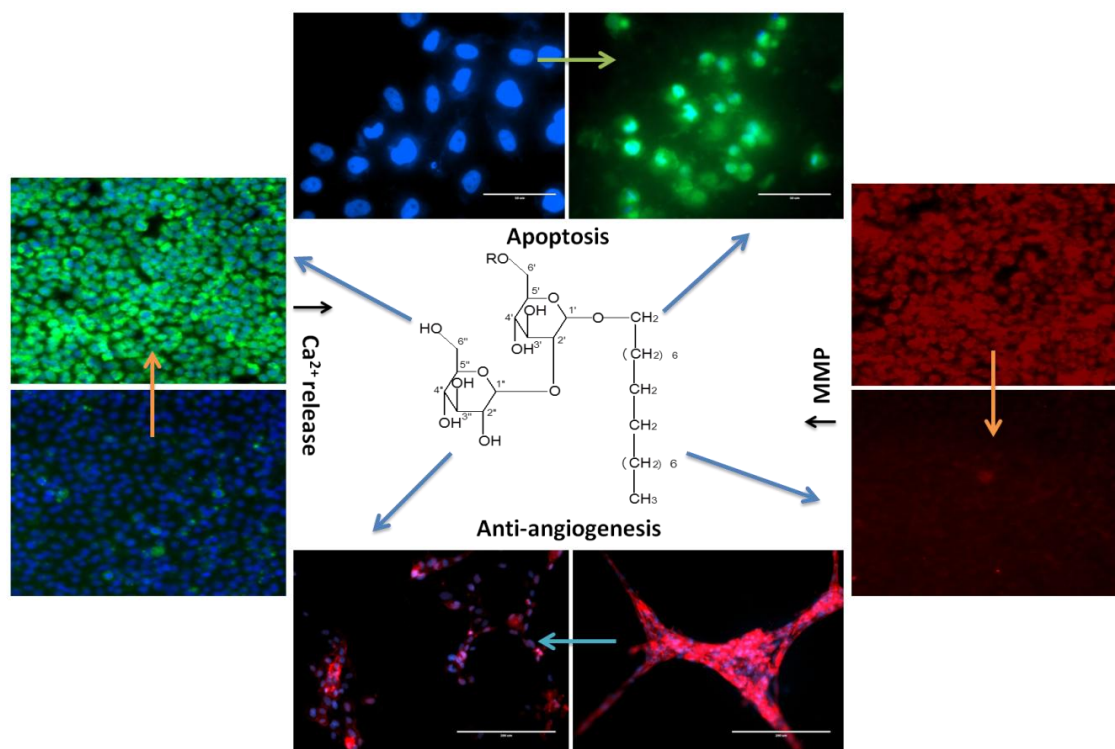
Sophorolipids	Gram-positive ( <i>S. aureus</i> )	Gram-negative ( <i>E. coli</i> )
	MIC <sub>100</sub>	MIC <sub>100</sub>
SLCA <sup>a</sup>	300 µg/mL	300 µg/mL
SLLA <sup>b</sup>	0.6 mg/mL	3 mg/mL
N-SL <sup>c</sup>	>512 µg/mL	>512 µg/mL

## 2.4 Conclusion

To summarize the chapter we have successfully demonstrated the use of cetyl alcohol as the lipophilic carbon feed source for *Candida bombicola*. The primary fatty alcohol (cetyl alcohol) was successfully incorporated into the sophrolipid molecule synthesized by the yeast, yielding a mixture of product. The product synthesized was characterized for the presence of different components and their structure, present in the mixture. Two major forms differing in the type of terminal group present at the lipophilic end of the molecule were confirmed by HR-LCMS. These two forms further varied in degree of acetylation at 6' and 6'' group of sophorose. The effectiveness of the synthesized product as a surfactant was ascertained by measuring its surface tension lowering capacity. In comparison to oleic acid derived sophorolipids, SLCA was found to lower the surface tension of water to a remarkable value i.e. 31.349 mN/m and also had lower CMC value of 104mg/mL. The antibacterial activity against *Staphylococcus aureus* and *Escherichia coli* was found to be higher in comparison to natural sophorolipids and lauryl alcohol derived sophorolipids, thus indicating that SLCA have higher potent antibacterial activity against both Gram positive and Gram negative bacteria, compared to mentioned sophorolipids.

## Chapter 3

# Apoptosis mediated anti-proliferative effect of cetyl alcohol sophorolipids and their anti-angiogenic activity



This chapter elaborates about purified cetyl alcohol sophorolipid and their anti-cancerous studies. Antiproliferative effects of SLs in human carcinoma and primary cells were examined. SLs significantly inhibited the survival of two cell lines HeLa and HCT 116 and were found to be non-toxic towards normal human umbilical vein endothelial cells (HUVEC) even at high concentration. Sophorolipids, SLCA B at 16.32  $\mu\text{g/ml}$  and SLCA C at 14.14  $\mu\text{g/ml}$  enhanced cell cycle arrest at G1/S phase and caspase-3,8,9 expression and reduced mitochondrial membrane potential in HeLa cells in time-dependent manner.  $\text{Ca}^{2+}$  was also found to be involved in mitochondrial depolarization during SLs-induced apoptosis. Further the SLs ability to act as anti-angiogenic molecule in HUVEC cells was explored. Interestingly, these SLs also disrupted the endothelial tubulogenesis. These findings suggest that cetyl alcohol derived SLs could penetrate into HeLa cells and execute anti-tumor activities possibly via inducing caspase dependent mitochondrial apoptotic pathway.

### 3.1 Introduction

Glycolipid molecules and their derivatives have gained importance in therapeutic applications owing to several biological properties displayed by them.<sup>[95]</sup> Sophorolipids (SLs), belong to class of glycolipid biosurfactants that are synthesized extracellularly by certain non-pathogenic yeasts. SLs initially gained attention because of the alkane utilizing ability of the yeasts. But later they exponentially attained recognition owing to possession of several properties such as emulsification, anti-microbial, anti-viral, anti-cancer that played role in detergent industry, cosmetics, pharmaceutical etc.

Anti-cancer property of SLs has been extensively studied in past owing to their promising potential and biocompatibility. Researchers have elucidated the cytotoxic effects of SLs produced from *Wickerhamiella domercqiae* against human lung cancer A549, liver cancer H7402 and esophageal cancer KYSE109, KYSE450 respectively.<sup>[50,96]</sup> The antiproliferative activity of SL against H7402 liver cells was accounted to its apoptosis inducing ability marked by morphological changes such as cell shrinkage, chromatin condensation and membrane blebbing.<sup>[137]</sup> Enhanced cytotoxic effect of SL obtained from *Candida bombicola* against human pancreatic carcinoma cells was demonstrated by their selective derivatization into alkyl esters.<sup>[95]</sup> Additionally, promising anticancer activity of SL against hepatocellular carcinoma HepG2 and lung adenocarcinoma A549, due to inhibition of urokinase and histone deacetylase activities has also been reported.<sup>[164]</sup>

Structurally classical sophorolipids comprise of a hydrophilic dimeric sugar head group known as sophorose, linked glycosidically to a hydrophobic tail of 16-18 carbon fatty acid chain length. But, SLs structure-bioactivity relationship has been tested with a view to achieve enhanced properties by varying the lipophilic feed of the yeast ranging from alkane, fatty acid to fatty alcohol. Similarly to achieve superior biological properties chemoenzymatic modification of SLs has also been done.<sup>[162]</sup> Thus, sophorolipid synthesis has opened new facet for direct applicability and employment of several hydrophobic molecules which being water insoluble have limited biological applications or other setbacks.

Microbial conversion of similar water insoluble lipophilic substrate, cetyl alcohol also commonly known as palmityl alcohol  $[\text{CH}_3(\text{CH}_2)_{14}\text{CH}_2\text{OH}]$  into amphiphilic sophorolipid molecule was carried out as described in chapter 2 section 2.2.3.<sup>[160]</sup> Prior presence of hydroxylated  $-\text{OH}$  group in the fatty alcohol probably bypasses the hydroxylation step in the

SL biosynthetic pathway. Thus altered SLs differing in the hydrophobic tail end with  $-CH_3$  and  $-CH_2OH$  end group are synthesized. This modification from the classical SLs (C18, acidic and lactonic) is expected to impart enhanced or suppressed biological properties comparatively.

Since glycolipids have been shown to possess anticancer activity, novel SL synthesized using cetyl alcohol were column purified and studied for their toxicity against different human cancer cell lines: acute monocytic leukemia THP-1, cervical carcinoma HeLa, colon carcinoma HCT 116, lung adenocarcinoma A549, breast adenocarcinoma MCF-7, pancreas carcinoma PANC-1, and squamous carcinoma A431. Further, the underlying mechanism of anti-proliferative behaviour of SL on HeLa and its anti-angiogenic potential was investigated.

## **3.2 Materials and methods**

### **3.2.1 Sophorolipid production and extraction**

Sophorolipid synthesis and extraction was carried out as described in chapter 2 section 2.2.3. The synthesized product was referred as SLCA (cetyl alcohol derive sophorolipid) and subjected to purification as mentioned below.

### **3.2.2 Column Purification of SLCA**

Silica gel column chromatography was carried out for the separation of crude sophorolipid obtained by fermentation. Brown viscous SLCA was chromatographed on a silica gel column (100-200 mesh size). Elution was performed using chloroform/methanol with increasing amount of methanol (99:1, 98:2 up to 95:5). Successive fractions were collected at regular time interval and solvent was dried under vacuum by rota evaporation. The purity of the compound was primarily checked by thin layer chromatography using chloroform/methanol in 9:1 ratio as solvent and finally liquid chromatography mass spectroscopy was carried out for confirming the molecular weight, thus structure, of the purified sophorolipid.

### **3.2.3 LC-MS of purified cetyl alcohol derived sophorolipids**

The column purified sophorolipids were identified by LC-MS in order to confirm the structure by comparing with already reported data in previous chapter, section 2.3.3d.<sup>[160]</sup> LC-MS Agilent Quadrapole with atmospheric pressure chemical ionization was used to

identify the molecular weight of cetyl alcohol derived sophorolipid. 1mg of purified, concentrated fraction was dissolved in 1 mL methanol and subjected to analysis. The two identified sophorolipids were referred as SLCA B and SLCA C, described later in the result section.

### **3.2.4 Cell Lines and Cell Culture**

The cytotoxic effect of cetyl alcohol derived sophorolipid (SLCA) was determined on HUVECs-primary Human umbilical vein endothelial cells, L929-areolar and adipose tissue fibroblast cells and on different human tumour cells including: THP-1 -acute monocytic leukemia, HeLa-cervix adenocarcinoma, HCT 116-colon carcinoma, MCF-7 -breast adenocarcinoma, A549-lung adenocarcinoma, PANC-1 -pancreatic adenocarcinoma, A431-squamous carcinoma. All cell lines (THP-1, HeLa, HCT 116, A549, MCF-7, PANC-1, A431, L929 and HUVEC) were procured from NCCS Cell Repository, Pune.

Different media were used for maintaining above mentioned cells i.e. for HUVECs, M200 media enriched with 50X Large vessel endothelial supplement (LVES) (Gibco, Invitrogen) was used; for THP-1, RPMI 1640; and for L929, A549, PANC-1 cells, Dulbecco's Modified Eagle Medium (DMEM) was used. Eagle's Minimum Essential Medium (EMEM) was used for culturing HeLa and MCF-7 cells. Serum supplement i.e. fetal bovine serum at 10% concentration (FBS; Gibco) was added to all above media and the atmosphere of 5% CO<sub>2</sub> was created to maintain the cells at 37°C.

### **3.2.5 High Content Screening (HCS) Analysis**

The ability to study multiple features simultaneously in complex biological systems has imparted significant impetus to automated microscope based High Content Screening (HCS, or HCA, HCI). Thus, HCS was employed to predict and validate cell cycle distribution analysis, annexin V-FITC apoptosis analysis, mitochondrial depolarization, release of intracellular [Ca<sup>2+</sup>]<sub>i</sub> study and to investigate anti-angiogenic activity of sophorolipids.

### **3.2.6 Experimental assays**

#### **a) Cell viability assay**

Dose-dependent anti-proliferative effects of SLs was investigated by MTT assay.<sup>[165]</sup> It is the best known enzyme-based assay that determines mitochondrial dehydrogenase activity in

the metabolically active living cells. In this method, MTT, a yellow tetrazolium dye (3-(4,5-dimethylthiazol-2-yl)-2,5-diphenyltetrazolium bromide) is reduced into an insoluble dark purple color formazan product, by the action of NADPH dependent mitochondrial reductase enzyme. The formazan crystals are then solubilized using organic solvent and the absorbance is measured spectrophotometrically.

Cells with a density of  $1 \times 10^5$  cells/ml were seeded in growth media containing all supplements with 10% FBS and grown overnight on a 96-well plate. After 24 h incubation, cells were treated with increasing concentrations of sophorolipids (10, 20, 40, 80, 160, 200, 250, 320  $\mu\text{g/ml}$  final concentrations) at  $37^\circ\text{C}$  with 5%  $\text{CO}_2$  for 48 h. Doxorubicin and Paclitaxel were used as positive controls. Doxorubicin is DNA-intercalating drug that inhibits enzymatic activity of DNMT1 *in vitro* <sup>[166]</sup> while paclitaxel is a chemotherapy drug that interferes with the normal breakdown of microtubules during cell division and is used to treat cancers including ovarian, breast and non-small cell lung cancer. <sup>[167]</sup> Wells containing culture medium and MTT but no cells acted as blanks. *In vitro* efficacies of two SLs (SLCA B & C) were studied against HUVECs and human cancer cell lines. After 48 h of SL treatment, antiproliferative effect was assessed using modified MTT cell viability assay. <sup>[168]</sup> The treated cells were first washed three times with 1 mL phosphate buffer saline. Then 0.01 ml MTT solution prepared in PBS at 5mg/mL concentration was added to each well and incubated for 4 h at  $37^\circ\text{C}$ . The cells were then treated with acidified (0.2 mL of 0.04 N HCl) isopropanol to solubilize the formazan crystals formed in viable cells and measured spectrophotometrically. Optical density was measured at 570 nm using SPECTRAmax PLUS 384 plate reader (Molecular Devices Inc, USA). <sup>[169]</sup> Each experiment was corrected for the presence of sophorolipid in media (sophorolipid control). These controls were incubated in the same experimental assay 96-well plate. All experiments were conducted in triplicates, and respective measurements were presented as the average  $\pm$  standard deviation.  $\text{IC}_{50}$  value for both the sophorolipids was calculated from the data as concentration that results in 50% growth inhibition *in vitro*.

### **b) Cell cycle distribution**

The cell cycle assay allows determination of different cell cycle stages. The cell cycle has four sequential phases: G0/G1 (first growth phase), S (synthesis), G2 (second growth phase), and M (mitosis). Normal cells in the G0/G1 phase of the cell cycle have 2N DNA content (i.e., two

copies of each chromosome), and after DNA replication in the S phase, the DNA content doubles to 4N (four copies of each chromosome) in the G2 phase.<sup>[170]</sup> Thus, by quantifying the DNA content by using fluorescent nuclear stain DAPI (4',6-diamidino-2-phenylindole) that binds to A-T rich region of DNA, the cell cycle stage of a cell can be determined. The DAPI fluorescence intensity measured within the nucleus is proportional to the cell's DNA content. For the study carboplatin and paclitaxel were used as positive control. Carboplatin is an antineoplastic drug used to treat certain forms of cancers (ovarian, lung, breast etc.) by hampering DNA repair.

The effects of SLCA B (16.32  $\mu\text{g/ml}$ ), SLCA C (14.14  $\mu\text{g/ml}$ ) at  $\text{IC}_{50}$  concentration determined by cell viability assay, carboplatin (0.85  $\mu\text{g/ml}$ ), paclitaxel (0.13  $\mu\text{g/ml}$ ) on cell cycle distribution was evaluated for time interval of 6, 12, 18 and 24 h respectively. Treated cells were harvested by centrifugation at 1,000 rpm for 5 min at room temperature. Supernatant was discarded and cells were washed with cold 1X PBS. Cells were fixed with 3.7 % paraformaldehyde at 37°C for 15 minutes. Fixed cells were again washed with PBS and then resuspend in a staining solution containing DAPI (1 $\mu\text{M/ml}$ ) and incubated at room temperature for 15 min in the dark. The DNA content was measured by acquiring images using a laser-scanning confocal microscope as 4X4 binning with an X20 objective (Olympus FV1000). The acquired images were processed using Thermo Scientific™ HCS Studio™ 2.0 Cell Analysis Software and different cell percentages in G1 phase, S phase, and G2/M phase were calculated.

### **c) *Annexin V-FITC Apoptosis Assay***

The process of apoptosis is marked by flipping of phosphatidyl serine (PS) from the cytoplasmic leaflet to outer layers of the plasma membrane. A phospholipid binding protein Annexin V, has high affinity for PS and can bind to it in a  $\text{Ca}^{2+}$  dependent manner.<sup>[171]</sup> Thus to evaluate the occurrence of apoptosis, binding of annexin V-FITC to PS was used as the principle of apoptosis assay, followed by high content screening. HeLa cells were treated with sophorolipids SLCA B (16.32  $\mu\text{g/ml}$ ) and SLCA C (14.14  $\mu\text{g/ml}$ ) for the time interval of 2, 24, 48 and 72 h. Post-incubation after harvesting, the cells were subsequently treated with annexin V-binding buffer comprising of annexin V-FITC, DAPI and propidium iodide (PI) at 3  $\mu\text{g/ml}$ , 1 $\mu\text{M/ml}$  and 10 $\mu\text{g/ml}$  concentration respectively.<sup>[172]</sup> The number of cells undergoing apoptosis were examined using LSCM (20X magnification, Olympus FV1000) and Thermo

Scientific™ HCS studio™ 2.0 software was used for three dimensional multichannel-image processing.

**d) Mitochondrial membrane depolarization Assay**

In order to determine mitochondrial dysfunction, mitochondrial membrane potential (MMP) was investigated using Mito Tracker Red (Invitrogen), a mitochondrial potential sensor.<sup>[173]</sup> MitoTracker® Red is a cationic non-cytotoxic fluoro-chrome dye that stains viable cells by passively diffusing through the plasma and sequestering in mitochondria with active mitochondrial membrane potential ( $\Delta\psi_m$ ).<sup>[174]</sup> HeLa  $1 \times 10^5$ /ml cells treated with sophorolipids SLCA B (16.32  $\mu\text{g/ml}$ ) and SLCA C (14.14  $\mu\text{g/ml}$ ) for 2, 24, 48 and 72 h were stained with 0.1  $\mu\text{mol/L}$  Mito Tracker Red and incubated at 37°C for 15 mins. Post-incubation, the cells were washed, fixed and then stained with 1 $\mu\text{M/ml}$  DAPI. Further, LSCM was used to acquire images of the stained cells and analysis was carried out by employing HCS using fluoresces red, excitation 525 nm, emission 590 nm. The uptake of Mito Tracker Red in sophorolipid treated cells represented an alteration in the  $\Delta\psi_m$  whereas a decrease in red fluorescence intensity signified mitochondrial membrane dysfunction.

**e) Intracellular cytoplasmic calcium release [ $\text{Ca}^{2+}$ ]<sub>i</sub> Assay**

The effect of SLs on [ $\text{Ca}^{2+}$ ]<sub>i</sub> release was examined quantitatively and qualitatively using Fluo 4-acetoxymethyl ester (Fluo 4-AM); a fluorescent  $\text{Ca}^{2+}$  sensitive dye.<sup>[175]</sup> Briefly, HeLa  $1 \times 10^5$ /ml cells were stimulated with sophorolipids for 4, 8 and 12 h. After incubation, the cells were washed twice with phosphate buffer saline (PBS) and solution of Fluo-4/AM (4  $\mu\text{mol/L}$ , Invitrogen) was prepared in HEPES buffer saline (20 mmol/L HEPES, 115 mmol/L NaCl, 13.8 mmol/L glucose, 0.8mmol/L  $\text{MgCl}_2$ , 1.8 mmol/L  $\text{CaCl}_2$ , 5.4 mM KCl, pH 7.4)<sup>[176]</sup> which was used to stain the cells. Nuclei were stained with DAPI. An alteration in released calcium level was detected using LSCM by measuring the green fluorescence (excitation 490 nm, emission 530 nm).

**f) Caspases activity assay**

Caspase activities were quantified using Caspase Activity Assay Kit (Promega, USA) according to the manufacturer's instructions. The fold increase in the activity of caspases was calculated for sophorolipid treated cells with respect to the control cells. For measuring the

activity of caspase-3, HeLa cells were treated with sophorolipids for indicated time and lysed at 4°C for 10 mins using lysis buffer provided by Molecular probes, USA in EnzChek® Caspase-3 Assay Kit. Briefly, to determine the caspase activity respective substrate and reversible aldehyde inhibitors are added and the plates are incubated at 37°C for 1h.<sup>[173,177]</sup> The detection of caspase 3 is done using a weakly fluorescent aminomethylcoumarin (AMC) derived substrate (Z-DEVD-AMC) and its inhibitor (Ac-DEVD-CHO). The enzymatic cleavage of the substrate yields bright fluorescent product that can be detected spectrophotometrically (excitation/emission maxima ~342/441 nm). The use of inhibitor confirms that fluorescent signals arise exclusively by the enzymatic caspase activity. Similarly for caspase 8 and caspase 9 the substrates used for detection are Acetyl-Ile-Glu-Thr-Asp p-nitroaniline (Ac-IETD-pNA) and acetyl-Leu-Glu-His-Asp-p-nitroaniline (Ac-LEHD-pNA) respectively. During incubation these substrates are cleaved by caspases 8 and 9 and p-nitroaniline (p-NA) is released. The resultant fluorescence intensity of the cleaved product at 405 nm was quantified using VarioskanFlash plate reader. The increase in caspases activity was calculated for sophorolipid treated cells with respect to the control cells.

### **3.2.7 Anti-angiogenesis activity of sophorolipids**

The anti-angiogenic potential of sophorolipids was evaluated by *in vitro* capillary tube formation assay with HUVECs.<sup>[168]</sup> For the HUVEC tube formation assay the cells were plated onto a matrigel in standard eppendorf 96-well clear-bottom microtiter plates. Cells with a density of  $2 \times 10^4$  cells/well were treated with the established pro-angiogenic compounds, Vascular Endothelial Growth Factor (VEGF) at the concentration of 1 ng/ml for 16 h. VEGF helps to promote angiogenic tube formation. Tube formation was prevented by the use of SLCA B (16.32 µg/ml) and SLCA C (14.14 µg/ml) sophorolipids and suramin (40 µM) as a positive control.<sup>[178–182]</sup> After 16 h incubation, the media was removed and cells were washed, fixed (0.5% buffered paraformaldehyde), and tubes were stained with rhodamine conjugated phalloidin (2 Units) and the nuclei were labelled with nuclear stain, DAPI (1 µM). The rhodamine phalloidin is a whole cell stain that enables identification of entire tube by labelling F-actin. The DAPI labelled cells enabled estimation of the number of nuclei per tube. 96-well plate was automatically imaged on HCS Reader Cellomics' ArrayScan®.

### 3.3 Results and Discussion

#### 3.3.1 Purified Sophorolipid Structure

The two sophorolipids that showed promising biological activity in this study were confirmed to be cetyl alcohol derived sophorolipid. The significant ions that occurred at  $m/z$  589 and  $m/z$  631 for fraction B and C were sodium adducts (Figure 3.1a,b). The structures were determined as the non-acetylated and mono-acetylated forms of sophorolipid with sophorose head group and 16 carbon fatty tail ending with terminal methyl group, respectively. These two compounds were further abbreviated as SLCA B and SLCA C for cell studies.

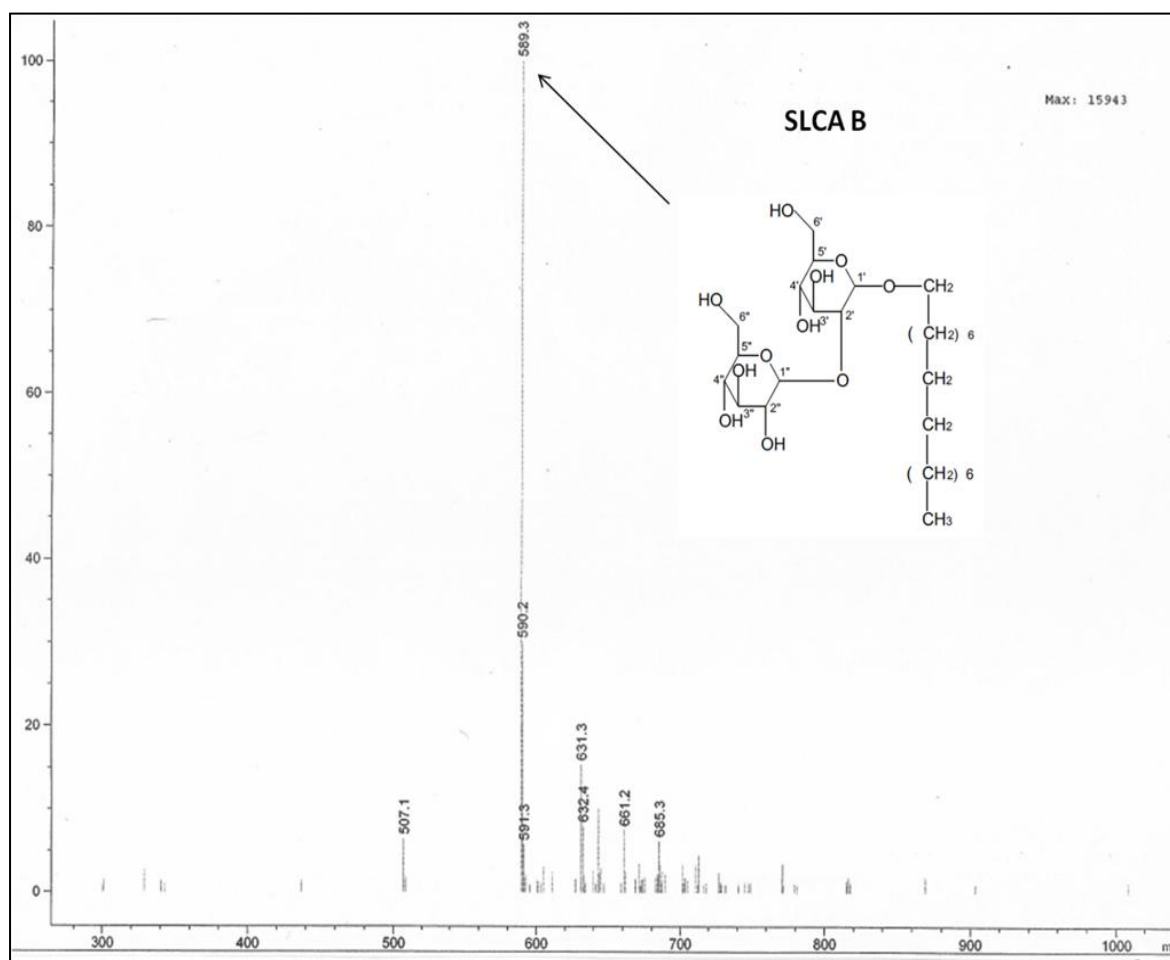


**Figure 3.1a** Ion Spectra and structure of sodium adduct of non-acetylated form of cetyl alcohol sophorolipid with methyl end group.

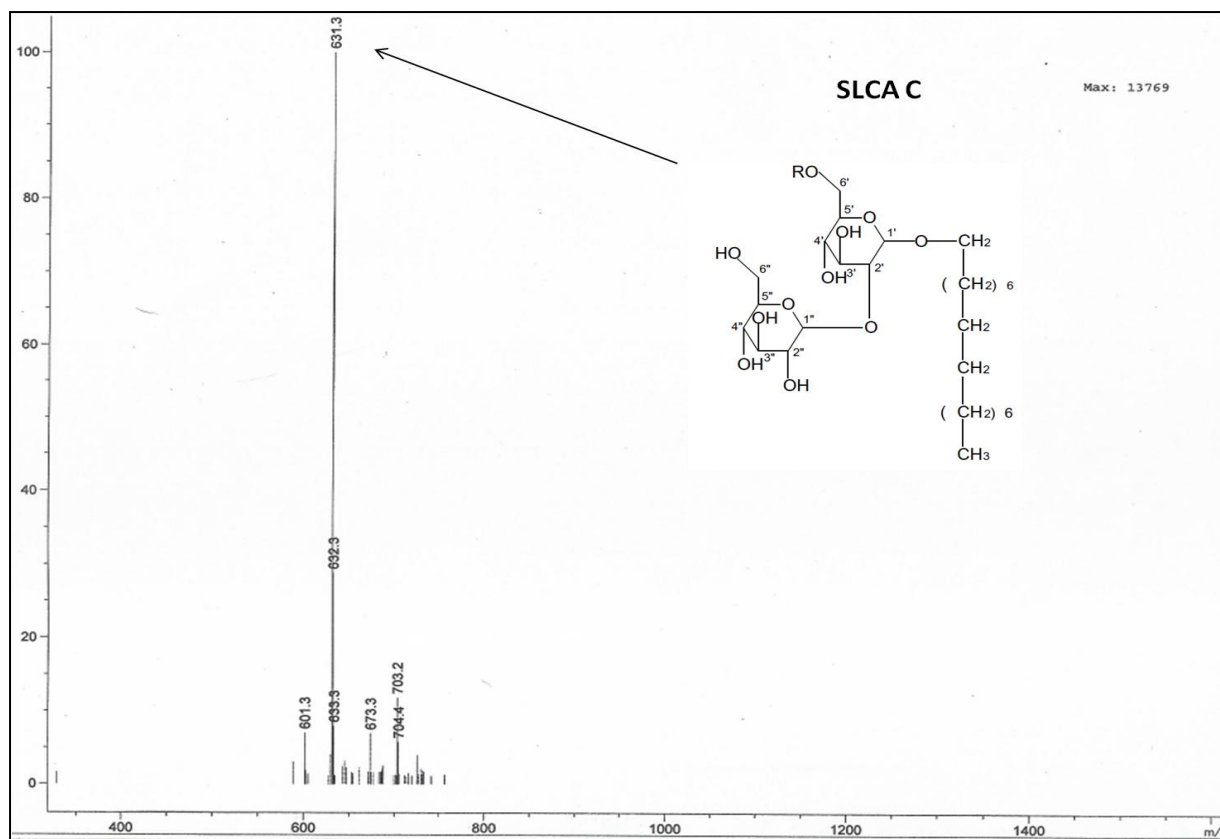


**Figure 3.1b** Ion Spectra and structure of sodium adduct of monoacetylated form of cetyl alcohol sophorolipid with methyl end group.

### 3.3.2 Determination of cell viability

Sophorolipids being amphiphilic in nature partially resemble the cell membrane lipids, thus they are able to span through the membrane and gain entry inside the cell. Also, sophorolipids possess unique ability to negatively impact cancerous cells and remain indifferent towards normal cells. On the contrary current therapeutic regimes lack this additional property. Thus, use of SLs can prove to be beneficial over them in curtailing the associated side effects.<sup>[136]</sup>

Different glycolipids have been reported to possess anticancer effects on lung, cervical, breast and brain cancers.<sup>[183]</sup> To examine the antitumor activity of two sophorolipids derived from cetyl alcohol (SLCA B and SLCA C) in human carcinoma cells, exponentially dividing primary (HUVECs) and human cancer cells (THP-1, HeLa, HCT 116, A549, MCF-7, PANC-1 and A431), the cells were treated with increasing concentrations of SLs, and cell viability was measured over time by the MTT assay (Figure 3.2a-c). As a reference, two different types of anticancer drugs, doxorubicin and paclitaxel were used.

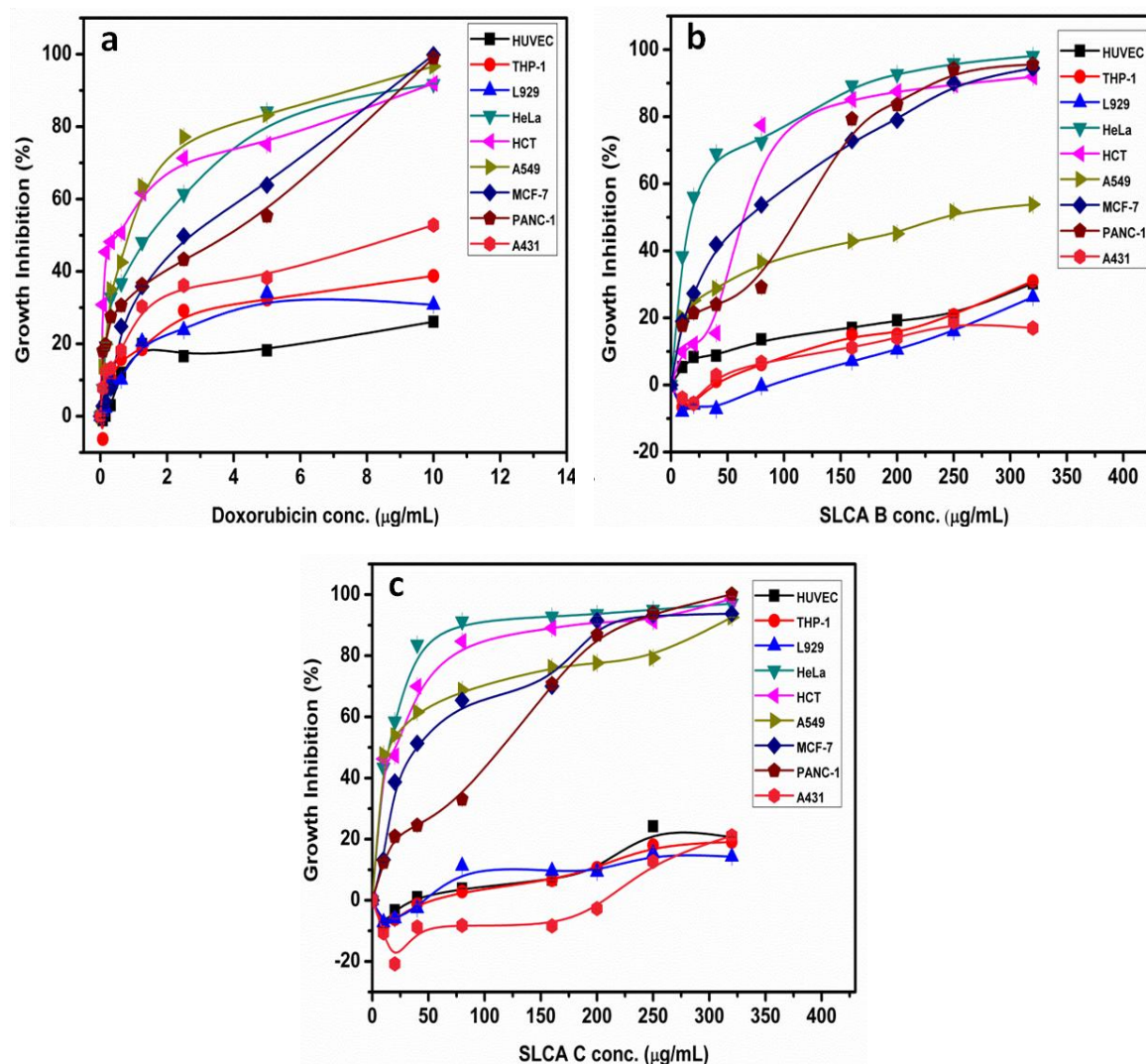


**Figure 3.2** MTT assay. HUVEC cells and varied cancer cell lines subjected to different concentrations of doxorubicin, SLCA B, SLCA C for 48 h and the % growth inhibition as calculated for different treatments; (a) doxorubicin (b) SLCA B (c) SLCA C by MTT assay,  $n=3$ , Mean value  $\pm$  SD

In comparison to DMSO treated control, SLs markedly resulted in growth inhibition and significant decrease in the viability of HeLa cells with  $GI_{50}$  value (SLCA B-16.32 µg/ml; SLCA C-14.14 µg/ml) and  $GI_{90}$  (SLCA B-162.08 µg/ml; SLCA C-71.47 µg/ml) and HCT 116 cells with  $GI_{50}$  value (SLCA B-62.77 µg/ml; SLCA C-23.22 µg/ml) and  $GI_{90}$  (SLCA B-262.9 µg/ml; SLCA C-170.68 µg/ml) in a concentration-dependent fashion (Table 3.1). It is noteworthy that sophorolipids did not demonstrate the cell toxicity towards HUVECs and L929 cells (<20% at 320 µg/ml), implying its non-toxicity towards normal cells. Thus, the application of SLs for cancer prevention or therapy might be safe. Also, 50% of cell growth inhibition was observed in A549, MCF-7, PANC-1 and A431 cells at concentration above 65 µg/ml and 14 µg/ml in SLCA B and SLCA C respectively. These preliminary data suggested that both the

sophorolipids had high inhibitory effect on human cervix adenocarcinoma (HeLa) and colon carcinoma (HCT 116), but dose required for inhibition of HeLa cells was lower. In order to understand the mechanism by which SLCA functioned, the effects of sophorolipid on HeLa cells was further investigated.

**Table 3.1** Growth Inhibition (GI): GI<sub>50</sub>/GI<sub>90</sub> in µg/ml values of Sophorolipids on different cell lines derived from MTT assay

Cell Name	SLCA B		SLCA C		Doxorubicin		Paclitaxel	
	GI <sub>50</sub>	GI <sub>90</sub>						
HUVEC	> 320	> 320	> 320	> 320	>10	>10	>10	>10
THP-1	> 320	> 320	> 320	> 320	>10	>10	0.1374	5.814
L929	> 320	> 320	> 320	> 320	>10	>10	>10	>10
HeLa	<b>16.32</b>	<b>162.08</b>	<b>14.14</b>	<b>71.47</b>	1.45	8.83	0.0048	0.075
HCT 116	<b>62.77</b>	<b>262.9</b>	<b>23.22</b>	<b>170.68</b>	0.54	9.62	0.026	5.21
A549	236.32	> 320	14.95	308.93	0.87	7.91	0.0035	0.0706
MCF -7	65.7	250.86	37.71	197.11	2.52	8.71	0.0021	0.0502
PANC-1	113.52	229.55	116.33	224.01	3.96	9.01	0.1279	5.715
A431	> 320	> 320	> 320	> 320	9.05	>10	1.64	4.83

### 3.3.3 Monitoring cell cycle progression

The cytotoxicity caused by SLs may be resultant of anti-proliferative and pro-apoptotic effects. Thus, to affirm the association of apoptosis with decreasing cell viability, induced by sophorolipids in HeLa cells, cell cycle arrest was investigated.<sup>[181]</sup> The effect of SLs on cell cycle was determined by HCS-DAPI staining. In exponentially dividing cultures of HeLa cells treated with dimethyl sulfoxide (DMSO), the percentages of cells in different stages of cell cycle i.e. G<sub>0</sub>/G<sub>1</sub>, S, and G<sub>2</sub>-M phases were calculated (Figure 3.3).<sup>[165]</sup> The DAPI fluorescence intensity measured within the nucleus is proportional to the cell's DNA content. As shown in Figure 3.3, exposure of HeLa cells to SLs resulted in an increase in the G<sub>1</sub>/S phase population at G<sub>1</sub> phase (~ 55 % populations till 24 h) and partly at S phase (~ 33 % populations till 24 h), as compared to 7.13 – 2.2% in untreated cells, indicative of early

G1-S block. There was an approximate 89% decrease at M phase in SL treated cells in comparison to the untreated cells. Hence, SLs exerted proliferation-inhibitory effects on the HeLa cells via G1/S phase arrest in a time-dependent manner; arresting the cells at G1/S phase for 6, 12, 18 and 24 h (Figure 3.3). It was found that (6 h) treatment with doxorubicin resulted in G2 phase (~ 60 % population) arrest whereas further continuous treatment for 24 h resulted in arrest at G0/G1 phase in HeLa cells. The control cells exhibited all the cell cycle phases i.e. G0/G1, S and G2/M whereas paclitaxel treatment resulted in G2/M phase (~ 55 % / ~ 25 % populations till 24 h) arrest.

The hindrance in the normal functioning of the cell cycle thus results into SL induced anti-proliferative effects. Additionally, a remarkable increase in the hypodiploid DNA content pertaining to G1 phase in HeLa cell lines resulted in an increase in SL induced apoptotic cell death. For mammalian development, cell growth and proliferation progress via normal functioning of the cell cycle whereas its failure can trigger apoptosis.<sup>[136,184]</sup> Subsequently, the ability of SLs to cause apoptosis in HeLa cells was examined by Annexin V/PI analysis with HCS.

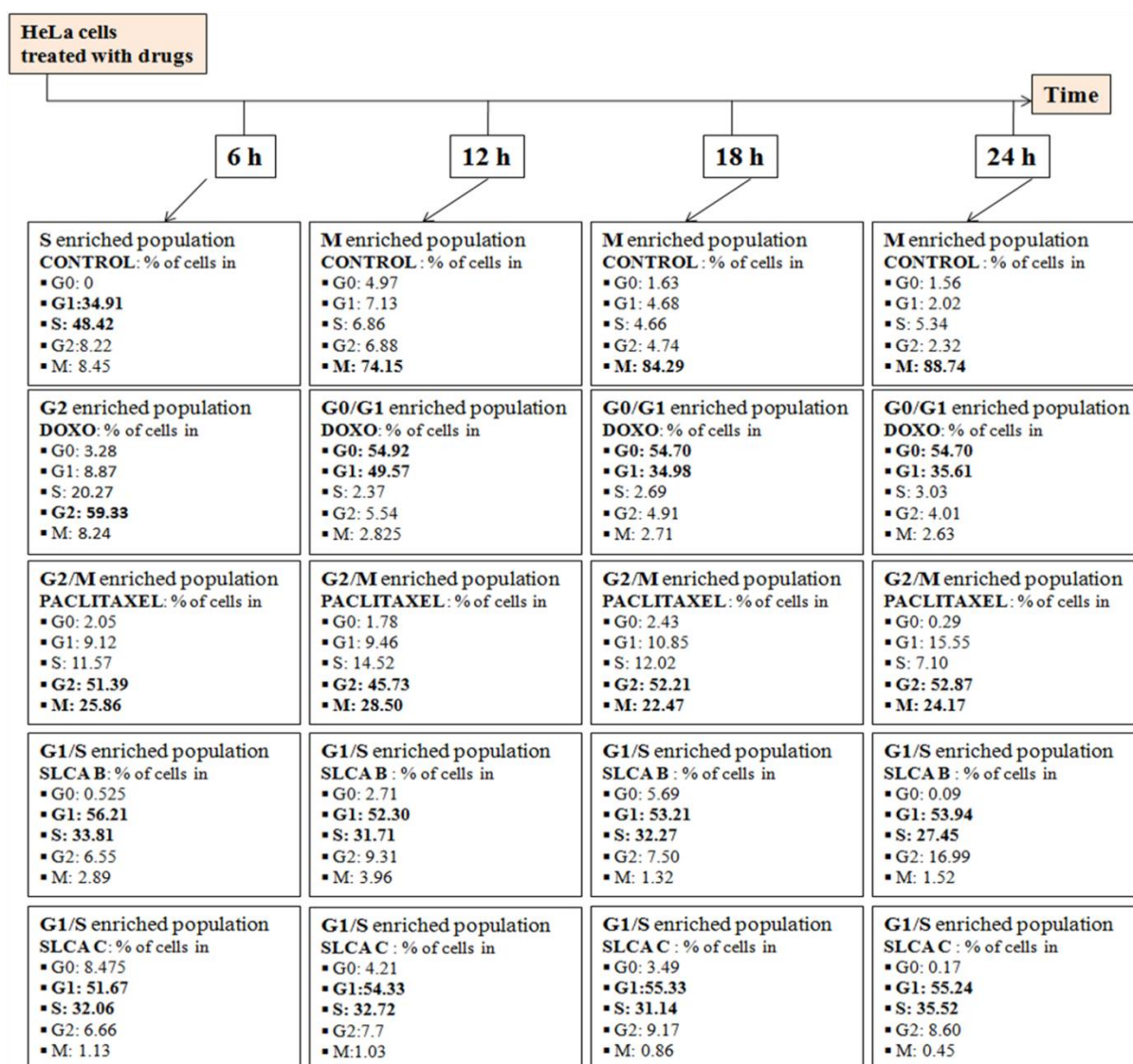


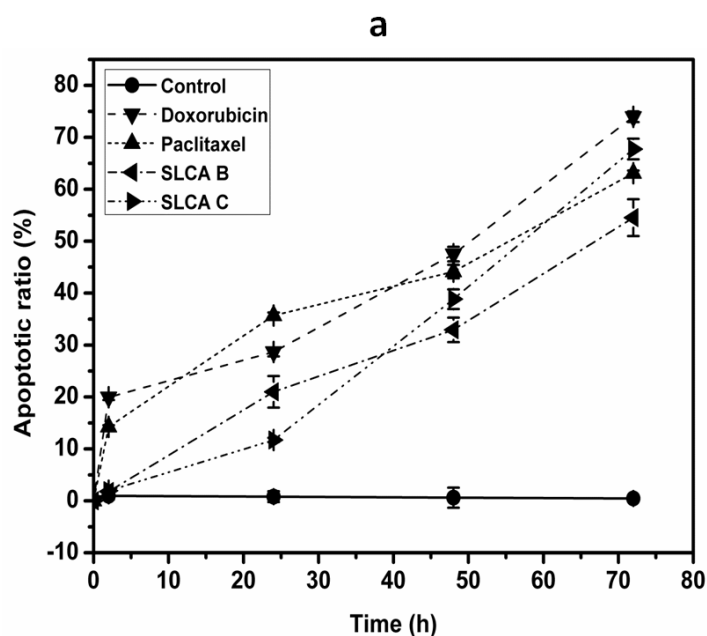
**Figure 3.3** Effect of SLCA B (16.32  $\mu\text{g/ml}$ ), SLCA C (14.14  $\mu\text{g/ml}$ ), Doxorubicin (1.45  $\mu\text{g/ml}$ ) and Paclitaxel (0.0048  $\mu\text{g/ml}$ ) on cell cycle phases. The alterations in cell cycle were monitored with DAPI staining after time interval of 6, 12, 18 and 24 h of sophorolipid treatment. The highlighted values reflect the arrested cell percentage in different cell cycle phases.

### 3.3.4 SLCA induced apoptosis in HeLa cells

Evading apoptosis has been recognized as one of the hallmarks of cancer cells.<sup>[185]</sup> Apoptosis is a tightly regulated cell death process that is marked by characteristic cellular changes such as cell shrinkage, nuclear and chromosomal DNA fragmentation and activation of caspases.<sup>[186]</sup> The tumor growth is governed by rate of cell proliferation whereas the balance between cell proliferation and death is controlled by apoptosis. Therefore, induction of apoptosis in tumor cells is being sought to strategically treat cancer using chemotherapeutic or chemopreventive agents.<sup>[184][187]</sup>

Sophorolipids have been shown to induce apoptosis in H7402 human liver cancer cells.<sup>[137]</sup> Similarly, the apoptotic effect of SLs on HeLa cells was investigated by quantifying the binding of annexin V-FITC/PI and DAPI staining. Normally present in the inner membrane, phosphatidyl serine (PS) in early apoptotic phase translocates to the outer leaflet of the plasma membrane. Annexin V, an intracellular proteins can then bind to flipped phosphatidyl serine depending upon the calcium concentration.<sup>[188]</sup>

Quantification of apoptosis by Annexin V/PI analysis that also differentiates between viable, apoptotic and necrotic cell showed that treatment of HeLa cells with  $GI_{50}$  concentration (SLCA B-16.32  $\mu\text{g/ml}$ ; SLCA C-14.14  $\mu\text{g/ml}$ ) of SLs resulted in gradual increase of apoptotic cells in a time-dependent manner whereas no significant change was observed in untreated cells (Fig 3.4). The calculated percentage of cells that bound annexinV-FITC ranged from 20 % to ~38 % and 65 % at 24, 48 and 72 h respectively, indicating that both SLCA B and C lead to apoptosis in HeLa cells (Figure 3.4a). Absence of PI-positive cells in the entire experimental time frame (72 h) clearly indicated that sophorolipid induced death in HeLa cells is due to apoptosis and not necrosis (Fig 3b). These results indicated that SLs impacted HeLa cells by inhibiting their growth and inducing cell death via apoptosis.



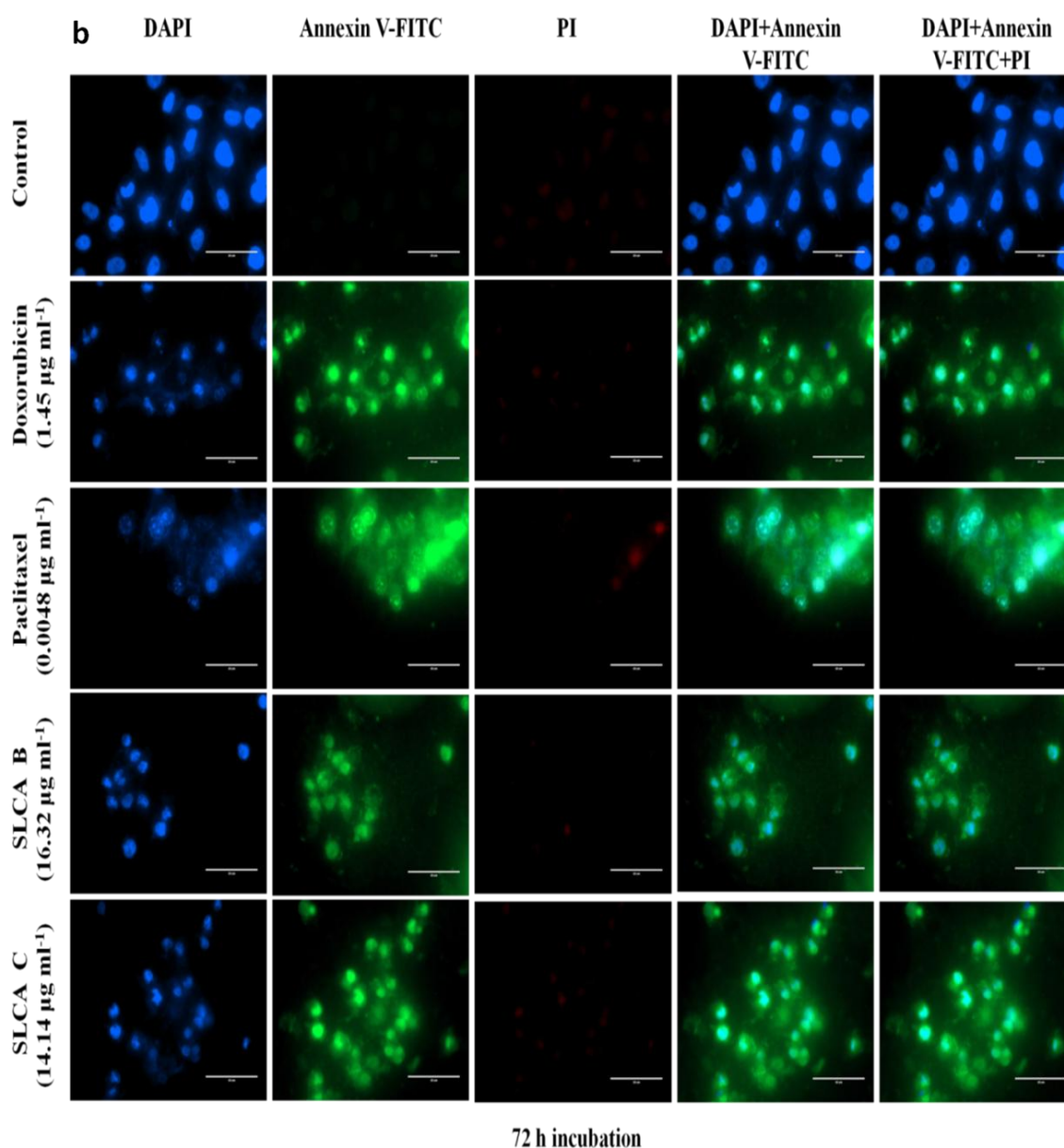


**Figure 3.4** (a) Apoptotic ratio in HeLa cells subjected to different drug treatments (b) Assay of Annexin V-FITC (green) binding and PI (red) incorporation in sophorolipid-treated HeLa cells after 72 h. The overlay images in the second last and last column represent the apoptotic cells and absence of necrosis respectively. The analysis was conducted using confocal microscopy, Magnification 20X (scale, 100  $\mu\text{m}$ ).

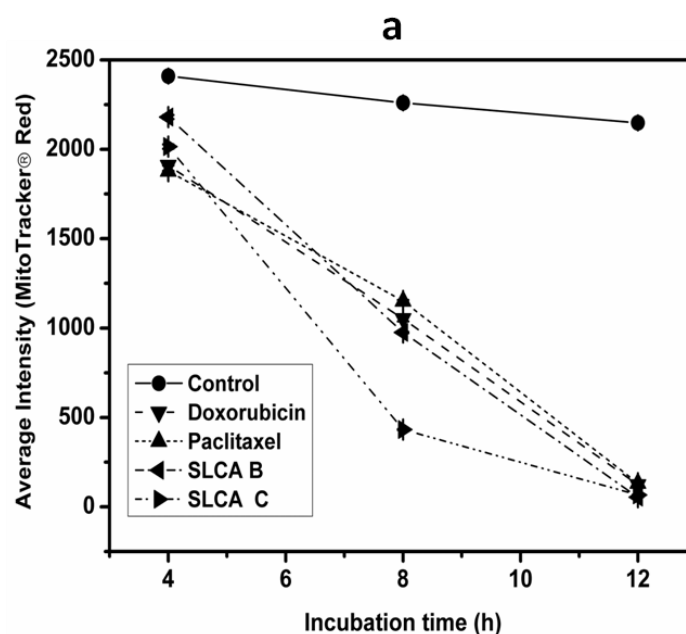
### 3.3.5 Evaluation of mitochondrial membrane potential

Apoptosis is known to occur via two pathways, extracellular and intracellular. Upon signalling by external factors extrinsic pathway or death receptor mediated pathway comes into action, whereas the release of specific intracellular signals under stressed condition activates intrinsic or mitochondrial pathway.<sup>[173]</sup> The intrinsic pathway is initiated by

disturbance in the mitochondrial membrane by pore formation or increased permeability that leads to the release of apoptogenic molecules from the mitochondria into the cytosol.<sup>[189]</sup> The immediate effect of mitochondrial membrane depolarization is the release of cytochrome c and  $Ca^{2+}$ , which then together with Apaf-1 and caspase-9 promote caspase activation.<sup>[186]</sup> Eventually the activated caspases execute the steps necessary for cell death. Thus monitoring of mitochondrial function can be indicative of intracellular apoptosis pathway participating in SL induced cell death in HeLa cells.

Sophorolipids that are amphiphilic in nature and partially resemble cell membrane lipids can possibly span through the cellular membrane and gain entry inside the cell. Hence they can affect integrity of the cell in yet not understood ways. To test whether the SL induced apoptosis in the HeLa cells is associated with mitochondrial dysfunction,  $\Delta\psi_m$  was determined that represents disruption of mitochondrial membrane potential, after staining with mitochondrial-specific dye, Mito Tracker Red.

As can be seen in Figure 3.5a, a significant decrease in red fluorescence intensity of Mito Tracker Red was evident within 8 h of sophorolipid treatment and it subsequently diminished upon further incubation for 12 h. The microscopic images in Figure 3.5b, also exemplify loss in red intensity at 12 h. Thus, it could be concluded that SLs caused mitochondrial membrane depolarization in HeLa cells.



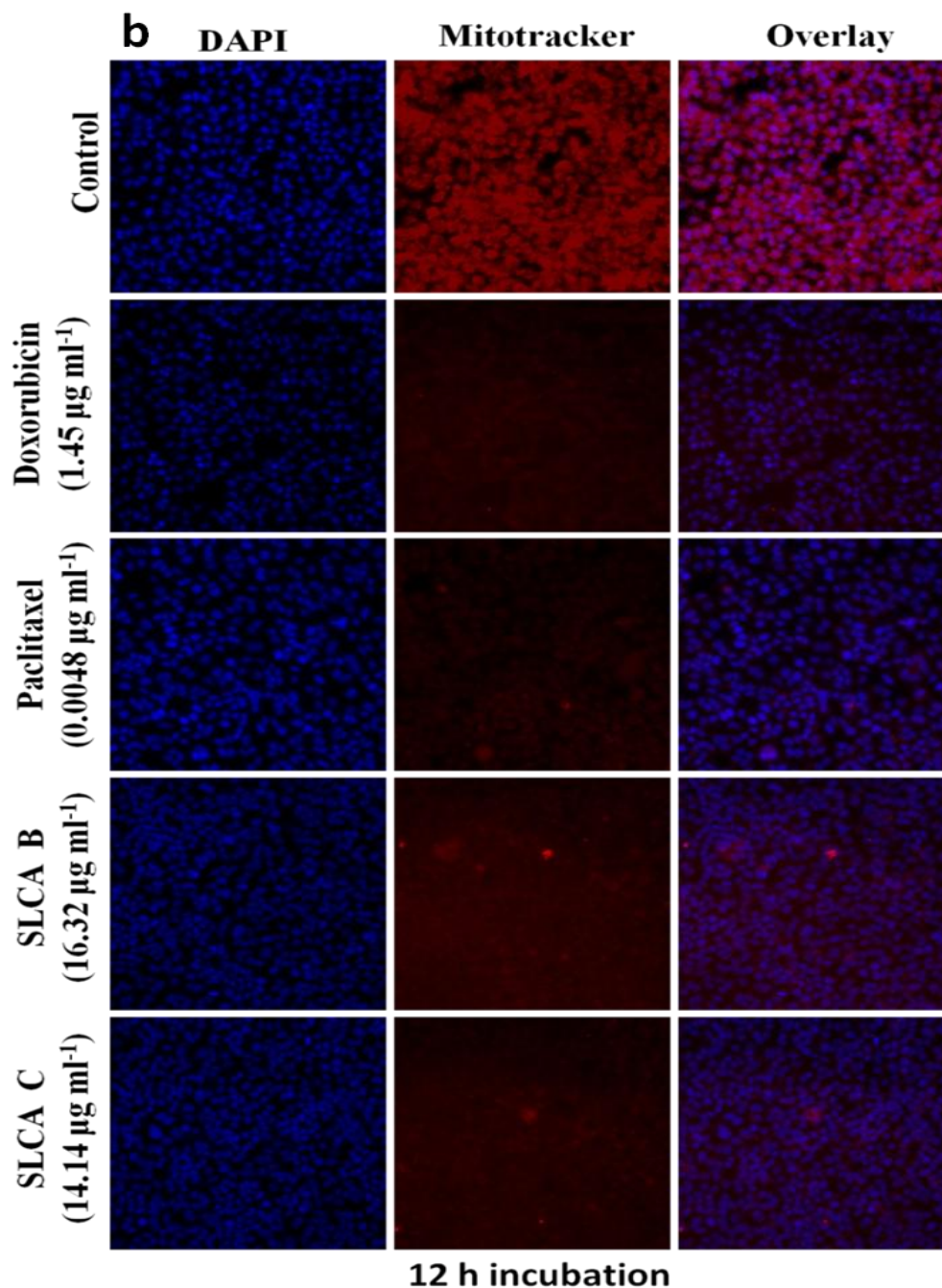


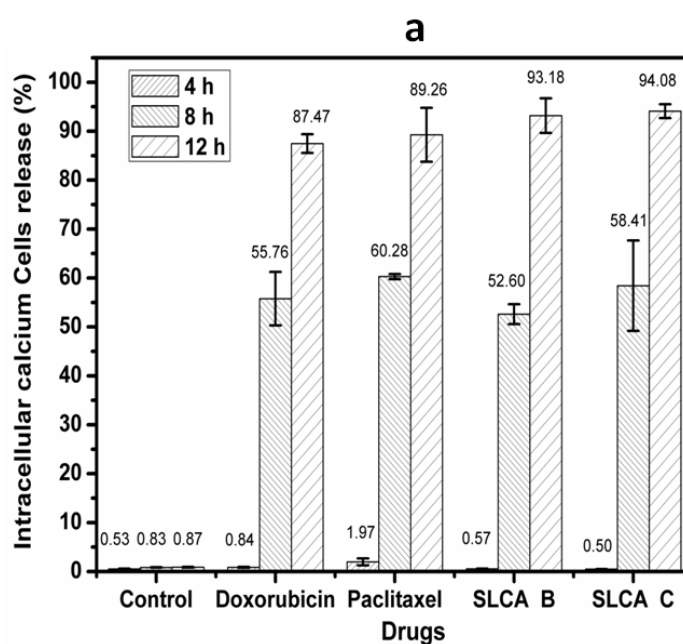
**Figure 3.5** Alteration of mitochondrial transmembrane potential in sophorolipid stimulated HeLa cells. Sophorolipid treated cells were incubated for different time intervals and later stained with Mito Tracker Red. (a) Average dye intensity signifying depolarized cells. Data from triplicate experiments represented as mean $\pm$ SD (b) Fluorescence intensity of bound dye as recorded by confocal microscope (20X magnification, scale-100  $\mu\text{m}$ ). Loss in red intensity exemplifies the disruption of MMP.

### 3.3.6 $\text{Ca}^{2+}$ release indicator of apoptosis.

$\text{Ca}^{2+}$  is known to be an important regulator of apoptosis and alteration in intracellular  $\text{Ca}^{2+}$  ion homeostasis possibly lead to induction of apoptosis.<sup>[190]</sup> The treatment of H7402 human liver cancer cells with sophorolipids also showed that the dramatic

increase in cytoplasmic calcium ions, due to influx across the cell membrane, was a triggering event for apoptosis.<sup>[137]</sup> To evaluate if cetyl alcohol derived sophorolipids affect the intracellular  $\text{Ca}^{2+}$  level, calcium sensitive dye Fluo 4-AM was used. The results showed that the cells treated with  $\text{GI}_{50}$  concentration (16.32/14.14  $\mu\text{g}/\text{ml}$ ) of SLCA B and SLCA C displayed a higher increase in the green fluorescence than the control cells in time-dependent manner (Figure 3.6a). The number of cells releasing calcium ions was measured as 93.2 % (SLCA B), 94.1 % (SLCA C) and 87.4 % (Doxorubicin), while the control showed 0.87 % at 12 h.

As shown in Figure 3.6b, in HeLa cells treatment with SLs lead to intracellular  $\text{Ca}^{2+}$  release from the mitochondria into the cytosol. These results are conclusive towards SLs direct or indirect role in mitochondrial damage followed by the mitochondrial depolarization and release of intracellular  $\text{Ca}^{2+}$ . Although, SLs treatment on HeLa cells results in mitochondrial depolarization and involvement of  $\text{Ca}^{2+}$  in mitochondrial dysfunction, but it is still unclear how this is linked to the apoptotic process.<sup>[188,189]</sup> These results suggest  $\text{Ca}^{2+}$  are important signalling intermediates that lead to depolarization of the mitochondrial membrane. The impaired mitochondria release cytochrome c which forms apoptosome complex and activates caspase-9. This eventually leads to the activation of executioner caspase resulting in apoptosis.<sup>[190]</sup>



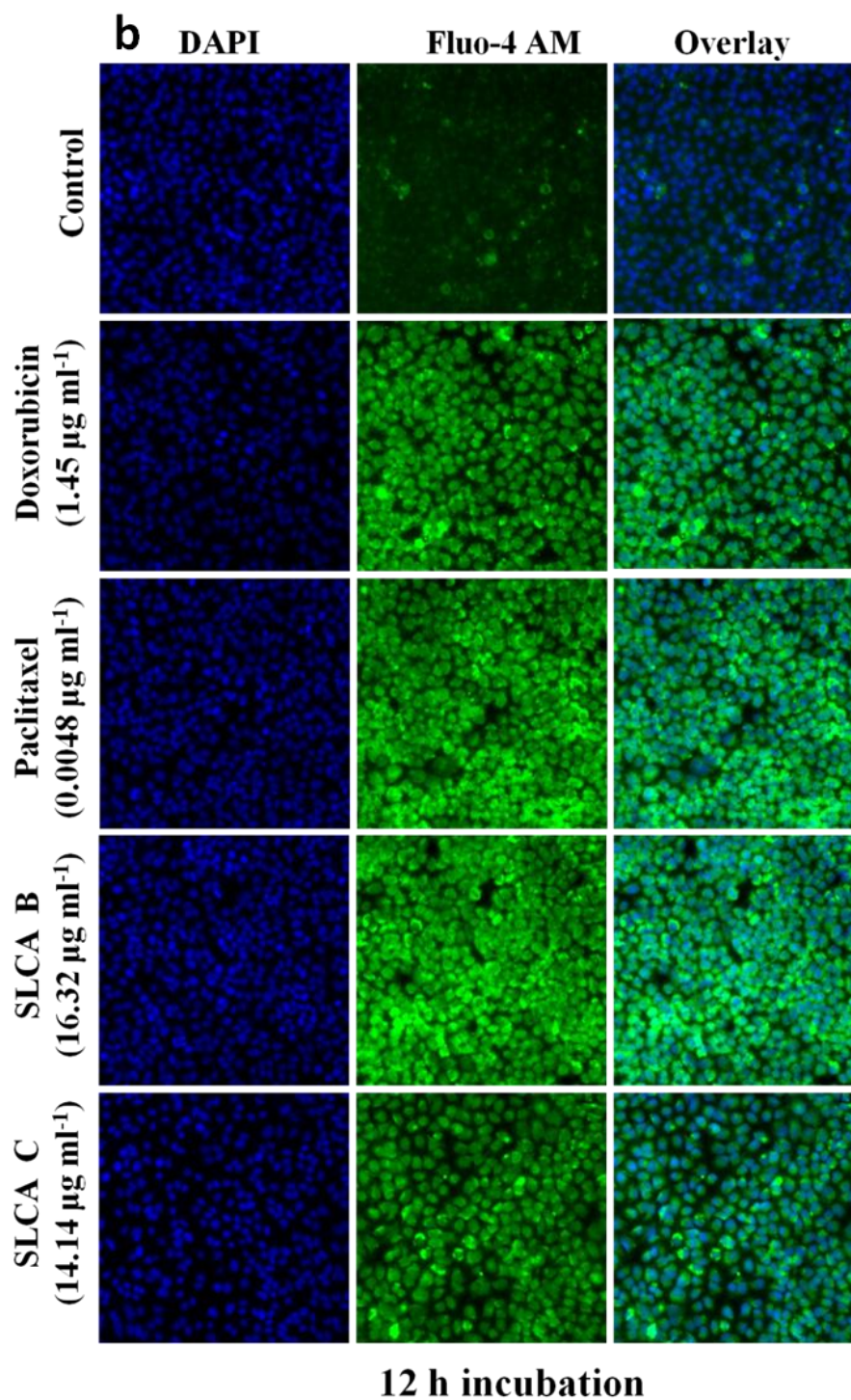


**Figure 3.6** Elevation in intracellular  $[\text{Ca}^{2+}]_i$  on sophorolipid treatment of HeLa cells. The treated cells were incubated for 4, 8 and 12 h, stained with DAPI (blue) and Fluo-4/AM (green). (a) Bar diagram represents cell percentage releasing calcium at different time intervals. (b) Overlay of confocal microscopy images exemplifying increased Fluo-4 AM intensity after 12 h that indicates increase in cytoplasmic calcium. Magnification 20X (scale, 100  $\mu\text{m}$ ).

### 3.3.7 *Functioning of caspase cascade (intrinsic/extrinsic apoptotic pathways)*

The apoptotic cell death occurs through a biochemical cascade that seems to involve activation of certain cysteine proteases called as caspases and additionally release of cytochrome c from mitochondria, that eventually induces condensation and fragmentation of nuclear DNA.<sup>[191]</sup> In the apoptotic process, caspases serve as both initiators and executors of cell death.<sup>[192]</sup> Death receptor and mitochondrion apoptosis pathways come into play by the interdependence of initiator and effector caspases.<sup>[193]</sup> The known initiator caspases are -2, -8, -9, -10, and -12 while the effector caspases include -3, -6, and -7. These proteases are present in inactive form as pro-caspases and participate in a caspase cascade to initiate apoptosis.<sup>[194]</sup> Caspase-8, activated by extracellular signals, is one of the cysteine proteases that is involved in both apoptosis and cytokine processing and is also responsible for early caspase-9 activation. The apoptotic extrinsic and intrinsic pathways converge at the proteolytic activation of caspase-3. Thus, caspases-3 execute apoptosis by cleavage of key cellular proteins such as cell cycle proteins, cellular DNA repair machinery proteins, apoptotic and structural proteins that cause typical cellular morphological changes observed in apoptotic cells.<sup>[173][195]</sup>

To investigate whether induction of apoptosis by SL involves the activation of caspases-aspartate-specific cysteine proteases, procaspases processing associated with both the apoptotic pathways (intrinsic and extrinsic) was calculated. The impact of SLs on caspase-3, caspase-8 and -9 activation was measured in HeLa cells. Fluorescent caspase activity analysis demonstrated that certain procaspases get processed in HeLa cells upon subjection to SL treatment in concentration dependent manner (Figure 3.7).

It was observed that SLs at GI<sub>50</sub> concentration, 16.32 and 14.14 µg/ml of SLCA B and SLCA C respectively, enhanced caspase-3, 8 and 9 expressions strongly in a time-dependent manner in HeLa cells when compared to the untreated cells (Figure 3.7a, b, c respectively). To confirm this, complete inhibition of caspase-3/8/9 activity, respective enzyme inhibitors were added to the cell cultures as per manufacturer's instructions. The enzyme activity was reduced to negligible level in the presence of inhibitors. On the other hand, pre-treatment of caspase-8 inhibitor inhibited caspase-9 activation. Thus, from these results it could be concluded that both SLCA B & SLCA C induce cell death via pro-apoptotic molecules and activate extrinsic and intrinsic pathways to induce cell death in HeLa cancer cells.

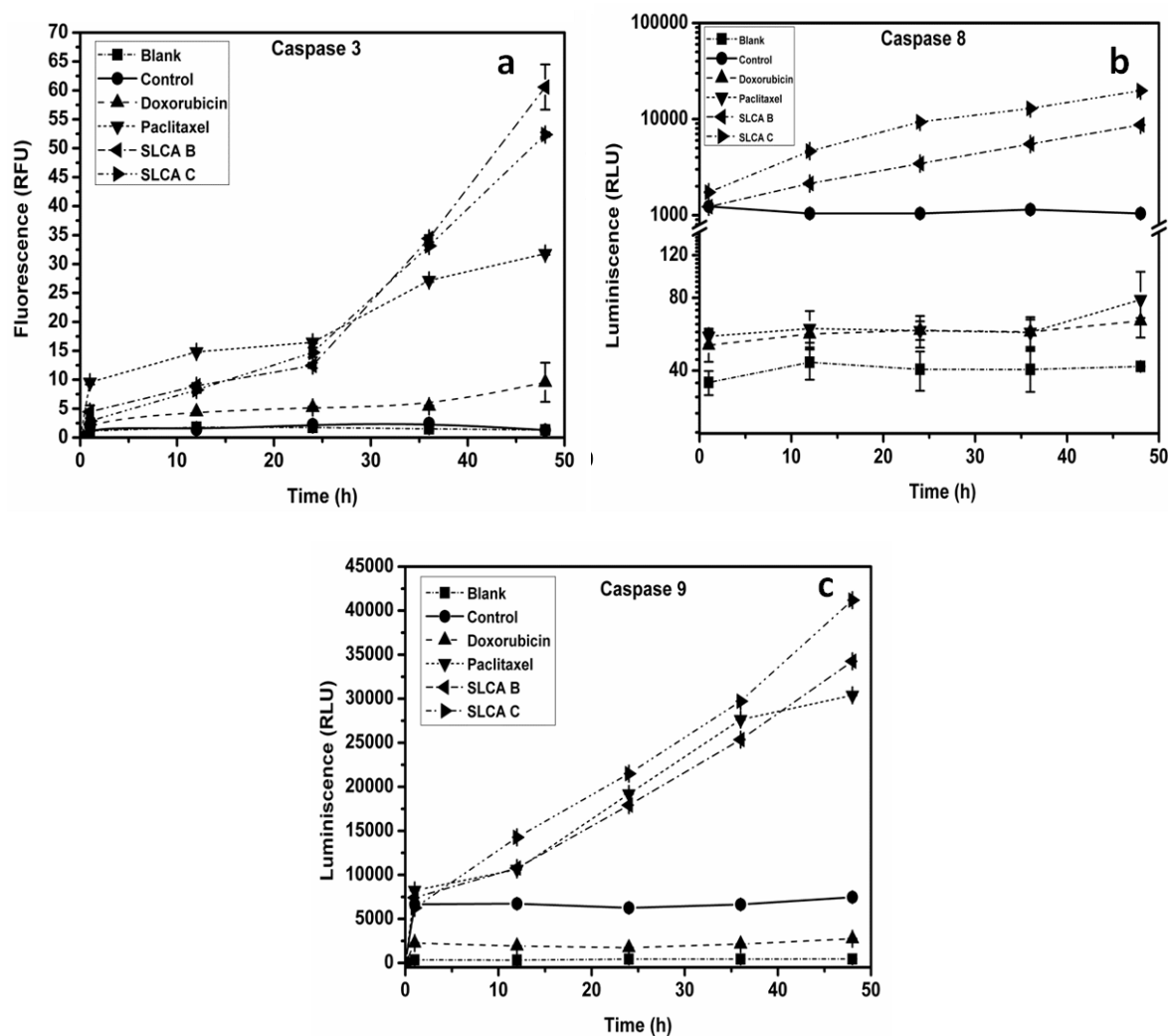


**Figure 3.7** Effect of SLCA B and SLCA C on activation of caspases. The sophorolipid treated cells were incubated for different time intervals and caspase activity was assessed by spectrometric method. (a) caspase-3, (b) caspase-8 and (c) caspase-9 activity was measured in comparison to the control. Data represented from three independent experiments as mean  $\pm$  SD values.

### 3.3.8 Cetyl alcohol sophorolipids as anti-angiogenic agents

For tumor growth and progression, angiogenesis; formation of new vessels from the pre-existing ones, is critical in order to provide required blood supply and allow circulation of metastatic cells.<sup>[196]</sup> Recently angiogenesis is considered as an exciting target for novel anticancer therapies as it provides tumor accessibility and independence, and wide range applicability to many tumor types.<sup>[197]</sup> Since sophorolipids have already been shown to display anticancer property, additionally the effects of sophorolipids, (SLCA B: 16.32  $\mu\text{g}/\text{ml}$ ; SLCA C: 14.14  $\mu\text{g}/\text{ml}$ ) on regulation of angiogenesis was investigated. When the endothelial cells are plated on matrigel, supplemented with LVES and VEGF, their proliferation ceases and they undergo rapid reorganization forming capillary like tubular structures. On the

other hand, in absence of LVES and VEGF cells only tend to proliferate. In cytotoxicity studies, it is shown that both the sophorolipids did not inhibit the growth of HUVECs but interestingly they displayed inhibition of vascular tube formation *in vitro* (Figure 3.8). As can be seen in Figure 3.8, when compared to untreated control, SLs treatment resulted in decreased count of connected tubes, their length and percentage of area covered by HUVECs. This inhibitory effect of SLs on angiogenesis may possibly be due to decreased expression of VEGF, a protein which is important in sustaining angiogenesis. In addition, HUVECs' tube formation inhibitory effect could be due to blockage of the co-receptor binding site for VEGFs. These inhibiting angiogenesis data suggest that SLs play important role in inhibition of endothelial tube formation and prevention of vascular growth. Anti-angiogenic therapy could be a promising strategy for anti-cancer therapeutics.<sup>[198]</sup>

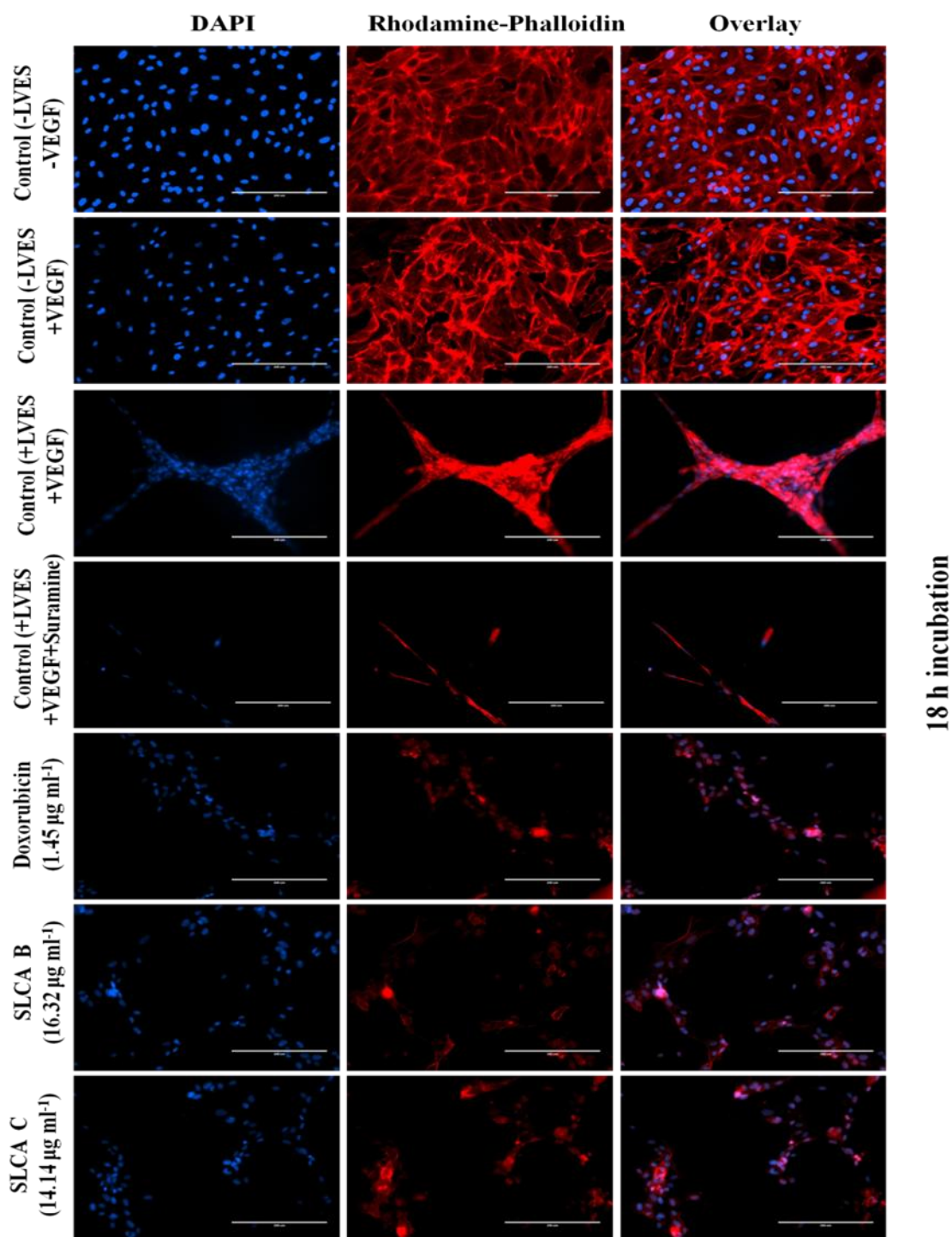


**Figure 3.8** Inhibition of neovascularisation upon SLCA B and SLCA C treatment. HUVECs were plated on 96 well plate precoated with matrigel ( $\pm$  LVES+VEGF) as control. Sophorolipid treated cells were stained with rhodamine conjugated phalloidin (red) and DAPI (blue) to stain tubes and nuclei respectively. Cell imaging was done using HCS Reader Cellomics' ArrayScan®.

Thus, to summarize this chapter, the cytotoxicity studies of SLCA B and SLCA C assessed by MTT assay in primary and human cancer cells revealed that both the sophorolipids show higher inhibitory effect on human cervix adenocarcinoma and do not

affect the survival of normal human endothelial cells, HUVECs. Thus, the application of SLs for cervical cancer prevention or therapy might be safe.

Physiological processes such as proper tissue development and homeostasis essentially require a balance between apoptosis and cell proliferation. Both these processes are affected and connected by cell-cycle regulators and apoptotic stimuli.<sup>[199]</sup> In SLs treated HeLa cells, apoptotic like morphological and nuclear changes were observed in time dependent manner as enhancement of phosphatidyl serine externalization and increase in DNA cleavage with G1/S phase arrest.

Present study also shows that there is an elevation of  $Ca^{2+}$  in the SLs-induced cells. There is a possibility that the intracellular elevation of  $Ca^{2+}$  in the SLs-induced cells might be due to proteolytic degradation of protein that participate in pumping cytosolic  $Ca^{2+}$  into the endoplasmic reticulum, after treatment of SLs.<sup>[200]</sup> Also, elevation of  $Ca^{2+}$  in the cytosol is likely to be result of perturbation in the mitochondrial permeability due to depolarization of the mitochondrial redox potential that consequently induces apoptosis (Figure 3.5). Thus,  $Ca^{2+}$  is an important signalling intermediate in SL-induced apoptosis. Cetyl alcohol derived sophorolipids SLCA B and SLCA C, induce apoptosis through mitochondrial depolarization and elevation of intracellular  $Ca^{2+}$  has been reported for the first time.

The enhanced activities of caspase-3 and -9 was observed in SL treated HeLa cells (Figure 3.7a, c), that confirmed involvement of mitochondria-mediated apoptosis pathway. In this study, SLs increased cytoplasmic  $Ca^{2+}$  concentration in HeLa cells that further resulted in the disruption of MMP. The loss of MMP caused cytochrome c release from the mitochondria to cytosol. This cytochrome c participates in apoptosome formation that cleaves pro-caspase-9 and releases its activated form i.e. caspase-9. Once activated caspase-9 then processes the downstream effector caspases-3 and ultimately triggers apoptosis of HeLa cells. Thus, this study also demonstrates involvement of  $Ca^{2+}$  in activation of caspase-3 during SLs-induced apoptosis.<sup>[186]</sup>

Death receptor-dependent apoptosis pathway is known to be modulated by initiator caspase-8. Significantly high caspase-8 activity in SLs-treated HeLa cells (Fig 6b) indicated that extrinsic apoptosis pathway might also be participating in the sophorolipid induced apoptosis in HeLa cells. From the results, it could be concluded that induction of initiator caspase-8, -9 and execution by caspase-3 might have resulted in cell apoptosis.<sup>[201]</sup>

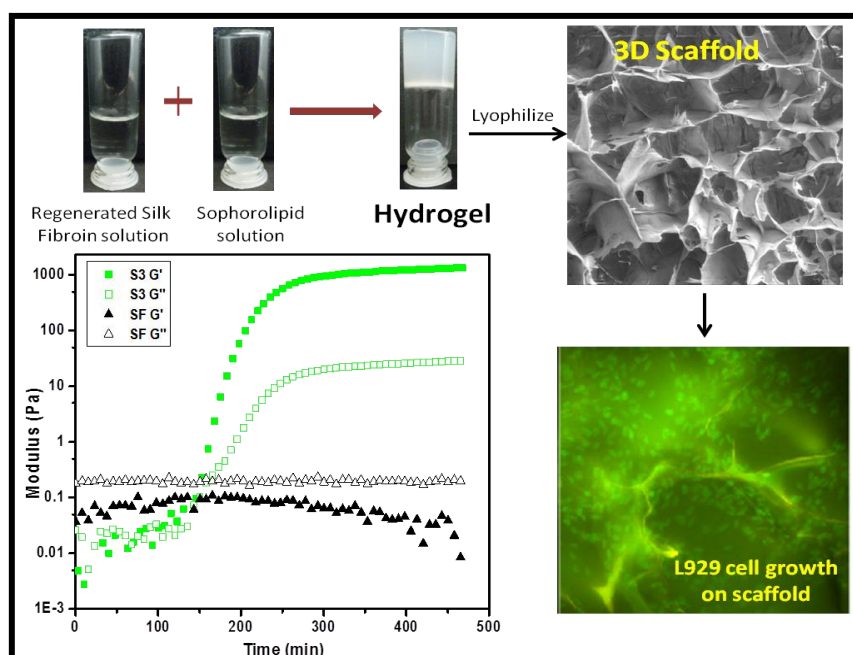
Formation of new blood vessels, termed as angiogenesis is regarded essential for intrusive tumor growth and metastatic spread. Hence, it is considered crucial stage to control tumour progression.<sup>[202]</sup> Thus, angiogenesis inhibitors can be employed to inhibit different steps in the angiogenic cascade, such as endothelial cells proliferation, adhesion to the matrix proteins and tube meshwork formation. In this work to investigate the anti-angiogenic property of sophorolipids SLCA B and SLCA C, tube formation assay in HUVECs was employed. This *in vitro* angiogenesis assay employs the three-dimensional capillary-like tubule formation ability of endothelial cells on the matrigel. Here, both the sophorolipids efficiently inhibited the tubule formation and remained ineffective on the HUVECs viability, also evident from MTT assay. In the available literature, there are no reports mentioning sophorolipids anti-angiogenic property at reported concentration.

### **3.4 Conclusions**

In conclusion, this study indicates that two sophorolipids (SLCA B and SLCA C) have potential growth regulatory role in human cervical HeLa cancer cells via inducing apoptosis. SL stimulates the activation of caspases -3, -8 and -9 with alteration of mitochondrial membrane potential. Among these two SLs, SLCA C was found to be more cytotoxic than SLCA B. Both SLs showed similar apoptotic effect in human cervical cancer cells in a time-dependent manner; arresting the cells at G1/S phase for 6, 12, 18 and 24 h. The underlying mechanism of apoptosis was found to involve intrinsic as well as extrinsic pathways resulting in depolarization of mitochondrial membrane and elevation in intracellular calcium level leading to activation of caspases. Additionally, it was interesting to find that, both the SLs also inhibited endothelial tubule formation. Thus, both SLCA B and SLCA C exhibited potential anti-tumor and anti-vascular agents that could improve common anticancer therapies.

## Chapter 4

# Sophorolipid assisted tunable and rapid gelation of silk fibroin to form porous biomedical scaffolds



Three dimensional polymer hydrogels, based on both natural and synthetic polymers, are increasingly being used as scaffolds and drug delivery vehicles for biomedical applications. Fibrous protein, silk fibroin (SF), obtained from *Bombyx mori* silkworm is a promising candidate in this area. However, SF has a long gelation time of about few weeks that can only be reduced by non-physiological treatments (e.g. high temperature, ultrasonication and low pH) or by addition of a chemical and non-biodegradable polymer and/or surfactant. We report here, accelerated gelation of SF, under physiological conditions, using a biosurfactant, sophorolipid (SL) as a gelling agent. SL and SF are completely miscible and form a very clear solution upon mixing. Hence it is interesting to see that this clear solution gels in a time span of just few hours. The hydrogels so formed have pore architecture, porosities and mechanical stability ideally suitable for tissue culture applications. Here we also demonstrate that mouse fibroblasts cells not only adhere to but also extensively proliferate on these SF-SL scaffolds.

#### 4.1 Introduction

Silk fibroin (SF) protein, derived from *Bombyx mori* silkworm, has been extensively studied in the biomedical field, due to its inherent and remarkable properties such as excellent biocompatibility, tunable biodegradability, excellent thermo-mechanical stability and minimum inflammatory reaction. SF can be processed in versatile forms such as thin films, sponges, composites, fibers, microspheres, tubes and hydrogels.<sup>[203]</sup> Polymer hydrogels can form 3D porous and stable scaffolds and thus are increasingly being used for biomedical applications such as controlled drug release, repair and regeneration of defective tissues and organs.<sup>[117,204–206]</sup> Biodegradable polymers are being evaluated as templates to facilitate the three dimensional culture of cells and also provide the guidance for the formation of new tissue.

SF hydrogels have been extensively studied in the last two decades. SF hydrogels can be prepared by employing non-toxic cross-linking agents such as genipin,<sup>[207]</sup> which results in inter and intra covalent cross-links between SF molecules. SF hydrogels can also be prepared by physical mechanisms such as, vortexing, sonication, electrical currents and acidic pH.<sup>[208–211]</sup> Here, the gelation is driven by change in conformation of the SF molecule from random coil to beta sheet structures. Aqueous solutions of SF are extremely sensitive to the pH. The gelation of aqueous SF solution can vary from 10-16 hours (below the isoelectric pH) to a period of few days and weeks (slightly above the isoelectric pH). This long gelation time limits the clinical applications of SF.<sup>[212]</sup>

Researchers have also demonstrated use of other methods to accelerate gelation of SF. Additives such as polyethylene oxide (PEO)<sup>[133]</sup> and Pluronic (Poloxamer)<sup>[213]</sup> and an anionic surfactant, sodium dodecyl sulphate (SDS),<sup>[117]</sup> have been used as gelling agents for silk fibroin under mild conditions. However, PEO (5 wt%, 60°C) reduces the gelation time in limited fashion only to approximately 9 days whereas in case of Polaxamer (15 wt%, 35°C) gelation occurs within 5 minutes. SDS at 8-12 mM concentration reduces the gelation time from few hours to 15-18 minutes. Apart from polymers researchers have also demonstrated the use of inorganic material such as nano-silica for accelerated gelation of silk.<sup>[214]</sup> These additives are not ideal for forming biologically relevant hydrogels because of their chemical and non-biodegradable nature.<sup>[117]</sup>

In the present work, a new molecule - sophorolipid was evaluated as a gelling agent for silk fibroin. Sophorolipids (SL) are carbohydrate based amphiphilic biosurfactants

derived from non-pathogenic yeast *Candida bombicola*. Sophorolipid structure comprises of a disaccharide known as sophorose (2 glucose monomers linked by unusual  $\beta$ 1-2 bond) linked to hydrophobic fatty acid chain preferably of 16-18 carbons. Additional esterification step within the molecule leads to formation of a closed ring form of SL.<sup>[46]</sup> Thus the two SL forms are known as acidic and lactonic. The hydroxyl fatty acid moiety remains free in acidic form whereas upon esterification with 4'' OH group of sophorose, it converts into lactonic form. Of the two forms, acidic SL has better assembling nature and water solubility whereas the lactonic form gives SL its biological properties. Thus, optimal performance can be achieved by the mixture of these two forms.

Sodium dodecyl sulfate has been successfully used as an inducer for gelation of silk fibroin.<sup>[117]</sup> SL has a chemical structure similar to SDS and hence it might have the potential to induce and accelerate gelation of SF through hydrophobic interactions. Also, SLs have several advantages over earlier reported gelling agents. SLs are natural compounds derived using a completely biological process. Thus, SL's have improved biocompatibility and reduced environmental impact as compared to the synthetic counterparts.<sup>[135]</sup> These biological properties have been exploited in a variety of applications including antimicrobial activity against bacteria,<sup>[215]</sup> inhibition of HIV virus,<sup>[104]</sup> anticancer activity<sup>[50]</sup> and ability to induce cell differentiation<sup>[94]</sup>. The dermal fibroblast metabolism stimulating activity<sup>[216]</sup> of SLs as well as increasing efficacy of topical antibiotics against microorganisms responsible for the majority of skin and soft tissue infections<sup>[108]</sup> makes them promising candidates for wound dressing application.

Thus these biological properties of SL make it an interesting gelling agent. The hydrogels of silk fibroin so formed can be used for wound dressing applications. Further, these hydrogels can be lyophilized into 3D scaffolds, which may be useful in tissue regeneration.

Here, in this study, addition of SL to SF solutions results in accelerated gelation of SF near physiological pH, with gelation time reduced from few weeks to few hours. The method involves simple mixing of aqueous SF and SL solutions. These hydrogels are further lyophilized to form three dimensional SF-SL scaffolds with controlled porosity, pore architecture and excellent mechanical properties. These lyophilized scaffolds have been evaluated for the growth and proliferation of fibroblast L929 cells, considering their future use in wound dressing applications. This is the first report showing the use of biosurfactants

for the accelerated gelation of SF at near physiological pH and a provisional patent has been filed for this formulation.

## **4.2 Materials and methods**

### **4.2.1 Preparation of regenerated silk fibroin**

Regenerated silk fibroin solutions were prepared from bivoltine *Bombyx mori* cocoons procured from Central Sericultural Research and Training Institute, Mysore, India. The cocoons were boiled in 0.05% w/v of NaHCO<sub>3</sub> (Merck) solution twice for 30 minutes each to remove sericin. The extracted fibroin mass was then dissolved in 9.3 M Lithium Bromide (Sigma Aldrich) solution at 60°C for 4 h.<sup>[217]</sup> The solution was then extensively dialyzed for 48 h with at least 6 changes of water to ensure complete removal of the salt. After dialysis, the concentration of Regenerated silk fibroin (RSF) solution was determined by drying known volume of RSF solution at 60°C in a vacuum oven and weighing the remaining solid. The final ~5% (w/v) dialyzed RSF solution was then diluted to 3% (w/v) with deionized water for further studies. The pH of the regenerated silk solution was measured to be 7.3 ± 0.2.

### **4.2.2 Sophorolipid synthesis and solutions**

Sophorolipid synthesis was carried out by growing seed culture of *Candida bombicola* (ATCC 22214) in 10mL medium comprising of malt extract 0.3%, yeast extract 0.3%, peptone 0.5% and glucose 2% followed by incubation at 28°C, 180rpm for 24 h. The seed culture was transferred to 40 mL medium for developing the starter culture, and incubated for 24 hours at 30°C with 180 rpm orbital shaking. The fermentative production was further carried out by transferring the starter culture into 200 mL of above mentioned medium in 1 litre Erlenmeyer flask and incubated for 120 h at 28°C with 180 rpm orbital shaking. The grown yeast cells were harvested by centrifugation at 5,000 rpm at 4°C for 10 min. Harvested cells were transferred to production medium comprising of 10% glucose supplemented with 1% v/v oleic acid and incubated for 120h at 28°C, 180 rpm. The synthesized sophorolipid was extracted using procedure reported by Gupta & Prabhune (2012).<sup>[57]</sup> Equal volume of ethyl acetate was added to supernatant. The aqueous layer was re-extracted until no emulsion was formed at the interface. Next 0.5 g sodium sulphate per 100 mL of ethyl acetate was added to remove any traces of water left. The solvent was filtered and reduced by rotary evaporation under vacuum to yield a brown coloured viscous product. The synthesized

sophorolipid was washed twice with n-hexane to remove any unreacted oleic acid. To determine the effect of sophorolipid concentration on gelation time of RSF, Oleic acid derived sophorolipid solutions were prepared at different concentrations i.e. 1%, 3% and 5% (w/v) respectively. The pH of each concentration solution was adjusted to 8 ( $\pm 0.2$ ) using 0.1 N NaOH.

### 4.2.3 Formulation of hydrogels and characterization

The purified silk solution of 3% w/v concentration was mixed with sophorolipid solution at various concentrations (1%, 3% and 5% w/v) in 1:1 (v/v) ratio and allowed to stand till gelation. These samples are further referred to as S1, S3 and S5 respectively.

#### a) Rheological characterization

Apart from the two states of matter (liquid and solid) there are in between states as well that require additional terms for description. Liquids are characterized by viscosity whereas solids are characterized by elasticity. Thus in between states are either viscoelastic liquids or solids (such as jellies, creams etc.). Thus, rheology is used to characterize these complex fluids using rheometer. In typical rheological experiment, storage modulus ( $G'$ ) (measure of elastic properties) and loss modulus ( $G''$ ) (describes viscous properties or dissipation of energy) are measured as a function of time. The cross-over of  $G'$  over  $G''$  describes the transformation of material from viscous to elastic nature (in present study, sol to gel state). In conventional oscillatory shear experiment, a sinusoidal shear strain  $\gamma = \gamma_0 \sin \omega t$  is applied on the sample, where  $\gamma_0$  is the amplitude and  $\omega$  is the frequency. The stress measured during this oscillatory deformation is then given by:

$$\text{Equation 4.1} \quad \sigma(t) = G'(\omega) \gamma_0 \sin \omega t + G''(\omega) \gamma_0 \cos \omega t$$

The coefficient  $G'$  as mentioned above is storage modulus and remains in phase with strain, while  $G''$ , the loss modulus is in phase with rate of strain. Viscosity of the system is measured as ratio of stress and shear rate.

To monitor the gelation process and determine the gelation time (GT), rheological measurements of the SF-SL hydrogels were performed using Anton Paar MCR 301 rheometer equipped with Couette flow geometry (CC17). A time sweep experiment was

performed at 0.5% strain using a frequency of 6.28 rad/s at 25°C. The experiment was started immediately after mixing the required quantities of SF solution into the pH adjusted SL solution. The cross-over of  $G'$  and  $G''$  was considered to be the gelation time.

#### ***b) Fourier transformed Infrared Spectroscopy (FTIR)***

The gelation of the SF-SL solutions was also investigated through FTIR Spectroscopy (Protégé 460, Nicolet, USA), using an Attenuated Total Reflectance (ATR) ZnSe cell. After mixing SL to SF, the solution was drop casted on ZnSe cell and spectrum was measured. As the gelation progressed the gels were loaded for IR measurements. The FTIR spectrum in the amide I region ( $1580\text{-}1720\text{cm}^{-1}$ ) was deconvoluted using the Peakfit v 4.12 software. The spectrum was corrected for baseline using a linear two-point method. A second derivative method was used to identify the peaks and the spectrum was smoothed till 12 peaks ( $1595\text{-}1605$ ,  $1605\text{-}1615$ ,  $1616\text{-}1621$ ,  $1622\text{-}1627$ ,  $1628\text{-}1637$ ,  $1638\text{-}1646$ ,  $1647\text{-}1655$ ,  $1656\text{-}1662$ ,  $1663\text{-}1670$ ,  $1671\text{-}1685$ ,  $1686\text{-}1696$ ,  $1696\text{-}1703\text{ cm}^{-1}$ ) could be fit. These peak positions have been defined by Hu et al.<sup>[218]</sup> A Gaussian fit with fixed peak width was used for automatic curve fitting and the spectrum was deconvoluted into 12 peaks. The % beta sheets was then calculated as the sum of % area under the four beta sheet peaks ( $1616\text{-}1621$ ,  $1622\text{-}1627$ ,  $1628\text{-}1637$ ,  $1696\text{-}1703\text{ cm}^{-1}$ ).

#### ***4.2.4 Preparation of scaffolds and their characterization***

The SF-SL solutions were allowed to gel in a 96 well cell culture plate at room temperature. The cell culture plate was then immersed in Liquid Nitrogen for 30 minutes. This frozen plate was then stored in  $-80^\circ\text{C}$  freezer overnight and the plate was lyophilized for 16-20 h, to obtain 3D SF-SL porous scaffolds.

#### ***a) Measurement of dry compression modulus***

Dry compression modulus measurements were performed on an MCR 301 Anton Paar rheometer using 8mm parallel plate geometry. Cylindrical scaffolds of approximately 5mm diameter and 5mm height were used for the measurement. A cross-head displacement speed of  $5\mu\text{m/s}$  was used to displace the top plate and the normal force was measured. At least 3 samples per measurement were recorded. A graph of stress vs strain was then

manually plotted and the dry compression modulus was determined to be the slope of initial linear region in the plot.

#### ***b) Scanning Electron Microscopy***

Scanning electron microscope (Quanta 200 3D, FEI) was employed to observe the cross-sectional morphology of the prepared scaffolds. The accelerating voltage was set to 15 kV. Cut section of the scaffolds was mounted on aluminum stubs and coated with a thin layer of gold to prevent charging. Representative images of each sample were captured at suitable magnifications.

#### ***4.2.5 Cell adhesion and proliferation studies on scaffolds***

Cell proliferation activity was determined in mouse fibroblast cell line L929 (ATCC CCL-1) obtained from National Center for Cell Science, Pune. The adherent L929 mouse fibroblast cells were cultured in DMEM (Gibco, Invitrogen) complemented with 10% fetal bovine serum (FBS; Gibco 10082-139) and routinely maintained at 37°C with 5% CO<sub>2</sub>. The culture medium was replaced every 2 days.

#### ***a) Fibroblast seeding and culture on porous scaffolds***

The scaffolds were autoclaved and UV sterilized for 25 min before any cell culture study. Adherent fibroblast cells were permitted to achieve 90% confluence and harvested in log phase by trypsinization using 0.05% trypsin prepared in PBS (with 0.02% EDTA). The cell counts were performed by haemocytometry. The cell suspensions were diluted in DMEM medium to obtain the cell density of  $1 \times 10^4$  cells/mL. An aliquot of 100  $\mu$ L of each suspension was seeded in a drop-wise manner on the top of the sterilized scaffolds disc in 96-well cell culture plates. The plate was then left undisturbed at 37°C in 5% CO<sub>2</sub> atmosphere and 95% relative humidity in a CO<sub>2</sub> incubator. The culture medium was replaced every 2 days.

#### ***b) Cell adhesion assay***

For cell adhesion assay, the cells were seeded in 96 well plate on top of the sterilized scaffold disc and incubated in a humidified atmosphere with 5% CO<sub>2</sub> at 37°C as mentioned above. At 4 and 8 h, the cells were gently harvested in 100  $\mu$ L PBS at pH 7.4 and then counted using a haemocytometer. By subtracting the number of washed out fibroblasts

from  $1 \times 10^4$  cells per scaffold, the number of cells remained adhering to each scaffold disc was calculated (Equation 1).

$$(1 \times 10^4 \text{ cells per scaffold} - \text{number of washed out L929 fibroblast cells}) = \text{Number of cells adhering to each scaffold} \quad (\text{Equation 1})$$

**c) Cell proliferation assay to study the metabolic activities of cells within scaffolds**

An enzyme-based assay was performed to quantify the proliferation of L929 fibroblast cells within the constructs (scaffolds with cells) at intervals of 2, 4 and 7 days. The *in vitro* cytotoxic effect of the fabricated scaffold was investigated by a standard MTT assay (refer section 3.2.6a, a widely adopted method of measuring cellular proliferation as described by Mosmann (1983).<sup>[165,219]</sup>

The scaffolds were sectioned to disc weighing approximately  $1.5 \text{ mg} \pm 0.2$  and used for all cell culture studies. A  $100 \mu\text{L}$  suspension of  $1 \times 10^4$  cells/mL was seeded on sterilized scaffold disc kept in 96-well cell culture plates. The plates were then left undisturbed at  $37^\circ\text{C}$  in an atmosphere of 5%  $\text{CO}_2$  and 95% relative humidity within a  $\text{CO}_2$  incubator. At the end of the incubation, the suspensions containing the unattached cells was discarded and each well containing the scaffold and attached cells was washed thrice with 1 mL of phosphate buffer saline. 0.01 ml MTT solution prepared at a concentration of 5 mg/mL in PBS was then added to each well and incubated for 4 h at  $37^\circ\text{C}$ . 0.2 mL of acidified (0.04 N HCl) isopropanol was used to solubilize the formazan product. Optical density was measured on a SPECTRAMax PLUS 384 plate reader (Molecular Devices Inc, USA), at 570 nm. The assay was carried out with only MTT solution as negative control and cell suspension as positive control. All the experiments were performed in triplicates, and the values were expressed as mean  $\pm$  standard deviation.

**d) Confocal microscopy**

The morphology of the adhered cells on constructs (cell laden scaffold disc) was studied using a Thermo Scientific™ ArrayScan™ XTI High Content Analysis (HCA) Reader. After incubation for 24 hours the cell laden scaffold discs were washed thrice with PBS (pH 7.4) and incubated in 4% paraformaldehyde for 25 minutes to fix the constructs. For

fluorescence microscopic study, the fixed constructs were stained with 1  $\mu\text{M}$  DAPI (4', 6-Diamidino-2-Phenylindole, Sigma) and 1  $\mu\text{M}$  Nile red (Sigma). For staining, 100  $\mu\text{L}$  dye solutions (prepared in DMSO) were mixed with the cell suspension (9.9 mL) and kept at room temperature for 30 minutes in dark. The cells were then washed thrice before acquiring images. The images were acquired using a confocal laser-scanning microscope as 4X4 binning with a 20X objective (Olympus FV1000). The 3D multichannel-image processing was done using Thermo Scientific™ HCS Studio™ 2.0 Cell Analysis Software.

### 4.3 Results and discussion

#### 4.3.1 Studying time kinetics of gelation

Gelation of silk fibroin solutions has been conventionally monitored using time sweep experiment in Couette geometry in a rheometer.<sup>[212,220]</sup> The results on gelation of pure SF and SF-SL solutions at near physiological pH are reported. As can be seen from Figure 4.1, the pure SF solution at pH  $8.0 \pm 0.2$  shows a near flat storage modulus ( $G'$ ) and loss modulus ( $G''$ ) during the entire experimental time frame. The SF solution does not exhibit gel-like behaviour even after storage at room temperature for a period of 20 days. When 1% w/v SL solution is mixed with 3% w/v SF solution, a clear solution with a pH of about  $7.4 \pm 0.2$  is obtained. This S1 sample was then used for the rheology experiments.

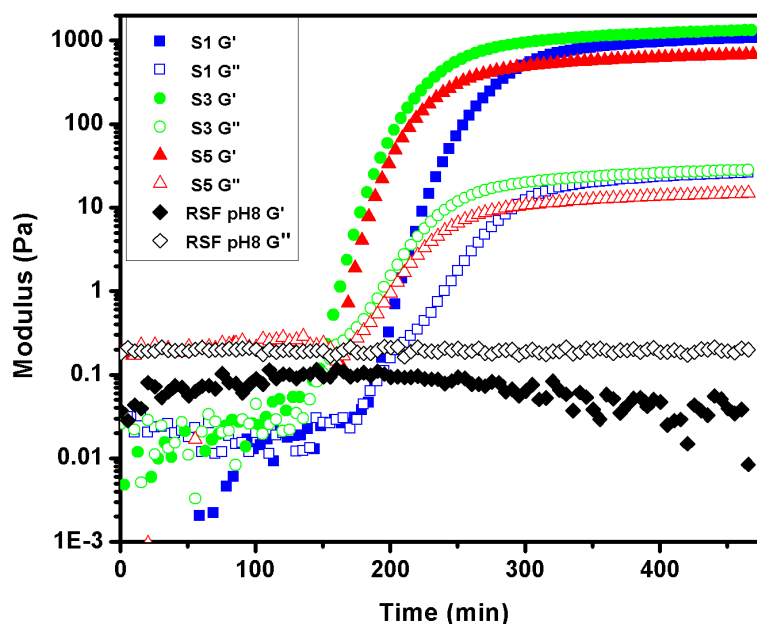


**Figure 4.1** Time sweep rheology experiments on pure SF, S1, S3 and S5 samples.

As shown in Figure 4.1, S1 shows a dominant  $G''$  for the initial 180 minutes. However, the storage modulus rapidly builds up after 180 minutes. After 189 minutes, the  $G'$  dominates the  $G''$ . This indicates the formation of gel. A corresponding increase in  $G''$  is also seen at this time interval. Similar results were also observed for the SF-SL solutions with increasing concentrations of SL to 3% w/v. The gelation time was considered to be the time at which  $G'$  and  $G''$  had equal values and after this the  $G'$  was always greater than  $G''$ , indicating a solid like behaviour. The gelation time of the S3 hydrogel further decreased to 140 minutes as compared to 189 minutes for the S1 sample. But, further increasing the SL concentration did not result in further reduction of gelation time. S5 had a gelation time of about 164 minutes. Hence higher concentrations of SL were not evaluated. Figure 4.1 also suggests that the S5 sample has the lowest storage modulus values. The S1 and S3 have comparable modulus, but the modulus of S1 has still not reached a plateau due to slower gelation kinetics.

This implies that the effective modulus of the hydrogel is essentially governed by the amount of SF present. Addition of SL negatively affects the storage modulus. However, these trends were not observed in the wet compression modulus studies on these hydrogels. The compression modulus of the wet hydrogels was found to be of the order of  $\sim 9000\text{Pa}$  with no significant change with respect to formulation.

### 4.3.2 Conformational changes in silk fibroin upon gelation

The gelation of SF is accompanied by change in conformation of the silk fibroin molecules from a predominantly random coil structure to highly crystalline beta sheet structures. To verify the same, Fourier Transform Infrared (FTIR) spectroscopy was used. FTIR is a powerful and widely used technique for investigating the molecular conformations, and is especially employed to study the structure of silk protein.<sup>[218]</sup> The major conformations of SF are random coil,  $\alpha$ -helix,  $\beta$ -sheets and  $\beta$ -turns. Sample S3 was chosen for this study and a time dependent (ATR) measurement was performed on this sample as shown in Figure 4.2a. The amide peak between  $1600\text{-}1700\text{ cm}^{-1}$  was monitored and further deconvoluted to quantify the beta sheets present in the sample. The amide I peak corresponding to C=O stretching, progressively shifted to lower wavenumbers, indicating a conversion from a predominant random coil structure to crystalline beta-sheet conformation. The initial peak, corresponding to the homogeneously mixed SF and SL sample centred at  $1646\text{ cm}^{-1}$ , shifted to values of  $1637$ ,  $1636$ ,  $1633$  and  $1622\text{ cm}^{-1}$  after 2, 4, 6 h and 24 h respectively. The peak

centred at  $1646\text{ cm}^{-1}$  is attributed to a random coil conformation, while the peaks located in the range of  $1623\text{--}1637\text{ cm}^{-1}$  attributed to anti-parallel beta-sheet structures.<sup>[218]</sup>

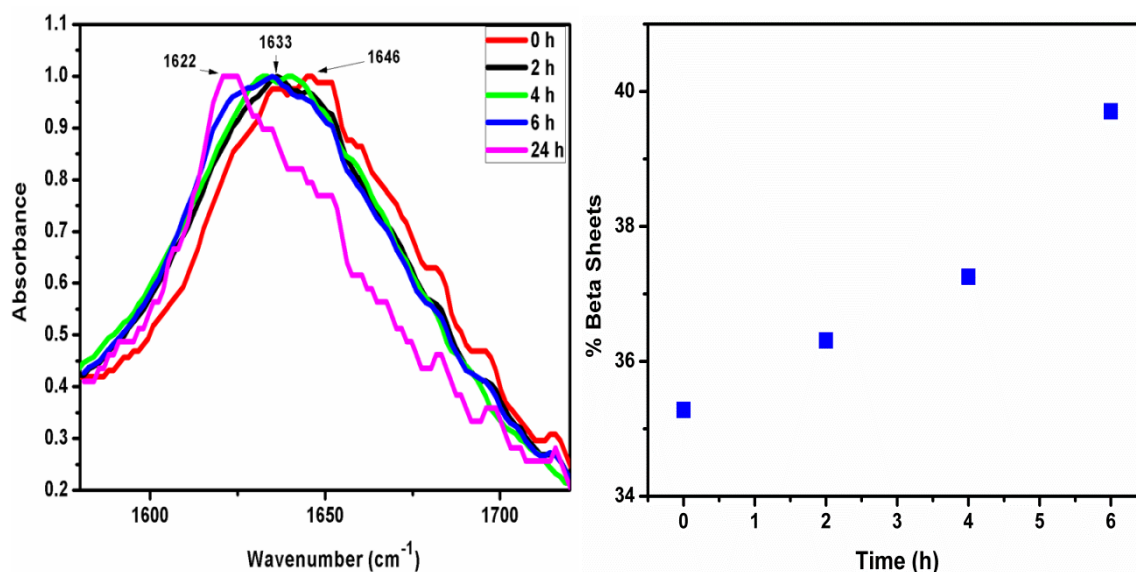


**Figure 4.2** (a) ATR-FTIR spectra of S3 solution as a function of time (b) % beta sheet change in S3 as a function of time after amide I peak deconvolution.

Time dependent ATR-FTIR measurements of S3 sample showed an increase in  $\beta$ -sheet content during gelation (Figure 4.2b). A gradual increase in the % beta sheets in different samples was observed with increase in concentration of SL (Refer Figure 4.3). The S5 sample showed the highest beta sheets content at  $40.4\% \pm 0.2$  (std. error) when measured at 6h. This indicates that the concentration of SL plays a significant role in conversion of random coil to beta sheet structure. Higher the concentration of SL present, higher is the % beta sheet structure in the sample at a given time.

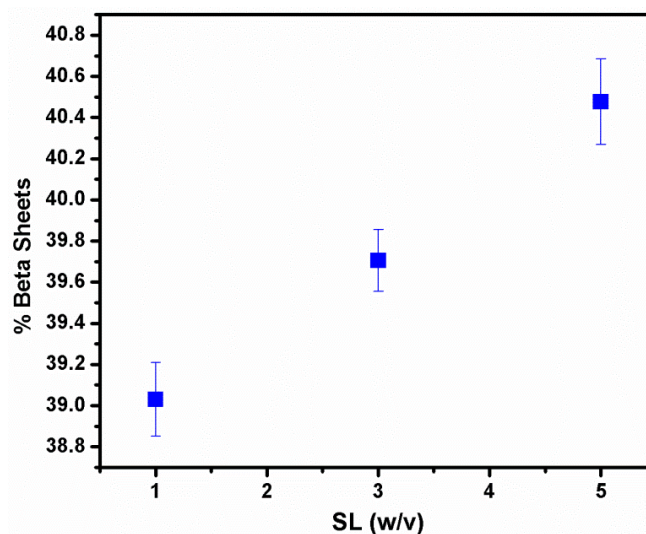


**Figure 4.3** % Beta sheets of SF + SL hydrogel for S1, S3 and S5 samples.

### 4.3.3 Compressive modulus of scaffolds

The three gelled samples were further frozen and lyophilized to obtain 3D porous scaffolds. Several different characterization techniques were used to evaluate the suitability of these scaffolds for cell culture experiments. First, the dry compression modulus of the lyophilized scaffolds of SF-SL was measured (Figure 4.4). With increasing concentration of SL from 1 to 5% w/v, the corresponding dry compression modulus of the hydrogels decreased from 1.23 to 0.4 MPa. The SF-SL hydrogels with higher protein and lower sophorolipid content i.e. 3:1 concentration ratio had maximum compression modulus. As SF takes more than 20 days to gel, scaffolds of SF could not be prepared and hence could not be compared with the SF-SL hydrogels. However, the dry compression modulus of SF scaffolds reported by Vepari & Kaplan (2007), prepared by freezing and lyophilizing have moduli in the range of few MPa, which is comparable to that obtained for our sample S1.<sup>[203]</sup> Clearly, addition of a small organic molecule like SL deteriorates the modulus of the scaffold. However, the measured compression moduli indicate that the mechanical integrity of these 3D structures is sufficient to be evaluated for tissue engineering applications.

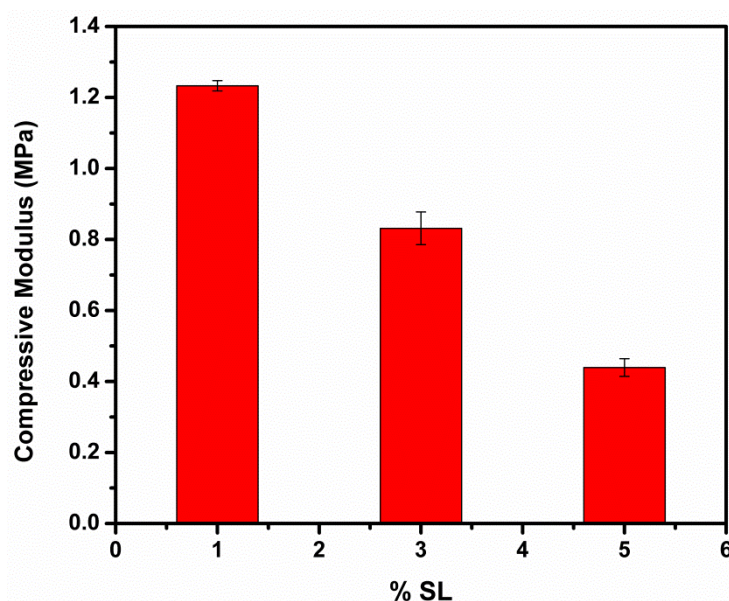


**Figure 4.4** Compressive modulus of SF + SL scaffolds as a function of SL concentration (i.e. 1%, 3% and 5% (w/v)) at 25°C.

### 4.3.4 Morphology and pore size of scaffolds

The cross-sectional morphology of these 3D scaffolds was visualized using a scanning electron microscope. The scaffolds represented a continuous porous morphology. A clear trend in pore size was observed i.e., with increasing SL concentration from 1% w/v to 3%

w/v to 5% w/v, pore size decreased from  $143 \pm 32 \mu\text{m}$  to  $114 \pm 23 \mu\text{m}$  to  $32 \pm 8 \mu\text{m}$  respectively (Figure 4.5). The internal architecture of the hydrogels was dependent on SL concentration. The % porosity as calculated by liquid displacement method reported by Gil et al. (2011) <sup>[221]</sup> was found to be  $90 \pm 3\%$  for all the scaffolds. This high porosity and large pore sizes in scaffolds is also desirable for tissue engineering applications for easy transport of nutrients and cell migration.

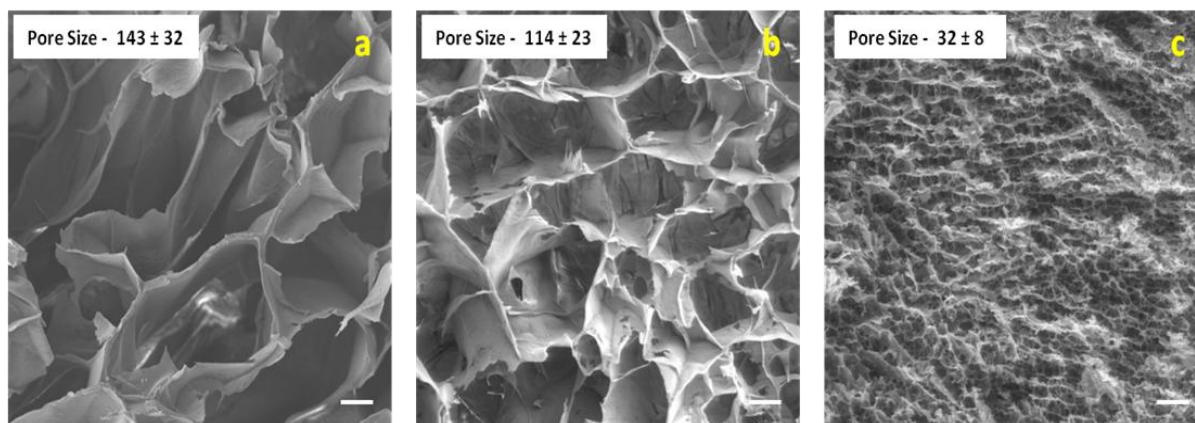


**Figure 4.5** Scanning electron micrographs of cut surface of lyophilized scaffolds for (a) S1, (b) S3 and (c) S5 samples. Scale bar for all images is 50  $\mu\text{m}$ .

#### 4.3.5 *Fibroblast adhesion and proliferation on scaffolds*

These scaffolds were then evaluated in cell culture studies using mouse fibroblast L929 cells. The adhesion of mouse fibroblast to the SF-SL scaffolds was characterized after 4 and 8 h (Figure 4.6). The porous structure of the scaffolds provides a 3D space with enhanced surface area thus increasing the available space for the cells to adhere. This was proved by higher percentage of cells attached to scaffolds in comparison to control polystyrene culture plates. Also, an increase in SL content resulted in small improvements in the ability of the cells to attach to the scaffold. Not a very significant difference in the % cell adhesion was found between the three samples, which well corroborated with the minor variation in % porosity of the scaffolds.

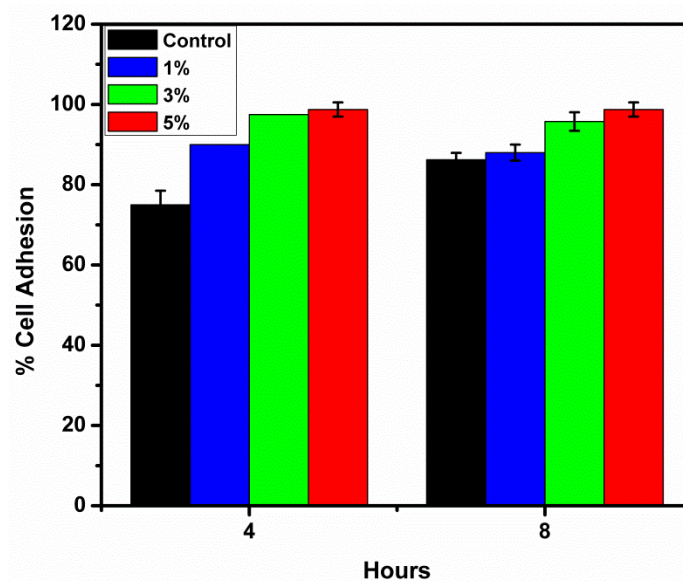


**Figure 4.6** Adhesion of Mouse fibroblast (L929) cells as a function of time on lyophilized scaffolds prepared using S1, S3 and S5 solutions.

The cell viability was investigated at day 2, 4 and 7 by performing MTT assay (Figure 4.7). Short term observation (day 2) exhibited significant difference between the cells cultured within the scaffolds and control, demonstrating scaffolds lacking any adverse effect on cell growth. This indicates that the scaffold material is non-toxic. On day 4 it was observed that cells within S3 and S5 scaffolds showed significantly greater cellular activity than the control polystyrene plates. The higher cell proliferation could be attributed to the higher surface area available for cell attachment in a 3D scaffold as compared to that available in 2D culture plates. On day 7, significant difference in cellular activity as compared to the culture plate was found only in S5 scaffolds. This result clearly showed that sophorolipid does not exert any significant adverse effect on the viability of cells and higher SL proved to be even more nourishing for the increased cellular activity.

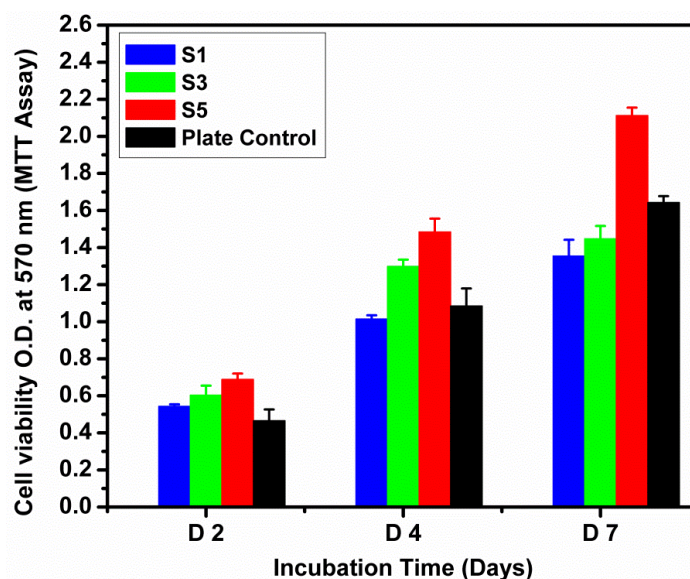


**Figure 4.7** MTT assay showed that fibroblasts exhibited high metabolic activity cultured on three dimensional scaffold matrices for up to 7 days.

Also, confocal microscopy done on day 2 confirmed effective migration and distribution of cells within the scaffolds. The confocal images reinforced the profile obtained from MTT assay, as more profuse population of cell was found habitating within the scaffolds made of highest SL concentration (5% w/v) (Figure 4.8a). Cells in S5 sample were observed to be covering the scaffold surface and the pores entirely. With decrease in SL concentration, lower cell proliferation was observed in case of S3 and S1 scaffolds. The colored background is a result of the matrix staining along with the cells. Fibroblast cells with rounded nuclei were observed throughout the matrix surface suggesting their normal growth on these 3D SF-SL scaffolds (Figure 4.8b).

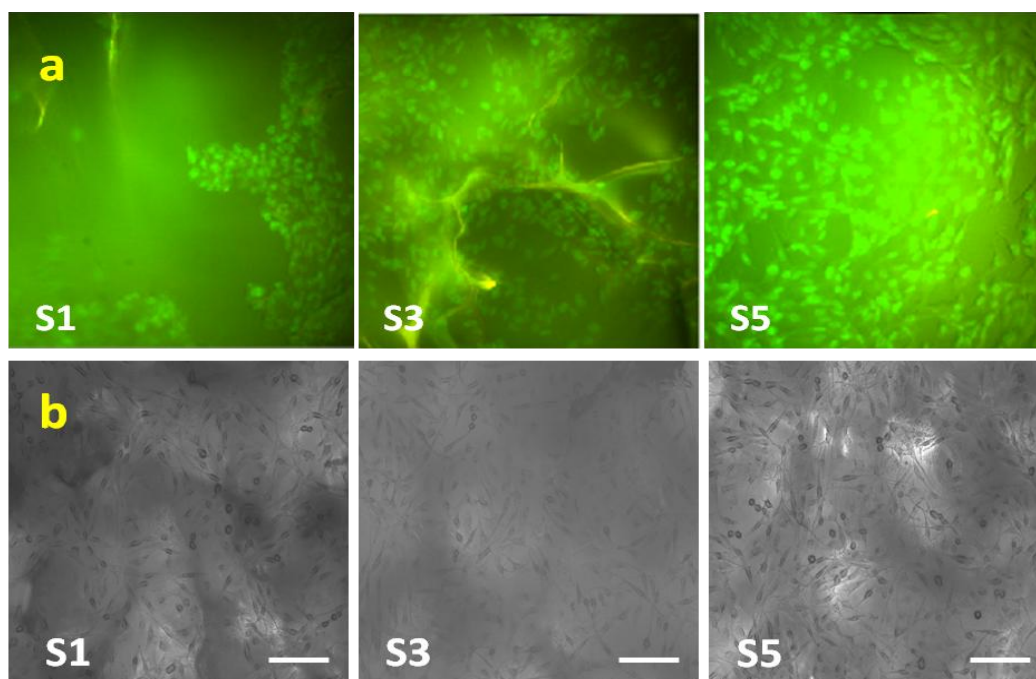


**Figure 4.8** (a) Confocal images of DAPI and Nile red stained L929 fibroblast cells and scaffold matrices. (b) Adherent cell morphology on scaffolds 48 h post seeding and fixing with 2.5 % glutaraldehyde using Floid® Cell Imaging System with fixed 20X Plan Fluorite objective having Image resolution – 1296 x 964 pixels. Scale bar for all images is 100  $\mu$ m.

To summarize the results, present work deals with the development of silk fibroin – sophorolipid hydrogels for use in wound dressing applications and 3D SF-SL scaffolds for tissue engineering applications. It has been demonstrated that, gelation time of regenerated silk fibroin solution can be considerably reduced from few weeks to few hours by simply mixing it with sophorolipid (biosurfactant) solution. The effective pH of SF-SL solution on mixing was  $7.4 \pm 0.2$ . Increasing the SL concentration from 1% w/v to 3% w/v resulted in the decrease in gelation time from 189 minutes to 140 minutes. However, further reduction in gelation time could not be achieved even after increasing the concentration of sophorolipid.

Sol to gel transition in silk fibroin is marked by conversion of random coil to  $\beta$ -sheet and the ATR-FTIR analysis clearly showed that beta sheet formation is the mechanism of gelation for these solutions. Also, higher concentrations of SL resulted in higher beta sheet contents in the sample. This result implies that the percent  $\beta$ -sheet crystallinity in the sample at a given time can be tuned by varying sophorolipid concentration.

These SF-SL hydrogels may be frozen and lyophilised to form 3D scaffolds useful for tissue regeneration. Dry compressive modulus of the 3D scaffolds increases with decrease in SL concentration.<sup>[133]</sup> The compressive modulus of the SF-SL scaffold with higher percentage

of regenerated silk fibroin i.e. S1 sample was found to be maximum.

Cross-sectioned SEM pictographs demonstrated that increasing concentration of sophorolipid leads to development of smaller pore diameters. SF concentration being constant, increasing concentration of SL, leads to the formation of larger number of micelles. Each of these micelle further acts as an interacting site for SF chains which results in higher number of nuclei causing faster gelation and smaller pore sizes. In addition, all the SEM images showed no phase separation suggesting homogenous entanglement of sophorolipid and silk fibroin.

Moreover, pore size ranging from 110-350  $\mu\text{m}$  are most favourable for fibrovascular tissue ingrowth due to the balance in two factors, the channel size of sponges for cell infiltration and their surface area for cell attachment.<sup>[222]</sup> Thus, the pore sizes of resultant 3D scaffold are expected to support neonatal tissue ingrowth. Also it has already been shown by authors D'britto et al.<sup>[223]</sup> that sophorolipid molecules support and enhance proliferation of cells and our cell culture studies corroborate these findings. The 1% w/v SL scaffolds show less cell viability as compared to the other scaffolds due to low concentration of SL. With increasing concentration of SL higher cell viability and proliferation could be achieved. Comparison with the pure SF scaffolds could not be accomplished due to its extremely high gelation time thus preventing the formation of consistent and non-contaminated gelled scaffolds.

The present approach of hydrogel fabrication is simple, feasible and requires relatively mild conditions without the employment of any extraneous chemical or cross-linking agent. Such a scaffolding matrix may have immense potential applications in wound dressing and tissue engineering. Further studies to develop a deeper understanding of SF–SL intermolecular interactions leading to hydrogel formation have been discussed in detail in Chapter 5.

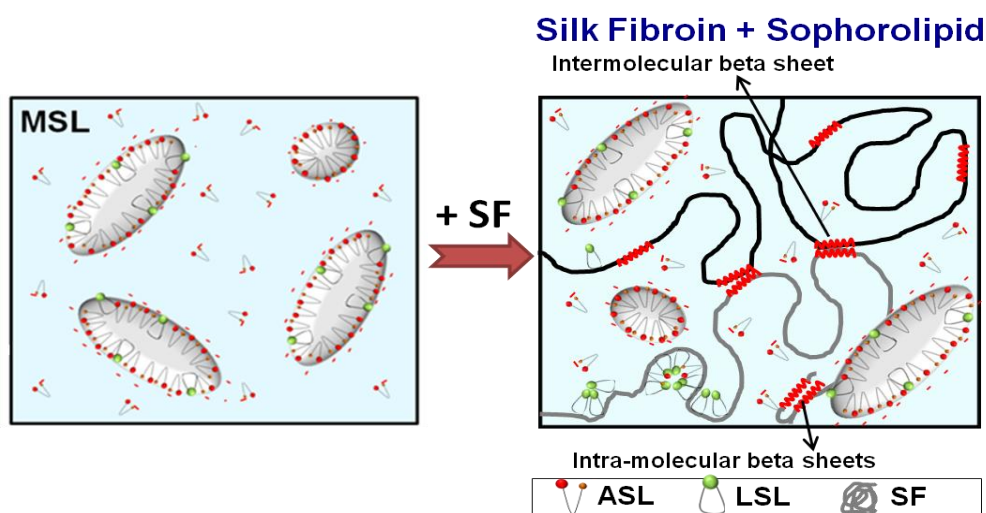
#### **4.4 Conclusion**

The accelerated gelation of silk fibroin is achieved in this investigation by a simple method that involves addition of sophorolipid, a biosurfactant solution. The addition of sophorolipid reduces the gelling time of SF solutions from few weeks to few hours. These SF-SL hydrogels can be further lyophilized to form 3D scaffolds. The compression modulus and pore size of the scaffolds can be very easily tuned by controlling the SL concentration.

Additionally, adherence and proliferation of L929 cells on these constructs is demonstrated. The SF-SL hydrogels will find applications in wound dressing while the SF-SL 3D scaffold may have potential use in tissue regeneration.

## Chapter 5a

# Silk Fibroin - Sophorolipid gelation: Deciphering the underlying mechanism



Silk fibroin (SF) protein, produced by silkworm *Bombyx mori*, is a promising biomaterial while sophorolipid (SL) is an amphiphilic functional biosurfactant synthesized by non-pathogenic yeast *Candida bombicola*. SL is a mixture of two forms: acidic (ASL) and lactonic (LSL), which when added to SF results in accelerated gelation of silk fibroin. LSL is known to have multiple biological functionalities and hence these SF-SL hydrogels have promising applications in the biomedical sector. In this work, SANS, NMR and rheology are employed to examine the assembling properties of individual and mixed SLs and their interactions with SF to understand the mechanism which leads to rapid gelation. SANS and NMR studies show that ASL assembles to form charged micelles while LSL forms aggregates of fractal nature. ASL and LSL together form larger mixed micelles all of which interact differently with SF. It is shown that preferential binding of LSL to SF causes rapid unfolding of the SF chain leading to the formation of intermolecular beta sheets which trigger fast gelation. Based on the observations, gelation of SF in the presence of different sophorolipids is proposed.

### 5a.1 Introduction

Silk fibroin protein (SF) derived from *Bombyx mori* silkworm is a naturally occurring polymer that is acknowledged and widely studied for biomedical applications attributable to its mechanical strength, biocompatibility and easy processability.<sup>[224]</sup> SF has been processed into different materials such as sponges, films, tubes, electrospun mats, spheres and hydrogels for use in tissue engineering, disease models, implant devices and drug delivery.<sup>[203]</sup>

SF hydrogels have been extensively studied because they provide stable 3D porous scaffolds for applications including controlled drug release, repair and regeneration of damaged tissue and organs. Aqueous solution of silk fibroin undergoes gelation over a period of few days to weeks. Hence, physical methods such as vortexing, sonication, electric currents and low pH have been employed for constructing quick SF hydrogels.<sup>[225]</sup> Apart from these non-physiological methods, chemical additives of non-biodegradable nature such as surfactants,<sup>[117]</sup> acutely toxic natural cross-linker-genipin,<sup>[207]</sup> non-ionic triblock copolymer-ploxamers<sup>[213]</sup> and polyethylene oxide<sup>[133]</sup> have also been used to accelerate gelation of silk fibroin solutions. In the previous chapter 4, a simple method for accelerating gelation of SF which involves physical mixing of a novel biosurfactant molecule - sophorolipid (SL) with silk fibroin solution is described.<sup>[169]</sup> The gelation time of SF was reduced to 2.3h by using 3% w/v solution of SL (pH 8.0±0.2). Sol to gel transition of silk fibroin was confirmed to be driven by conformational changes in SF molecules from random coil to beta sheet structures. The increase in % beta sheet content with increasing concentration of SL from 1% w/v to 5% w/v clearly indicated that SL played an important role in driving the gelation process. However, the SF-SL interactions that lead to the accelerated gelation of SF+SL solutions upon mixing is still not understood. To elucidate this mechanism it is necessary to understand the chemical and physical properties of SL.

Sophorolipid is a functional biomolecule synthesized by a non-pathogenic yeast *Candida bombicola* ATCC 22214 when supplemented with glucose as a hydrophilic carbon source and fatty acid as lipophilic feed. Structurally SLs are composed of a polar disaccharide head group with an unusual  $\beta$  1-2 glycosidic linkage known as sophorose that is linked to the  $\omega$  or  $\omega$ -1 carbon of the hydrophobic fatty acid tail.<sup>[46]</sup> SLs are extracellularly produced by the yeast as a mixture that comprises of two forms: acidic and lactonic form. When the carboxylic end of the fatty acid tail remains free it is known as acidic SL (ASL) whereas

internal esterification of this carboxylic group with the 4' OH of the sugar molecule, results in a closed ring structure i.e. lactonic SL (LSL).<sup>[46]</sup> The percentage of each form in the mixture entirely depends upon the duration for which SL production is carried out. Prolonged incubation results in higher conversion of ASL to LSL, thus leading to a predominance of LSL in the mixture. For our experimental conditions, we observed the molar ratio of ASL: LSL to be 3:1 (shown by NMR characterization later in this study).

ASL is a water soluble asymmetrical bolaamphiphile and is known to form different self assembled structures under varied conditions such as pH, concentration and time. ASLs have been reported to self assemble into twisted giant helical ribbons; 5-11  $\mu\text{m}$  wide and several hundreds of micrometers in length under acidic conditions (pH 2.0 - 4.1).<sup>[59]</sup> The influence of the degree of ionization of the COOH group of acidic SL on its assembling behavior have also been reported using small angle neutron scattering.<sup>[60]</sup> Low and medium degrees of ionization led to the formation of neutral and charged micelles whereas at higher degree of ionization large net like aggregates were formed. Apart from pH, concentration of ASL has also been shown to remarkably influence its assembly. Evolution of micelles from spherical to cylindrical has been reported when the solution concentration of ASL was varied from 1% w/v to 5% w/v.<sup>[62]</sup> Differences in fatty acid tail saturation of ASL have also been shown to greatly impact the nature of assembly.<sup>[65]</sup>

Hydrophobicity and closed ring structure of LSL results in severe constraints on solubility and packing; hence assembling properties of LSL have not been extensively studied. Penfold et al. reported complex and unusual evolution in phase behavior with increasing concentration of LSL from small unilamellar vesicle to disordered dilute phase of tubules.<sup>[226]</sup> LSLs are hydrophobic, but have better surface tension lowering ability and useful biological properties such as antimicrobial,<sup>[215]</sup> spermicidal, cytotoxic, proinflammatory<sup>[104]</sup> and anticancerous<sup>[96]</sup>. Degree of acetylation of LSL exhibits different cytotoxic effects on human esophageal cancer cell lines KYSE 109 and KYSE 450. Diacetylated LSL promotes a better inhibition than monoacetylated LSL. These biological functionalities corroborate the usefulness of SL over other gelling agents for SF hydrogels, more specifically for biological applications. In chapter 4, it is shown that a mixture of ASL and LSL can be used to accelerate the gelation of SF. The hydrogels so produced have interesting biological properties and they enhance attachment and proliferation of cells as compared to pure SF hydrogels. Although optimal gelling can be achieved by the mixture of

these two forms, it is necessary to elucidate the role of individual molecules of ASL and LSL in SF-SL gelation. Interactions of proteins and surfactants have been studied for close to a century; however it remains an active area of research till date.<sup>[109]</sup> These interactions are governed by several factors such as protein sequence (hydrophobicity, charge and propensity towards various secondary conformations), type of surfactant (head group charge, alkyl chain length) and also the ratio of protein to surfactant.<sup>[109]</sup> Apart from this pH, ionic strength of the solvent and temperature also affect these interactions and hence govern the stability and shape of micellar structures. The surfactant molecules can interact individually with the protein or as micellar aggregates. Various models such as rod-like particle model, decorated micelle model or bead necklace model have been developed to understand protein-surfactant interactions.<sup>[109]</sup>

In this work, the two different forms of SL namely non-acetylated ASL and diacetylated LSL have been isolated and purified. These forms were characterized for purity using Nuclear Magnetic Resonance (NMR) spectroscopy and their assembling properties were studied using Small Angle Neutron Scattering (SANS) technique. The gelation of a 3% w/v solution of SF in the presence of 3% w/v solutions of ASL, LSL and their mixture in 3:1 ratio (MSL) at pH  $8.0 \pm 0.2$  were examined by rheology, NMR spectroscopy and SANS. Rheology probes the bulk gelation behavior, SANS probes the microstructure at the nm -  $\mu\text{m}$  length scales whereas NMR spectroscopy probes the SF-SL system at the atomic level and is also sensitive to the dynamical aspects of the SF-SL interaction. Although there have been some studies on understanding the gelation of SF using ionic surfactants,<sup>[117,227]</sup> this is the first study that uses a combination of multiple complementary techniques to probe the microstructure in this complex system at various length scales. Here, the complexity in the system arises due to the interactions of a mixture of ionic and non-ionic molecules with a fibrous hydrophobic protein having a predominant beta sheet conformation. These investigations provide a deeper understanding of the mechanism of accelerated SF gelation in the presence of SL.

## ***5a.2 Materials and methods***

### ***5a.2.1 Preparation of regenerated silk fibroin***

Regenerated silk fibroin solutions were prepared as per the protocol described in Section 4.2.1<sup>[169]</sup> The final ~5% (w/v) dialyzed RSF solution was then diluted to 3% (w/v) with

deionized water for further studies. The pH of the RSF was measured to be  $7.3 \pm 0.2$ . This RSF solution was also lyophilized at  $-55^{\circ}\text{C}$  using a (SCANVAC-coolsafe) lyophilizer for 8 h. The lyophilized SF powder was used for preparation of samples for NMR and SANS analysis.

### **5a.2.2 Sophorolipid synthesis and solutions**

Oleic acid derived sophorolipid (SLOA) was synthesized by supplementing *Candida bombicola* (ATCC 22214) with glucose and oleic acid using a method described in Section 4.2.2.<sup>[21]</sup> Further, for purification of diacetylated lactonic form of sophorolipid, column chromatography was used.<sup>[228]</sup> Briefly, the SLOA was first treated with hexane to remove any unreacted oleic acid. It was then purified on a silica gel (60–120 mesh) column and eluted with a chloroform/methanol gradient ranging from 99.9:0.1% to 95:5%.<sup>[228]</sup> Eluted fractions were pooled and the solvent was evaporated. Remaining solvent was completely removed by vacuum evaporation, followed by lyophilisation. This lyophilized LSL was then used in preparation of samples for NMR, SANS and rheology studies.

Alkaline hydrolysis of the sophorolipid was carried out separately to synthesize ASL as mentioned by Rau et al. (1999).<sup>[229]</sup> Hydrolysis was accomplished by suspending 20g SLOA in 50mL 5M NaOH solution and refluxing the mixture at  $100^{\circ}\text{C}$  for 10 min. After cooling, aqueous hydrochloric acid was added to give pH 4. The non-acetylated sophorolipid-acid was extracted using n-pentanol to obtain desalted form of sophorolipid. Excess solvent was removed by distillation under reduced pressure. The chemically purified product was dissolved in water and lyophilized to obtain ASL powder. The silk fibroin gelation process was studied using 3% w/v solutions of different SLs. The pH of all SL solutions was adjusted to  $8.0 \pm 0.2$  using 0.1N NaOH solution.

### **5a.2.3 Nuclear Magnetic Resonance Spectroscopy**

All NMR experiments were carried out on a 700 MHz Bruker Avance III HD spectrometer using a 5mm BBO probe with z-axis gradient. The synthesized samples of SL (ASL, LSL and SLOA) and lyophilized RSF were characterized by employing various NMR spectroscopic techniques at 298K to establish sample composition and purity. The SL samples for characterization were dissolved in deuterated methanol ( $\text{CD}_3\text{OD}$ ) at a concentration of 20mg/mL. Samples of SF for characterization by NMR were prepared by dissolving lyophilized RSF in  $\text{D}_2\text{O}$  at a concentration of 30mg/mL. The spectrum of the amide protons

of SF which exchange with the solvent were recorded in a 9:1 mixture of H<sub>2</sub>O-D<sub>2</sub>O at 298K. One dimensional (1D) <sup>1</sup>H and <sup>13</sup>C NMR spectra and two dimensional (2D) NMR experiments (correlation spectroscopy-COSY, total correlation spectroscopy-TOCSY, rotating frame Overhauser effect spectroscopy-ROESY, nuclear Overhauser effect spectroscopy-NOESY, heteronuclear single quantum spectroscopy-HSQC, heteronuclear multiple bond correlation-HMBC) were employed for sample characterization and to obtain complete spectral assignments for the SL samples. The 1D spectra were recorded using a 30° flip angle and an interscan delay of 2s. <sup>1</sup>H and <sup>13</sup>C spectra were typically recorded with 128 and 20000 scans respectively. Homonuclear and heteronuclear 2D NMR experiments were recorded with 256 × 2K and 256 × 1K data points respectively and a relaxation delay of 2s. All experiments were carried out employing standard Bruker pulse sequences.

The association behavior and mobility of SL molecules was monitored by NMR diffusion and relaxation rate measurements using the same sample concentrations as employed for gelation studies reported below. Diffusion measurements were carried out employing pulsed field gradient stimulated echo (PFGSE) experiments using bipolar gradients and a longitudinal storage period before data acquisition. A pair of magnetic field gradient pulses of strength G, and duration δ separated by a gradient recovery delay τ was applied, with the diffusion time set to Δ. Molecular diffusion over the timescale Δ, results in dephasing of the NMR signal leading to an attenuation of the observed signal. Spectra were acquired for 16 different values of G and the diffusion coefficient was determined by fitting the signal amplitude decay to the equation 5a.1,

$$\text{Equation 5a.1} \quad I = I_0 \exp \left[ -D(\gamma G \delta)^2 \left( \Delta - \frac{\delta}{3} - \frac{\tau}{2} \right) \right]$$

Where I<sub>0</sub> is the signal amplitude at zero gradient strength and γ is the <sup>1</sup>H gyromagnetic ratio. The experiments were performed using the Bruker pulse sequence 'ledbpgp2s', with the delays δ, τ and Δ set to 2.4, 0.2 and 80ms respectively while the gradient strengths ranged from 1 to 47 G cm<sup>-1</sup>. Proton spin-lattice relaxation rate (R<sub>1</sub>) was determined by inversion recovery experiments employing 20 delays. The spin-spin relaxation rates (R<sub>2</sub>) were determined by relaxation under a 2KHz spin lock field applied on-resonance for 12 delays. Signal intensities as a function of the delays were fit to I(t) = I(0)[1-2exp(-tR<sub>1</sub>)] and I(t) = I(0)exp(-tR<sub>2</sub>) respectively to extract R<sub>1</sub> and R<sub>2</sub> rates.

Sophorolipid solutions (ASL, LSL and MSL) for gelation studies by NMR were prepared in D<sub>2</sub>O at 3% w/v concentration and the pH was adjusted to  $8.0 \pm 0.2$  using a 0.1N NaOH solution in D<sub>2</sub>O. 3% w/v silk fibroin solution was prepared by dissolving the lyophilized SF powder in D<sub>2</sub>O. The un-dissolved protein was removed by centrifugation and the protein concentration was verified by UV-visible spectrophotometer (Thermo, Nanodrop) before using for NMR experiments.

To study gelation kinetics at the molecular level, the SL and SF solutions were mixed in 1:1 ratio and immediately transferred to the NMR tube and <sup>1</sup>H spectra were recorded every 15 minutes until gelation was complete. The <sup>1</sup>H spectra with suppression of residual H<sub>2</sub>O signal using the 3-9-19 sequences were recorded using a 90° pulse, relaxation delay of 6s and 144 scans. The progress of gel formation was monitored by measuring the decrease in intensity of the well separated tyrosine proton of the SF molecule at ~7.0 ppm (refer Figure 5a.1a). The maximum signal intensity at t = 0h; corresponds to the first spectrum recorded immediately after mixing SF and SL solutions. As gel formation progresses, the signal intensity decreases and formation of the gel phase is assumed to be complete when the signal intensity shows no perceptible decrease with time (time = ∞). The fraction of gel phase formed at time t is given by  $X_t = (I_0 - I_t) / (I_0 - I_\infty)$ , where I<sub>0</sub>, I<sub>t</sub> and I<sub>∞</sub> are the intensities at time 0, t and ∞ respectively.

#### **5a.2.4 Bulk Rheology measurements**

The SF solution of 3% w/v concentration was mixed with different sophorolipid solutions viz. ASL, LSL and MSL in 1:1 (v/v) ratio. Rheological measurements were performed as described in section 4.2.3a.

#### **5a.2.5 Small angle neutron scattering**

Small angle neutron scattering is a widely used technique for studying behaviour of soft matter in solution. SANS can hence be employed to study microstructures of complex fluids at mesoscopic scale. In a typical SANS experiment, when a monochromatic beam of neutron is directed at a sample, the neutrons are elastically scattered by nucleus of atoms present in the sample.<sup>[230]</sup>

SANS data is generally presented as a spectrum of intensity against the magnitude of scattering vector q ( $q = (4\pi/\lambda) \sin\theta/2$ ), where θ and λ represent scattering angle and

wavelength of incident radiation respectively.<sup>[231]</sup> The scattered intensity can be represented as:

$$\text{Equation 5a.2} \quad I = nV^2 (\Delta\rho)^2 P(q)S(q) + B$$

Where  $n$  and  $V$  represent the number density and volume of scattering objects,  $(\Delta\rho)$  is the scattering density difference between the particle and the solvent,  $P(q)$  is the form factor, which gives information about the structure, shape and size of the scatterers and  $S(q)$  is the structure factor, which gives information about interactions between the scatterers.<sup>[232]</sup>  $B$  is a constant term representing incoherent background. If for a given solution the term  $nV^2 (\Delta\rho)^2$  can be considered constant the scattered intensity mainly depends upon the form factor and structure factor.

$$\text{Equation 5a.3} \quad I(q) \sim P(q)S(q)$$

where  $I(q)$  represents scattered intensity of neutrons in absolute scale as a function of scattering vector  $q$ . For very dilute solution, where particles remain isolated, structure factor  $S(q)$  can be considered as unitary and analysis of  $I(q)$  provides information on the micellar shape depending on the form factor  $P(q)$ . But this structure factor cannot be neglected in case of repulsive interactions between defined particles and it results into strong interaction peaks in the intermediate  $q$ -range. In case of particles with undefined shape and size such as fractal objects, the scattered intensity in the low  $q$  range increases linearly and slope is used to relate the fractal dimension of the object.

The details of  $P(Q)$  and  $S(Q)$  used for data analysis of different systems are as follows:

For a sphere of radius  $R$ ,  $P(Q)$  is given by<sup>[230,233,234]</sup>

$$\text{Equation 5a.4} \quad P(Q) = \frac{16\pi^2 R^6}{9} (\rho_p - \rho_s)^2 \left[ \frac{3\{\sin(QR) - (QR)\cos(QR)\}}{(QR)^3} \right]^2$$

where  $\rho_p$  and  $\rho_s$  are the scattering length densities of the particles and the solvent, respectively. For prolate ellipsoidal particles,  $P(Q)$  may be expressed as<sup>[230,233,234]</sup>

$$\text{Equation 5a.5} \quad P(Q) = \frac{16\pi^2}{9} (\rho_p - \rho_s)^2 (ab^2)^2 \int_0^1 [F(Q, \mu)]^2 d\mu$$

where the functions are given by:

$$F(Q, \mu) = \frac{3(\sin x - x \cos x)}{x^3} \quad \text{and} \quad x = Q[a^2 \mu^2 + b^2(1 - \mu^2)]^{1/2}$$

where  $a$  and  $b=c$  and represent semi-major and semi-minor axes of prolate ellipsoid respectively ( $a>b=c$ ).  $\mu$  is a variable that signifies cosine of the angle between the directions of  $a$  and  $Q$ .<sup>[235]</sup>  $S(Q)$  correlates particles present in the system and is Fourier transform of the radial distribution function  $g(r)$ .<sup>[236]</sup> Hayter and Penfold analysis has been used to calculate  $S(Q)$  under rescaled mean spherical approximation (RMSA). RMSA assumes that charged particles interact by screened Coulomb forces.<sup>[237–239]</sup>

In the case of particle aggregation<sup>[240]</sup> or bead-necklace structure<sup>[241]</sup> formation that is marked by mass fractal structure,  $S(Q)$  is determined by using following equation:

$$S_{mf}(Q) = 1 + \frac{1}{(Qr_m)^{D_m}} \frac{D_m \Gamma(D_m - 1)}{\left[1 + (Q\xi)^{-2}\right]^{(D_m - 1)/2}} \sin\left\{(D_m - 1) \times \tan^{-1}(Q\xi)\right\}$$

Equation 5a.6

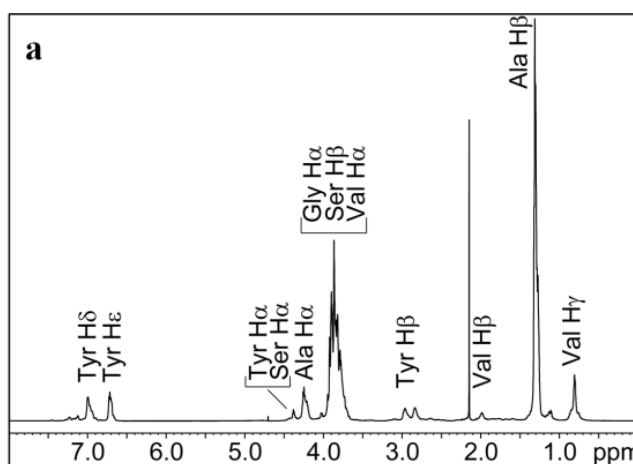
where  $\xi$  signifies the maximum length up to which fractal microstructure exists,  $r_m$  is the size of building block and  $D_m$  is the mass fractal dimension.<sup>[242]</sup> For the data analysis the corrected scattering data has been compared with different theoretical models. Non-linear least-square fitting program has been employed to optimize the parameters under study.<sup>[235]</sup> Instrumental smearing was corrected throughout the data analysis. The modelled scattering profiles were smeared by the appropriate resolution function to compare with the measured data.<sup>[230,243,244]</sup>

### 5a.3 Results and Discussion

The objective of this work is to decipher the mechanism of accelerated gelation of SF-SL systems. It is therefore necessary to independently characterize the SF and SL molecules to understand their chemical structure and assembling behavior in aqueous solution and investigate the interactions between SF and SL molecules. In the following sections results obtained by employing spectroscopic and scattering techniques are described to investigate these properties.

### 5a.3.1 Characterization of Silk Fibroin by NMR and SANS

SF from *Bombyx mori* has been studied extensively by NMR, especially in the solid state.<sup>[245]</sup> The  $^1\text{H}$  NMR spectrum of SF shown in Figure 5a.1a agrees well with previously published spectra<sup>[246,247]</sup> and displays characteristic signals from the Glycine, Alanine, Serine, Valine and Tyrosine residues. The purity of regenerated silk fibroin (RSF) was confirmed by recording  $^1\text{H}$ - $^{13}\text{C}$  and  $^1\text{H}$ - $^{15}\text{N}$  HSQC spectra (Figure 5a.1b right and left respectively) and comparing with reported data.<sup>[126,248]</sup>  $^1\text{H}$ - $^{15}\text{N}$  TROSY spectrum in Figure 5a.1b (left) clearly shows that one set of NH resonance can be assigned to Tyr and Val, minimum two sets of NH resonance were assigned to Ser, three sets to Ala, and at least 7 sets to Gly. Multiple sets of resonances for a given residue correspond to the location of the residue in different repetitive motifs in the SF protein. For example, depending on the flanking residues, glycine can have slightly different chemical shifts in ala-gly-ala, ala-gly-ser, ala-gly-tyr etc.  $^1\text{H}$ - $^{13}\text{C}$  HSQC spectrum (Figure 5a.1b, right) shows the chemical shift correlations for the protonated carbons in the backbone and side chains of the protein. The tyrosine correlations are shown in the inset.



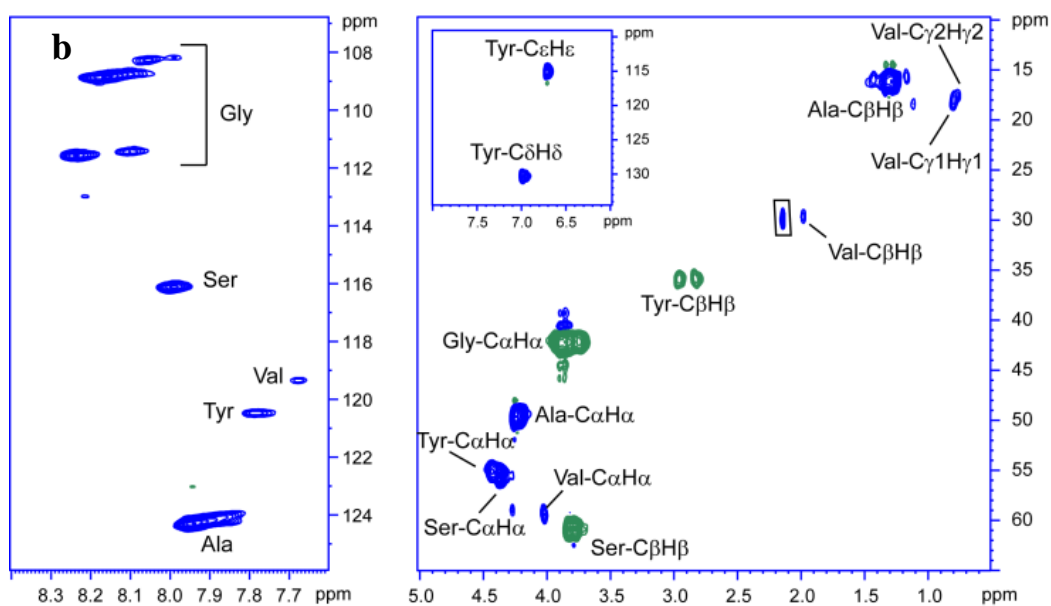


**Figure 5a.1** (a)  $^1\text{H}$  spectrum of SF in  $\text{D}_2\text{O}$  obtained on a 700 MHz spectrometer at 298K. (b)  $^1\text{H}$ - $^{15}\text{N}$  TROSY (transverse relaxation optimized spectroscopy) spectrum in  $\text{H}_2\text{O}$  at 278K (left) and  $^1\text{H}$ - $^{13}\text{C}$  HSQC spectrum in  $\text{D}_2\text{O}$  at 298K (right) of SF. The tyrosine correlations are shown in the inset. In the multiplicity edited spectrum the positive  $\text{CH}_3$  and  $\text{CH}$  correlations are shown in blue while the negative  $\text{CH}_2$  correlations are shown in green.

Figure 5a.2 depicts the SANS data of 3% w/v pure silk fibroin in  $\text{D}_2\text{O}$ . The data shows a monotonically decreasing scattering cross-section as a function of  $Q$  indicating  $S(Q) \sim 1$ . The fit using prolate ellipsoidal form factor predicts a semi-major and minor axis of 130Å and 37Å respectively and a radius of gyration ( $R_g$ ) of about 62 Å. The inset shows the Guinier analysis of the initial data points, which also calculates a  $R_g$  of 60 Å. This clearly indicates the existence of silk fibroin in random Gaussian conformation.

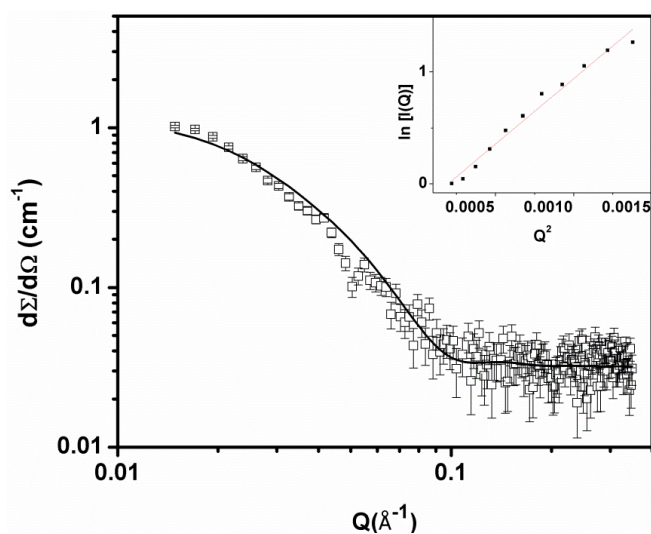
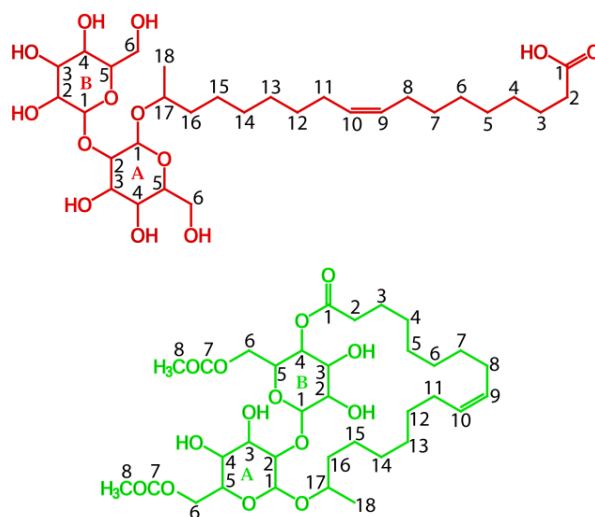


**Figure 5a.2** Small angle neutron scattering from 3% w/v pure silk fibroin in  $\text{D}_2\text{O}$ . Inset depicts Guinier analysis of the initial data points.

### 5a.3.2 Characterization of Sophorolipids by NMR and SANS

The numbering of the protons in ASL and LSL molecules is indicated in Scheme 5a.1. The spectral assignments were obtained from 1D and 2D NMR spectra of purified ASL and LSL samples in deuterated methanol ( $\text{CD}_3\text{OD}$ ) (shown in Figure 5a.3, 5a.4).



**Scheme 5a.1** Representation of acidic and lactonic SL molecules with labeling of atoms.

The NMR spectra of SL samples in deuterated methanol shown in Figure 5a.3, display characteristic signals from the sugar rings and the fatty acid chain in agreement with published spectra.<sup>[229,249]</sup> The BH4 signal of LSL showed a significant downfield shift compared to its chemical shift in the ASL spectrum due to the formation of a lactone ring between carboxylic group and C2 -OH group of the sugar B shown in Scheme 5a.1. In addition, the H2 methylene protons which are shifted downfield with respect to the other aliphatic protons of the fatty acid chain, showed distinctly different chemical shifts in LSL (2.4 ppm) and ASL (2.3 ppm). The LSL sample was obtained in the diacetylated form as indicated by the strong methyl signals from the acetyl groups of the sugar. The alkaline hydrolysis procedure for the synthesis of ASL from SLOA, resulted in deacetylation of the sugars in ASL, marked by absence of AH6 and BH6 signal corresponding to acetyl groups at A6 and B6 position of sugars.

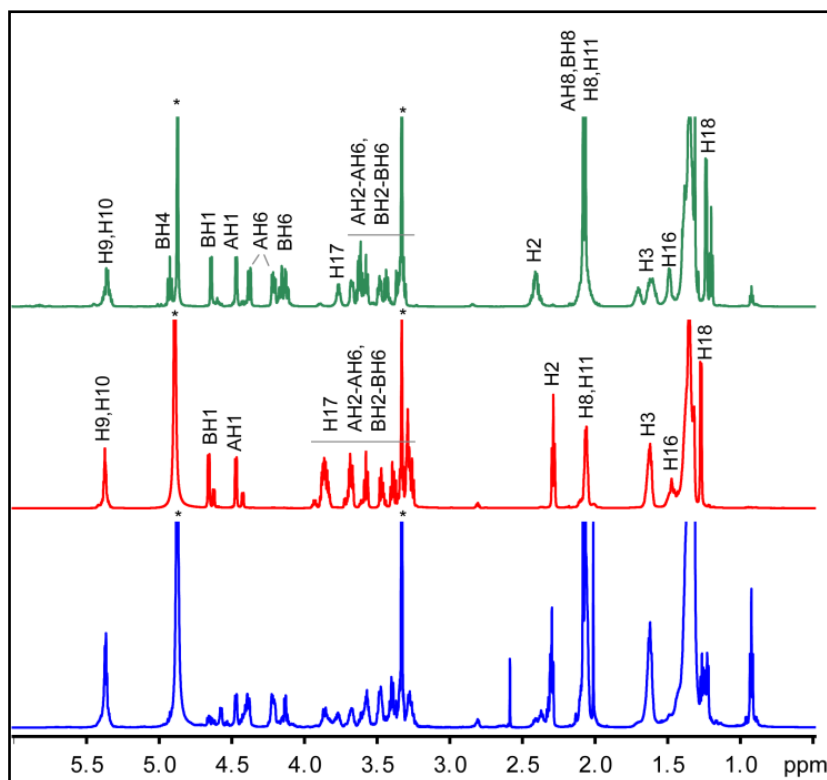


**Figure 5a.3**  $^1\text{H}$  NMR spectra of LSL (green), ASL (red) and SLOA (blue) obtained on a 700 MHz spectrometer at 298 K. Signal assignments are indicated for LSL and ASL, with residual solvent signal marked by asterisks.

In Figure 5a.4 the comparison of the HSQC and HMBC spectra show the characteristic sugar to fatty acid linkages and disaccharide linkages in ASL and LSL. In both the sophorolipid forms, long range correlation (BH1-AC2) confirmed the disaccharide linkage of sophorose connecting sugar rings A and B while the correlation between AH1-C17 confirmed linking of sugar ring A to the fatty acid to form the sophorolipid. Additionally, LSL showed long range correlation (BH4-C1) between the BH4 proton and the carbonyl group due to lactone formation. In both ASL and LSL, a second glycolipid with linkage to the  $\omega$  carbon of the fatty acid, was observed which is present as a minor form as indicated by the correlations shown by dotted lines in Figure 5a.4. This form could not be eliminated by the purification procedures and has also been observed in previously reported NMR spectra of ASL by Baccile et. al. (2013).<sup>[249]</sup>

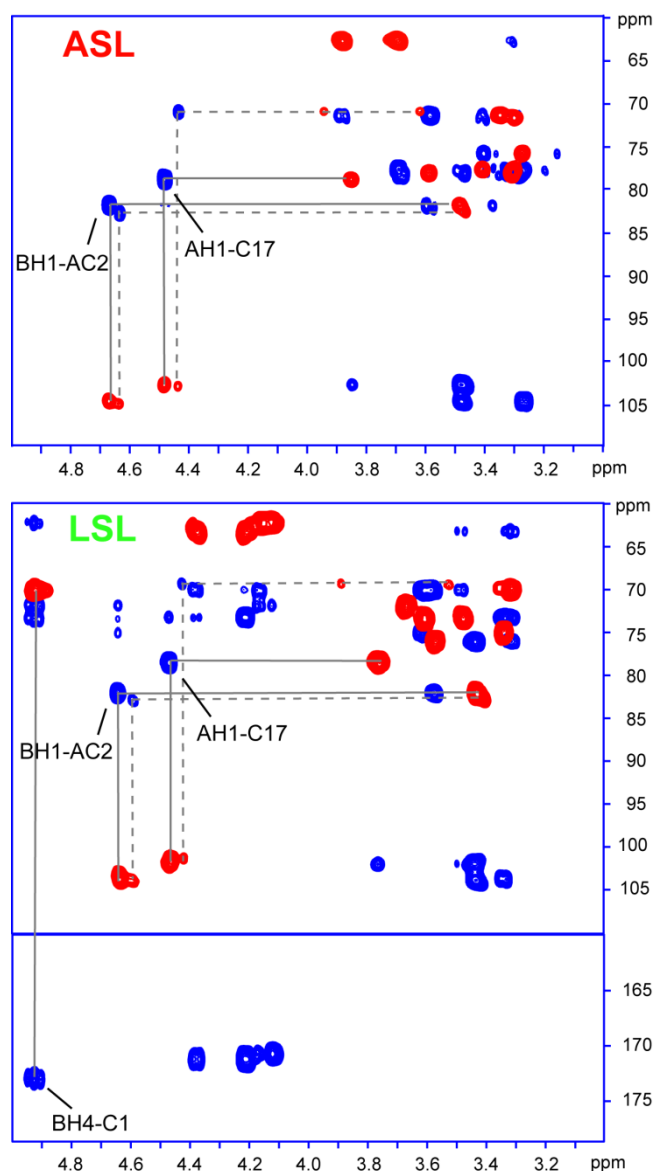


**Figure 5a.4** Overlay of HSQC spectrum (red) showing single bond C-H correlations and HMBC spectrum (blue) showing long range C-H correlations in ASL and LSL at 298K.

The presence of both ASL and LSL as major components in oleic acid derived sophorolipid (SLOA) isolated from *Candida bombicola* ATCC 22214 was confirmed by comparing the NMR spectra of SLOA with those of the pure forms. The ASL and LSL components present in SLOA are readily visible in the HSQC spectrum (Figure 5a.5), which is better resolved and has less overlapping signals as compared to the 1D spectrum. The ratio of ASL:LSL present in the SLOA used in this study was calculated to be 3:1 mole ratio from the integration of the H2 signal in the  $^1\text{H}$  NMR spectrum. The two pure forms ASL and LSL mixed in the same ratio of 3:1 form the mixed sophorolipid (MSL). MSL has been later used in mechanistic studies.

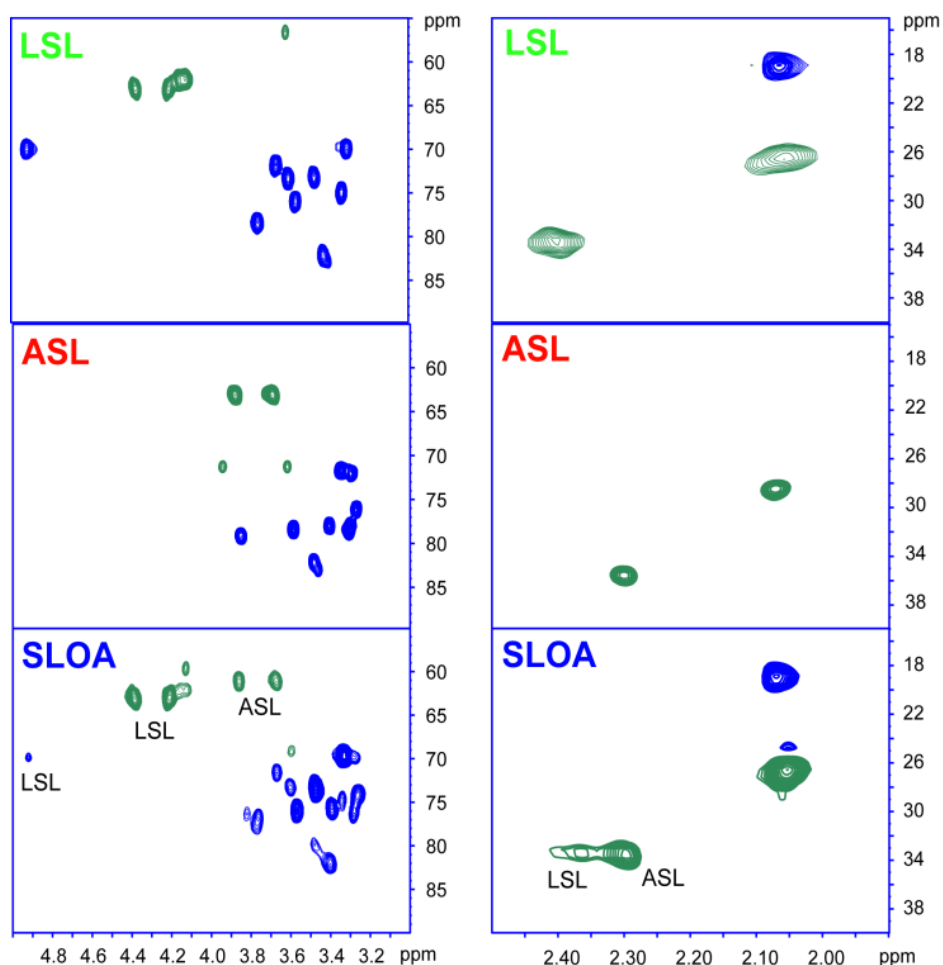


**Figure 5a.5** Parts of the multiplicity edited  $^1\text{H}$ - $^{13}\text{C}$  HSQC spectra showing the sugar region (left) and aliphatic region (right). The positive " $\text{CH}_3$ " and " $\text{CH}$ " group correlations are shown in blue while the negative " $\text{CH}_2$ " group correlations are shown in green. Spectra of Oleic acid derived SL from *Candida bombicola* (SLOA), column purified diacetylated lactonic SL (LSL) and non-acetylated acidic SL (ASL) are shown in separate panels.

These pure forms of SLs were then used to study their assembling properties in aqueous solutions by SANS. Micellar assembly of SLs has been studied using SANS before.<sup>[62]</sup> However, the main focus was on examining the assembly of pure ASL as a function of its concentration and degree of ionization. Figure 5a.6 shows the SANS data of 3% w/v ASL, LSL and MSL solutions and the results have been summarized in Table 5a.1.

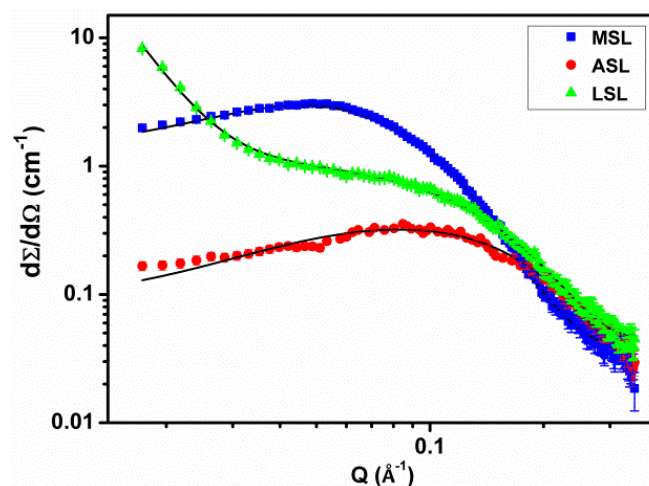


**Figure 5a.6** SANS on individual sophorolipids, namely mixed SL, acidic SL, lactonic SL at pH  $8.0 \pm 0.2$

**Table 5a.1** The fitted parameters of the sophorolipid systems

System	Semi-major axis (Å)	Semi-minor axis (Å)	Equivalent radius $(ab^2)^{1/3}$ (Å)	Charge (e.u.)	Fractal dimension
ASL	16.0	12.0	12.9	7.6	-
LSL	25.0	12.0	15.3	-	2.8 (mass)
MSL	39.0	16.5	21.9	10.0	-

The non-acetylated ASL solution was observed to be visually clear indicating the presence of small assemblies with highly curved micellar structures, as reported by Penfold et al. (2011)<sup>[226]</sup> The SANS data for ASL can be fitted<sup>[226]</sup> using a prolate ellipsoidal form factor. The scattering data of ASL in Figure 5a.6 also shows a clear and broad correlation peak indicating the presence of interacting charged micelles.

The analysis was performed using a structure factor,  $S(Q)$ , as calculated by Hayter and Penfold analysis for charged macroions since deprotonation of  $\text{COOH}$  into  $\text{COO}^-$  introduces electrical charges located at the surface of the micellar objects.<sup>[62]</sup> The parameters in Table 5a.1 show that ASL forms nearly spherical charged micelles. Also, it may be noted here that the calculated radius of semi-minor axis (12 Å) is significantly lower than the fully extended chain length of a C18 fatty acid chain ( $\sim 24$  Å). This suggests that ASL molecule assumes a highly bent conformation within the ASL micelle. These observations are in agreement with those reported by Baccile et al.<sup>[62]</sup> However, it is not possible to conclusively state whether the ASL molecules assume a parallel or antiparallel

conformation. In addition to SANS, the size of the ASL micelle can also be determined by NMR. The well separated H<sub>2</sub> signal in ASL solution (D<sub>2</sub>O) was used to estimate the diffusion coefficient which was found to be  $1.052 \times 10^{-10} \text{ m}^2 \text{ s}^{-1}$  at 298K. Based on this diffusion coefficient, radius of hydration ( $r_H$ ) of 18.9 Å (assuming spherical micelle and validity of Stokes Einstein equation) was calculated. Since the solvent viscosity was employed in the calculation, the estimated  $r_H$  value may be considered as an upper bound for the size of ASL micelles in D<sub>2</sub>O. Thus, the NMR data corroborated the micellar size predicted from the SANS analysis.

For LSL, at 3% w/v concentration, the solution was found to be turbid. This turbidity may be attributed to poor solubility of LSL in water. In contrast to ASL, the scattering data of LSL did not show any correlation peak indicating very low charge on these micelles. The observation of a strong linear increase in  $I(q)$  in the low Q region indicated the existence of large aggregates. In comparison to ASL the larger size of LSL assemblies may be attributed to its lactone ring structure and diacetylation of the head group which results in increased hydrophobicity. LSL avoids interacting with the surrounding hydrophilic environment and assembles into structures in mass fractal form. The LSL data has been fit by combining power law behavior from the aggregates and scattering from the individual assemblies.

The nature of scattering data of MSL was found to be very similar to the ASL system. However, the intensity for MSL was much higher as compared to that of ASL; thereby suggesting larger size of these micelles. This implies that the small amount of LSL present in the mixture, imposes packing constraints resulting in a slightly larger hydrophobic core and thus, increasing the size of the micelle. NMR diffusion measurements also indicated larger micellar size in the MSL system compared to ASL. The  $r_H$  value calculated, assuming a spherical shape for the micelle, was 28 Å at 298K (similar to the equivalent radius calculated by SANS given in Table 5a.1).

The rationale for the large micelle size in case of the MSL system was sought by probing the association between the two molecules i.e. ASL and LSL in solution by NMR. LSL by itself has very low solubility in aqueous medium owing to its relatively hydrophobic nature shown in Figure 5a.7.

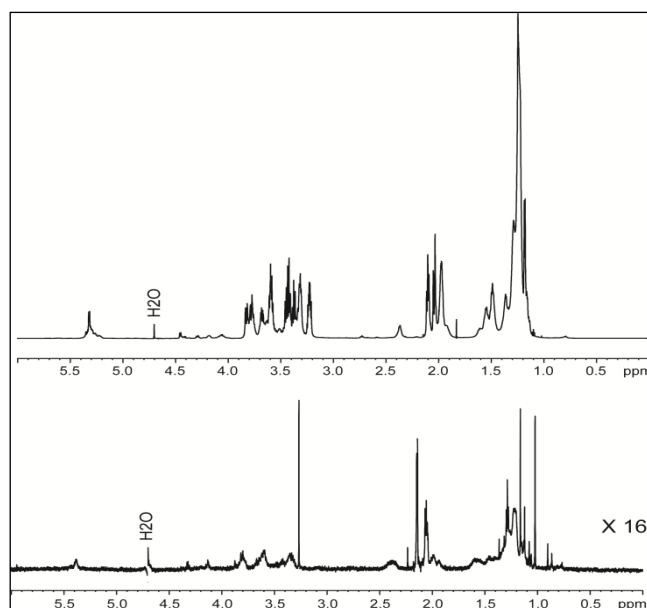


**Figure 5a.7** <sup>1</sup>H NMR spectra of a saturated solution of LSL (below), and solution of MSL with LSL:ASL ratio 1:3 (above) recorded on a 700 MHz spectrometer at 298 K with 128 scans. LSL spectrum is shown with 16 times magnification since signals were very weak due to poor solubility. The sharp signals in the LSL spectrum are from residual impurities.

However, in the MSL sample, the presence of ASL enhances the solubility of LSL suggesting that the LSL molecules may be incorporated in the hydrophobic regions of the ASL assemblies in solution. The NMR spectrum shows the presence of both ASL and LSL in solution and integration of the peaks corresponding to ASL and LSL indicates that the two components are present in a molar ratio of 3:1 (Figure 5a.8).

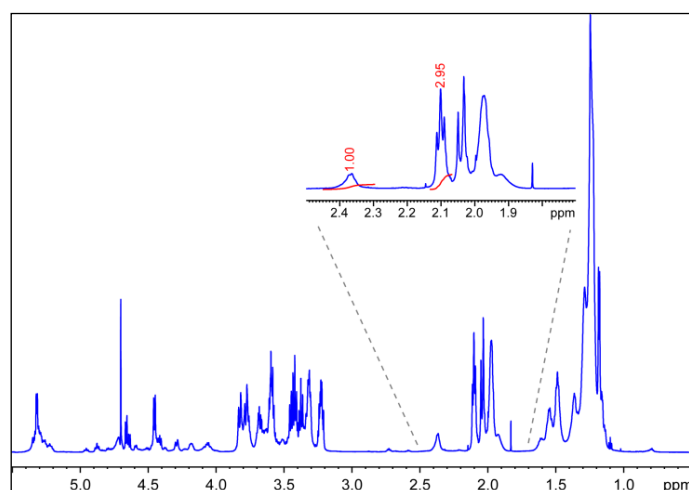


**Figure 5a.8** <sup>1</sup>H spectrum of ASL and LSL mixture in D<sub>2</sub>O obtained on a 700 MHz spectrometer at 298 K. The H<sub>2</sub> signals of ASL and LSL show a ratio of 3:1 for the two components in solution. The presence of signature corresponding to LSL molecule in the mixed solution of ASL and LSL confirms its enhanced solubility in the presence of acidic SL.

A series of spectra obtained in the temperature range 278 - 318K shows that this ratio is maintained, suggesting that relatively stable micellar structures incorporating the two types of sophorolipids are formed. In order to understand the nature of the association between LSL and ASL, we carried out diffusion measurements by employing PFGSE NMR experiments. The well separated H<sub>2</sub> signals from the methylene protons were chosen as probes to monitor LSL and ASL separately in the diffusion experiments.

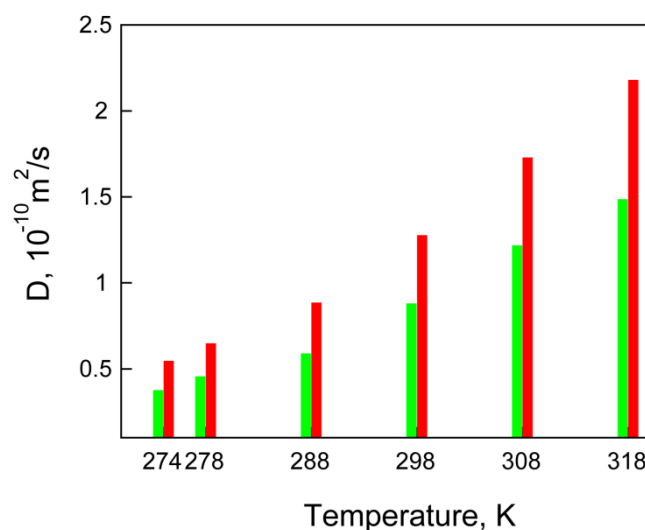


**Figure 5a.9** Temperature dependence of the diffusion coefficients of ASL (red) and LSL (green) in a mixture of ASL and LSL forms in 3:1 molar ratio in D<sub>2</sub>O.

In the MSL solution, the diffusion coefficients corresponding to the LSL signal is lower compared to that measured for the ASL signal at all temperatures (Figure 5a.9). The H<sub>2</sub> signal of LSL is expected to arise entirely from a mixed micelle, since LSL itself has very low solubility in aqueous solution. The H<sub>2</sub> signal from ASL on the other hand could have contributions from the mixed micelle, micelles composed of only ASL and non-associated ASL molecules in solution. The ASL molecule could be in fast exchange between mixed micelles, ASL micelles and non-associated forms since we do not see separate signals corresponding to these different environments. Thus, the diffusion coefficient measured for ASL would be a population weighted average of the diffusion coefficients of the different species present in solution. The lower diffusion coefficient measured for H<sub>2</sub> signal of LSL is thus, representative of the mixed micelle and is consistent with its larger size. Further evidence for the larger size of the mixed micelle is obtained from relaxation rate

measurements. At 298K the  $R_2$  value measured for the H2 signal of LSL is  $19.3 \text{ s}^{-1}$  while that of ASL is  $7.3 \text{ s}^{-1}$  indicating that the mixed micelle in which LSL is incorporated is larger in size. In order to determine the spatial proximity of the ASL and LSL molecules in the mixed micelles, nuclear Overhauser effect spectroscopy (NOESY) spectra of the MSL solution at 298K was recorded (Figure 5a.10).

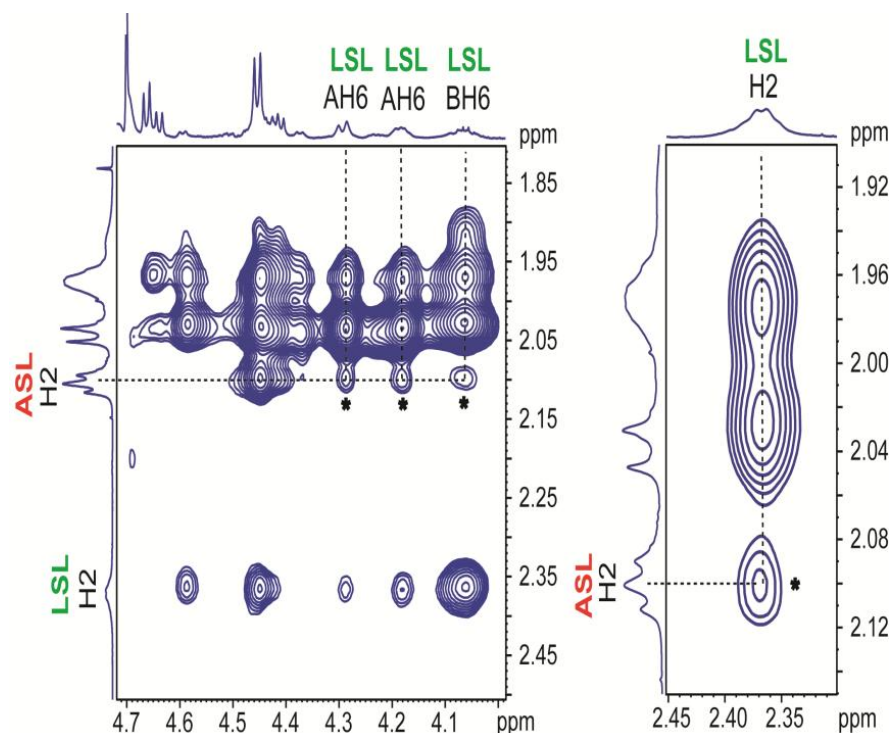


**Figure 5a.10** NOESY spectrum of a mixture of ASL and LSL forms in 3:1 molar ratio in  $\text{D}_2\text{O}$  obtained on a 700 MHz spectrometer at 298K. The mixing time employed was 800 ms. The cross peaks between ASL and LSL forms are indicated by asterisks.

While most of the  $^1\text{H}$  NMR signals of ASL and LSL were overlapped, the H2 signals of ASL and LSL as well as the signals from the H6 protons of the acetylated sugars in LSL were fairly well separated. Hence, unambiguous evidence for spatial proximity of ASL and LSL in a mixed micelle could only be obtained by detecting NOE cross peaks between H2 of ASL and H2 or H6 protons of LSL. All cross peaks in the NOESY spectra were positive indicating the presence of molecular assemblies which have rotational correlation times,  $\tau_c$  that falls in the long correlation limit ( $\omega_0\tau_c \gg 1$ ,  $\omega_0$  being the frequency) typically observed for macromolecules. Cross peaks between H2 of ASL and LSL protons were not observed at low mixing times implying that the two species are at a distance exceeding  $5\text{\AA}$ . However at a mixing time of 800ms, weak cross peaks were observed between H2 of ASL and LSL as well

as H2 of ASL and the H6 sugar protons of LSL (Figure 5a.10). This implies that the two species approach close enough to allow magnetization transfer through spin diffusion. The micelles were highly dynamic, existing in an equilibrium between different types of assemblies (mixed ASL/LSL micelles, ASL micelles) as well as non-associated forms, hence ASL and LSL molecules were not expected to form a close association showing direct NOE cross peaks between them. On the basis of the observations from SANS and NMR experiments, the micellar assemblies formed in ASL, LSL and MSL maybe represented as shown in Figure 5a.11.

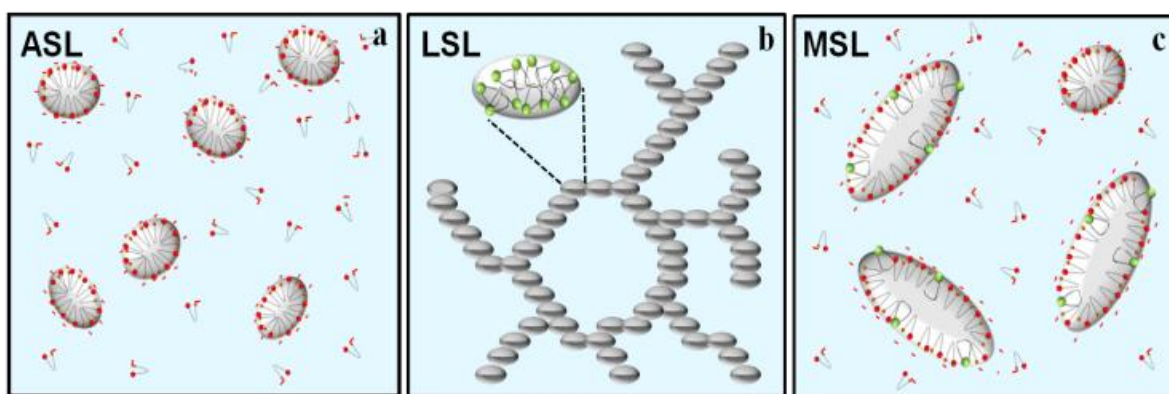


**Figure 5a.11** Diagrammatic representation of different SL systems in solution.

### 5a.3.3 Bulk gelation in different SF-SL systems

The role of sophorolipid in accelerating the gelation of regenerated silk fibroin solution has already been described in chapter 4.<sup>[169]</sup> The sol to gel transformation was shown to be the result of a transition in silk fibroin from amorphous random coil conformation to crystalline beta sheet form.<sup>[169]</sup> Figure 5a.12a depicts the bulk gelation kinetics of different SF-SL samples monitored using time sweep experiment in couette geometry in a rheometer. As can be seen in the Figure 5a.12a, the pure SF solution does not gel and its storage modulus ( $G'$ ) and loss modulus ( $G''$ ) remain unaltered during the entire experimental time frame. On the other hand, upon addition of sophorolipid, gelation commences at different time points depending upon the type of sophorolipid used. For the ASL, gelation is a two step process. A slow building up of  $G'$  is observed for the first  $\sim 10$ h followed by a rapid increase in  $G'$  and a corresponding rise in  $G''$ , until complete gelation has been achieved. ASL can electrostatically interact with cationic side chains of amino acid residues. However, the SF chain has less than 6 mol% of cationic amino acids. Thus, individual ASL molecules probably

interact with the SF chain and cause slight unfolding of the chain, which is not enough to trigger gelation. However, co-operative binding of ASL molecules above the critical aggregation concentration for the ASL-SF system, could be the reason for the rapid gelation after 10h.<sup>[109]</sup> These interactions may be non-ionic in nature. Also, the isoelectric pH for SF molecule is 3.9.<sup>[250]</sup> Thus, at the experimental pH of  $8.0 \pm 0.2$ , the SF molecule has an overall negative charge. Hence, interactions between the ASL molecules and SF molecules are hindered due to electrostatic repulsion.

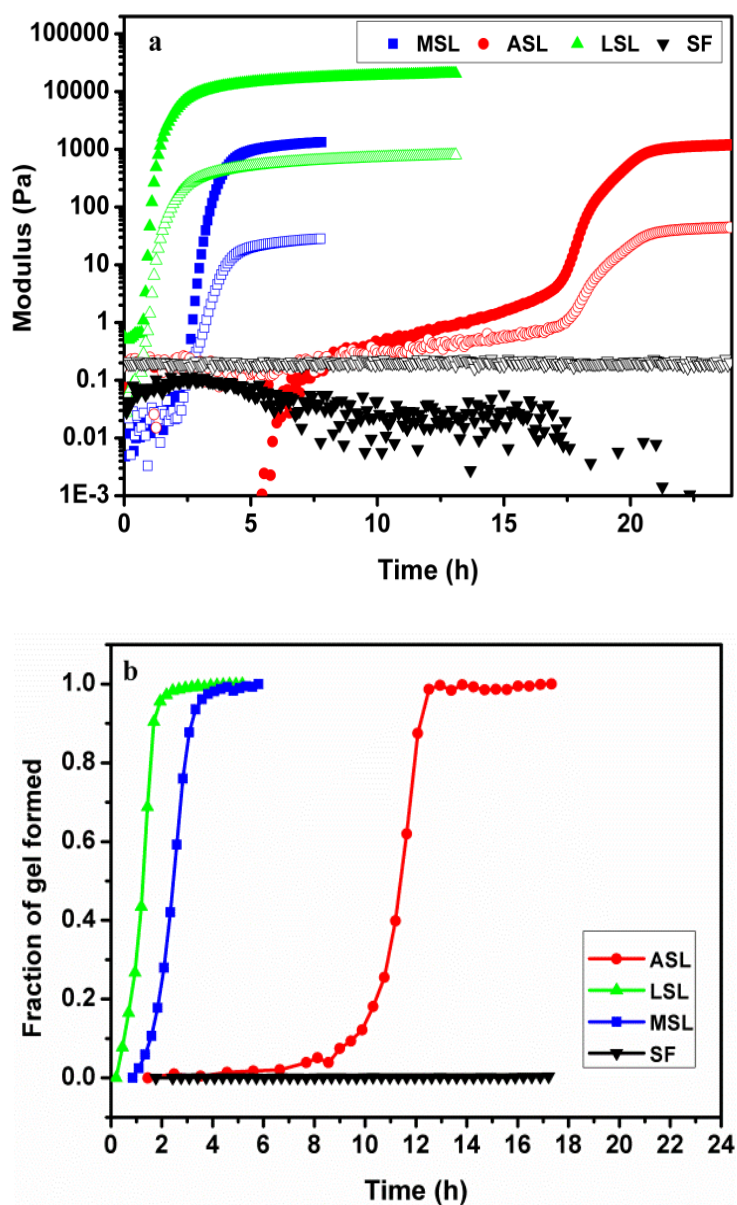


**Figure 5a.12** Rheological time sweep experiment (a) (Filled symbols –  $G'$  ; Unfilled symbols -  $G''$ ) and molecular gelation studies using  $^1\text{H}$  NMR (b) on pure SF, SF+ASL, SF+LSL and SF+MSL systems

The induction time for gelation of SF-LSL system was found to be the lowest i.e. about 0.8h. The SF - MSL system gels at an intermediate time frame of ~2.3h. Since LSL is a non-ionic surfactant molecule, it interacts with the protein predominantly through its hydrophobic tail and the hydrophobic domains on the SF chains. These results indicate that although sphorolipids accelerate the gelation process, the presence of the relatively hydrophobic LSL plays a crucial role in reducing gelation time.

#### ***5a.3.4 Molecular gelation in different SF-SL systems***

In order to further understand the SF-SL gelation mechanism, the gelation kinetics was also studied by NMR spectroscopy. Initially, the SF and SL molecules are in the solution phase and have considerable mobility resulting in narrow spectral lines. However, as the sol-gel transformation begins, the mobility of the SF and SL molecules incorporated in the gel phase is significantly reduced, leading to broad spectral lines which cannot be detected. Thus, gelation kinetics maybe monitored by measuring the decrease in signal intensity as a function of time.

The molecular gelation kinetics data shown in Figure 5a.12b corroborates the observations from rheological measurements and confirms that rate of gelation is fastest in the presence of LSL. Thus, rate of gelation exhibits the following trend: LSL > MSL >> ASL >> SF. Although the trend in rate of gelation measured by both the techniques is similar, the induction time for gelation is always smaller for the NMR experiment as compared to the corresponding rheological measurement. This difference is a result of two factors; (i) NMR sense the restrictions in molecular mobility imposed by the onset of gelation and reports on the initial stages of the assembling process, by monitoring the species in solution. Rheology on the other hand probes bulk behavior (solution and gel states), hence in addition to the initial assembling process it can sense further development of the gel network by interaction of the initial aggregates. (ii) NMR experiments were done using D<sub>2</sub>O as a solvent as against the use of H<sub>2</sub>O for rheological measurements. We have observed that SF gels faster in D<sub>2</sub>O compared to H<sub>2</sub>O.

### 5a.3.5 Mechanistic understanding of SF-SL systems

The difference in gelation observed for the three SF-SL systems is primarily governed by the assembly of SL molecules in solution, as discussed earlier, and their interaction with the SF protein. The ASL and LSL molecules assemble differently owing to their chemical structure as shown above and their interaction with the protein depends upon the stability of the assembly. The interaction of SF with the different sophorolipids (ASL/LSL/MSL) was probed using SANS and the data along with model fits are shown in Figure 5a.13. The details of model fits and parameters are summarized in Table 5a.2.

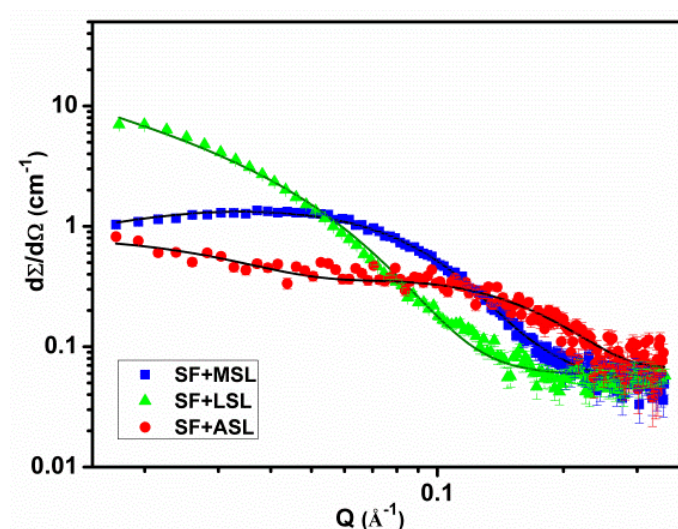


**Figure 5a.13** SANS data and model fits for SF + LSL/ASL/MSL systems at pH  $8.0 \pm 0.2$ .

**Table 5a.2** The fitted parameters of SF+SL systems.

System	Semi-major axis a (Å)	Semi-minor axis b (Å)	Charge (e.u.)
SF+ASL*	15.5	12	7.6
SF+MSL	35.0	16.6	5.2

\*  $R_g = 57 \text{ \AA}$

System	Radius of micelle $r_m$ (Å)	Fractal dimension $D_f$	Overall length radius of fractal $\xi$ (Å)
SF+LSL	33.0	1.3	180

It is important to note here that the SANS data were collected for 4h immediately after mixing SF and SL solutions. In this time frame, ASL+SF solutions do not gel whereas SF+LSL solutions undergo sol-gel transition.

The SANS data for the SF+ASL system shows distinctive signatures of charged micelles in the intermediate Q range, while the low Q region shows characteristic features for SF chain in random Gaussian coil conformation (Figure 5a.14).

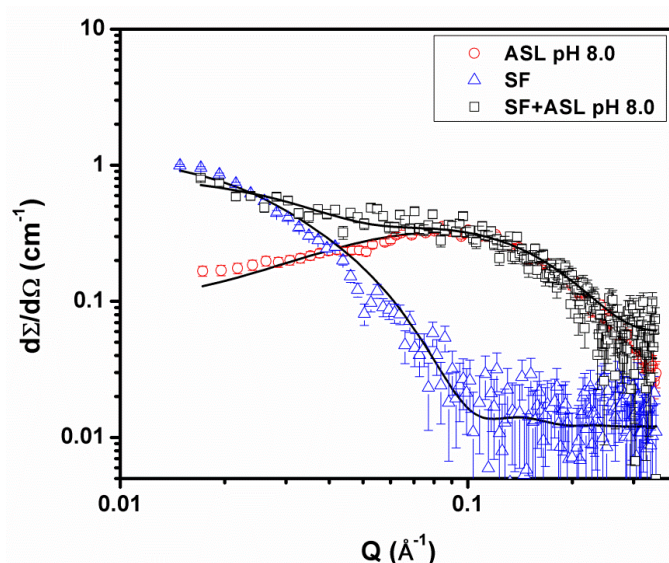


**Figure 5a.14** SANS data of ASL, SF, SF+ASL. Experimental data of SF+ASL solution depict features of both SF and ASL.

This indicates that there is no significant interaction between the ASL micelles and SF molecules immediately on mixing (as illustrated in Figure 5a.15). The models used to represent surfactant-protein interactions, for fitting the experimental data, also results in parameter values that are very similar to those of the individual components. Refer to Table 5a.1 and 5a.2.

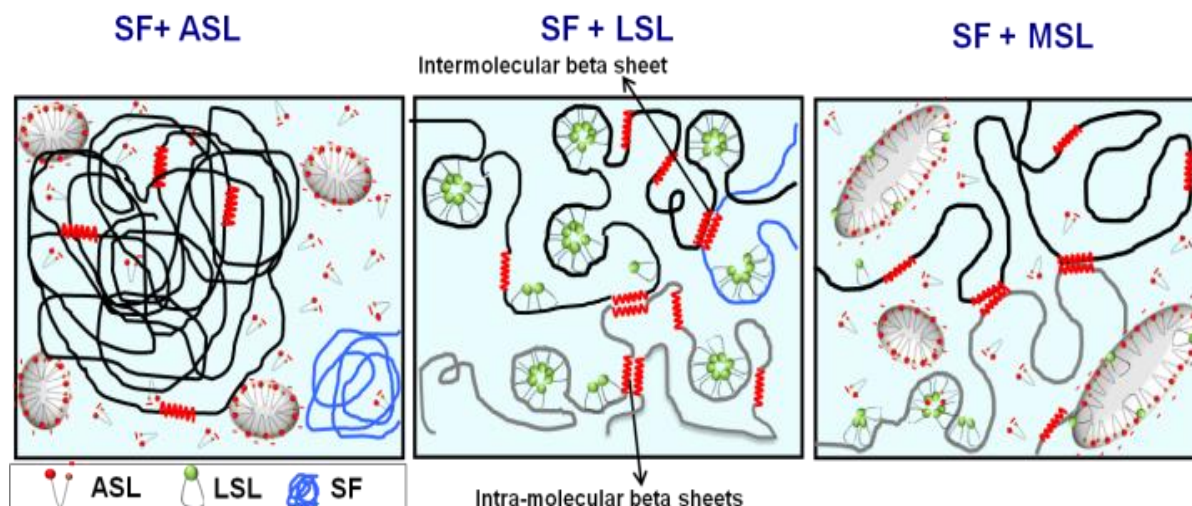


**Figure 5a.15** Schematic representation of SF-SL gelation mechanism, with individual SF chains shown in different colors.

In case of the SF+LSL system, comparison of the SANS scattering data before (Figure 5a.6) and after (Figure 5a.13) the addition of SF solution shows a marked difference that could only arise due to a change in microstructure of individual components. This implies that the self-interaction of LSL molecules and random Gaussian coil of SF molecules must be disrupted. The LSL adsorbs on the SF protein, forming small micelle-like clusters leading to a bead-necklace kind of morphology as widely described for various protein-surfactant systems in the literature (Figure 5a.15).<sup>[251,252]</sup> The SANS data has been fitted using this bead necklace model. Since LSL is an uncharged molecule, the interactions between LSL and SF chains are predominantly hydrophobic in nature. Adherence of few molecules or micelles results in unfolding of the SF molecule chain, thus exposing the hydrophobic patches embedded in the interior of the random coil.<sup>[253]</sup> Further, the opening of the SF chains allows the formation of intra and inter-molecular beta sheets as shown in Figure 5a.14, which eventually leads to the three dimensional hydrogel networks.

Unlike LSL, the scattering of MSL sample after the addition of SF does not appear to change significantly. In SF+MSL, the SANS data shows a correlation peak indicating the presence of freely interacting charged micelles, which is similar to the observation in MSL solution. Also, SANS data of SF+MSL does not show independent signatures of the SF molecule. This is in contrast to SANS scattering from SF+ASL sample which shows (Figure

5a.15) signature of both the components as they do not interact with each other for a prolonged period.

The presence of lactonic SL in the MSL solution allows some molecules of LSL to interact with the hydrophobic domains of SF by escaping from the mixed SL micelles (refer Figure 5a.15). This LSL driven unfolding of SF chains suppresses the distinct scattering signal of the pure SF chain in SF+MSL. On the other hand, the ASL micelles still exist in solution and thus their signature (charged micelles) persists in scattering. The data has been fitted to prolate micelles as it does not show signatures of bead necklace model. As a result, a medium stage micellization is observed in MSL. Acidic SL micelles could also be attaching to the silk fibroin protein chain but repulsion due to high charge restricts them from coming close or allowing multiple micelles to bind to a single chain.

In LSL and MSL samples, unlike ASL, the presence of lactonic sophorolipid is a common factor and they differ only in terms of the percentage and micellar nature of LSL present. Rheology and NMR kinetics experiments clearly show that among all three samples LSL gels fastest followed by MSL. This clearly indicates the significance of LSL in the gelation process. In order to understand the role of LSL in enhancing the gelation rate, we carried out NMR investigations of the SF+MSL sample. As discussed earlier, the solubility of LSL in D<sub>2</sub>O increases significantly in presence of ASL. A mixture of ASL and LSL in 3:1 molar ratio gives a clear solution and NMR spectra shows the presence of both ASL and LSL signals. The larger size of micelles in MSL as inferred from the SANS data (refer Table 5a.1) and NMR diffusion measurements indicate the formation of mixed micelles incorporating the two forms of sophorolipids. Figure 5a.16a shows the aliphatic region of a series of HSQC spectra recorded during successive additions of 10 $\mu$ l of SF (20mg/ml) solution to a solution of MSL. Unlike the ASL signal, the intensity of the LSL signal decreases significantly with increasing SF. Also, the overlay of the HSQC (Figure 5a.16b) of MSL and MSL+SF (80 $\mu$ l) shows that the LSL signals undergo a significant loss of intensity and are too weak to be observed while the intensity of ASL signals are relatively unchanged. Signal loss arising from the broadening of spectral lines as a result of intermediate exchange on the NMR time scale is a signature of binding interactions.

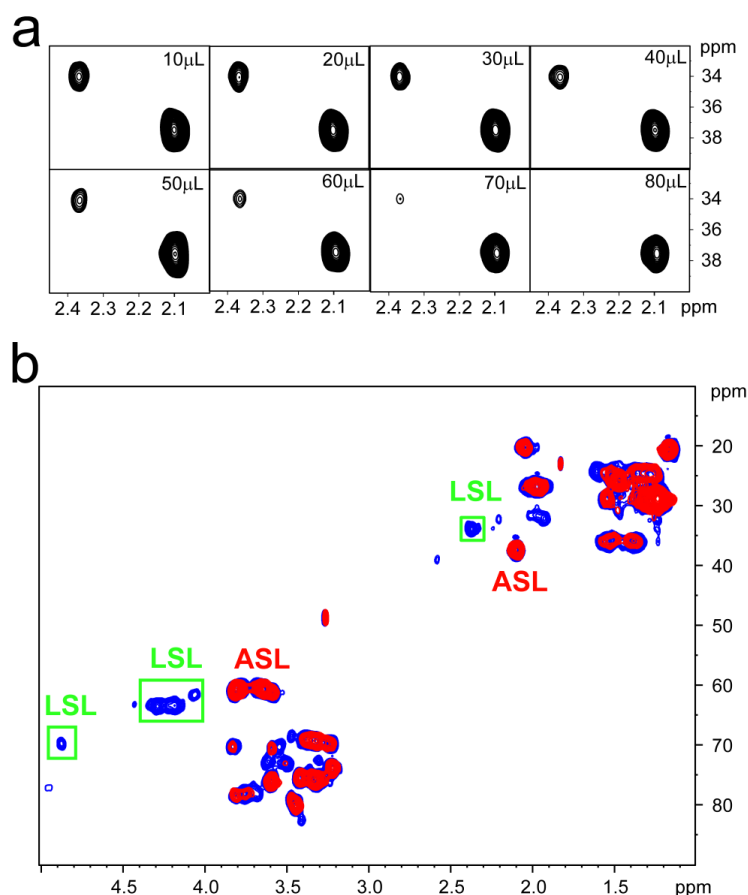


**Figure 5a.16** (a) HSQC spectra showing the aliphatic region upon successive addition of SF to MSL solution (b) Overlay of the HSQC spectra of a 3:1 mixture of ASL and LSL in the absence (blue) and presence (red) of SF. The well separated signals of LSL which are indicated in boxes are absent on addition of SF.

In the mixed SL solution, the LSL molecules bind to the protein and could be in exchange equilibrium between the mixed micelles and the SF bound form leading to exchange broadening of the LSL signals. It is likely that the hydrophobic LSL molecules bind to the hydrophobic regions of SF whereas the hydrophilic ASL molecules may have a relatively weaker binding affinity to SF. The results from NMR are consistent with the SANS scattering data of the MSL sample in which the signature from charged ASL micelles persist even after the addition of SF.

The binding of LSL to SF could act as the nucleating step in the SF gelation process in the presence of sophorolipids. When SF is added to LSL, the hydrophobic LSL preferentially binds to the hydrophobic pockets of SF there by triggering fast gelation. In MSL solutions, the LSL is solubilised within a mixed micellar assembly with ASL molecules. On adding SF, the

LSL molecules escape from the mixed micelles and bind to the protein. This could account for the slightly slower gelation in MSL solution.

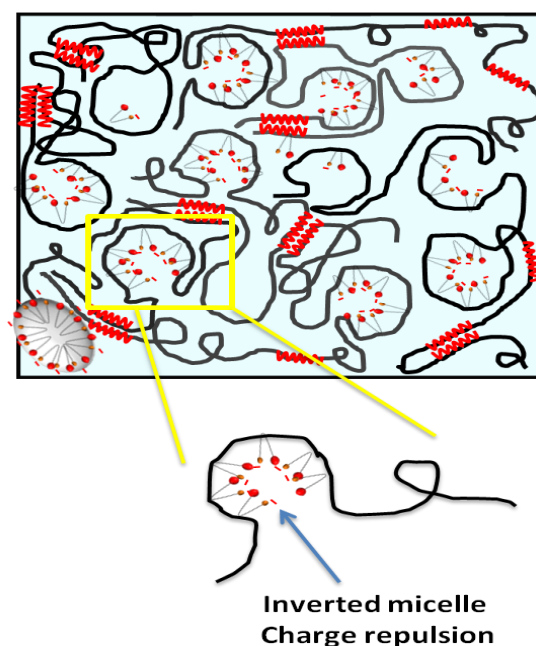
Gel formation on adding SF to ASL solution is slow, suggesting that the rate determining step maybe a diffusion controlled process leading to a long induction time for the onset of gel formation. The ASL micelles are in equilibrium with non-associated ASL molecules in solution. The free ASL molecules could diffuse to binding pockets on the protein; with the shifting equilibrium causing further disruption of the micellar assembly till the gelation process is complete.

#### **5a.4 Conclusion**

Silk Fibroin is a promising material for biomedical applications and sophorolipid is a bio-functional molecule. It is interesting to see that sophorolipids accelerate the gelation of silk fibroin to produce functional hydrogels. Here, the mechanism for accelerated gelation of silk fibroin upon using a biological surfactant i.e. sophorolipid has been probed. The findings of the work clearly indicate the role of the structure and thus assembling property of SLs in controlling the time of gelation. Bola-amphiphilic acidic sophorolipids were shown to form stable charged prolate micelles whereas the lactonic sophorolipid randomly aggregate in solution to form mass fractal and thus minimize interaction with hydrophilic environment. The third sample under study i.e. mixed SL, as the name suggest forms mixed micelles in solution in which LSL molecules are incorporated within the ASL micelles. Upon addition of SF to these SL samples, the gelation time and mechanism differ depending upon the type of sophorolipid. In case of SF+ASL, gelation commences only after 10 h, prior to which both the components were found to exist in solution without any interaction. The shift in equilibrium between the ASL micelles and non-associated molecules leads to diffusion dependent onset of gelation. In case of both LSL and MSL samples that comprise of lactonic SL molecules gelation was found to be faster. NMR studies of SF+MSL sample confirmed that the underlying reason for faster gelation of the sample was due to preferential binding of lactonic sophorolipid to silk fibroin chain leading to unfolding of the protein. The formation of intra- and intermolecular beta sheets as a result of chain opening facilitates the gelation process.

## Chapter 5b

# pH dependent sophorolipid assemblies and their influence on gelation of silk fibroin protein



Protein surfactant interactions are known to be governed by several factors. Among several, pH has been reported to have marked influence on both, surfactants assembling behaviour and protein properties. Thus, it becomes essential to evaluate the impact of pH on the system under investigation i.e. silk fibroin-sophorolipid. Here, the influence of pH on sophorolipid assembly has been investigated with view to examine its impact on gelation of silk fibroin protein. The gelation of a 3wt% solution of SF in the presence of 3wt% solutions of different SLs at pH  $6.0 \pm 0.2$  and pH  $8.0 \pm 0.2$  were examined by analytical techniques such as rheology, NMR, SANS and fluorescent spectroscopy. The study focuses on acidic sophorolipid that comprises of pH responsive carboxylic group at the fatty acid tail end, and it's assembling behavior and interaction with silk fibroin is thus expected to be influenced by pH. Thus, this study investigates the reason behind delayed gelation in silk fibroin and acidic sophorolipid sample in comparison to lactonic and mixed SL as seen in chapter 5a.

### 5b.1 Introduction

In heterogeneous colloidal systems, bulk properties are governed by the interactions between the different constituents. Among such colloidal systems amalgam between protein and surfactant is considered imperative for detergent, food, cosmetic and pharmaceutical products. Diverse surfactants and proteins have thus excited researchers and today a large body of literature exists on their interactions.<sup>[109]</sup> Various factors such as the charge on the protein and surfactant, their concentrations and amphiphilicity are known to affect these interactions.<sup>[254]</sup> It has been shown that in case of ionic surfactants at low concentration, electrostatic binding plays a significant role whereas above critical aggregation concentration hydrophobic interactions take over the binding process. At higher surfactant concentration, the binding of surfactants to the polypeptide chain leads to denaturation, which is regarded as surfactant-induced protein unfolding.<sup>[255]</sup>

In model globular proteins such as bovine serum albumin (BSA), irrespective of the charge on the surfactant, the cooperative binding of surfactant to the protein leads to micelle-like clusters of surfactant forming along the unfolded protein chain. The cooperative binding is predominantly hydrophobic so both anionic and cationic surfactants such as sodium dodecyl sulfate (SDS) and dodecyl trimethyl ammonium bromide (DTAB) undergo quite similar binding with BSA which is anionic.<sup>[256]</sup> On the other hand, another widely studied globular protein lysozyme does not unfold even at very high concentration of SDS.<sup>[257]</sup>

Silk fibroin (SF), a natural fibrous protein spun by silkworms and spiders is studied extensively for its varied applications. In biomedical field, it is recognised as a scaffolding material for tissue regeneration. Different physical and chemical conditions (temperature, pH, additives) have been reported which transform silk fibroin solution to hydrogel. This process is triggered by a conformational transition of SF from random coil to  $\beta$ -sheets. As pH dictates the protonation and deprotonation of acidic and basic amino acids, it has a marked effect on the gelation of SF. At acidic pH, SF solutions form gels within a few hours since minimized repulsion among molecules leads to enhanced hydrophobic interactions between the chains resulting in  $\beta$ -sheet formation.<sup>[212,258]</sup> At near neutral and alkaline pH (pH 6-9) gelation of SF takes 10-25 days depending on concentration of SF solution used. This clearly reflects the critical role of pH on SF gelation.

Reports on employment of surfactant to induce gelation in SF are very few. Researchers have investigated the use of all three types of chemical surfactants viz. non-ionic, cationic and anionic, to induce SF gelation. Among the three, minimum gelation time was achieved with anionic surfactant; SDS.<sup>[117]</sup> Cationic surfactants such as OTAB, DTAB, HTAB etc. which are oppositely charged in comparison to SF show concentration dependent aggregation.<sup>[118]</sup> Non-ionic surfactant (Triton X-100) was shown to induce gelation in 15 h at 100 mM concentration. Absence of charge on the surfactant molecules resulted in gelation driven mainly by salting out of water molecules from the SF chain, leading to the possibility of hydrophobic interactions and hydrogen bonding to form beta sheets.

In contrast to usual nonionic surfactants that are characterized by polar but uncharged head groups which do not ionize in solution, a microbial derived glycolipid biosurfactant, sophorolipid (SL) marks an exception. Apart from being non-ionic it falls into the category of bolaamphiphiles. This property asserts characteristics that differ from the conventional non-ionic surfactants such as Triton X 100. Presence of a carboxylic group at the end of the fatty acid tail in acidic sophorolipid confers it with pH responsive behaviour. Thus, change in pH can have a profound effect on surfactant-protein interaction.

In previous chapter 5a, we have shown that the presence of lactonic SL (LSL) in sophorolipid synthesized by *Candida bombicola* ATCC 22214, results in accelerated gelation of silk fibroin protein. The sophorolipid synthesized by yeast naturally comprises of a mixture of acidic (ASL) and lactonic (LSL) forms. Even though the preferential binding of lactonic SL via hydrophobic interactions with silk fibroin chain results in faster gelation, its poor solubility makes it less preferable as a gelling agent. Presence of ASL with LSL in 3:1 ratio in the SL mixture from yeast markedly increases LSL's solubility rendering the combination a slightly delayed gelation when compared with LSL alone but overcomes the solubility issues. When ASL alone was used as a gelling agent for silk fibroin solution, gelation was greatly delayed in comparison to LSL and mixed SL systems comprising both ASL and LSL (MSL) (refer Figure 5a.12). This observation prompted us to investigate the reason behind this difference. An obvious difference between the two molecules (ASL and LSL) lies in their structure. ASL has a free carboxylic acid group at the end of the fatty acid tail which distinguishes it from other non-ionic surfactants and makes it a bolaamphiphile, whereas no such structural feature is present in LSL due to its closed ring structure. The presence of a carboxylic acid group in ASL makes it an interesting pH responsive surfactant.

At low pH (<5) neutral micelles are formed whereas at an intermediate pH range (5<pH<8) charged micelles exist in solution. On further increasing the pH (>8) these micellar structures transform into large net-like aggregates.<sup>[62]</sup> This implies that the interaction of MSL/ASL with SF can differ depending on the pH of the solution.

In this chapter, experimental techniques such as rheology, small angle neutron scattering (SANS), fluorescence spectroscopy and nuclear magnetic resonance (NMR) spectroscopy were employed to gain insights into the influence of pH on the assembling behavior of sophorolipids, mechanism of interaction between sophorolipid and silk fibroin and subsequent gel formation

## **5b.2 Materials and methods**

### **5b.2.1 Preparation of RSF and sophorolipid solution**

Regenerated silk fibroin (RSF) solutions were prepared as described earlier (section 4.2.1). Final concentration of RSF solution was adjusted to 3% w/v using deionized water and it was also lyophilized to powder for NMR and SANS studies.

Sophorolipid synthesis was carried out by supplementing oleic acid to *Candida bombicola* (ATCC 22214) using a method described in section 4.2.2. The crude sophorolipid was subjected to column chromatography<sup>[228]</sup> and alkaline hydrolysis<sup>[229]</sup> to obtain pure diacetylated lactonic and non-acetylated acidic sophorolipid respectively. The purified products were lyophilized to obtain powder. The two purified forms i.e. ASL and LSL were mixed in 3:1 ratio and are referred to as mixed sophorolipid (MSL). Similar to silk fibroin the concentration of different SLs were adjusted to 3% w/v which is significantly above the reported critical micelle concentration of sophorolipids.<sup>[259]</sup> The pH of SL solutions were adjusted to  $6.0 \pm 0.2$  and  $8.0 \pm 0.2$  using 0.1N NaOH solution.

### **5b.2.2 NMR Spectroscopy, Rheology and SANS**

The NMR experiments were conducted as described in chapter 5a Section 5a.2.3. The rheological measurements of SF and SL solutions (MSL, ASL) were carried out as described in Section 5a.2.4. Similarly small angle neutron scattering experiments were carried out following protocol mentioned in Section 5a.2.5.

### **5b.2.3 Fluorescence measurements**

The micropolarity changes in sophorolipid-induced silk fibroin gelation were studied by using pyrene as a fluorescent probe and measuring its spectra at room temperature using Bruker system. Pyrene was used at a concentration of  $5 \times 10^{-3}$  mM. The fluorescence measurements were done within 350-660 nm and excitation wavelength was set as 334 nm. The slit width of 2nm was used for both excitation and fluorescence measurements and fluorescence intensities at 373 and 384 nm were recorded using sample cells with a 1 cm path length. Each experiment was conducted in triplicates.

## **5b.3 Results and discussion**

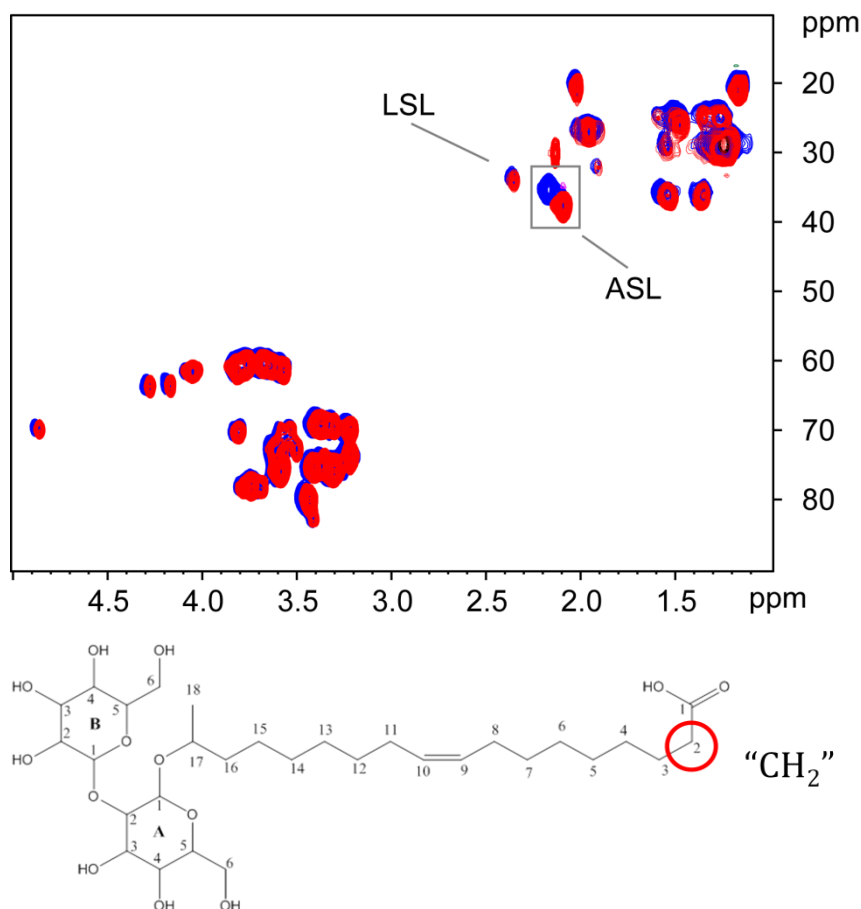
### **5b.3.1 Influence of pH on sophorolipids**

The objective of this work is to examine the effect of pH on gelation of SF-SL systems. The pH of SL solution is usually 4 or less depending on the concentration and is close to the isoelectric point of silk fibroin (3.9). We observed that when SL solution is added to SF in solution, instead of gelation immediate aggregation and precipitation of SF occurs as a result of localised pH reduction at the point of contact on mixing. However if the pH of the SL solution is adjusted to values  $> 4.0$  prior to mixing, gelation occurs without phase separation. While gelation rate increases in the pH range 5 to 8, further increase does not lead to acceleration in gelation. We therefore examined the gelation behaviour at pH 6 and pH 8 in MSL+SF and ASL+SF systems to understand the effect of pH on the sophorolipid-silk fibroin interaction by employing SANS, rheology, NMR and fluorescence spectroscopy.

In chapter 5a, Figure 5a.16 we have shown that in MSL+SF, the preferential binding of LSL to SF triggers fast gelation of SF. While LSL has very poor solubility in aqueous solution, the presence of ASL in MSL helps to solubilize LSL in mixed micelles. On the other hand, when ASL alone is mixed with SF, gelation is slower compared to MSL+SF but is much faster than gelation of pure SF solution. In this case gelation is a diffusion controlled process in which ASL molecules diffuses from the micellar assembly and binds to SF. Clearly the gelation rate is determined by the nature of the SL assembly and its interaction with SF.

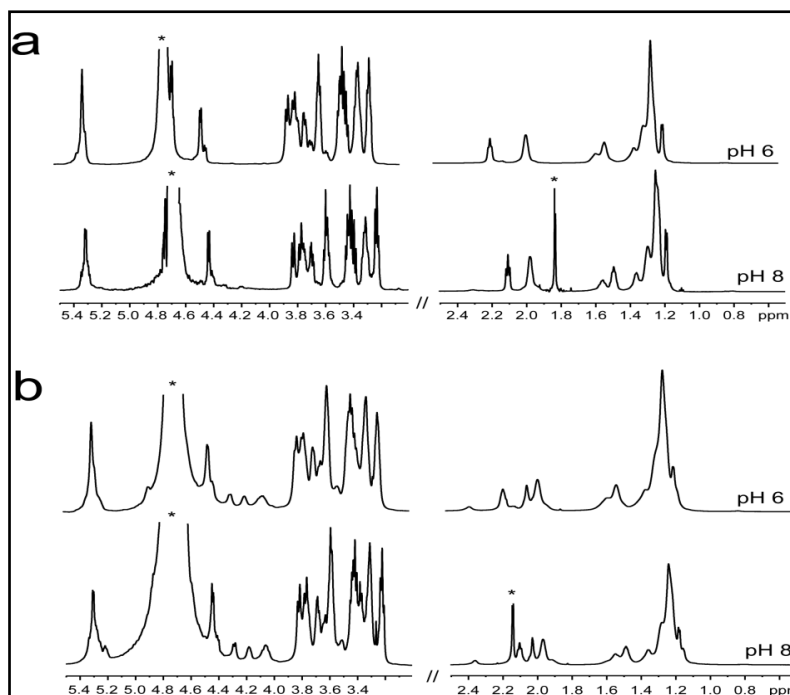
It is well known that the nature of self assemblies in aqueous solution depends on the pH of the medium. Figure 5b.1 shows an overlay of the HSQC spectra of MSL at pH 6 and 8. Signals from LSL overlaps at both pH while in ASL the methylene signal which is sensitive to the environment of the adjacent carboxylic group is shifted. Unlike LSL, ASL has a free

carboxylic acid group and the degree of ionization is influenced by the pH of the solution which in turn dictates the assembling behaviour.



**Figure 5b.1** Overlay of the HSQC spectra of MSL at pH 6 (blue) and pH 8 (red). The signal from the methylene group indicated in the structure is marked by a square in the spectrum.

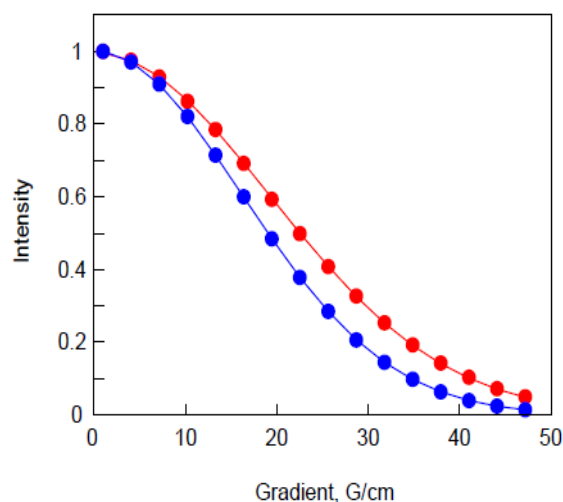
In addition, a comparison of the proton spectra of ASL and MSL at the two pHs shows that signals are significantly broadened at lower pH indicating the presence of larger assemblies in solution at pH 6 (Figure 5b.2). This was confirmed by measuring diffusion coefficients by NMR at pH 6 and 8. The well separated signal of the methylene proton adjacent to the carboxylic group was monitored to estimate the diffusion coefficient.



**Figure 5b.2** Proton spectra of (a) ASL and (b) MSL in D<sub>2</sub>O at pH 6 and 8. The signals marked by asterisks are from solvent, acetone (~1.8 ppm) and acetic acid (~2.2 ppm).

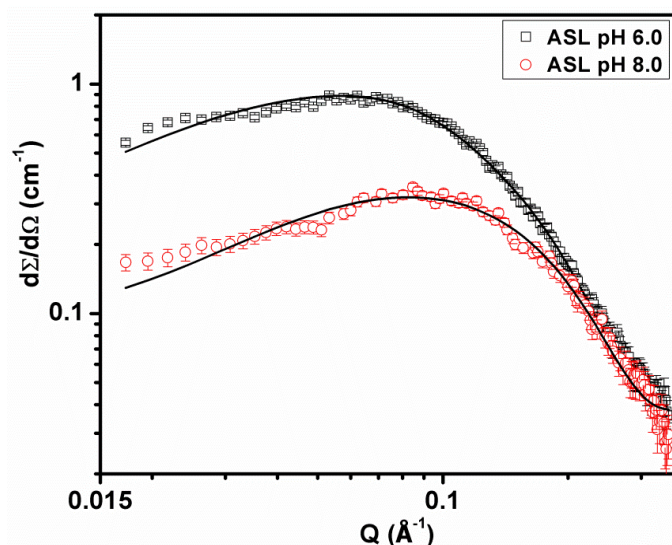
### 5b.3.2 Diffusion and size analysis of sophorolipid assemblies

Figure 5b.3 shows the decay curves obtained for ASL at pH 6 and 8 and the calculated diffusion coefficients are  $0.791 \times 10^{-10} \text{ m}^2/\text{s}$  and  $1.052 \times 10^{-10} \text{ m}^2/\text{s}$  respectively. The lower diffusion coefficient value at pH 6 indicates the presence of larger micellar assemblies in solution. Assuming spherical micelles and employing the Stokes-Einstein equation, the estimated hydrodynamic radius ( $r_H$ ) is 25.1 Å at pH 6 and 18.9 Å at pH 8.



**Figure 5b.3** Diffusion decay curve of ASL (in D<sub>2</sub>O) at pH 6.0 (blue) and 8.0 (red).

In order to obtain quantitative information on the size and shape of ASL molecular assemblies, we carried out further investigations employing SANS. Figure 5b.4 depicts the scattering data of ASL sample in D<sub>2</sub>O at pH 6 and 8. The scattering profile of ASL at both the pH was found to be very similar with the presence of a strong and broad interaction peak in the middle Q region which indicates the existence of charged micelles in the system. However the scattering intensity in the low Q region was observed to be higher at pH 6 compared to pH 8 thus confirming the larger size of assemblies at lower pH, which was also observed by NMR diffusion coefficient measurements. The fitted parameters of the scattering data tabulated in Table 5b.1 shows that even though the calculated semi minor axis at both pH remains the same, the semi major axes are 25.5 and 16.0 Å at pH 6 and 8 respectively which mirror the rH estimates based on NMR. Apart from the difference in size, higher de-protonation at pH 8 also results in higher charge, which increases the effective surface area of the head group thereby reducing the packing parameter ( $V/av$ ). This leads to a shift in the shape of the micelles from ellipsoidal to nearly spherical at pH 8.



**Figure 5b.4** SANS scattering data of ASL in D<sub>2</sub>O at pH 6.0 and 8.0.

**Table 5b.1** Fitted parameters for SANS data of ASL at different pH.

System	Semi-major axis (Å)	Semi-minor axis (Å)	Charge (e.u.)
ASL-pH 6	25.5	12.0	5.4
ASL-pH 8	16.0	12.0	7.6

### 5b.3.3 Gelation kinetics in SF-SL system at different pH

The differences in molecular assembling behaviour with pH and its effect on SF-SL gelation was studied by monitoring the bulk gelation kinetics of the system at pH 6 and 8 employing time sweep experiments in Couette geometry in a rheometer. As shown in Figure 5b.5a, upon addition of MSL, gelation commences at different time points depending upon the pH of the sophorolipid solution. At pH 6, gelation is highly delayed in comparison to pH 8. At near neutral/slightly acidic pH (6) gelation commences only after  $\sim 10$ h whereas at alkaline pH (8) the gelation time is 2.3 h.

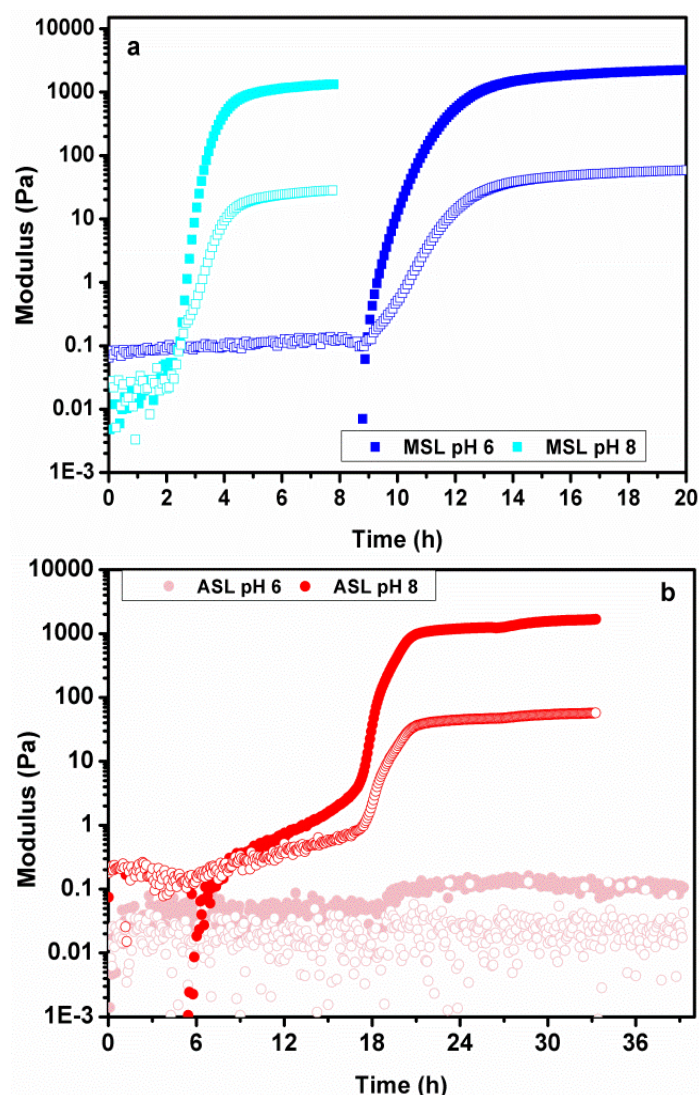


**Figure 5b.5** Rheological time sweep experiment on (a) MSL+SF and (b) ASL+SF in H<sub>2</sub>O at pH 6.0 and 8.0 (Filled symbols – G' ; Unfilled symbols – G'').

In chapter 5a, we have already shown that gelation of SF in the presence of ASL is much slower when compared to MSL+SF. At pH 8 gelation in the SF+ASL system occurs as a two step process. Initially up to  $\sim 10$ h a slow build up of G' occurs followed by a rapid increase in

$G'$  and a corresponding rise in  $G''$ , until gelation is complete (Figure 5b.5b). In contrast, at pH 6 the loss ( $G''$ ) and storage ( $G'$ ) modulus remains nearly flat in the time frame studied (Figure 5b.5b). This indicates that gelation does not commence even 36 h after the addition of ASL to SF solution.

Even though rheology does not provide indications of gel formation in SF+ASL at pH 6, SANS (see below) and NMR measurements show that gelation occurs after a prolonged delay (Figure 5b.6). This discrepancy is due to the different solvents used for the experiments. In  $D_2O$  which is employed as a solvent for SANS and NMR experiments, gelation is faster compared to that in  $H_2O$  which is used in the rheology measurements (Figure 5b.7). Solvent isotope effects are known to have an influence on the size and stability of micellar assemblies.<sup>[260]</sup> At pH 6, gelation rate in  $H_2O$  is far too slow to be detected during the rheology measurements. The pH dependence on the gelation rate is dictated by the effect of pH on the degree of ionization of ASL, hence we examined gelation in the ASL+SF system by SANS in more detail.

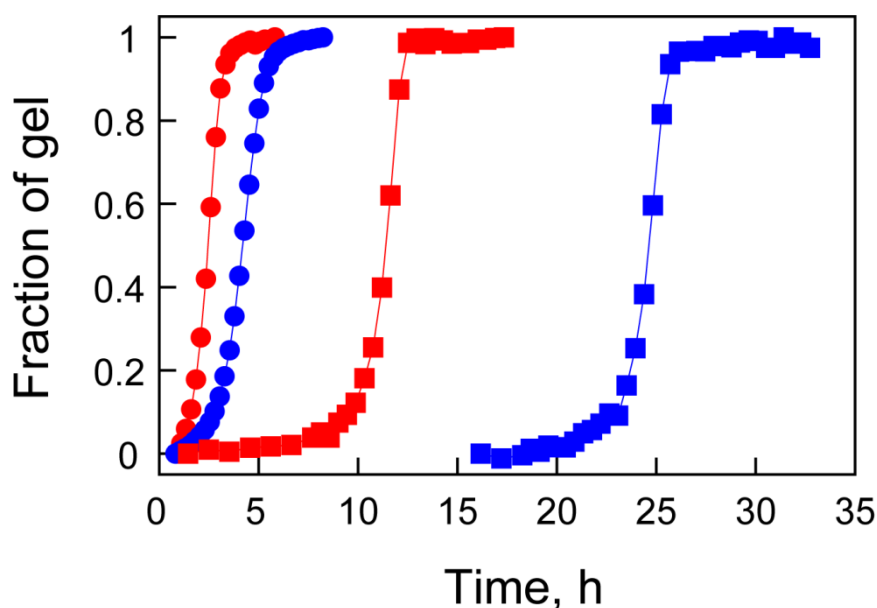


**Figure 5b.6** Gelation kinetics of MSL+SF (circles) and ASL+SF (squares) in  $D_2O$  at pH 6 (blue) and 8 (red) monitored by NMR.

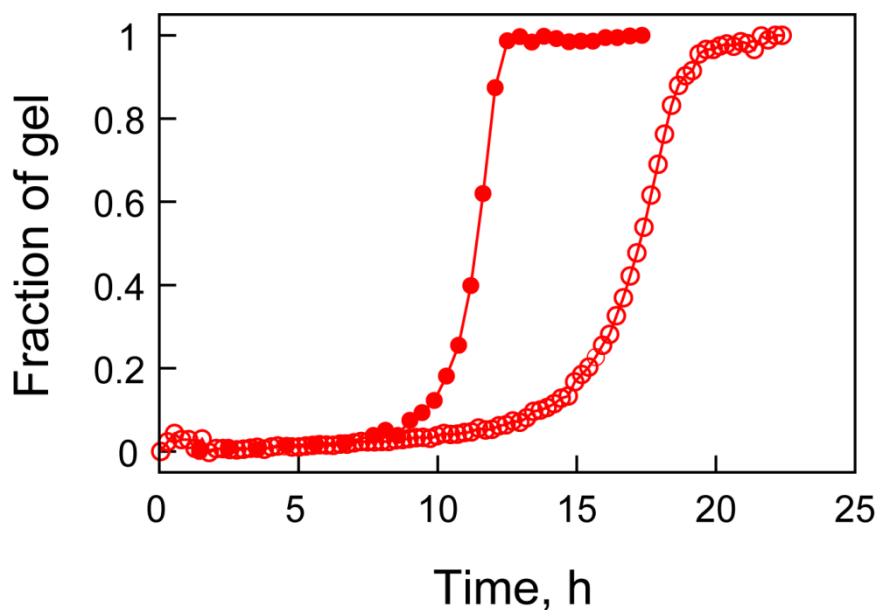


**Figure 5b.7** Comparison of difference in gelation time of SF+ASL samples prepared in D<sub>2</sub>O (filled circle) and H<sub>2</sub>O (empty circle) at pH 8.

#### 5b.3.4 SANS analysis of SF + acidic SL system at different pH

Similar to observations from rheology studies at pH 8, the SANS data of SF+ASL system at both pH shows that gelation occurs in two steps at different time points. For the initial few hours (~6h) during which build up of  $G'$  is not very evident, SANS data at both the pH show distinctive signatures of charged micelles in the intermediate Q range, while the low Q region shows characteristic features of SF chain in random Gaussian coil conformation (Figure 5b.8a and 8b). This clearly indicates the absence of any significant interaction between the ASL micelles and SF molecules in the initial stages and the system typically remains in the solution state (Figure 5b.8c). Sol to gel transition and the subsequent gel state is marked by scattering data which is distinctly different from that observed in the solution state. As shown in Figure 5b.8d the presence of a linear region in the intermediate Q region is characteristic of the bead necklace model of protein surfactant interaction.<sup>[243]</sup> According to this model, ASL molecules interact with SF to form micelle like clusters on the SF polypeptide chain thereby initiating chain unfolding as shown schematically in Figure 5b.9. Adherence of few molecules or micelles on the chain further unfolds the protein and exposes the embedded hydrophobic patches in the interior.<sup>[253]</sup> The exposed hydrophobic domains comprise of amino acid sequences that aid intra and inter-molecular beta sheet

formation<sup>[261]</sup> as shown in Figure 5b.9, which eventually links different SF polypeptide chains into a three dimensional hydrogel network.

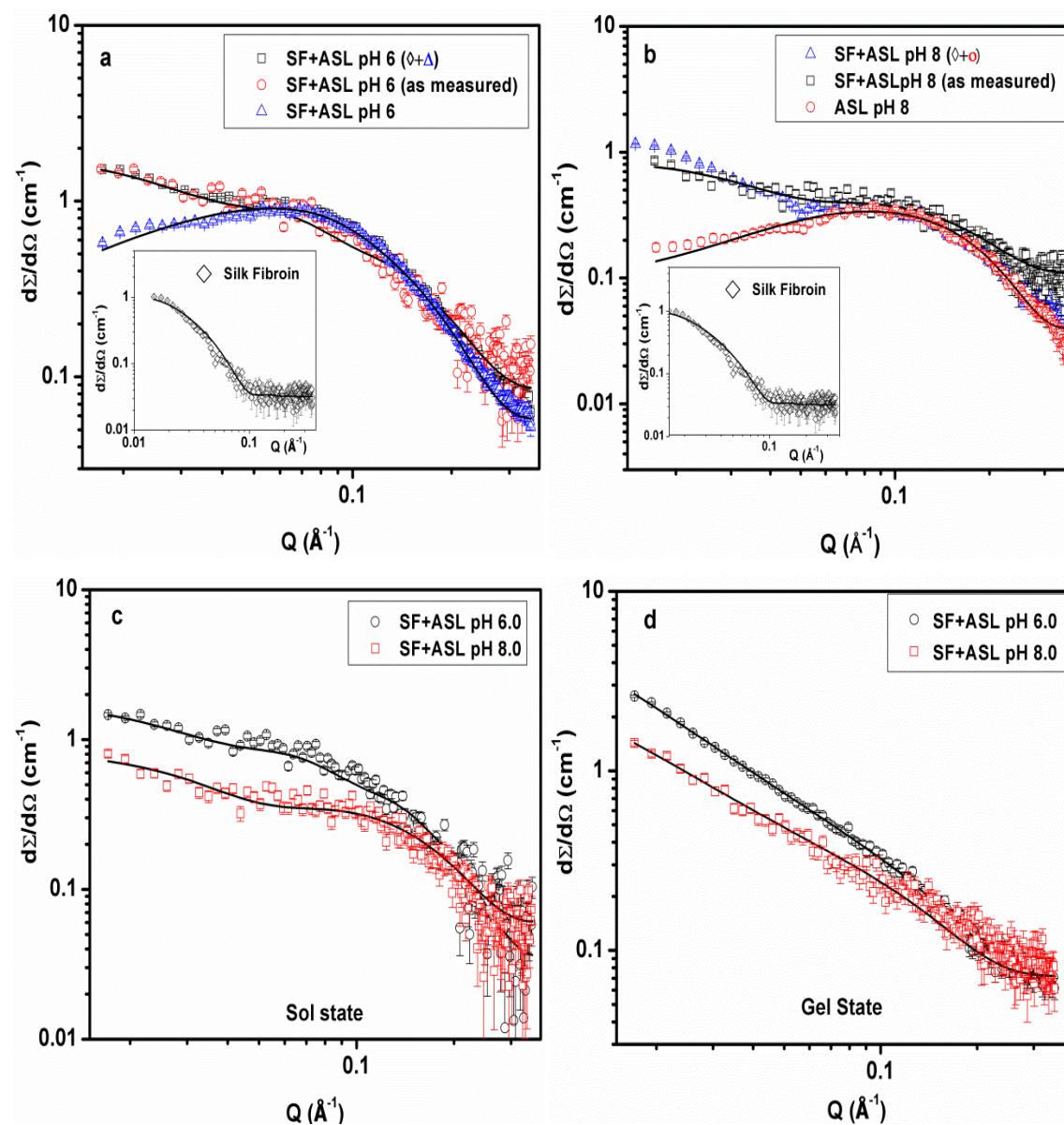


**Figure 5b.8** SANS scattering data of SF+ASL (in D<sub>2</sub>O) depicting as measured and summed up scattering from SF and ASL individually (a) at pH 6 (b) at pH 8. SF+ASL scattering data (c) in sol state (initial ~6h), (d) in gelled state.

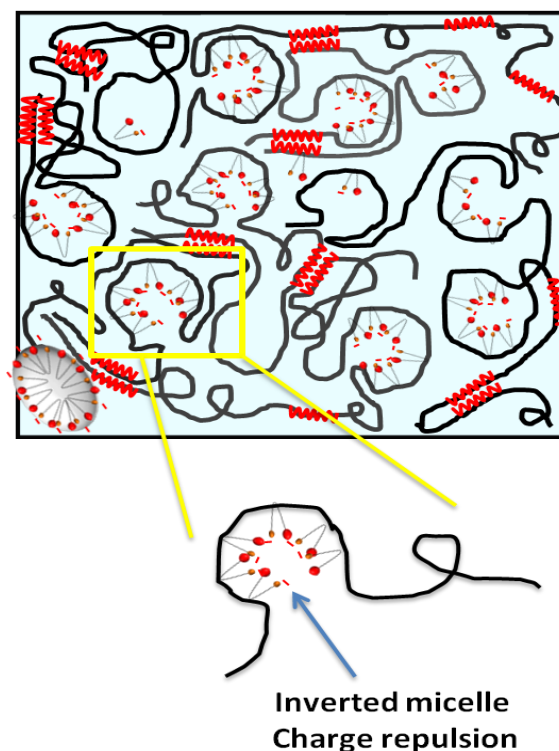


**Figure 5b.9** Schematic representation of SF-ASL interaction according to the bead necklace model.

**Table 5b.2** Fitted parameters of SF+ASL system at different pH.

Silk + Acidic	Radius of micelle	Fractal dimension	Overall length radius of fractal
pH 6.0	16 Å	1.5	170 Å
pH 8.0	20 Å	1.2*	190 Å

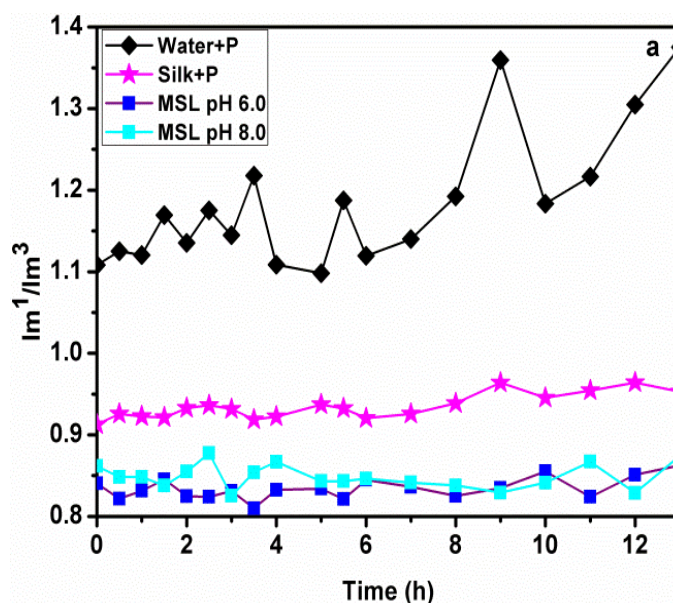
SANS data clearly shows that the mechanism of gelation in SF+ASL system at both the pH is similar. Since ASL is negatively charged, it could interact electrostatically with the cationic side chains of SF. However, the percentage of cationic amino acids (6 mol%) is relatively low in SF, thus limiting the contribution of electrostatic forces in the association between SF and ASL. Instead, the interactions may be hydrophobic in nature where the ASL molecules bind to the hydrophobic regions of the SF polypeptide chain by escaping from the ASL micelles. As more ASL molecules escape the ASL micelles and bind to SF, the equilibrium between the ASL molecules and ASL micelles is further disrupted resulting in increased interaction between ASL and SF. At pH 6, the size and stability of the ASL micelles is higher compared to that at pH 8, making it more difficult for the ASL molecules to escape from the micelle. This could be one of the factors leading to a longer induction time for gelation at pH

6. The eighteen carbon fatty acid tail of ASL has a *cis* configuration at the C9-C10 double bond which enables bending of the molecule bringing the sophorose and carboxylic group closer. This orientation allows the fatty acid chain of ASL to interact with the hydrophobic regions of SF as depicted in Figure 5b.9 resulting in micelle like bead structures along the polypeptide chain. The micellar beads so formed are inverted i.e. the polar groups of ASL molecules are oriented inwards. At both the experimental pHs studied, the negative charge on the carboxylic group could lead to repulsion within the micellar bead. Thus higher repulsion would lead to increased spacing of the molecules within the micellar bead thereby unfolding the polypeptide chain. This hypothesis is supported by the fit of the bead necklace model to the SANS data. The fitted parameters in Table 5b.2 show that the size of the micellar bead is 20 Å at pH 8 and 16 Å at pH 6. Bigger bead size could only arise due to higher charge repulsion between ASL molecules within the bead. Also the calculated fractal dimension of SF+ ASL system at pH 8 is 1.2 which is lower than the value of 1.5 calculated at pH 6. A lower fractal dimension value reflects greater opening of the polypeptide chain in the SF+ASL system at pH 8 than at pH 6. Increased degree of chain opening further exposes the hydrophobic domains in SF leading to the formation of inter and intra molecular beta sheets, resulting in faster gelation.

### **5b.3.5 Microenvironment change determination by fluorescent spectroscopy**

In order to confirm that SF-SL gelation is largely driven by hydrophobic interactions, the hydrophobic microenvironment of the system was studied using fluorescence spectroscopy with pyrene as an external probe. Pyrene's fluorescence emission spectrum is very sensitive to solvent polarity. The formation of a hydrophobic environment in aqueous media leads to a decrease in the intensity ratio of the first and third vibronic peak ( $I_1/I_3$ ) in emission spectra, whereas in a hydrophilic environment the  $I_1/I_3$  ratio is high. This difference in spectra helps to identify the changes in the solvent environment of a system. Figure 5b.10a and b depict the intensity ratio change ( $I_1/I_3$ ) of pyrene emission spectra as a function of time for SF-SL systems. Since H<sub>2</sub>O is used as the solvent in fluorescence spectroscopy, we selected the MSL+SF system for this study because the gelation time is shorter compared to ASL+SF. The conclusions drawn for the MSL+SF system is also valid for ASL+SF since MSL comprises of ASL and LSL in 3:1 ratio.

The fluorescence data in Figure 5b.10a shows that, pyrene in 3% w/v of SF and SL solution separately has an intensity ratio of  $0.9 \pm 0.2$ , and  $0.85 \pm 0.2$  respectively revealing the existence of a hydrophobic environment due to the amphiphilic nature of both silk fibroin and sophorolipid. In the MSL+SF solution at pH 6,  $I_1/I_3$  intensity ratio fluctuates between 0.85 and 0.9 without any significant variation (Figure 5b.10b). In contrast, at pH 8 similar fluctuations are observed up to  $\sim 4$  hours followed by a rapid increase in the  $I_1/I_3$  ratio. Pyrene molecule being hydrophobic in nature remains associated within the hydrophobic interior of the SL micelles or hydrophobic domains of SF in the initial stages of mixing. Rheology data shows that at pH 8, gelation in MSL+SF is initiated at 2.3h after mixing (Figure 5a). As the SL molecules start interacting with the SF chain the hydrophobic environment associated with the SL micelles is reduced. Thus, with the progress of sol to gel transition, the number of accessible hydrophobic sites available to pyrene diminishes. The gelation process reaches a plateau in  $\sim 4$ h (Figure 5b.5a) which correlates with the time point at which a rapid increase in the  $I_1/I_3$  intensity ratio of pyrene is observed (Fig 5b.10b). When the gelation process approaches completion pyrene encounters a relatively hydrophilic environment present in the 3D gelled network thus resulting in a corresponding increase in the  $I_1/I_3$  intensity ratio to values comparable to that of pyrene in water (Fig 5b.10a). At pH 6, the MSL+SF system in  $H_2O$  does not gel within the time frame of the fluorescence experiments and we do not observe any significant change in the  $I_1/I_3$  ratio.



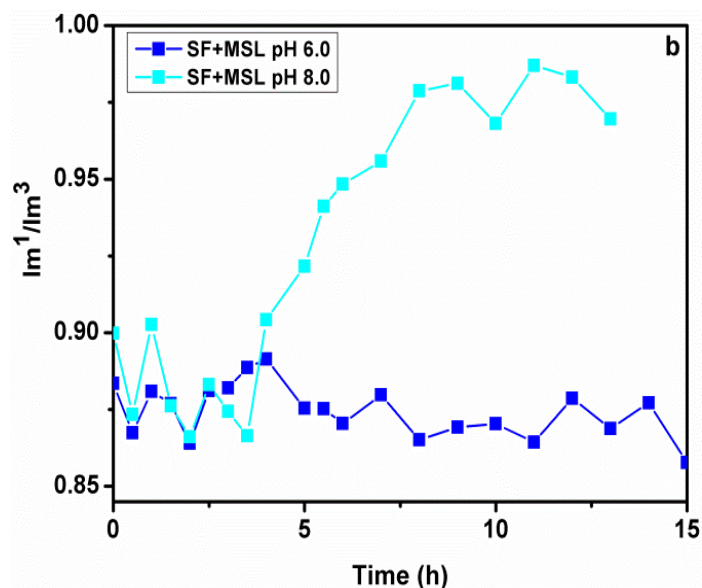


**Figure 5b.10** Fluorescence spectroscopy graph depicting  $I_1/I_3$  intensity ratio of pyrene (a) in different environments (comprising of components under study), (b) SF+SL system at different pH. Fluorescence emission data depicting the  $I_1/I_3$  intensity ratio of pyrene in (a) solutions of individual components and (b) solution of SF+MSL.

Even though there is a sharp increase in the  $I_1/I_3$  ratio of MSL+SF at pH 5b.10, the value remains below 1.0 unlike that in a solution of pyrene in water where the ratio can be up to 1.3 or more (Figure 5b.10). This is because of the presence of some sophorolipids remaining in the solution which are not part of the gel. Thus, in a water solution pyrene is in an entirely hydrophilic environment whereas some degree of hydrophobicity is present in MSL+SF even after gelation is complete.

### 5b.3.6 NMR diffusion analysis of SF+ASL system

We also carried out NMR diffusion experiments to probe the changes occurring in the solution environment during the gelation process. We chose the ASL+SF system at pH 6 in  $D_2O$  for this study, since gelation is sufficiently slow to allow diffusion experiments to be carried out as a function of time during the sol-gel transition process. Figure 5b.11a shows the variation of the diffusion coefficient of ASL as a function of time following mixing of ASL and SF solutions. Figure 5b.11b monitors the gel formation process as a function of time. On mixing ASL and SF, initially there is no significant interaction between the two components hence the diffusion coefficient measured for ASL remains close to that of a solution of ASL alone. When gelation is initiated by the interactions between ASL and SF, the ASL molecules start to get incorporated in the gel phase hence remaining ASL molecules in solution which

are not bound to SF begin to experience a relatively less viscous environment and diffuse faster. As observed in the case of the  $I_1/I_3$  ratio of pyrene, a sharp increase in diffusion coefficient is observed at the time point where gelation reaches a plateau. On completion of gelation, the solution still contains some ASL molecules which are not part of the gel in a less viscous environment leading to an upper limit for the diffusion coefficient. These observations mirror the results from fluorescence experiments thus providing insights into the changes in the microscopic environments during the gelation process.

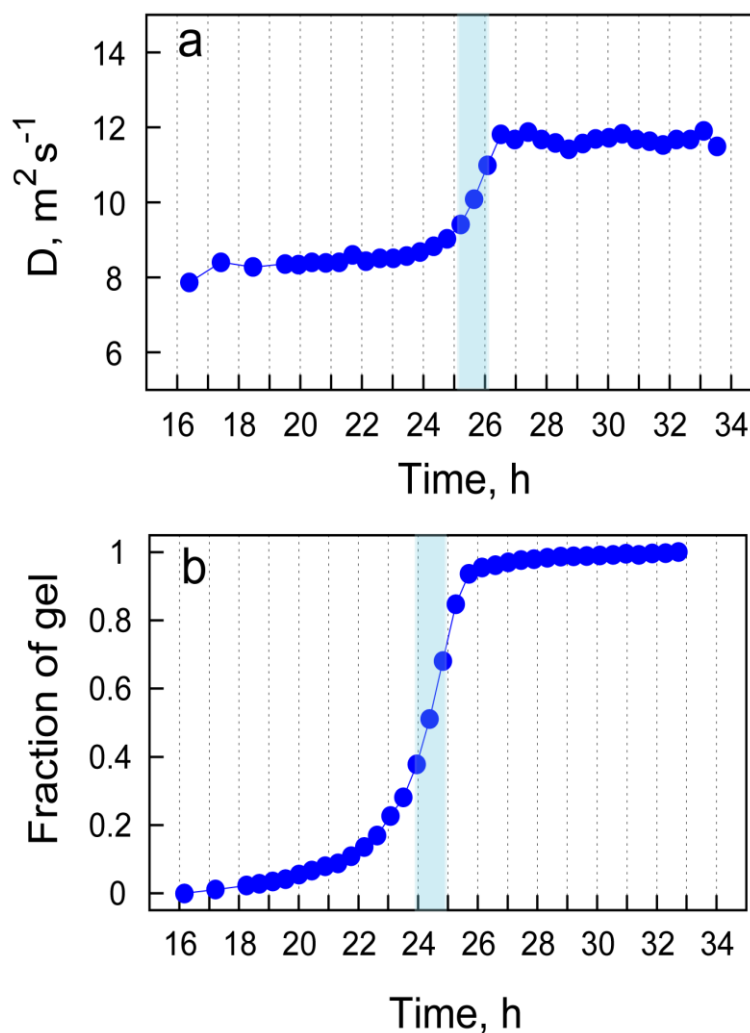


**Figure 5b.11** (a) Variation of the diffusion coefficient ( $D$ ) of ASL with time during gel formation in ASL+SF. (b) Gel formation kinetics in ASL+SF at pH 6. The time axis shift of the inflection in the two plots is highlighted.

Investigations of sophorolipid-SF systems show that the rate at which SF gelation occurs in the presence of sophorolipids, depends on the pH of the medium. At lower pH, the micellar assemblies of sophorolipids are larger in size. The observed pH dependence arises due to the degree of ionization of the free carboxyl group in ASL. Hydrophobic interactions

between the fatty acid chain of the sophorolipids and silk fibroin induces protein chain unfolding thus triggering gel formation. The mechanism is best described in terms of the bead necklace model where a higher pH results in greater charge repulsion between the molecules within the SL micellar bead bound to the protein chain. This leads to rapid chain unfolding and subsequent gel formation.

From fluorescence spectroscopy we understand that hydrophobic interactions play the major role in driving gelation of SF+ASL system. The pH of ASL solution dictates the charge on the molecule which holds responsible for the repulsion between the molecules within the micelle formed as a bead in the protein chain necklace. Hence pH directly affects ASL molecule that in turn indirectly effects the SF gelation.

#### **5b.4 Conclusion**

Protein surfactant interactions are known to be governed by several factors. Among several, pH has been reported to have marked influence on both, surfactants assembling behavior and protein properties. Thus, it was essential to evaluate the impact of pH on the system under investigation i.e. silk fibroin-sophorolipid. Hence, the two forms of sophorolipid, acidic and lactonic when subjected to pH change demonstrated that lactonic SL that lacks pH responsive group due to closed ring structure is not influenced by pH, whereas in case of acidic SL, changes were evident upon varying the pH due to the presence of carboxylic acid group. The extent of carboxylic group deprotonation determined the molecular size and charge on the assembly. Similar to lactonic SL, the acidic SLs were also found to interact with silk fibroin by hydrophobic interactions but difference that led to delayed gelation was more stable assemblies formed in case of acidic SL that preferred to remain self associated. In absence of any driving force the gelation was observed to be diffusion dependent. Increasing interaction of individual acidic SL molecules with SF probably shifted the equilibrium towards gelation after a prolonged time period. The higher electrostatic repulsions between ASL molecules at pH 8.0 resulted in the formation of a more open structure causing faster gelation of ASF-SL systems. Thus, the study clearly indicated that faster gelation could be induced in SF+ASL solution by increasing the pH to 8.0 but for substantially reduced gelation time, employment of lactonic sophorolipid was essential.

## Conclusions and Future work

At the end, this chapter summarizes the work presented in this thesis. Highlights of the work conducted towards completion of the thesis have been noted. Also, certain leads encountered during the work that are interesting and have significant potential have been described in detail.

The main objective of the thesis was to widen the structural variation in sophorolipids and hence to synthesize novel SLs that displayed enhanced properties. An additional aim was to explore the mechanism of biological property with a view to understand the action pathway adopted by the SLs to certain extent. Oleic acid derived SL also referred as classical sophorolipids have been extensively studied for their assembling behaviour. As a second part of the work these sophorolipids were subjected to an entirely new application and we discovered their potential as gelling agent for proteins. In the due course to understand the mechanism of gelation, assembling property of these SLs was studied to gain insight into their contribution during the process and to understand how they influence gelation.

In **Chapter 2**, the work carried out towards synthesis of novel sophorolipids has been described in detail. Water insoluble primary fatty alcohol with C16 chain i.e. cetyl alcohol has been supplemented to the yeast *Candida bombicola*. The SL product thus synthesized (SLCA) displayed enhanced properties than the substrate and other SLs due to addition of hydrophilic head group to water insoluble tail, making it amphiphilic. Thus, improved solubility and hence applicability of SLCA could be achieved. The physico-chemical properties were found to superior than the substrate and other SLs. Analytical characterization ensured incorporation of the fatty alcohol in the SL molecule. Studies on biological properties such as anti-microbial revealed that SLCA, in comparison to other SLs that do not display effective activity against Gram-negative bacteria, remarkably killed both Gram-negative and Gram-positive bacteria at significantly low concentrations. These interesting findings add a new facet to the known range of sophorolipids that can be explored for potential applications in diverse fields.

**Chapter 3** was continuation of the previous chapter and SLCAs biological properties and their mechanism was further explored. Sophorolipids and their derivatives have been reported to display anti-cancerous properties, thus with this knowledge SLCA was also investigated for its anti-proliferative nature and additionally for the first time anti-angiogenic property of SLs was investigated and reported. Two purified SLCA were shown to be effective against human colorectal cancer cells and human cervical cancer cells at significantly low concentrations. The mechanism studies revealed that both SLCAs functioned in a similar manner by inducing apoptosis in the cervical cancer cells.

Interestingly, both the pathways of apoptosis i.e. death receptor/extracellular and mitochondrial/intracellular pathway were found to be activated by SLCA. Further in-depth studies can help us understand that in what way a single molecule can activate both the pathways. The ability of the SLCA to obstruct the tubule formation by endothelial cells was reported for the first time. These findings indicate that the use of SLCA as a therapeutic drug to fight against the cancer cells can be advantageous as it does not kill the normal cells and displays anti-angiogenic property.

**Chapter 4 and 5** concerned with the new property of oleic acid derived Sophorolipid reported for the first time.

Certain proteins such as silk fibroin (SF) find application in biomedical field in several forms due to their biocompatibility and strength. SF has been fabricated into hydrogels that are applicable in tissue engineering and wound dressings. But, for SF to gel naturally a time period of 15-20 days is required that is a drawback for clinical applications. Therefore several attempts have been made and different methods have been described to reduce the gelation time of SF in-order to increase its applicability. With this view, we significantly brought down the SF gelation time from days to few hours by using sophorolipid as a gelling agent. The biological properties of SL make it an interesting gelling agent. The SL induced SF gelation was shown to be resultant of conformational changes in protein from random coil to beta sheet structure. Additionally these hydrogels could further be used for fabrication of three dimensional scaffolds for tissue engineering applications. Apart from reduced gelation time SLs enhanced the bio-applicability of the hydrogels as show by adhesion and proliferation studies on L929 mouse fibroblast cells. Employment of SL as a gelling agent gave us the leverage of tuning the scaffold strength, pore size and porosity to suit the need. Thus, these SF-SL hydrogels showed great potential for biomedical applications.

**Chapter 5** was an extension of chapter 4 as it described in-depth mechanism of SF-SL gelation. The deciphered mechanism employed sophisticated techniques such as Rheology, NMR and SANS. The data generated was huge hence the chapter was split into two parts, 5a and 5b.

**Chapter 5a** comprised of detailed study on two sophorolipid forms i.e. acidic and lactonic and their mixture. The characterization of different SL carried out using NMR and SANS

elaborated on their purity, composition, assembling behaviour and interactions within the assembly. This detailed analysis proved to be significant in probing their interaction with the silk fibroin protein that leads to accelerated gelation. Silk fibroin was also characterized by NMR and SANS to establish its purity and solution state in order to understand the changes witnessed after addition of sophorolipid. The gelation kinetic studies conducted by Rheology and NMR reflected upon the order (lactonic SL > mixed SL >>>> acidic SL) in which different SLs accelerate gelation. SANS and NMR further highlighted the molecular changes occurring in the process of gelation and how the assembling behaviour of SL changes upon encounter with silk fibroin. These investigations showed that preferential binding of lactonic sophorolipid played a significant role in significantly reducing the gelation time of silk fibroin. Hydrophobic binding of lactonic sophorolipid resulted into rapid unfolding of the SF chain leading to the formation of intermolecular beta sheets which triggered fast gelation. On the other hand acidic sophorolipid induced delayed gelation in silk fibroin. The reason behind this happening was further deciphered in the following chapter.

**Chapter 5b** described the impact of pH on acidic sophorolipid molecule and its assembly that ultimately reflected on its interaction with silk fibroin and resulted in delayed gelation. Presence of pH responsive group, carboxylic group at fatty acid tail end, along with sophorose head group makes it bola-amphiphilic. Alterations in pH to alkaline conditions lead to deprotonation of the carboxylic group and induce negative charge on the molecular self-assembly. Acidic SL in comparison to lactonic SL forms stable micellar assembly and thus prefers to remain self associated. The stability of the assembly further governs interaction of sophorolipid with the protein chain. Thus, it was shown by different techniques that upon addition of silk fibroin solution to acidic SL solution, both the components do not interact for an extended period of time and hence gelation is delayed. Rheological studies show that these SF+ASL solutions undergo gelation at a faster rate when the pH of sophorolipid solution is basic. Further, the gelation in case of acidic SL and SF was proposed to be diffusion dependent. The SF-SL gelation was confirmed to be driven by hydrophobic interactions as shown by spectroscopic measurements. Thus, these understandings add value to the growing literature of protein-surfactant systems that are of prime interest to the healthcare, food and cosmetic industry and will be helpful in designing SF-SL hydrogels and scaffolds to suit our need.

### ***Future Prospects***

Interestingly while conducting the above described works, we came across two leads that can be pursued in future and have remarkable potential.

#### ***1) Self assembling behaviour of cetyl alcohol derived sophorolipid***

There are number of reports on self assembly of oleic acid derived SL and their analogues. Cetyl alcohol derived sophorolipids reported in Chapter 2 differ structurally from classical SLs and are thus expected to assemble differently. So far, there are no reports on effect of sonication on self assembling behaviour of sophorolipids. Thus, SLCA was subjected to sonication, with an expectation of supramolecular structures with different morphology and functionality. Two different concentration of SLCA were selected for the study, 2mg/mL and 5mg/mL, and were subjected to sonication for 1 h. SEM images were acquired pre and post sonication and are represented in Figure 1a.

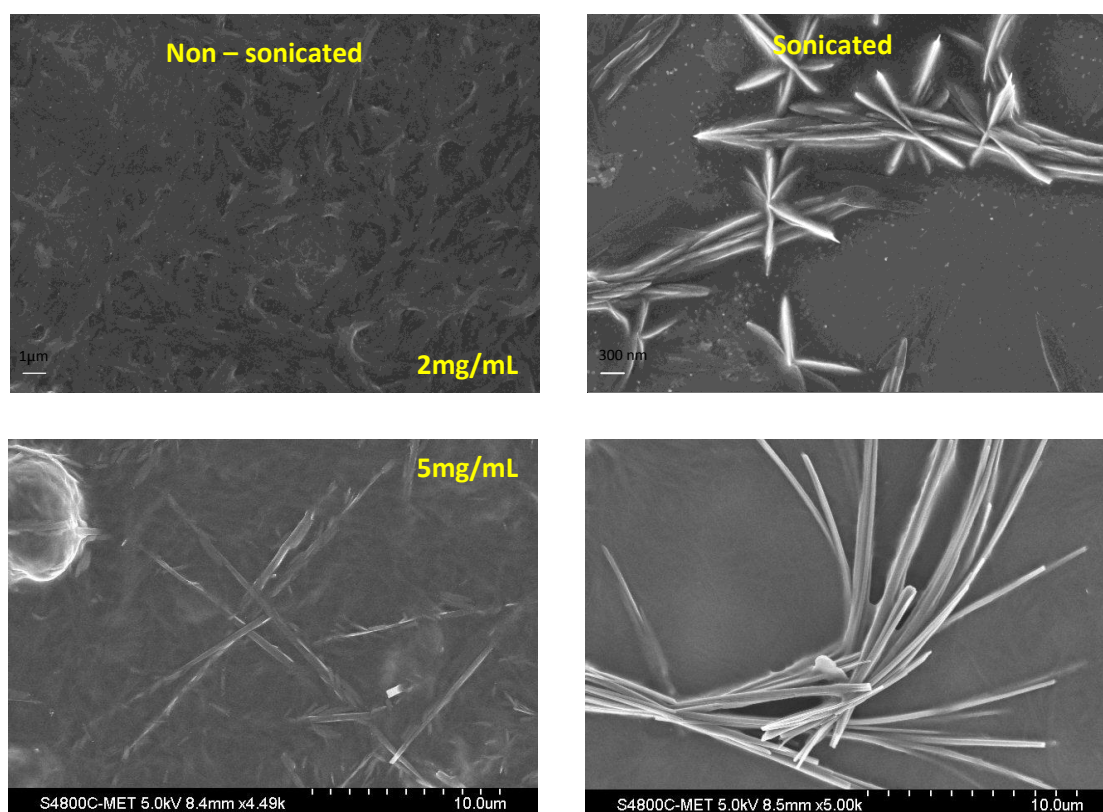


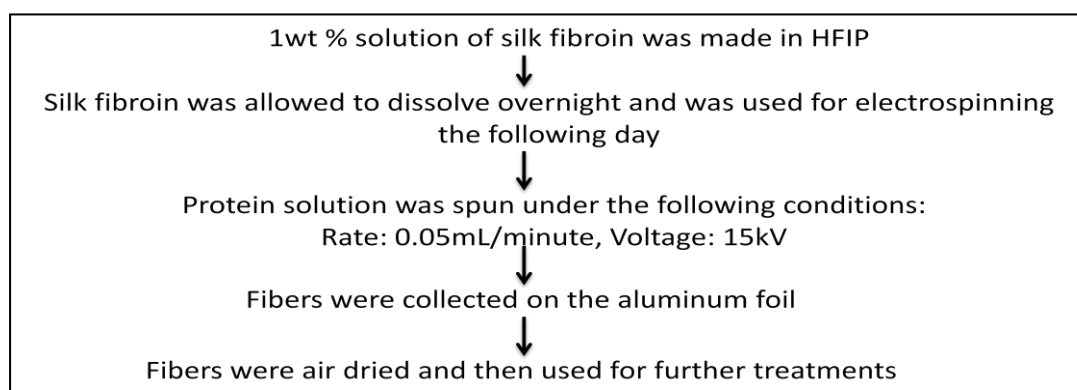
**Figure 1a** SEM images of SLCA solutions at different concentration before and after sonication.

Preliminary data of assembly experiments suggest that sonication is playing a role in ordering of the molecules into particular morphology – ranging from flower to flexible

cylindrical rods as a function of concentration, which can be further explored to understand the assembling behavior. To gain better understanding on the role of different structural forms of SLCA in development of these molecular structures, further purification of SLCA can be carried out and individual forms can be investigated for their assembling nature.

## 2) *Enhancing the bio-applicability of electrospun silk fibres*

Surface modification of silk fibroin has been carried out from time to time in order to enhance its applicability as a biomaterial.<sup>[262]</sup> With the similar view, sophorolipid was employed to coat the surface of silk fibroin nano-fibers formed by electrospinning. The procedure employed was as follows:



These SF-HFIP (Hexafluoroisopropanol) fibres were further subjected to different treatments such as methanol, ammonia plasma and sophorolipid. Methanol treatment imparted crystallinity by inducing beta sheet formation, whereas ammonia plasma treatment of electrospun fibers exposed positively charged group on the surface with which the carboxylic group of acidic sophorolipid could interact or hydrophobic interactions could also participate in surface modification. The SEM micrographs at three different magnifications obtained after these treatments are presented as follows (Figure 2a):

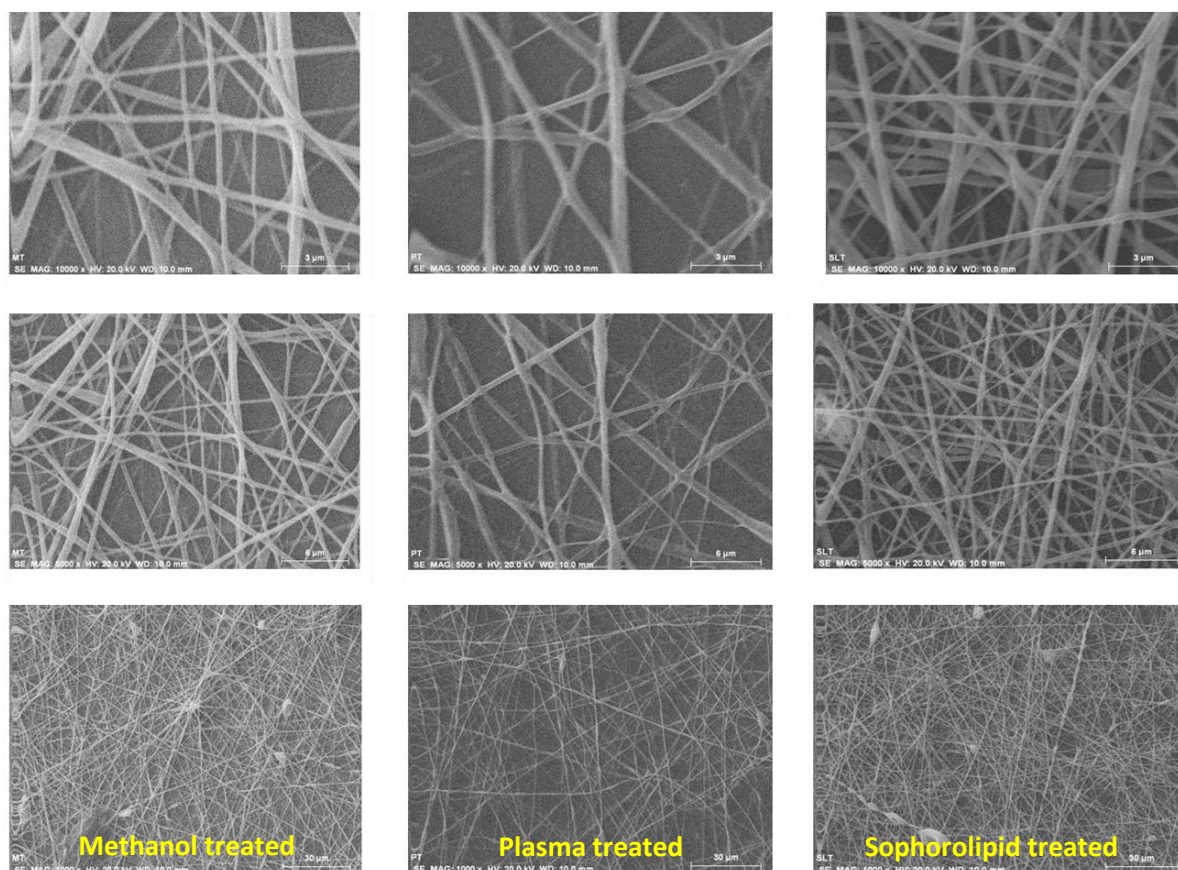


**Figure 2a** SEM images of electrospun silk fibroin after different treatments.

As can be seen, sophorolipid treated fibers did not lose their integrity and were observed to be intact and evenly coated without any clumping. The functional group analysis was carried out to ascertain the sophorolipid coating on SF fibers using FT-IR. In IR spectrum of ASL treated SF fibers (Figure 2b) significant peak corresponding to silk fibroin protein was not evident but sharp peak corresponding to methylene stretch of fatty acid tail was prominent. This implicated that SF fiber surface was completely coated with ASL. On the other hand, in mixed sophorolipid treated fibers peak corresponding to anti-parallel beta sheet confirmation of SF was evident whereas signatures from SL were not very prominent. Thus, it could be concluded that the coating was not as good as ASL (Figure 2c).

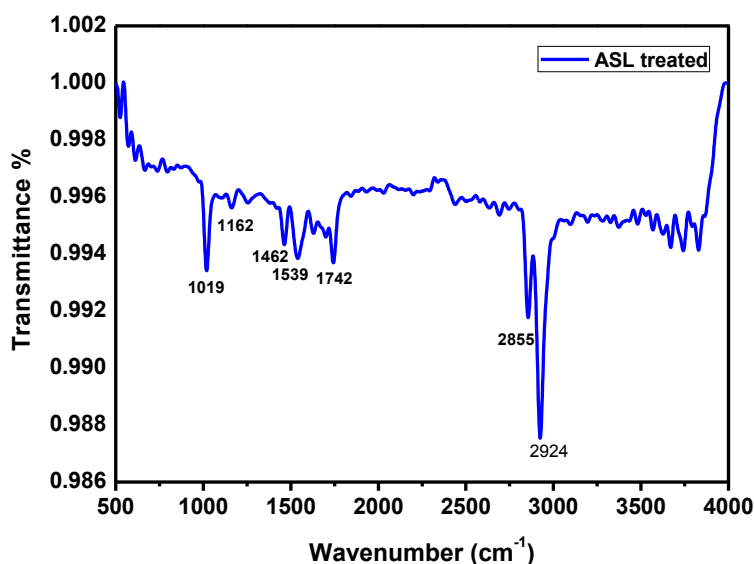


**Figure 2b** FTIR spectrum of electrospun SF fibers with acidic sophorolipids

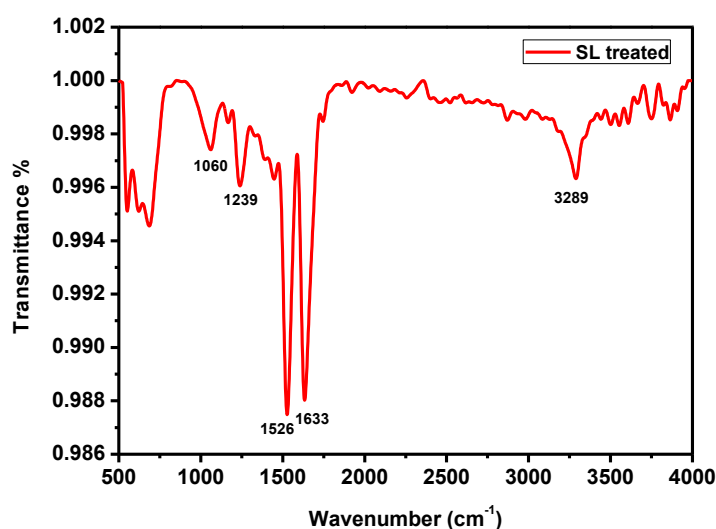


**Figure 2c** FTIR spectrum of electrospun SF fibers with mixed sophorolipids.

To evaluate the biocompatibility and enhanced effect of surface modification with sophorolipid, cell studies on these constructs were carried out. Growth and proliferation of mouse fibroblast L929 cells was monitored and cytotoxicity of these constructs on cancer cells was evaluated. As shown in figure 2d, if we compare the growth of fibroblast cells in these scaffolds, growth in methanol treated constructs was least, whereas in plasma treated constructs, cells showed higher proliferation. But because different studies have demonstrated that plasma treatment is unstable and it deteriorates over the time hence it cannot be used alone. Constructs that were treated overnight with mixed SL showed more proliferation than methanol and 6 hr treated samples but lesser proliferation than ASL treated fibers. This could be attributed to better coating in case of acidic SL due to

electrostatic interaction between the positive charge on SF fibers and negatively charged SL carboxylic group. The cytotoxicity studies conducted on human lung cancer A549 cells demonstrated that fibers treated with mixed SL for overnight showed maximum inhibition (Figure 2e). This could be attributed to the presence of lactonic SL in mixed SL sample which is known to be more biologically active than ASL.

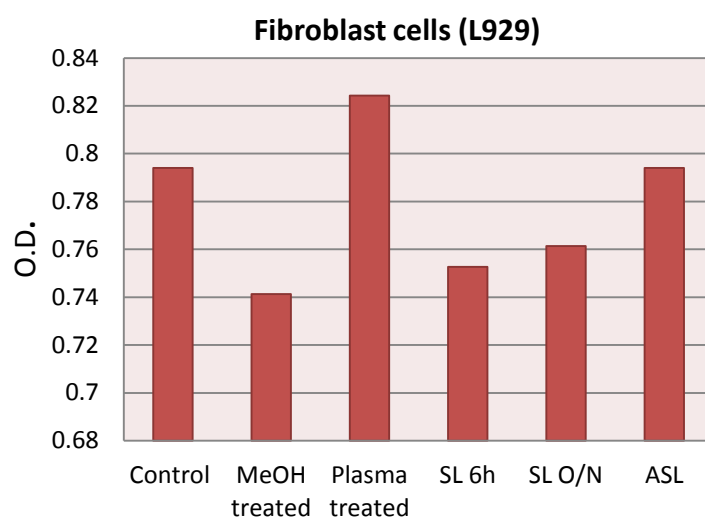


**Figure 2d** MTT assay showing proliferation of L929 fibroblast cells in silk fibroin electrospun fibers subjected to different treatments

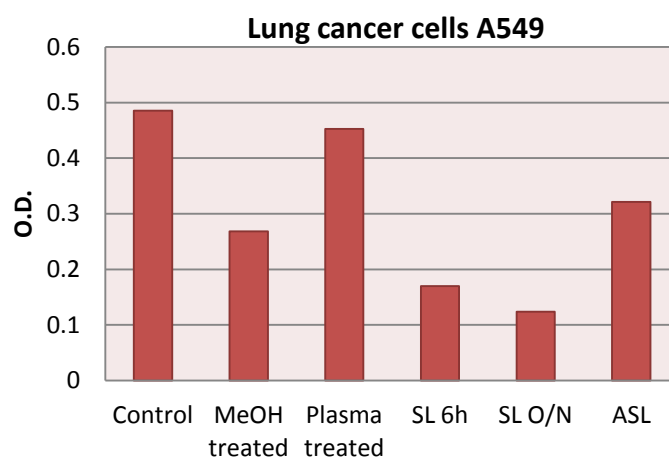


**Figure 2e** MTT assay showing cytotoxicity studies on human lung cancer A549 cells in silk fibroin electrospun fibers subjected to different treatments.

The results obtained in this study are novel and encouraging and can be regarded as a proof-of-concept that can be further taken to design similar materials for different biomedical application such as SF mats for antimicrobial wound dressing applications.

## ***Bibliography***

- [1] A. Singh, J. D. Van Hamme, O. P. Ward, *Biotechnology Advances* **2007**, *25*, 99.
- [2] K. Rakutani, Y. Onda, T. Inaoka, *Industrial Applications of Surfactants IV*, **1999**.
- [3] D. W. G. Develter, L. M. L. Lauryssen, *European Journal of Lipid Science and Technology* **2010**, *112*, 628.
- [4] I. M. Banat, *Acta Biotechnologica* **1995**, *15*, 251.
- [5] N. Kosaric, *Pure and Applied Chemistry* **1992**, *64*, 1731.
- [6] S. Lang, D. Wullbrandt, *Applied microbiology and biotechnology* **1999**, *51*, 22.
- [7] S. G. V. A. O. Costa, E. D??ziel, F. L??pine, *Letters in Applied Microbiology* **2011**, *53*, 620.
- [8] E. Haba, A. Pinazo, O. Jauregui, M. J. Espuny, M. R. Infante, A. Manresa, *Biotechnology and Bioengineering* **2003**, *81*, 316.
- [9] A. Franzetti, I. Gandolfi, G. Bestetti, T. J. P. Smyth, I. M. Banat, *European Journal of Lipid Science and Technology* **2010**, *112*, 617.
- [10] P. Rapp, H. Bock, V. Wray, F. Wagner, *J Gen Microbiol* **1979**, *115*, 491.
- [11] D. G. Cooper, S. N. Liss, R. Longay, J. E. Zajic, *Journal of fermentation technology* **1981**, *59*, 97.
- [12] Y. Uchida, S. Misawa, T. Nakahara, T. Tabuchi, *Agricultural and Biological Chemistry* **1989**, *53*, 765.
- [13] V. I. Golubev, T. V Kulakovskaia, a S. Shashkov, E. V Kulakovskaia, N. V Golubev, *Microbiology* **2008**, *77*, 201.
- [14] E. O. Puchkov, U. Zähringer, B. Lindner, T. V. Kulakovskaya, U. Seydel, A. Wiese, *Biochimica et Biophysica Acta - Biomembranes* **2002**, *1558*, 161.
- [15] S. Spoeckner, V. Wray, M. Nimtz, S. Lang, *Applied Microbiology and Biotechnology*

- 1999, 51, 33.
- [16] S. Hewald, K. Josephs, M. B??lker, *Applied and Environmental Microbiology* **2005**, 71, 3033.
- [17] M. Konishi, T. Morita, T. Fukuoka, T. Imura, K. Kakugawa, D. Kitamoto, *Applied Microbiology and Biotechnology* **2007**, 75, 521.
- [18] M. Konishi, T. Morita, T. Fukuoka, T. Imura, K. Kakugawa, D. Kitamoto, *Applied Microbiology and Biotechnology* **2008**, 78, 37.
- [19] J. H. Im, T. Nakane, H. Yanagishita, T. Ikegami, D. Kitamoto, *BMC biotechnology* **2001**, 1, 5.
- [20] J. I. Arutchelvi, S. Bhaduri, P. V. Uppara, M. Doble, *Journal of Industrial Microbiology and Biotechnology* **2008**, 35, 1559.
- [21] I. N. A. Van Bogaert, K. Saerens, C. De Muynck, D. Develter, W. Soetaert, E. J. Vandamme, *Applied microbiology and biotechnology* **2007**, 76, 23.
- [22] C. P. Kurtzman, N. P. J. Price, K. J. Ray, T. M. Kuo, *FEMS Microbiology Letters* **2010**, 311, 140.
- [23] J. Chen, X. Song, H. Zhang, Y. B. Qu, J. Y. Miao, *Applied Microbiology and Biotechnology* **2006**, 72, 52.
- [24] M. Konishi, T. Fukuoka, T. Morita, T. Imura, D. Kitamoto, *Journal of oleo science* **2008**, 57, 359.
- [25] J. Zhang, K. M. J. Saerens, I. N. A. van Bogaert, W. Soetaert, *Biotechnology Letters* **2011**, 33, 2417.
- [26] R. K. Hommel, L. Weber, A. Weiss, U. Himmelreich, O. Rilke, H. P. Kleber, *Journal of Biotechnology* **1994**, 33, 147.
- [27] V. Dingle Pulate, S. Bhagwat, A. Prabhune, *Journal of Surfactants and Detergents* **2012**, 1.
- [28] G. Pekin, F. Vardar-Sukan, N. Kosaric, *Engineering in Life Sciences* **2005**, 5, 357.

- [29] J. D. Desai, I. M. Banat, *Microbiology and molecular biology reviews : MMBR* **1997**, *61*, 47.
- [30] H. J. Daniel, R. T. Otto, M. Reuss, C. Syldatk, *Biotechnology Letters* **1998**, *20*, 805.
- [31] I. N. A. Van Bogaert, J. Zhang, W. Soetaert, *Process Biochemistry* **2011**, *46*, 821.
- [32] A. Mor, *Drug Development Research* **2000**, *50*, 440.
- [33] R. Maget-Dana, F. Peypoux, *Toxicology* **1994**, *87*, 151.
- [34] M. N. Nasir, F. Besson, *Biochimica et Biophysica Acta - Biomembranes* **2012**, *1818*, 1302.
- [35] C. R. Macdonald, D. G. Cooper, J. E. Zajic, *Applied and Environmental Microbiology* **1981**, *41*, 117.
- [36] J. L. Beebe, W. W. Umbreit, *Journal of Bacteriology* **1971**, *108*, 612.
- [37] E. Rosenberg, A. Zuckerberg, C. Rubinovitz, D. L. Gutnick, *Applied and Environmental Microbiology* **1979**, *37*, 402.
- [38] E. Rosenberg, C. Rubinovitz, R. Legmann, E. Z. Ron, *Applied and environmental microbiology* **1988**, *54*, 323.
- [39] M. C. Cirigliano, G. M. Carman, *Microbiology* **1985**, *50*, 846.
- [40] N. G. K. Karanth, P. G. Deo, N. K. Veenanadig, *Current Science* **1999**, *77*, 116.
- [41] P. A. J. Gorin, J. F. T. Spencer, A. P. Tulloch, *Canadian J. of Chemistry* **1961**, *39*, 846.
- [42] S. Lang, A. T. Hubbard, in *Novel Surfactants: Preparation, Applications and Biodegradability*, **2003**, pp. 279–315.
- [43] A. M. Davila, R. Marchal, J.-P. Vandecasteele, *Applied Microbiology and Biotechnology* **1992**, *38*, 6.
- [44] U. Rau, S. Hammen, R. Heckmann, V. Wray, S. Lang, *Industrial Crops and Products* **2001**, *13*, 85.

- [45] P. K. Singh, K. Bhardwaj, P. Dubey, A. Prabhune, *RSC Adv* **2015**, *5*, 24513.
- [46] J. A. Casas, F. García-Ochoa, *Journal of Bioscience and Bioengineering* **1999**, *88*, 488.
- [47] L. Zhang, P. Somasundaran, S. K. Singh, A. P. Felse, R. Gross, *Colloids and Surfaces A: Physicochemical and Engineering Aspects* **2004**, *240*, 75.
- [48] A. P. Tulloch, J. F. T. Spencer, M. H. Deinema, *Canadian Journal of Chemistry* **1968**, *46*, 345.
- [49] J. F. T. Spencer, P. A. J. Gorin, A. P. Tulloch, *Antonie van Leeuwenhoek* **1970**, *36*, 129.
- [50] J. Chen, X. Song, H. Zhang, Y. Qu, *Enzyme and Microbial Technology* **2006**, *39*, 501.
- [51] R. D. Ashby, D. K. Y. Solaiman, T. A. Foglia, *Biotechnology Letters* **2008**, *30*, 1093.
- [52] N. Vedaraman, N. M. Venkatesh, *Polish Journal of Chemical Technology* **2010**, *12*, 9.
- [53] S. Ito, M. Kinta, S. Inoue, *Agricultural and Biological Chemistry* **1980**, *44*, 2221.
- [54] F. C. Huang, A. Peter, W. Schwab, *Applied and Environmental Microbiology* **2014**, *80*, 766.
- [55] P. A. Felse, V. Shah, J. Chan, K. J. Rao, R. A. Gross, *Enzyme and Microbial Technology* **2007**, *40*, 316.
- [56] N. P. J. Price, K. J. Ray, K. E. Vermillion, C. A. Dunlap, C. P. Kurtzman, *Carbohydrate Research* **2012**, *348*, 33.
- [57] R. Gupta, A. A. Prabhune, *Biotechnology Letters* **2012**, *34*, 701.
- [58] P. Dubey, K. Selvaraj, A. Prabhune, *World Journal of Pharmacy and Pharmaceutical Sciences* **2013**, *2*, 1107.
- [59] S. Zhou, C. Xu, J. Wang, W. Gao, R. Akhverdiyeva, V. Shah, R. A. Gross, *Langmuir* **2004**, *20*, 7926.
- [60] N. Baccile, N. Nassif, L. Malfatti, I. N. a. Van Bogaert, W. Soetaert, G. Pehau-Arnaudet, F. Babonneau, *Green Chemistry* **2010**, *12*, 1564.

- [61] Y. Ishigami, Y. Gama, H. Nagahora, M. Yamaguchi, H. Nakahara, T. Kamata, *Chemistry letters* **1987**, 763.
- [62] N. Baccile, F. Babonneau, J. Jestin, G. Pehau-Arnaudet, I. Van Bogaert, *ACS Nano* **2012**, *6*, 4763.
- [63] A. Stradner, O. Glatter, P. Schurtenberger, *Langmuir* **2000**, *16*, 5354.
- [64] S. Iglauer, Y. Wu, P. Shuler, Y. Tang, W. A. Goddard, *Tenside, Surfactants, Detergents* **2010**, *47*, 87.
- [65] P. Dhasaiyan, A. Banerjee, N. Visaveliya, B. L. V Prasad, *Chemistry - An Asian Journal* **2013**, *8*, 369.
- [66] P. Dhasaiyan, P. R. Pandey, N. Visaveliya, S. Roy, B. L. V Prasad, *Chemistry - A European Journal* **2014**, *20*, 6246.
- [67] A. S. Cuvier, F. Babonneau, J. Berton, C. V. Stevens, G. C. Fadda, I. Genois, P. Le Griel, G. Péhau-Arnaudet, N. Baccile, *Chemistry - An Asian Journal* **2015**, *10*, 2419.
- [68] A. S. Cuvier, F. Babonneau, J. Berton, C. V. Stevens, G. C. Fadda, G. Péhau-Arnaudet, P. Le Griel, S. Prévost, J. Perez, N. Baccile, *Chemistry - A European Journal* **2015**, *21*, 19265.
- [69] P. K. Singh, R. Mukherji, K. Joshi-Navare, A. Banerjee, R. Gokhale, S. Nagane, A. Prabhune, S. Ogale, *Green Chemistry* **2013**, *15*, 943.
- [70] A. M. Shete, G. Wadhawa, I. M. Banat, B. A. Chopade, *Journal of Scientific and Industrial Research* **2006**, *65*, 91.
- [71] R. Cited, O. City, R. U.-A. Data, **2003**, *1*, 0.
- [72] N. Lourith, M. Kanlayavattanakul, *International Journal of Cosmetic Science* **2009**, *31*, 255.
- [73] M. Maingault, *Utilization of Sophorolipids as Therapeutically Active Substances or Cosmetic Products, in Particular for the Treatment of the Skin*, **1999**.
- [74] H. Mager, R. Röthlisberger, F. Wagner, *Use of Sophoroselipid-Lactone for the*

- Treatment of Dandruffs and Body Odour*, **1986**.
- [75] D. Develter, S. Fleurackers, **2008**, *1*, 1.
- [76] K. Joshi-Navare, P. Khanvilkar, A. Prabhune, *Biochemistry Research International* **2013**, DOI 10.1155/2013/169797.
- [77] D. Pierce, T. J. Heilman, *Germicidal Composition*, **2001**.
- [78] V. Dengle-pulate, J. Joshi, S. Bhagwat, A. Prabhune, B. S. Division, **2014**, *3*, 1630.
- [79] P. Singh, K. Joshi, D. Guin, A. A. Prabhune, *RSC Advances* **2013**, *3*, 22319.
- [80] R. Marchant, I. M. Banat, *Trends in Biotechnology* **2012**, *30*, 558.
- [81] N. Saborimanesh, C. N. Mulligan, *Journal of Bioremediation & Biodegradation* **2015**, *06*, DOI 10.4172/2155-6199.1000314.
- [82] A. E. Elshafie, S. J. Joshi, Y. M. Al-Wahaibi, A. S. Al-Bemani, S. N. Al-Bahry, D. Al-Maqbali, I. M. Banat, *Frontiers in Microbiology* **2015**, *6*, 1.
- [83] C. N. Mulligan, R. N. Yong, B. F. Gibbs, *Journal of Hazardous Materials* **2001**, *85*, 111.
- [84] S. H. Baek, X. X. Sun, Y. J. Lee, S. Y. Wang, K. N. Han, J. K. Choi, J. H. Noh, E. K. Kim, *Journal of Microbiology and Biotechnology* **2003**, *13*, 651.
- [85] N. Field, S. Giessler-blank, O. Tlhum, E. Sleverdng, **2012**, *1*.
- [86] M. Kasture, S. Singh, P. Patel, P. A. Joy, A. A. Prabhune, C. V. Ramana, B. L. V Prasad, *Langmuir* **2007**, *23*, 11409.
- [87] S. Singh, P. Patel, S. Jaiswal, a. a. Prabhune, C. V. Ramana, B. L. V. Prasad, *New Journal of Chemistry* **2009**, *33*, 646.
- [88] S. Dhar, E. M. Reddy, A. Prabhune, V. Pokharkar, A. Shiras, B. L. V Prasad, *Nanoscale* **2011**, *3*, 575.
- [89] N. Baccile, R. Noiville, L. Stievano, I. Van Bogaert, *Phys Chem Chem Phys* **2013**, *15*, 1606.

- [90] P. A. Darne, M. R. Mehta, S. B. Agawane, A. A. Prabhune, *RSC Advances* **2016**, *6*, 68504.
- [91] P. K. Singh, K. Wani, R. Kaul-Ghanekar, A. Prabhune, S. Ogale, *RSC Adv* **2014**, *4*, 60334.
- [92] Y. Ikeda, T. Sunakawa, S. Tsuchiya, M. Kondo, K. Okamoto, *The Journal of toxicological sciences* **1986**, *11*, 197.
- [93] H. Isoda, D. Kitamoto, H. Shinmoto, M. Matsumura, T. Nakahara, *Bioscience, biotechnology, and biochemistry* **1997**, *61*, 609.
- [94] K. Joshi-Navare, A. Shiras, A. Prabhune, *Biotechnology Journal* **2011**, *6*, 509.
- [95] S. L. Fu, S. R. Wallner, W. B. Bowne, M. D. Hagler, M. E. Zenilman, R. A. Gross, M. H. Bluth, *The Journal of Surgical Research* **2008**, *148*, 77.
- [96] L. Shao, X. Song, X.-J. Ma, H. Li, Y. Qu, *The Journal of surgical research* **2012**, *173*, 286.
- [97] M. M. Rashad, M. U. Nooman, M. M. Ali, a E. Mahmoud, *Grasas Aceites* **2014**, *65*, 1.
- [98] M. A. Díaz De Rienzo, I. M. Banat, B. Dolman, J. Winterburn, P. J. Martin, *New Biotechnology* **2015**, *32*, 720.
- [99] J. N. Sleiman, S. A. Kohlhoff, P. M. Roblin, S. Wallner, R. Gross, M. R. Hammerschlag, M. E. Zenilman, M. H. Bluth, *Annals of Clinical and Laboratory Science* **2009**, *39*, 60.
- [100] V. Shah, D. Badia, P. Ratsep, *Antimicrobial Agents and Chemotherapy* **2007**, *51*, 397.
- [101] K. Kim, D. Yoo, Y. Kim, B. Lee, D. Shin, E. K. Kim, *Journal of Microbiology and Biotechnology* **2002**, *12*, 235.
- [102] V. Dingle Pulate, S. Bhagwat, A. Prabhune, *Journal of Surfactants and Detergents* **2012**, *16*, 173.
- [103] R. A. Gross, V. Shah, *Anti-Herpes Virus Properties of Various Forms of Sophorolipids*, **2007**.
- [104] V. Shah, G. F. Doncel, T. Seyoum, K. M. Eaton, I. Zalenskaya, R. Hagver, A. Azim, R. Gross, *Antimicrobial Agents and Chemotherapy* **2005**, *49*, 4093.

- [105] M. H. Bluth, E. Kandil, C. M. Mueller, V. Shah, Y.-Y. Lin, H. Zhang, L. Dresner, L. Lempert, M. Nowakowski, R. Gross, R. Schulze, M. E. Zenilman, *Critical care medicine* **2006**, *34*, 188.
- [106] R. Hardin, J. Pierre, R. Schulze, C. M. Mueller, S. L. Fu, S. R. Wallner, A. Stanek, V. Shah, R. A. Gross, J. Weedon, M. Nowakowski, M. E. Zenilman, M. H. Bluth, *Journal of Surgical Research* **2007**, *142*, 314.
- [107] C. S. Lengsfeld, R. A. Shoureshi, **2008**, *1*.
- [108] K. Joshi-Navare, A. Prabhune, *BioMed Research International* **2013**, *2013*, DOI 10.1155/2013/512495.
- [109] D. Otzen, *Biochimica et Biophysica Acta - Proteins and Proteomics* **2011**, *1814*, 562.
- [110] A. Chakraborty, D. Seth, P. Setua, N. Sarkar, *Journal of Physical Chemistry B* **2006**, *110*, 16607.
- [111] A. D. Nielsen, K. Borch, P. Westh, *Biochimica et Biophysica Acta - Protein Structure and Molecular Enzymology* **2000**, *1479*, 321.
- [112] G. Allen, *The Biochemical journal* **1974**, *137*, 575.
- [113] A. Valstar, W. Brown, M. Almgren, *Langmuir* **1999**, *15*, 2366.
- [114] J. Narayanan, A. S. Abdul Rasheed, J. R. Bellare, *Journal of Colloid and Interface Science* **2008**, *328*, 67.
- [115] S. Ghosh, *Colloids and Surfaces B: Biointerfaces* **2008**, *66*, 178.
- [116] D. E. Otzen, *Biophysical journal* **2002**, *83*, 2219.
- [117] X. Wu, J. Hou, M. Li, J. Wang, D. L. Kaplan, S. Lu, *Acta Biomaterialia* **2012**, *8*, 2185.
- [118] J. H. Park, M. H. Kim, L. Jeong, D. Cho, O. H. Kwon, W. H. Park, *Journal of Sol-Gel Science and Technology* **2014**, *71*, 364.
- [119] M. N. Jones, *Chemical Society Reviews* **1992**, *21*, 127.
- [120] M. Jones, *Biochemical Journal* **1975**, *151*, 109.

- [121] P. Hazra, D. Chakrabarty, A. Chakraborty, N. Sarkar, *Biochemical and Biophysical Research Communications* **2004**, 314, 543.
- [122] J. a Reynolds, C. Tanford, *Proceedings of the National Academy of Sciences of the United States of America* **1970**, 66, 1002.
- [123] J. A. Reynolds, C. Tanford, *Journal of Biological Chemistry* **1970**, 245, 5161.
- [124] K. Shirahama, K. Tsujii, T. Takagi, *Journal of biochemistry* **1974**, 75, 309.
- [125] C. The, Z. Shao, F. Vollrath, *Nature* **2002**, 418, 741.
- [126] S. W. Ha, A. E. Tonelli, S. M. Hudson, *Biomacromolecules* **2005**, 6, 1722.
- [127] C. Z. Zhou, F. Confalonieri, M. Jacquet, R. Perasso, Z. G. Li, J. Janin, *Proteins* **2001**, 44, 119.
- [128] S. Nagarkar, T. Nicolai, C. Chassenieux, A. Lele, *Physical chemistry chemical physics : PCCP* **2010**, 12, 3834.
- [129] I. Dal Pra, G. Freddi, J. Minic, A. Chiarini, U. Armato, *Biomaterials* **2005**, 26, 1987.
- [130] N. Minoura, M. Tsukada, M. Nagura, *Polymer* **1990**, 31, 265.
- [131] A. Sugihara, K. Sugiura, H. Morita, T. Ninagawa, K. Tubouchi, R. Tobe, M. Izumiya, T. Horio, N. G. Abraham, S. Ikehara, *Experimental {...}* **2000**, 225, 58.
- [132] R. Nazarov, H.-J. Jin, D. L. Kaplan, *Biomacromolecules* **2004**, 5, 718.
- [133] U. J. Kim, J. Park, C. Li, H. J. Jin, R. Valluzzi, D. L. Kaplan, *Biomacromolecules* **2004**, 5, 786.
- [134] I. Van Bogaert, S. Fleurackers, S. Van Kerrebroeck, D. Develter, W. Soetaert, *Biotechnology and Bioengineering* **2011**, 108, 734.
- [135] M. Kjellin, I. Johansson, *Surfactants from Renewable Resources*, **2010**.
- [136] S. L. Fu, S. R. Wallner, W. B. Bowne, M. D. Hagler, M. E. Zenilman, R. Gross, M. H. Bluth, *Journal of Surgical Research* **2008**, 148, 77.

- [137] J. Chen, X. Song, H. Zhang, Y. B. Qu, J. Y. Miao, *Applied Microbiology and Biotechnology* **2006**, 72, 52.
- [138] S. Ito, S. Inoue, *Applied and Environmental Microbiology* **1982**, 43, 1278.
- [139] F. Mousavi, K. Beheshti-Maal, A. Massah, *Current Microbiology* **2015**, 71, 303.
- [140] S. D. Wadekar, S. B. Kale, A. M. Lali, D. N. Bhowmick, A. P. Pratap, *European Journal of Lipid Science and Technology* **2012**, 114, 823.
- [141] P. Darne, M. Mehta, P. Dubey, A. Prabhune, *World Journal Of Pharmacy And Pharmaceutical Sciences* **2014**, 3, 792.
- [142] G. L. Maddikeri, P. R. Gogate, A. B. Pandit, *Chemical Engineering Journal* **2015**, 263, 479.
- [143] M. M. Rashad, A. S. Al-kashef, M. U. Nooman, A. E. E. D. Mahmoud, *Research Journal of Pharmaceutical, Biological and Chemical Sciences* **2014**, 5, 1515.
- [144] V. Klekner, N. Kosaric, Q. H. Zhou, *Biotechnology Letters* **1991**, 13, 345.
- [145] Q. H. Zhou, N. Kosaric, *Journal of the American Oil Chemists' Society* **1995**, 72, 67.
- [146] Q. H. Zhou, N. Kosaric, *Biotechnology Letters* **1993**, 15, 477.
- [147] D. K. Y. Solaiman, R. D. Ashby, A. Nuñez, T. A. Foglia, *Biotechnology Letters* **2004**, 26, 1241.
- [148] A. Brakemeier, S. Lang, D. Wullbrandt, L. Merschel, A. Benninghoven, N. Buschmann, F. Wagner, *Biotechnology Letters* **1995**, 17, 1183.
- [149] A. Brakemeier, D. Wullbrandt, S. Lang, *Biotechnology Letters* **1998**, 20, 215.
- [150] Y. Hu, L. K. Ju, *Enzyme and Microbial Technology* **2001**, 29, 593.
- [151] A. Prabhune, S. R. Fox, C. Ratledge, **2002**, 1041.
- [152] M. Morikawa, Y. Hirata, T. Imanaka, *Biochimica et Biophysica Acta - Molecular and Cell Biology of Lipids* **2000**, 1488, 211.

- [153] D. G. Cooper, B. G. Goldenberg, *Applied and Environmental Microbiology* **1987**, *53*, 224.
- [154] E. Antoniou, S. Fodelianakis, E. Korkakaki, N. Kalogerakis, *Frontiers in Microbiology* **2015**, *6*, DOI 10.3389/fmicb.2015.00274.
- [155] D. C. Mayo, D. W.; Pike, R. M.; Forbes, *Microscale Organic Laboratory with Multistep and Multiscale Synthesis*, **2010**.
- [156] C. Wei, L. S. Chupak, T. Philip, B. M. Johnson, R. Gentles, D. M. Drexler, *Journal of Biomolecular Screening* **2014**, *19*, 297.
- [157] D. Shaw, T. Corocoran, *Green Chemistry* **2002**, *4*.
- [158] R. T. Otto, H. J. Daniel, G. Pekin, K. Müller-Decker, G. Fürstenberger, M. Reuss, C. Sylдатk, *Applied Microbiology and Biotechnology* **1999**, *52*, 495.
- [159] V. Denge Pulate, S. Bhagwat, A. Prabhune, *Journal of Surfactants and Detergents* **2012**, *1*.
- [160] P. Dubey, K. Selvaraj, A. A. Prabhune, **2014**, *3*, 993.
- [161] K. Joshi-Navare, P. K. Singh, A. A. Prabhune, *European Journal of Lipid Science and Technology* **2014**, *116*, 1070.
- [162] A. Azim, V. Shah, G. F. Doncel, N. Peterson, W. Gao, R. Gross, *Bioconjugate Chemistry* **2006**, *17*, 1523.
- [163] M.-A. Liebert, *Journal of the American College of Toxicology* **1988**, *7*, 359.
- [164] M. M. Rashad, M. U. Nooman, M. M. Ali, A. E. Mahmoud, *Grasas Aceites* **2014**, *65*, 1.
- [165] T. Mosmann, *Journal of immunological methods* **1983**, *65*, 55.
- [166] T. Yokochi, K. D. Robertson, *Molecular pharmacology* **2004**, *66*, 1415.
- [167] E. K. Rowinsky, R. C. Donehower, *The New England Journal of Medicine* **1995**, *332*, 1004.
- [168] V. Iman, H. Karimian, S. Mohan, Y. H. Hobani, M. I. Noordin, M. R. Mustafa, S. M.

- Noor, *Drug Design, Development and Therapy* **2015**, *9*, 1281.
- [169] P. Dubey, L. Nawale, D. Sarkar, A. Nisal, A. Prabhune, *RSC Adv* **2015**, *5*, 33955.
- [170] B. Alberts, A. Johnson, J. Lewis, M. Raff, K. Roberts, P. Walter, *Molecular Biology of the Cell*, **2002**.
- [171] B. Janic, T. M. Umstead, D. S. Phelps, J. Floros, *J Immunol Methods* **2003**, *272*, 125.
- [172] A. M. Rieger, K. L. Nelson, J. D. Konowalchuk, D. R. Barreda, *Journal of Visualized Experiments* **2011**, DOI 10.3791/2597.
- [173] R. Singh, L. Nawale, D. Sarkar, C. G. Suresh, *Plos One* **2016**, *11*, e0146110.
- [174] R. Pujari, S. M. Eligar, N. Kumar, S. Barkeer, V. Reddy, B. M. Swamy, S. R. Inamdar, P. Shastry, *PLoS ONE* **2013**, *8*, e79311.
- [175] X. Cao, Z. Huo, M. Lu, D. Mao, Q. Zhao, C. Xu, C. Wang, B. Zeng, *Journal of insect science (Online)* **2010**, *10*, 164.
- [176] L. A. Voloboueva, S. W. Suh, R. A. Swanson, R. G. Giffard, *Journal of Neurochemistry* **2007**, *102*, 1383.
- [177] J. Chen, J. L. Mehta, N. Haider, X. Zhang, J. Narula, D. Li, *Circulation Research* **2004**, *94*, 370.
- [178] S. Takano, S. Gately, M. E. Neville, W. F. Herblin, J. L. Gross, H. Engelhard, M. Perricone, K. Eidsvoog, S. Brem, *Cancer Research* **1994**, *54*, 2654.
- [179] S. Takano, Y. Yoshii, S. Kondo, H. Suzuki, T. Maruno, S. Shirai, T. Nose, *Cancer research* **1996**, *56*, 2185.
- [180] E. Pesenti, F. Sola, N. Mongelli, M. Grandi, F. Spreafico, *British journal of cancer* **1992**, *66*, 367.
- [181] A. Firsching, P. Nickel, P. Mora, B. Allolio, *Cancer Res* **1995**, *55*, 4957.
- [182] A. R. Gagliardi, M. F. Taylor, D. C. Collins, *Cancer Lett* **1998**, *125*, 97.
- [183] J. R. Van Brocklyn, *Mini reviews in medicinal chemistry* **2007**, *7*, 984.

- [184] A.-Y. Du, B.-X. Zhao, D.-L. Yin, S.-L. Zhang, J.-Y. Miao, *Bioorganic & medicinal chemistry* **2005**, *13*, 4176.
- [185] D. Hanahan, R. a Weinberg, *Cell* **2000**, *60*, 319.
- [186] Y. M. Ham, J. H. Lim, H. K. Na, J. S. Choi, B. D. Park, H. Yim, S. K. Lee, *Journal of Pharmacology and Experimental Therapeutics* **2006**, *319*, 1276.
- [187] R. Hájek, *Casopis lékařů českých* **1996**, *135*, 393.
- [188] J. Polz, **2010**.
- [189] K. C. Chan, H. H. Ho, M. C. Lin, C. N. Huang, H. P. Huang, C. J. Wang, *Journal of the Science of Food and Agriculture* **2016**, *96*, 381.
- [190] L. Annunziato, S. Amoroso, A. Pannaccione, M. Cataldi, G. Pignataro, A. D'Alessio, R. Sirabella, A. Secondo, L. Sibaud, G. F. Di Renzo, in *Toxicology Letters*, **2003**, pp. 125–133.
- [191] Q. Guo, B. L. Sopher, K. Furukawa, D. G. Pham, N. Robinson, G. M. Martin, M. P. Mattson, *The Journal of neuroscience : the official journal of the Society for Neuroscience* **1997**, *17*, 4212.
- [192] X. mei Chen, J. Liu, T. Wang, J. Shang, *Toxicology in Vitro* **2012**, *26*, 649.
- [193] D. Sareen, S. R. Darjatmoko, D. M. Albert, A. S. Polans, *Molecular pharmacology* **2007**, *72*, 1466.
- [194] M. Diederich, K. Noworyta, *Natural Compounds as Inducers of Cell Death*, **2012**.
- [195] Z. Jin, W. S. El-Deiry, *Cancer Biology and Therapy* **2005**, *4*, 139.
- [196] D. Belotti, V. Vergani, T. Drudis, P. Borsotti, M. R. Pitelli, G. Viale, R. Giavazzi, G. Taraboletti, *Clin Cancer Res* **1996**, *2*, 1843.
- [197] F. a. Scappaticci, *Journal of Clinical Oncology* **2002**, *20*, 3906.
- [198] P. Carmeliet, R. K. Jain, *Nature* **2000**, *407*, 249.
- [199] F. Q. B. Alenzi, *British Journal of Biomedical Science* **2004**, *61*, 99.

- [200] X. Ding, Q. Xu, F. Liu, P. Zhou, Y. Gu, J. Zeng, J. An, W. Dai, X. Li, *Cancer Letters* **2004**, *216*, 43.
- [201] N. Chatterjee, S. Das, D. Bose, S. Banerjee, T. Jha, K. Das Saha, *PLoS ONE* **2015**, *10*, 1.
- [202] S. Aggarwal, S. N. Das, *Tumor Biology* **2015**, DOI 10.1007/s13277-015-4583-8.
- [203] C. Vepari, D. L. Kaplan, *Progress in Polymer Science (Oxford)* **2007**, *32*, 991.
- [204] S. Rammensee, D. Huemmerich, K. D. Hermanson, T. Scheibel, A. R. Bausch, *Applied Physics A: Materials Science and Processing* **2006**, *82*, 261.
- [205] L. Yu, J. Ding, *Chemical Society reviews* **2008**, *37*, 1473.
- [206] B. Balakrishnan, R. Banerjee, *Chemical Reviews* **2011**, *111*, 4453.
- [207] L. Wang, Y. Wang, J. Qu, Y. Hu, R. You, M. Li, *Journal of Biomaterials and Nanobiotechnology* **2013**, *04*, 213.
- [208] T. Yucel, P. Cebe, D. L. Kaplan, *Biophysical Journal* **2009**, *97*, 2044.
- [209] X. Wang, J. A. Kluge, G. G. Leisk, D. L. Kaplan, *Biomaterials* **2008**, *29*, 1054.
- [210] G. G. Leisk, T. J. Lo, T. Yucel, Q. Lu, D. L. Kaplan, *Advanced Materials* **2010**, *22*, 711.
- [211] T. Yucel, N. Kojic, G. G. Leisk, T. J. Lo, D. L. Kaplan, *J. Structural Biology* **2010**, *170*, 406.
- [212] A. Matsumoto, J. Chen, A. L. Collette, U. J. Kim, G. H. Altman, P. Cebe, D. L. Kaplan, *Journal of Physical Chemistry B* **2006**, *110*, 21630.
- [213] G.-D. Kang, J.-H. Nahm, J.-S. Park, J.-Y. Moon, C.-S. Cho, J.-H. Yeo, *Macromolecular Rapid Communications* **2000**, *21*, 788.
- [214] S. Nagarkar, A. Lele, *Accelerated Gelation of Regenerated Fibroin*, **2014**.
- [215] V. Dingle-Pulate, P. Chandorkar, S. Bhagwat, A. A. Prabhune, *Journal of Surfactants and Detergents* **2013**, *17*, 543.
- [216] F. Application, P. Data, **2000**.
- [217] J. A. Kluge, N. C. Rosiello, G. G. Leisk, D. L. Kaplan, A. Luis Dorfmann, *Journal of the*

- Mechanical Behavior of Biomedical Materials* **2010**, 3, 278.
- [218] X. Hu, D. Kaplan, P. Cebe, *Macromolecules* **2006**, 39, 6161.
- [219] G. Ciapetti, E. Cenni, L. Pratelli, A. Pizzoferrato, *Biomaterials* **1993**, 14, 359.
- [220] S. Nagarkar, A. Patil, A. Lele, S. Bhat, J. Bellare, R. A. Mashelkar, *Industrial and Engineering Chemistry Research* **2009**, 48, 8014.
- [221] E. S. Gil, J. A. Kluge, D. N. Rockwood, R. Rajkhowa, L. Wang, X. Wang, D. L. Kaplan, *Journal of Biomedical Materials Research - Part A* **2011**, 99 A, 16.
- [222] M. Yamamoto, Y. Tabata, H. Kawasaki, Y. Ikada, *Journal of Materials Science: Materials in Medicine* **2000**, 11, 213.
- [223] V. D'Britto, H. Kapse, H. Babrekar, A. A. Prabhune, S. V Bhoraskar, V. Premnath, B. L. V Prasad, *Nanoscale* **2011**, 3, 2957.
- [224] G. H. Altman, F. Diaz, C. Jakuba, T. Calabro, R. L. Horan, J. Chen, H. Lu, J. Richmond, D. L. Kaplan, *Biomaterials* **2003**, 24, 401.
- [225] D. N. Rockwood, R. C. Preda, T. Yücel, X. Wang, M. L. Lovett, D. L. Kaplan, *Nature protocols* **2011**, 6, 1612.
- [226] J. Penfold, M. Chen, R. K. Thomas, C. Dong, T. J. P. Smyth, A. Perfumo, R. Marchant, I. M. Banat, P. Stevenson, A. Parry, I. Tucker, I. Grillo, *Langmuir* **2011**, 27, 8867.
- [227] B. Kundu, R. Rajkhowa, S. C. Kundu, X. Wang, *Advanced Drug Delivery Reviews* **2013**, 65, 457.
- [228] R. Thavasi, V. R. M. Subramanyam Nambaru, S. Jayalakshmi, T. Balasubramanian, I. M. Banat, *Marine biotechnology (New York, NY)* **2009**, 11, 551.
- [229] U. Rau, R. Heckmann, V. Wray, S. Lang, *Biotechnology Letters* **1999**, 21, 973.
- [230] J. S. Pedersen, *Advances in Colloid and Interface Science* **1997**, 70, 171.
- [231] A. Manceau, M. A. Marcus, S. Grangeon, M. Lanson, B. Lanson, A. C. Gaillot, S. Skanthakumar, L. Soderholm, *Journal of Applied Crystallography* **2013**, 46, 193.

- [232] J. V Joshi, V. K. Aswal, P. S. Goyal, *Journal of Physics: Condensed Matter* **2007**, *19*, 196219.
- [233] S. H. Chen, E. Y. Sheu, J. Kalus, H. Hoffman, *Journal of Applied Crystallography* **1988**, *21*, 751.
- [234] J. B. Hayter, J. Penfold, *Colloid & Polymer Science* **1983**, *261*, 1022.
- [235] J. Dey, N. Sultana, S. Kumar, V. K. Aswal, S. Choudhury, K. Ismail, *RSC Advances* **2015**, *5*, 74744.
- [236] S. Kumar, V. K. Aswal, *Journal of physics Condensed matter : an Institute of Physics journal* **2011**, *23*, 035101.
- [237] J. B. Hayter, J. Penfold, *Molecular Physics* **1981**, *42*, 109.
- [238] J.-P. Hansen, J. B. Hayter, *Molecular Physics* **2006**, *46*, 651.
- [239] R. Kaur, S. Kumar, V. K. Aswal, R. K. Mahajan, *Langmuir* **2013**, *29*, 11821.
- [240] J. Teixeira, *Journal of Applied Crystallography* **1988**, *21*, 781.
- [241] S. H. Chen, J. Teixeira, *Physical Review Letters* **1986**, *57*, 2583.
- [242] S. Kumar, V. K. Aswal, J. Kohlbrecher, *Langmuir* **2011**, *27*, 10167.
- [243] S. Mehan, A. J. Chinchalikar, S. Kumar, V. K. Aswal, R. Schweins, *Langmuir : the ACS journal of surfaces and colloids* **2013**, *29*, 11290.
- [244] P. R. Bevington, *Data Reduction and Error Analysis for the Physical Sciences*, **1969**.
- [245] T. Asakura, Y. Suzuki, Y. Nakazawa, K. Yazawa, G. P. Holland, J. L. Yarger, *Progress in Nuclear Magnetic Resonance Spectroscopy* **2013**, *69*, 23.
- [246] K. Ohgo, F. Bagusat, T. Asakura, U. Scheler, *Journal of the American Chemical Society* **2008**, *130*, 4182.
- [247] Zainuddin, T. T. Le, Y. Park, T. V Chirila, P. J. Halley, A. K. Whittaker, *Biomaterials* **2008**, *29*, 4268.

- [248] Y. Suzuki, T. Yamazaki, A. Aoki, H. Shindo, T. Asakura, *Biomacromolecules* **2014**, *15*, 104.
- [249] N. Baccile, A. S. Cuvier, C. Valotteau, I. N. A. Van Bogaert, *European Journal of Lipid Science and Technology* **2013**, *115*, 1404.
- [250] C. W. P. Foo, E. Bini, J. Hensman, D. P. Knight, R. V. Lewis, D. L. Kaplan, *Applied Physics A: Materials Science and Processing* **2006**, *82*, 223.
- [251] A. Stenstam, G. Montalvo, I. Grillo, M. Gradzielski, *J Phys Chem B* **2003**, *107*, 12331.
- [252] C. Sun, J. Yang, X. Wu, X. Huang, F. Wang, S. Liu, *Biophysical journal* **2005**, *88*, 3518.
- [253] E. L. Gelamo, R. Itri, A. Alonso, J. V da Silva, M. Tabak, *J Colloid Interface Sci* **2004**, *277*, 471.
- [254] T. Imamura, in *Encyclopedia of Surface and Colloid Science*, **2006**, pp. 5251–5263.
- [255] S. Chodankar, V. K. Aswal, J. Kohlbrecher, R. Vavrin, a G. Wagh, *Journal of Physics: Condensed Matter* **2007**, *19*, 326102.
- [256] S. Mehan, V. K. Aswal, J. Kohlbrecher, *Langmuir* **2014**, *30*, 9941.
- [257] S. N. Chodankar, V. K. Aswal, A. G. Wagh, *AIP Conference Proceedings* **2008**, *989*, 107.
- [258] Z. Ayub, K. Hirabayashi, M. Arai, Sen-i Gakkaishi, **1992**, *48*, 141.
- [259] Y. Hirata, M. Ryu, K. Igarashi, A. Nagatsuka, T. Furuta, S. Kanaya, M. Sugiura, *Journal of Oleo Science* **2009**, *58*, 565.
- [260] C. A. Ericsson, O. Söderman, V. M. Garamus, M. Bergström, S. Ulvenlund, *Langmuir* **2005**, *21*, 1507.
- [261] M. S. Zafar, D. J. Belton, B. Hanby, D. L. Kaplan, C. C. Perry, *Biomacromolecules* **2015**, *16*, 606.
- [262] S. Sofia, M. B. McCarthy, G. Gronowicz, D. L. Kaplan, *Journal of Biomedical Materials Research* **2001**, *54*, 139.
- [263] I. M. Banat, *Bioresource Technology* **1995**, *51*, 1.

 <b>Synopsis of the Thesis to be submitted to the Academy of Scientific and Innovative Research for Award of the Degree of Doctor of Philosophy in Chemistry</b>	
<b>Name of the Candidate</b>	Ms. Parul Dubey
<b>Degree Enrolment No. &amp; Date</b>	Ph. D in Biological Sciences (10BB11A26057); August 2011
<b>Title of the Thesis</b>	Biosynthesis of novel glycolipids (Sophorolipids): Exploring the mechanism of assembling and biological properties
<b>Research Supervisor/Co-supervisor</b>	Dr. Narendra Kadoo/ Dr. Asmita Prabhune, (AcSIR, CSIR-NCL, Pune)

## Introduction

Chemical surfactants constitute an important class of industrial bulk chemicals. They find applications in cosmetics, detergents, foods, textiles and pharmaceuticals. These inevitably end up in the environment after use. Thus, ecotoxicity and bio-accumulation of traditional surfactants remain issues of major concern. Hence, safer alternatives i.e. Biosurfactants that are derived microbially have gained recognition as they are biocompatible, non-toxic and biodegradable<sup>[263]</sup>. Sophorolipids (SL) constitute an interesting class of extracellular glycolipid biosurfactants. They are generally considered as the most promising glycolipid biosurfactant, as the production organism is non-pathogenic, ease of product recovery, high productivity, and substrate conversion<sup>[21]</sup>. Apart from general characteristics of surfactants, SLs possess several remarkable biological and assembling properties<sup>[58]</sup>. The new potentials of sophorolipids are being realized ever since its introduction and unique facets are being added by carrying out extensive research on it. Multiple properties possessed by single class of molecules i.e. Sophorolipids, renders the opportunity of employing them in varied fields ranging from detergent industry to materials and biomedical.

## Statement of Problem, Aims and Objectives

1) SLs have unique property of being tailor made i.e. different forms of SL can be synthesized by supplementing the yeast with different lipophilic feed. The flexibility of modifying the sophorolipids structure has prompted researchers to synthesize numerous forms of SLs to enhance their biological properties<sup>[148]</sup>. With the aim to synthesize novel SL, cetyl alcohol was used as the lipophilic substrate. The novel SL synthesized is expected to have varied properties than the conventional sophorolipids. Thus biological properties of SL such as anti-microbial and anti-cancerous were explored.

2) Interaction of proteins with surfactants is widely studied. Silk fibroin (SF) protein due to its mechanical strength and integrity finds application in biomedical field<sup>[225]</sup>. Among different processed forms of SF, hydrogels mark great importance in tissue engineering. But enormously high gelation time of SF restricts its use<sup>[117]</sup>. Different physical and chemical methods have been reported to induce faster gelation in SF. But their non-physiological and

non-biodegradable nature imposes drawback from biological application point of view. Thus we aimed at accelerating the gelation of SF by employing SL as it is both biocompatible and biodegradable.

### Methodology used

1. SL synthesis was carried out by supplementing *Candida bombicola* with cetyl alcohol as the lipophilic substrates. Successful incorporation of cetyl alcohol in SL molecule (SLCA) was shown by different analytical techniques. Cell culture techniques were carried to explore the anti-proliferative and anti-angiogenic property of SLCA.
2. Accelerated gelation of SF was achieved by a simple physical method which involved mixing of the two solutions at different concentration and pH.
3. Mechanism of accelerated gelation was investigated by multiple sophisticated techniques such as Rheology, Nuclear magnetic Resonance spectroscopy, Small angle neutron scattering.

### Key Findings

#### 1) Production of Novel Sophorolipids using fatty alcohol, their physico-chemical, analytical and antimicrobial analysis

Novel sophorolipid (SLCA) synthesized using cetyl alcohol depicted promising surfactant and biological properties. Physicochemical characterization revealed that it significantly lowered the surface tension of water to 31.4 mN/m with critical micelle concentration of 104 mg/L. Interestingly, unlike other sophorolipids SLCA completely inhibited the growth of both *E. coli* and *S. aureus* at the same and relatively low concentration (300 µg/mL).

#### 2) Sophorolipids from primary alcohol: anti-proliferative and anti-angiogenic agents against human cervical cancer cells

Anti-proliferative effect of SLCA against different human cancer cell lines was evaluated. SLCA significantly inhibited the cell proliferation of two human cancer cell lines (HeLa – human cervical cancer cells, and HCT 116 – human colon cancer cells) and was non-toxic towards normal cells even at higher doses. The mechanism of cytotoxicity in HeLa was found to be apoptosis. Interestingly, these sophorolipids also showed anti-angiogenic activity in HUVEC cells by disrupting the endothelial tubulogenesis.

#### 3) Sophorolipid assisted tunable and rapid gelation of silk fibroin to form porous biomedical scaffolds

Potential use of SL as gelling agent for silk fibroin protein was studied. The long gelation time of SF was brought down to few hours using SL. The biological properties of SL make it an interesting gelling agent. The hydrogels of silk fibroin so formed can be used for wound dressing applications. Further, these hydrogels were lyophilized into 3D scaffolds, which

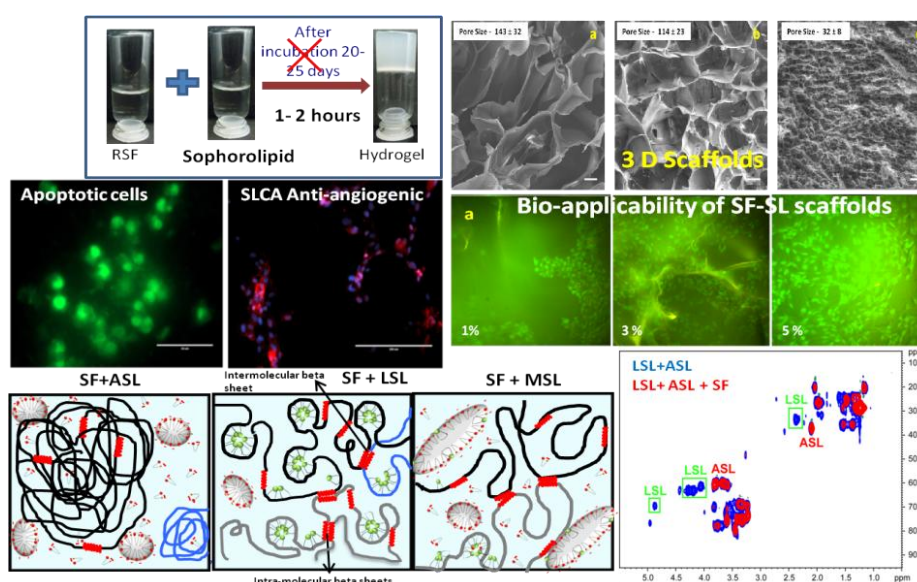
may be useful in tissue regeneration. Bio-applicability of scaffolds was ascertained by showing proliferation of fibroblast cells in scaffolds.

#### 4) Silk Fibroin Sophorolipid gelation: Deciphering the underlying mechanism

The mechanism of accelerated gelation of silk fibroin sophorolipid solutions was studied. Multiple characterization techniques such as Rheology, NMR, Fluorescence spectroscopy and Small Angle Neutron Scattering were used for the study. Preferential binding of lactonic SL to SF was found to be nucleating step of gelation.

#### 5) Influence of pH on assembly thus, gelation of sophorolipid-silk fibroin

The influence of pH on sophorolipids self assembling property and its role in gelation of sophorolipid-silk fibroin was deciphered. The study revealed that pH responsive group in acidic SL confers negative charge in alkaline condition. Higher charge leads to repulsion and opening of the SF chain. The molecular beta sheets thus formed lead to cross-linking of protein into 3D gelled network.



Signature of  
the candidate  
(Ms. Parul Dubey)

Signature of the  
Ph.D. co-supervisor  
(Dr. Asmita Prabhune)

Signature of the  
Ph.D. supervisor  
(Dr. Narendra Kadoo)

## List of Publications

- 1) **P. Dubey**, K. Selvaraj, A. Prabhune. Sophorolipids: in self assembly and nanomaterial synthesis. *World Journal of Pharmacy and Pharmaceutical Science*, 2(3), (2013) 1107-1133
- 2) **P. Dubey**, K. Selvaraj, A. A. Prabhune. Physico-chemical, analytical and antimicrobial studies of novel sophorolipids synthesized using cetyl alcohol. *World Journal of Pharmacy and Pharmaceutical Science*, 3(3), (2014) 993-1010
- 3) **P. Dubey**, L. Nawale, D. Sarkar, A. Nisal, A. Prabhune. Sophorolipid assisted tunable and rapid gelation of silk fibroin to form porous biomedical scaffolds. *RSC Advances*, 5, (2015) 33955
- 4) P. Darne, M. Mehta, **P. Dubey**, A. Prabhune. Bauhinia seed oil, a novel substrate for sophorolipid production. *World Journal of Pharmacy and Pharmaceutical Science*, 3(11), (2014) 792-804
- 5) V. Dengele-Pulate, **P. Dubey**, S. Bhagwat, A. Prabhune. HPLC-MS, HRMS analysis of microbial acid free, short chain alkyl sophorosides. *World Journal of Pharmaceutical Research*, 4(5), (2015) 2562-2576
- 6) P. K. Singh, K. Bhardwaj, **P. Dubey**, A. Prabhune. UV-assisted size sampling and antibacterial screening of *Lantana camara* leaf extract synthesized silver nanoparticles. *RSC Advances*, 5, (2015) 24513
- 7) **P. Dubey**, L. Nawale, D. Sarkar, A. Prabhune. Apoptosis mediated anti-proliferative effect of primary alcohol derived sophorolipid against human cervical cancer cells and their anti-angiogenic activity. (Manuscript communicated to PLOS ONE)
- 8) **P. Dubey**, S. Kumar, V. K. Aswal, S. Ravindranathan, P. R. Rajamohanam, A. Prabhune, A. Nisal. Silk Fibroin-Sophorolipid gelation: Deciphering the underlying mechanism. (Manuscript communicated to Biomacromolecules)
- 9) **P. Dubey**, S. Vasudevan S. Kumar, V. K. Aswal, S. Ravindranathan, P. R. Rajamohanam, A. Prabhune, A. Nisal. pH dependent sophorolipid assemblies and their influence on gelation of silk fibroin protein. (Manuscript communicated)

## Patent

- **P. Dubey**, P.P. Devi, A.A. Nisal, A.A. Prabhune. Sophorolipid mediated accelerated gelation of silk fibroin. WO2015170342 A1

## Poster Presentations

- 1) **P. Dubey**, K. Selvaraj, A. Prabhune. “Novel glycolipids: their surfactant and antimicrobial properties”, presented at 5<sup>th</sup> Asian Conference on Colloids and Interface Science, held at Department of Chemistry University of North Bengal Darjeeling, INDIA; 20-23 November 2013.
- 2) **P. Dubey**, L. Nawale, D. Sarkar, A. Nisal, A. Prabhune. “Mechanistic understanding of rapid gelation of Silk fibroin using a biosurfactant – Sophorolipid”, presented at Indo-Australian Conference on Biomaterials, Tissue Engineering, Drug Delivery system & Regenerative Medicine (BiTERM-2015), held at Department of Chemistry, Anna University, Chennai, India; 5-7 February 2015.
- 3) **P. Dubey**, A. Patil, K. Selvaraj, A. A. Prabhune. Physico-chemical, analytical and antimicrobial studies of novel sophorolipids synthesized using cetyl alcohol, during National Science Day, 2015, National Chemical Laboratory, Pune
- 4) **P. Dubey**, D. Joshi, A. Shete, A. Nisal, A. Prabhune and A. Lele. “Sophorolipid coated electrospun silk fibroin nano-fibers with enhanced biological activity”, during National Science Day, 2016, National Chemical Laboratory, Pune